Invited Speaker

1191 Breaking Resolution Limits with Ptychography using Topological Materials
Professor Kayla Nguyen[1]
[1]University of Oregon, Eugene, , United States
238 Progress in 3D phase-contrast imaging using 4D-STEM: increased dose-efficiency and depth of field
Philipp Pelz[1,2], Dr. Andrey Romanov[1,2], Dr. Shengbo You[1,2], Dr. Mary Scott[3,4], Dr Colin Ophus[4], Dr Min Gee Cho[3,4], Daniel Stroppa[5], Mingjian Wu[1]
[1]Department of Materials Science & Engineering, FAU Erlangen-Nürnberg, Erlangen, Germany, [2]Institute of Micro- and Nanostructure Research (IMN) \& Center for Nanoanalysis and Electron Microscopy (CENEM), Erlangen, Germany, [3]Department of Materials Science and Engineering, University of California Berkeley, Berkeley, United States, [4]The Molecular Foundry, Lawrence Berkeley National Laboratory, Berkeley, United States, [5]DECTRIS AG, Baden, Switzerland

Oral Presentation

177 Phase detection limits in electron holography with automatic stabilisation and direct electron detection
Dr Martin Hytch[1], Dr Cécile Marcelot[1], Dr Christophe Gatel[1,2]
[1]CEMES-CNRS, Toulouse, France, [2]University of Toulouse III, Toulouse, France
276 Holography with an Extended Reference in Transmission Electron Microscopy
Dr Wei Chao[1], Professor David Paganin[1], Dr Timothy Petersen[2], Professor Changlin Zheng[3], Professor Joanne Etheridge[1,2]
[1]School of Physics and Astronomy, Monash University, Clayton, Australia, [2]Monash Centre for Electron Microscopy, Monash University, Clayton, Australia, [3]Department of Physics, Fudan University, Songhu Road 2005, Shanghai, China
346 Off-Axis Electron Holography of In-Situ-Biased Highly-Doped p-AlGaAs/n-GaInP Junctions for Solar Cell Applications
Vita Mergner[1,2], Malte Klitzke[2], Dr. Patrick Schygulla[2], Dr. David Lackner[2], Dr. András Kovács[1], Prof. Dr. Wolfgang Jäger[3], Prof. Dr. Rafal E. Dunin-Borkowski[1], Dr. David Cooper[4]
[1]Ernst Ruska-Centre for Microscopy and Spectroscopy with Electrons, Forschungszentrum Jülich, 52425 Jülich, Germany, [2]Fraunhofer Institute for Solar Energy Systems ISE, 79110 Freiburg, Germany, [3]Materials Science, Christian-Albrechts-University, 24143 Kiel, Germany, [4]Univ. Grenoble Alpes, CEA, LETI, F-38000 Grenoble, France
807 Minimising the distortive effects of diffraction on magnetic STEM-DPC imaging of monocrystalline thin films
Sivert Dagenborg[1], Andrea D'Alessio[2], Nikolas Vitaliti[2], Alessandro Palliotto[2], Eric Brand[2], Associate Professor Ingrid Hallsteinsen[3], Professor Nini Pryds[2], Assistant Professor Daesung Park[2], Associate Professor Felix Trier[2], Associate Professor Magnus Nord[1]
[1]Department of Physics, Norwegian University of Science and Technology, Trondheim, Norway, [2]Department of Energy Conversion and Storage, Technical University of Denmark, Kongens Lyngby, Denmark, [3]Department of Materials Science and Engineering, Norwegian University of Science and Technology, Trondheim, Norway
1011 Sequential tilting 4D-STEM for reliable electric field mapping across junctions
Christoph Flathmann[1], Ulrich Ross[1], Andreas Beyer[2], Jürgen Belz[2], Kerstin Volz[2], Michael Seibt[1], Tobias Meyer[3]
[1]4th Physical Institute, Georg-August-University Goettingen, Göttingen, Germany, [2]Department of Physics and Materials Science CenterPhilipps-University Marburg, Marburg, Germany, [3]Institute of Materials Physics, Georg-August-University Goettingen, Göttingen, Germany

1083 Structured illumination near-field electron ptychography
Penghan Lu[1], Frederick Allars[2], Shengbo You[3], Thomas Schachinger[4], Rafal E. Dunin-Borkowski[1], Andrew M. Maiden[2,3]
[1]Ernst Ruska-Centre for Microscopy and Spectroscopy with Electrons, Forschungszentrum Jülich, Jülich, Germany, [2]Diamond Light Source, Harwell Science and Innovation Campus, Didcot, UK, [3]Department of Electronic and Electrical Engineering, University of Sheffield, Sheffield, UK, [4]University Service Centre for Transmission Electron Microscopy, TU Wien, Wien, Austria
74 Alternating-probe electron ptychography
Meng Zhao[1], Mr. Anton Gladyshev[1], Prof. Christoph Koch[1]
[1]Humboldt University of Berlin & Center for the Science of Materials Berlin,, Berlin, Germany
251 Full-field illumination ptychography with a structured electron beam
Hirokazu Tamaki[1,2], Dr. Koh Saitoh[3]
[1]Graduate School of Engineering, Nagoya University, Nagoya, Japan, [2]Research & Development group, Hitachi Ltd., Kokubunji, Japan, [3]Institute of Materials and Systems for Sustainability, Nagoya University, Nagoya, Japan
288 Quantitative comparison of HRTEM and electron ptychography
Felix Bennemann[1], Prof Peter Nellist[1], Prof Angus Kirkland[1,2]
[1]Department of Materials, University of Oxford, Oxford, United Kingdom, [2]Rosalind Franklin Institute, Harwell Science & Innovation Campus, Didcot, United Kingdom
315 Electron single pixel imaging enabled by ultrafast optical modulation of the illuminating wavefunction
Dr. Cameron Duncan[1], Beatrice Ferrari[1], Irene Ostroman[1], Maria Giulia Bravi[1], Sang Tae Park[2], Daniel Masiel[2], Jean Christophe Olaya[3], Paolo Rosi[4], Enzo Rotunno[4], Vincenzo Grillo[4], Giovanni Maria Vanacore[1]
[1]Unversità degli Studi di Milano-Bicocca, Milan, Italy, [2]JEOL-IDES, Pleasonton, United States of America, [3]Holoeye Photonics, Berlin, Germany, [4]Istituto Nanoscienze, Consiglio Nazionale delle Ricerche, Modena, Italy
375 Atomic transitions analogue in phased-shaped electron energy-loss spectroscopy
Simon Garrigou[1], Mr. Arnaud Arbouet[1], Mr. Hugo Lourenço-Martins[1]
[1]CEMES-CNRS, Université de Toulouse, CNRS, Toulouse, France
557 Multi-Convergence-Angle Ptychography with Simultaneous Strong Contrast and High Resolution
Mr. Wei Mao[1,2], Mr. Weiyang Zhang[2], Dr. Chen Huang[3], Prof. Liqi Zhou[1,2,5], Dr. Judy Kim[3,4], Prof. Si Gao[2,6], Mr. Yu Lei[1], Mr. Xiaopeng Wu[1], Mr. Xudong Pei[2], Prof. Yuefeng Nie[2], Prof. Angus Kirkland[3,4], Dr Peng Wang[1,2]
[1]Department of Physics, University of Warwick, Coventry, UK, [2]National Laboratory of Solid-State Microstructures, Jiangsu Key Laboratory of Artificial Functional Materials, College of Engineering and Applied Sciences and Collaborative Innovation Centre of Advanced Microstructures, Nanjing University, Nanjing, China, [3]The Rosalind Franklin Institute, Harwell Campus, Didcot, UK, [4]Department of Materials, University of Oxford, Oxford, UK, [5]Institute of Materiobiology, College of Science, Shanghai University, Shanghai, China, [6]College of Materials Science and Engineering, Nanjing Tech University, Nanjing, China
681 Mean inner potential change of latex sphere with temperature measured using off-axis electron holography
Dr. Yan Lu[1], Peng-Han Lu[1], Dominik Biscette[2], Denys Sutter[2], Prof. Giulio Pozzi[3], Prof. Rafal E. Dunin-Borkowski[1]
[1]Forschungszentrum Juelich, Juelich, Germany, [2]CondenZero AG, Zurich, Switzerland, [3]University of Modena and Reggio Emilia, Modena, Italy
707 Coherent inelastic scattering probed by holographic scanning transmission electron microscopy
Dr. Nora Bach[1], Tim N. Dauwe[1], Dr. Murat Sivis[1], Prof. Dr. Claus Ropers[1]
[1]Max Planck Institute for Multidisciplinary Sciences, Göttingen, Germany
54 Vibration-Corrected Electron Ptychography

Anton Gladyshev[1,2], Mr. Johannes Müller[1,2], Dr. Benedikt Haas[1,2], Prof. PhD Christoph Koch1[1,2]
[1]Humboldt-Universität zu Berlin, Berlin, Germany, [2]Center for the Science of Materials Berlin, Berlin, Germany

103 End-to-end learning of atomic resolution phase-contrast volumes from 4D-STEM measurements

Shengbo You[1], Dr Andrey Romanov[1], Dr Philipp Pelz[1]
[1]Institute of Micro- and Nanostructure Research (IMN) & Center for Nanoanalysis and Electron Microscopy (CENEM), Friedrich Alexander-Universität Erlangen-Nürnberg,, Erlangen, Germany

352 Ptychographic imaging of nanoscale 3D objects with soft x-ray synchrotron and EUV table-top sources

Dr Vitaly Krasnov[1], Dr Kevin Dorney[2], Dr Esben Larsen[2], Prof. Igor Makhotkin[3], Dr Jeroen Scheerder[2], Dr Victor Soltwisch[4], Dr Paul van der Heide[2], Prof. Claudia Fleischmann[1]
[1]imec / KU Leuven, Department of Physics and Astronomy, Quantum Solid-State Physics, Leuven, Belgium, [2]imec, Leuven, Belgium, [3]University of Twente, Enschede, Netherlands, [4]PTB, Berlin, Germany

583 Iterative Phase Retrieval Methods for Weakly Scattering Signals: Transfer of Information and Efficient Regularization

Georgios Varnavides[1,2], Dr Stephanie Ribet[2], Mr Reed Yalisove[2,3], Dr Mary Scott[2,3], Dr Colin Ophus[2]
[1]Miller Institute for Basic Research in Science, University of California, Berkeley, USA, [2]National Center for Electron Microscopy, Lawrence Berkeley Laboratory, Berkeley, USA, [3]Department of Materials Science and Engineering, University of California, Berkeley, USA

633 Consistency and reliability of ptychographic deconvolution approaches

Tizian Lorenzen[1], Dr. Benedikt Diederichs[1,2], Charles Ogolla[3], Prof. Benjamin Butz[3], Prof. Knut Müller-Caspary[1]
[1]Ludwig-Maximilians-Universität, Munich, Germany, [2]Institute of Biological and Medical Imaging, Helmholtz Zentrum Munich, Neuherberg, Germany, [3]Micro- and Nanoanalytics Group, University of Siegen, Siegen, Germany

1164 Quantum Measurements using Interferometric STEM-EELS

Professor Benjamin McMorran[1], Dr. Cameron Johnson[1,2], Dr. Amy Turner[1]
[1]Department of Physics, University of Oregon, Eugene, USA, [2]Molecular Foundry, Lawrence Berkeley National Laboratory, Berkeley, USA

85 Near-Ideal Direct-Electron Focused-Probe 4D-STEM Data for Open-Source Phase Reconstructions

Prof. Toma Susi[1], Niklas Dellby[2], Russ Hayner[2], Christoph Hofer[3], Jani Kotakoski[1], Tracy Clark Lovejoy[2], Clemens Mangler[1], Andreas Mittelberger[2], Timothy J. Pennycook[3], Benjamin Plotkin-Swing[2]
[1]University of Vienna, Faculty of Physics, Vienna, Austria, [2]Nion Co. R&D, Kirkland, USA, [3]EMAT, University of Antwerp, Antwerp, Belgium

390 Thermal vibrations in inverse dynamical electron scattering

Ziria Herdegen[1], Dr. Benedikt Diederichs[2], Prof. Dr. Knut Müller-Caspary[1]
[1]Depart. Chemistry, Ludwig-Maximilians-Universität München, Munich, Germany, [2]Institute of Biological and Medical Imaging, Helmholtz Zentrum München, Neuherberg, Germany

555 Influence of the loss function on gradient-based iterative ptychographic reconstructions in 4D-STEM

Max Leo Leidl[1,2], Carsten Sachse[2,3], Knut Müller-Caspary[1,2]
[1]Ludwig Maximilian University of Munich, Munich, Germany, [2]Ernst Ruska-Centre, Forschungszentrum Jülich GmbH, Jülich, Germany, [3]Heinrich Heine Universitöt Düsseldorf, Düsseldorf, Germany

969 Transport of Intensity Phase Retrieval in the Presence of Intensity Variations and Unknown Boundary Conditions

Daniel Wolf[1], Radmila Kyrychenko[1], Max Herzo[1], Oleksandr Zaiets[1], Axel Lubk[1]
[1]Leibniz Institute for Solid State and Materials Research, Dresden, Germany

Poster Presentation

50 Electron holography for electrostatic potential measurement and contrast enhanced imaging of biological samples
Dr Elio Karim[1,2,4], Mr. Bumsu Park[1], Mr. Christophe Gatel[1], Ms. Amélie Le Forestier[3], Ms. Vanessa Soldan[2], Ms. Stéphanie Balor[2], Ms. Célia Plisson-Chastang[2], Mr. Pierre-Emmanuel Gleizes[2], Mr. Etienne Snoeck[1]
[1] Centre d'élaboration de matériaux et d'études structurales (CEMES) - CNRS, Toulouse, France, [2]MCD and METi, Centre de Biologie Intégrative, Université de Toulouse, CNRS, Toulouse, France, [3] Laboratoire Physique des Solides (LPS) - Université Paris-Saclay, CNRS, Orsay, France, [4]Institut de Biologie Structurale (IBS) – University Grenoble Alpes, CEA, CNRS, Grenoble, France
51 Investigating the potential variation of in-operando semiconductor nanostructures in electron beam direction
Hüseyin Çelik[1], Mr. Robert Fuchs[2], Dr. Dirk Berger[3], Dr. Christian M. Günther[3], Mr. Simon Gaebel[4], Dr. Tolga Wagner[5], Prof. Dr. Michael Lehmann[1]
[1]Technische Universität Berlin, Institute of Optics and Atomic Physics, , Germany, [2]Technische Universität Berlin, Institute of Theoretical Physics, , Germany, [3]Technische Universität Berlin, Center for Electron Microscopy (ZELMI), , Germany, [4]Max-Born-Institut für Nichtlineare Optik und Kurzzeitspektroskopie, , Germany, [5]Humboldt-Universität zu Berlin, Department of Physics, , Germany
62 Optimized Bright Field STEM Imaging for Detecting Molecules absorbed within Zeolite Pores
Yu Xia[1], Mr. Tom WIllhammar[1]
[1]Department of Materials and Environmental Chemistry, Stockholm University, Stockholm, Sweden
162 Liquid Phase Transmission Electron Microscopy
Mads Søndergaard Larsen[1], Mr Ebrahim Chalangar[1], Mrs Sofie Tidemand-Lichtenberg[1], Mr Murat Nulati Yesibolati[1], Mr. Emil Jensen[1], Mr. Kristian Speranza Mølhave[1]
[1]DTU Nanolab, Kgs. Lyngby, Denmark
165 Assessing the sensitivity of 4D-STEM measurements for electric field mapping at the sub-micrometer scale
Pierpaolo Ranieri[1], Dr. Reinis Ignatans[1], Dr. Victor Boureau[2], Prof. Vasiliki Tileli[1]
[1]Institute of Materials, École Polytechnique Fédérale de Lausanne, Lausanne, Switzerland, [2]Interdisciplinary Centre for Electron Microscopy, École Polytechnique Fédérale de Lausanne, Lausanne, Switzerland
173 Mean inner potential variation with strain in III-nitrides studied by off-axis electron holography
Lou Denaix[1], Dr Jing Li[1], Dr Benoît Scklenard[1], Dr David Cooper[1], Dr Eva Monroy[2]
[1]Univ. Grenoble Alpes, CEA, Leti, F-38000 Grenoble, France, [2]Univ. Grenoble Alpes, CEA, Grenoble INP, IRIG, PHELIQS, F-38000 Grenoble, France
185 New paradigm for ultra-low-dose high-resolution imaging through a dedicated event-driven analytical ptychography methodology
Dr. Hoelen L. Lalandec-Robert[1,2], Prof. Dr. Jo Verbeeck[1,2]
[1]Electron Microscopy for Materials Science (EMAT), University of Antwerp , Antwerp, Belgium, [2]NANOlab Center of Excellence, University of Antwerp, Antwerp, Belgium
196 High Spatio-Temporal Resolution Differential Phase Contrast Imaging via Detector Signal Digitisation
Julie Marie Bekkevold[1,2], Dr. Jonathan J. P. Peters[1,2], Prof. Ryo Ishikawa[3], Prof. Lewys Jones[1,2]
[1]School of Physics, Trinity College Dublin, Dublin, Ireland, [2]Advanced Microscopy Laboratory, Dublin, Ireland, [3]University of Tokyo, Bunkyo, Tokyo, Japan
204 Distortions correction in HR-(S)TEM and low resolution TEM images: absolute size, strain and polarization measurements
Dr. Nikolay Cherkashin[1], Mrs Sylvie Schamm-Chardon[1]

[1]CEMES-CNRS, Toulouse, France

241 Information Transfer Improvement by Parallax Correction and Ptychography Reconstruction Applied to Large-Area 4D STEM Experiments

Daniel Stroppa[1], Dr. Stephanie Ribet[2], Dr. Georgios Varnavides[2], Dr. Colin Ophus[2], Dr. Philipp Pelz[3]
[1]DECTRIS, Baden-Daettwil, Switzerland, [2]NCEM, Molecular Foundry, Lawrence Berkeley National Laboratory,, Berkeley, USA, [3]Institute of Micro- and Nanostructure Research (IMN) & Center for Nanoanalysis and Electron Microscopy, Erlangen, Germany

246 Depth sensitivity of atomic resolution secondary electron imaging

Professor Koh Saitoh[1]
[1]Institute of Materials and Systems for Sustainability, Nagoya University, Nagoya, Japan, [2]Department of Applied Physics, Nagoya University, Nagoya, Japan, [3]Hitachi High-Tech Corporation, Hitachinaka, Japan

255 Investigation of electron-beam-induced charging in a dolomite needle using off-axis electron holography

Dr. Fengshan Zheng[1], Mrs Ingrid McCarroll[4], Dr Vadim Migunov[3], Dr Marco Beleggia[5], Prof Giulio Pozzi[6], Prof Julie Cairney[4], Prof Rafal Dunin-Borkowski[2]
[1]South China University of Technology, Guangzhou, China, [2]Forschungszentrum Jülich, Jülich, Germany, [3]RWTH Aachen University, Aachen, Germany, [4]The University of Sydney, Sydney, Australia, [5]Technical University of Denmark, Denmark, Denmark, [6]University of Modena and Reggio Emilia, Modena, Italy

293 Improving Control Signals for Interference Gating

Simon Gaebel[1,2], Hüseyin Çelik[2], Dr. Christian M. Günther[2], Dr. Tolga Wagner[3], Prof. Dr. Michael Lehmann[2]
[1]Max-Born-Institut, Berlin, Germany, [2]Technische Universität Berlin, Berlin, Germany, [3]Humboldt-Universität Berlin, Berlin, Germany

304 Influential factors affecting the quantification accuracy of magnetic moments with electron magnetic chiral dichroism technique

Dr Xiaoxiao Fu[1], Mr Zhixin Zeng[1], Miss Qiwen Hu[1], Dr Xiaoxu Huang[1]
[1]International Joint Laboratory for Light Alloys (MOE), College of Materials Science and Engineering, Chongqing University, Chongqing , China

312 3D atomic-resolution imaging of nanomaterials based on exit wave reconstruction

Sophie Kargo Kaptain[1], Mr. Joakim Kryger-Baggesen[1], Mrs. Rikke Egeberg Tankard[2], Mr. Fu-Rong Chen[3], Mr. Dirk van Dyck[4], Mr. Joerg R. Jinschek[1,5], Mr. Jakob Kibsgaard[2], Mr. Christian Danvad Damsgaard[1,5], Mr. Stig Helveg[1]
[1]Center for Visualizing Catalytic Processes (VISION), Department of Physics, Technical University of Denmark, Kgs. Lyngby, Denmark, [2]Surface Physics and Catalysis, Department of Physics, Technical University of Denmark, Kgs. Lyngby, Denmark, [3]Department of Materials Science and Engineering, City University of Hong Kong, Kowloon, Hong Kong, [4]Departments of Physics, EMAT, University of Antwerp, Antwerp, Belgium, [5]National Center for Nano Fabrication and Characterization, Technical University of Denmark, Kgs. Lyngby, Denmark

326 Identification of inorganic fibres in workplace air by SEM-EDS

Dr. Markus Mattenklott[1], Dennis Kaiser[1], Bianca Gasse[1]
[1]Institute for Occupational Safety and Health (IFA), Sankt Augustin, Deutschland

445 Assessing Ptychographic Methods for Maximum Low Dose Performance

Tamazouzt Chennit, Ph.D Christoph Hofer[1], Ph.D Biao Yuan[1,2], MS.c Songge Li[1], Ph.D, MEng Andrew Maiden[3,4], Prof. Dr. Timothy Pennycook[1]
[1]EMAT, University of Antwerp, 2020, Belgium, [2]Electron Microscopy Center, University of Technology, South China, China, [3]EEE. Dept, University of Sheffield, S13JD, UK, [4]Diamond Light Source, OX110DE, UK

447 Towards atom-counting from first-moment STEM images

Dr. Yansong Hao[1], Dr. Annick De Backer[1], Prof. Scott David Findlay[2], Prof. Sandra Van Aert[1]

[1]EMAT, University of Antwerp, Antwerp, Belgium, [2]School of Physics and Astronomy, Monash, Australia

459 Overcoming the aberration-limit of a non-corrected Transmission Electron Microscope with computational ghost imaging

Paolo Rosi[1,2], Lorenzo Viani[2], Dr Enzo Rotunno[1], Prof. Stefano Frabboni[2], Dr Amir Hossein Tavaby[3], Prof Rafal E. Dunin-Borkowski[3], Dr Alberto Roncaglia[4], Dr Vincenzo Grillo[1]
[1]CNR-Institute for Nanoscience, Modena, Italy, [2]University of Modena and Reggio Emilia, FIM department, Modena, Italy, [3]Ernst Ruska-Centre for Microscopy and Spectroscopy with Electrons, Forschungszentrum Jülich, Jülich, Germany, [4]CNR - Institute for Microelectronics and Microsystems, Bologna, Italy

481 Largely improved momentum resolution in STEM-DPC imaging of Si(110) with a segmented detector

Julius Bürger[1], Maja Groll[1], Aladin Ullrich[2], Manfred Albrecht[2], Jörg K. N. Lindner[1]
[1]Paderborn University, Paderborn, Germany, [2]University of Augsburg, Augsburg, Germany

486 Influence of dynamical diffraction on DPC measurements of 2D materials

Maja Groll[1], Julius Bürger[1], Prof. Dr. Jörg K. N. Lindner[1]
[1]Paderborn University, Paderborn, Germany

500 Zernike Phase Plates for aberration-corrected TEM in Material Science

Simon Hettler[1,2], Raul Arenal[1,2,3]
[1]Instituto de Nanociencia y Materiales de Aragón (INMA), CSIC-Universidad de Zaragoza, Zaragoza, Spain, [2]Laboratorio de Microscopías Avanzadas (LMA), Universidad de Zaragoza. Zaragoza, Zaragoza, Spain, [3]Araid Foundation, Zaragoza, Spain

551 4D-STEM Post measurement machine learning enhanced aberration correction for amorphous and magnetic samples

Maximilian Töllner[1], Xiaoke Mu[3], Di Wang[1], Christian Kübel[1,2]
[1]Institute of Nanotechnology - KIT, Karlsruhe, Germany, [2]KNMFi, Karlsruhe, Germany, [3]School of Materials and Energy and Electron Microscopy Centre, Lanzhou University, Lanzhou, China

612 Simultaneous acquisitions and applications of DPC/OBF STEM, EDS and EELS

Dr. Yuhiro Segawa[1], Dr. Akiho Nakamura[1], Mr. Hiroki Hashiguchi[1], Mr. Yuji Kohno[1], Dr. Shigemasa Ohta[1], Senior Assistant Professor Takehito Seki[2], Professor Naoya Shibata[2]
[1]JEOL Ltd., Akishima-shi, Japan, [2]The University of Tokyo, Bunkyo-ku, Japan

635 Innovative Designs For Enhancing the Functionality of MEMS-Based Phase Plates through Numerical Simulation and Optimisation

Mr Payam Habibzadeh Kavkani[1,2], Dr Vincenzo Grillo[2], Professor Marco Beleggia[1]
[1]Universitá di Modena e Reggio Emilia, Modena, Italy, [2]CNRNANO - Istituto di Nanoscienze - Centro S3, Modena, Italy

637 Accessible low-cost, open-source, single-shot phase imaging implemented on an openFrame-based microscope

Huihui Liu[1], Sunil Kumar[1,2], Edwin A Garcia Castano[1], Yasin Razak[3], William Flanagan[1], Jonathan Lightley[1], Ruiyang D Duan[1], Freen Liao[1], Xiaoyu Sun[1], Shanhe N Zeng[1], Brian D Robertson[4], Christopher W Dunsby[1,2], Paul (PHOT) M W French[1,2]
[1]Physics Department, Imperial College London, SW7 2AZ, London, United Kingdom, [2]Francis Crick Institute, 1 Midland Road, NW1 1AT, London, United Kingdom, [3]University of Cape Town, , South Africa, [4]Department of Life Sciences, Imperial College London, SW7 2AZ, , United Kingdom

646 Analytical Phase-Shifting Electron Holography using Fresnel-corrected holograms

Augustin Nogier[1], Aurélien Masseboeuf[1], Kévin Garello[1]
[1]SPINTEC, Grenoble, France

683 Ptychography at finite dose in SrTiO3

Dr Malcolm Dearg[1], Mr James Gilbert[1], Mr Nick Michaelides[1], Dr Laura Clark[1]
[1]School of Physics, Engineering and Technology; University of York, York, United Kingdom

799 Towards Quantitative analysis of electrostatic potential of monolayer WSe2 using electron ptychography
Yiran Lu[1], Alexis Wartelle[1], Djodje Dosenovic[2], Matthew Bryan[3], Hanako Okuno[2], Julio-Cesar da Silva[1], Jean-Luc Rouvière[4], Martien I. den Hertog[1]
[1]Univ. Grenoble-Alpes, CNRS, Grenoble INP, Institut Néel, Grenoble, France, [2]Univ. Grenoble-Alpes, CEA, Grenoble INP, IRIG, PHELIQS, Grenoble, France, [3]CEA, LETI, Grenoble, France, [4]Univ. Grenoble-Alpes, CEA-IRIG, MEM, Grenoble, France
814 An examination of exit-wave reconstruction algorithms for low dose imaging at atomic-scale resolution
Jacob Svane-Petersen[1], Andreas Nymand[1], Joerg R. Jinschek[1,2], Stig Helveg[1], Joakim Kryger-Baggesen[1], Sophie Kargo Kaptain[1]
[1]Center for Visualizing Catalytic Processes (VISION), Technical University of Denmark, Kgs. Lyngby, Denmark, [2]Nanolab, Technical University of Denmark, Kgs. Lyngby, Denmark
825 Entanglement in Bragg Scattering
Ao. Univ. Prof. Peter Schattschneider[1], Assoc.-prof. Stefan Löffler[1]
[1]TU Wien, Wien, Austria
887 Numerical study on high orbital angular momentum vortex electron beams in hafnium dioxide
Christian Bick[1], Dr. Dorothee Hüser[1]
[1]Physikalisch-Technische Bundesanstalt (PTB), Braunschweig, Germany
914 On the accuracy of atomic-resolution DPC-STEM measurements
Rafael V. Ferreira[1,2], Sebastian Calderon V.[3], Paulo J. Ferreira[1,2,4]
[1]INL – International Iberian Nanotechnology Laboratory, Braga, Portugal, [2]Mechanical Engineering Department and IDMEC, Lisbon, Portugal, [3]Department of Materials Science and Engineering, Carnegie Mellon University, Pittsburgh, USA, [4]Materials Science and Engineering Program, The University of Texas at Austin, Austin, Portugal
928 Reconstruction of Angstrom resolution exit-waves by the application of drift-corrected phase-shifting off-axis electron holography
Jonas Lindner[1], Ulrich Ross[2], Tobias Meyer[1], Victor Boureau[3], Michael Seibt[2], Christian Jooss[1,4]
[1]1 Institute of Materials Physics, University Goettingen, Goettingen, Germany, [2]2, 4th Institute of Physics – Solids and Nanostructures, University of Goettingen, Germany, [3]Interdisciplinary Center for Electron Microscopy, École Polytechnique Fédérale de Lausanne, Lausanne, Switzerland, [4]4 International Center for Advanced Studies of Energy Conversion (ICASEC), University of Goettingen, Goettingen, Germany
947 Engineering electron-electron interaction for advanced quantum metrology in electron microscopy

Phd Caterina Chiari[1,2], Prof Marco Beleggia[2], Dr Vincenzo Grillo[1]
[1]Centro S3, CNR - Istituto di Nanoscienze, Modena, Italy, [2]Department of Physics, Informatics and Mathematics, University of Modena, Modena, Italy
949 Mean inner potential measurement by correlated EFTEM and phase-shifting holography
Dr. Ing. Ulrich Ross[1], Dr. Christoph Flathmann[1], M.Sc. Jonas Lindner[2], Dr. Tobias Meyer[2], Dr. Andreas Beyer[3], Dr. Jürgen Belz[3], Prof. Dr. Kerstin Volz[3], Prof. Dr. Christian Jooss[2,4], Prof. Dr. Michael Seibt[1]
[1]4th Institute of Physics - Solids and Naonstructures, Georg-August-University Goettingen, Goettingen, Germany, [2]Institute of Materials Physics, Georg-August-University Goettingen, Goettingen, Germany, [3]Department of Physics and Materials Science Center, Philipps-University Marburg, Marburg, Germany, [4]International Center for Advanced Studies of Energy Conversion (ICASEC), Georg-August-University Goettingen, Goettingen, Germany
985 Thin Film Phase Plates for Cryo TEM: Fabrication,
and Characterization Using Electron Holography
Marcus Hufe[1], Mads Larsen[1], Prof. Stephan Keller[1], Prof. Marco Beleggia[1,2], Associate Professor Paul Kempen[1]

[1]Technical University of Denmark, Copenhagen, Denmark, [2]University of Modena and Reggio Emilia, Modena, Italy

989 Characterization of Cu doped zeolite by MicroED and electron ptychography

Mr. Masahiko Shimizu[1], Dr. Katsuaki Nakazawa[2], Dr. Kazutaka Mitsuishi[2], Dr. Hajime Matsumoto[1], Dr. Hisashi Shima[1], Dr. Takahiko Takewaki[1], Dr. Ayako Hashimoto[2,3]
[1]Mitsubishi Chemical corporation, Yokohama, Japan, [2]National Institute for Materials Science, Tsukuba, Japan, [3]University of Tsukuba, Tsukuba, Japan

1049 Revealing Nanostructural Dynamics: Exploring Inelastic Scattering in Electron Microscopy

Phd Caterina Chiari[1,2], Prof. Marco Beleggia[1], Dr Vincenzo Grillo[2]
[1]University of Modena and Reggio Emilia, Modena, Italy, [2]S3 CNR Nano, Modena, Italy

1066 Electrons phase reconstruction using Kramers-Kronig relations

Dr. Yang Yin[1], Dr. Wenhao He[1], Prof. Changlin Zheng[1]
[1]Department of Physics,Fudan University, Shanghai, China

1088 Quarantotto: a 48-segment STEM detector for enhanced STEM performance and new applications

Dr Stefano Vespucci[1], Dr Eric G.T. Bosch[1], Dr Ivan Lazić[1], Bert de Vries[1], Dr Ricardo Egoavil[1], Dr Bert Freitag[1], Dr Tim Grieb[2], Dr Florian F. Krause[2], Dr Martin Eickhoff[2], Prof Andreas Rosenauer[2]
[1]Thermo Fisher Scientific, Eindhoven, The Netherlands, [2]Institute of Solid-State Physics, University of Bremen, Bremen, Germany

1103 Low-dose 4D-STEM cryo-tomography of biological samples

Dr. Shahar Seifer[1], Shai Kiriati[1], Dr. Peter Kirchweger[1], Prof. Michael Elbaum[1]
[1]Weizmann Institute of Science, Rehovot, Israel

1128 Nanoparticle Self Diffraction in the TEM: A proposal

Prof. Stefan Nimmrichter[1], Prof. Dennis Rätzel[2,3], Prof. Peter Schattschneider[4,5], Prof. Philipp Haslinger[4,6]
[1]Naturwissenschaftlich-Technische Fakultät, Universität Siegen,, Siegen, Germany , [2]Institut für Physik, Humboldt-Universität zu Berlin, Berlin, Germany, [3]ZARM, University of Bremen, Bremen, Germany, [4]USTEM, TU Wien, Vienna, Austria, [5]Institute of Solid State Physics, TU Wien, Vienna, Austria, [6]Vienna Center for Quantum Science and Technology, Atominstitut, TU Wien, Vienna, Austria

Late Poster Presentation

1296 Optimized Bright Field STEM Imaging for Detecting Molecules absorbed within Zeolite Pores

Yu Xia[1], Tom Willhammar[1]
[1]Department of Materials and Environmental Chemistry, Stockholm University, Stockholm, Sweden

1191

Breaking Resolution Limits with Ptychography using Topological Materials

Professor Kayla Nguyen[1]
[1]University of Oregon, Eugene, , United States

IM-03 (1), Plenary, august 28, 2024, 10:30 - 12:30

Electrons play a pivotal role in stabilizing matter, but they are also tools that can reveal the underlying physics of complex systems from high energy physics to condensed matter. One advantage of electrons is that they can also be used imaging probes, where properties of matter such as ferroelectricity, magnetism or topology can be observed atom-by-atom. While previous works have used vortex beam to uncover changes in orbital angular momentum [1,2], we use a generation of new direct electron detectors [3] and develop a mathematical algorithmic approach to uncover the torque transfer of an electron beam as it imparts upon a topological ferroelectric vortex [4]. Furthermore, using these new detector systems, we can also push imaging resolution on a conventional, non-aberration corrected STEM to sub-angstrom 0.5 resolution with electron ptychography [5,6].

Firstly, I will discuss a new type of electron probe which can image orbital angular momentum and torque transfer of topological structures in ferroelectrics. Using these new electron probes, we show that the presence of an electric toroidal moment transfers a measurable torque and orbital angular momentum to a localized electron beam in the ballistic limit. In Figure 1, we showed that the torque transfer could be measured where the point of reference is at the center of the vortex [4]. Depending on the rotation of the polarization vortices in our structure, we obtain a signal for the change in orbital angular momentum in either a counter-clockwise or clockwise direction (Figure 1).

Secondly, I will show how electron ptychography, an iterative computation imaging technique, can improve resolution beyond the numerical aperture of the electromagnetic lenses to the sub-angstrom limit in a conventional electron microscope for a two-dimensional moiré system (Figure 2, right image). Using this technique, we essentially use a ‘computation lens’ approach to imaging, opening opportunities to explore new physics in emergent materials beyond physical lenses and providing high-resolution imaging access to institutions that lack the funds to house such expensive equipment [6].

Finally, the interplay between technological and computational progress will be discussed in my talk, including the challenges that still arise for electron microscopy. Moreover, our research efforts described in these works were pursued using non-aberration-corrected electron microscopes. We believe that combining new detector technologies with computation, we can make electron microscopy more accessible while still developing new efforts for investigating new physics in emergent topological materials.

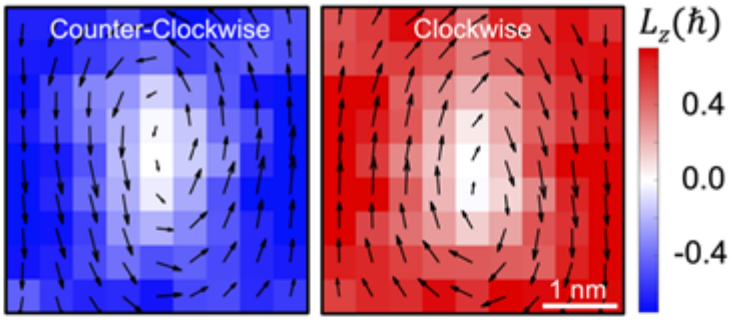

Figure 1: Change in orbital angular momentum observed as L_z in topological polarization vortices in superlattice of PbTiO3/SrTiO3. Using the reference point to be at the center of the vortex, we find that a (a) counter-clockwise rotation provides a negative L_z component while a (b) clockwise rotation provides a positive L_z.

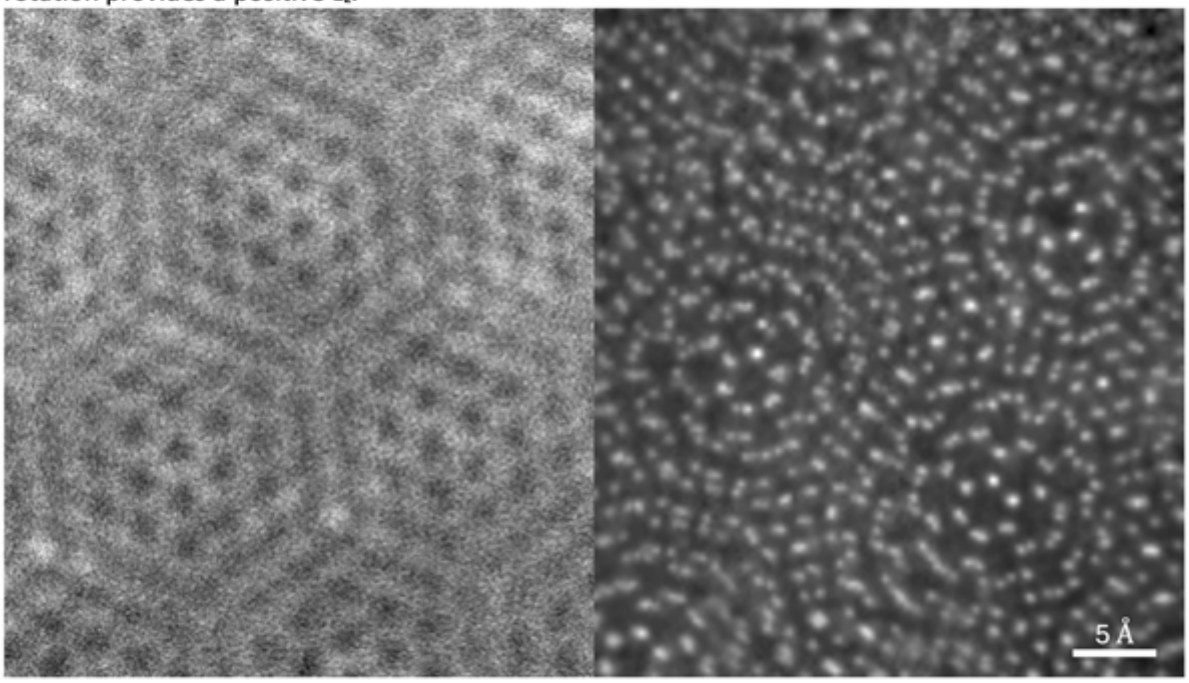

Figure 2: HAADF-STEM image on the left and electron ptychographic reconstructions on the right using a non-aberration-corrected electron microscope using bilayer, moiré MoS_2. In the image on the right, we are limited by the convergence angle of the STEM, ~ 10 mrad, where resolution is limited to 1.6 angstroms. Ptychography, on the other hand, is not limited by the convergence angle of the STEM probe, and thus has a resolution of 0.44 angstrom.

Keywords:

ptychography, 4D-STEM, orbital angular momentum, topological materials, 2D moiré

Reference:

[1] J Verbeeck, et al., Nature 467, 301-304 (2010).
[2] M Uchida, et al., Nature 464, 737-739 (2010).
[3] MW Tate, et al., Microscopy and Microanalysis 21, 237-249 (2016).
[4] KX Nguyen, et. al., Physical Review B 107, 205419 (2023).
[5] PD Nellist, et al., Nature 377, 6523 (1995).
[6] KX Nguyen, et. al., Science 383 (6685), 865-870 (2024).

238

Progress in 3D phase-contrast imaging using 4D-STEM: increased dose-efficiency and depth of field

Philipp Pelz[1,2], Dr. Andrey Romanov[1,2], Dr. Shengbo You[1,2], Dr. Mary Scott[3,4], Dr Colin Ophus[4], Dr Min Gee Cho[3,4], Daniel Stroppa[5], Mingjian Wu[1]
[1]Department of Materials Science & Engineering, FAU Erlangen-Nürnberg, Erlangen, Germany, [2]Institute of Micro- and Nanostructure Research (IMN) \& Center for Nanoanalysis and Electron Microscopy (CENEM), Erlangen, Germany, [3]Department of Materials Science and Engineering, University of California Berkeley, Berkeley, United States, [4]The Molecular Foundry, Lawrence Berkeley National Laboratory, Berkeley, United States, [5]DECTRIS AG, Baden, Switzerland

IM-03 (3), Plenary, august 29, 2024, 10:30 - 12:30

Scanning Transmission Electron Microscopy (STEM) is used extensively to study the atomic structure of materials at the nanoscale. So far, the dominant method for atomic resolution imaging is annular dark-field STEM, enabled by modern electron optics and popular because of its incoherent atomic number contrast. Developments in detector technology have caused the widespread adoption of fast direct electron detectors, which allow collecting a 2D momentum space image at every position of a 2D real-space scan, motivating the name 4D-STEM. Such 4D-STEM datasets allow recovery of phase information, and the high number of intensity measurements allows us to fit ever more complex models to the scattering data, increasing dose efficiency, resolution, and imaging throughput. Modern reconstruction algorithms can recover partial coherence effects, probe positions, and three-dimensional information beyond the numerical aperture limit from a single 4D-STEM dataset. However, the obtainable depth resolution in these approaches is currently more than a factor of ten away from the atomic scale needed for de novo structure determination. This motivates the collection of tilt-series 4D-STEM measurements, which allow higher dose efficiency to reach the 3D atomic resolution regime than 3D imaging approaches based on ADF-STEM.
Here, we show a series of advancements in instrumentation and 4D-STEM reconstruction methods that allow the determination of 3D atomic structure from 4D-STEM measurements and extend the sensitivity and volume limits of electron microscopy.

Methods & Results
Fig. 1a) shows an experimental demonstration of ptychographic electron tomography. We reconstructed a complex hybrid structure of a ZrTe nanowire encapsulated in a double-walled carbon nanotube [10]. We then solved the complete atomic structure from this 3D reconstruction. The nanowire comprises three unique structural motifs: an elliptic curved 2D material composed of ZrTe5 units, Te-Te chains, and a previously unobserved ZrTe2 core structure. The ZrTe2 core structure is closely related to the ZrTe5 structure, with the longer bond-length Te atoms removed and the stacking slightly modified. We also performed DFT to verify the stability of the proposed atomic structure of this nanowire [1].
In this study, we used a fast linear method for initial reconstruction and aberration parameter estimation, followed by iterative single-slice reconstruction, including partial coherence, and finally, tomographic reconstruction.
By explicitly modeling dynamical scattering within the sample using multi-slice ptychography, the accessible volume in ptychographic tomography can be significantly expanded beyond the conventional depth of field limit for 3D imaging in STEM. This allows for the retention of 3D atomic resolution in larger volumes.
Fig. 1b) shows an experimental demonstration of a sequential reconstruction approach to multi-slice ptychographic tomography on a Co3O4 nanocube. Here, we reconstruct a volume of 18.2nm side length and break the depth of field limit by a factor of >3x. The bottom panel of Fig 1b) shows cuts

through the 3D power spectrum of the reconstruction, indicating that a resolution of 2Å axial and 0.7Å lateral resolution has been reached.
Reconstructing the electrostatic potential in an end-to-end fashion directly from 4D-STEM data can further increase the coupling of the voxels in 3D space, allowing the recovery of missing wedge information. The reconstruction strategies developed above can be utilized to bootstrap all parameters of such an end-to-end reconstruction efficiently.

Conclusion
We have developed atomic resolution ptychographic electron tomography to solve 3D atomic structures containing light elements and spanning volumes larger than the depth of field. Future applications include the imaging of beam-sensitive polymers, hybrid organic-inorganic structures, battery materials, and biomolecules.

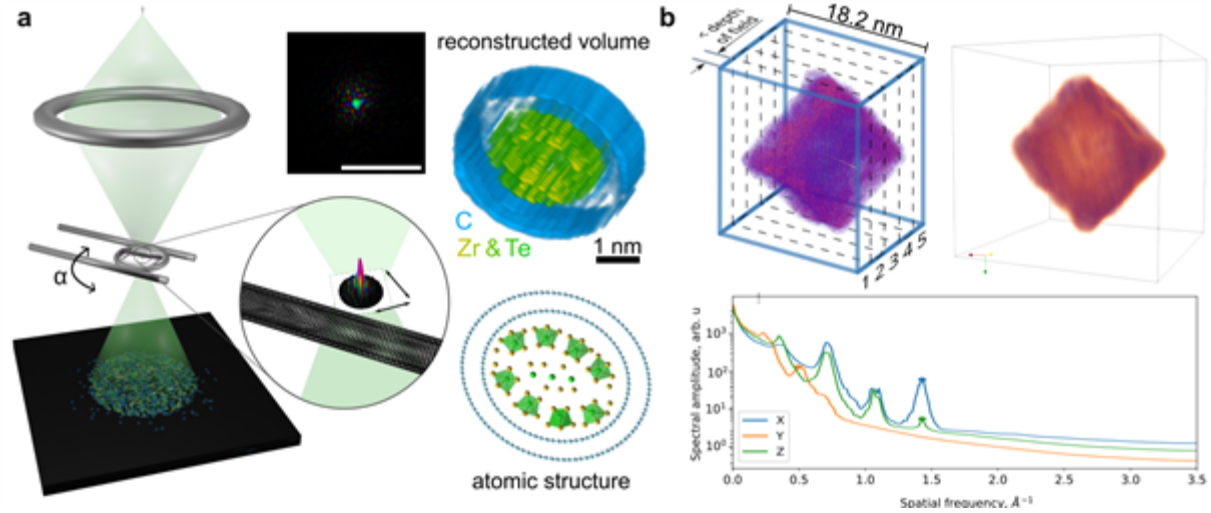

Keywords:

4D-STEM, multi-slice ptychography, tomography, reconstruction

Reference:

[1] Philipp M. Pelz, Sinéad M. Griffin, Scott Stonemeyer, Derek Popple, Hannah DeVyldere, Peter Ercius, Alex Zettl, Mary C. Scott, and Colin Ophus. Solving complex nanostructures with ptychographic atomic electron tomography. Nature Communications, 14:7906, November 2023.

177

Phase detection limits in electron holography with automatic stabilisation and direct electron detection

Dr Martin Hytch[1], Dr Cécile Marcelot[1], Dr Christophe Gatel[1,2]
[1]CEMES-CNRS, Toulouse, France, [2]University of Toulouse III, Toulouse, France

IM-03 (1), Plenary, august 28, 2024, 10:30 - 12:30

Electron holography can measure local electric, magnetic and elastic strain fields. Furthermore, the incident wave can be structured with the aid of a biprism in the illumination system for specialised interference configurations [1]. In all cases, the measurement precision is directly related to the precision with which the phase of the holographic fringes can be determined. Random errors from shot noise are related to the fringe visibility and the electron dose but also depend on the transfer characteristics of the detector and the mask used in the Fourier reconstruction:

$$\sigma(\varphi)=\sqrt{(2/N)}\times 1/V\times(MTF(q))/\sqrt{(DQE(q))}\times\sqrt{a} \quad (1)$$

where N is the number of incident electrons per pixel, V the observed visibility of the fringes, MTF(q) and DQE(q) the modulation transfer function and the quantum efficiency, respectively, of the detector at the spatial frequency corresponding to the hologram fringes and “a” a factor depending on the Fourier mask size [2]. We will test the limits of the theory and present two ways of maximising sensitivity: acquiring holograms over very long exposure times through automation [3] and with detect electron detection.

Methods

Automatically stabilised holograms were acquired on the I2TEM (Hitachi HF3300-C) microscope, operating at 300 kV and equipped with a cold-field emission gun (C-FEG), double stage, image aberration corrector (B-COR, CEOS), condenser biprism and three post specimen biprisms. In particular, two series were acquired: one on a conventional scintillator-coupled CMOS camera (OneView, Gatan Inc.) and the other on a direct detection device (K3, Gatan Inc.). Holograms covered the field of view of the detector and were adjusted to have indentical fringe spacing (5.5 pixels) using two post-specimen biprisms. Hologram phases were monitored in real-time using HoloLive! v1.1 (HREM Research Inc.) and dynamic automation was implemented through customised scripts [3]. Holograms were acquired continuously over 15 minutes (900 s) at comparable dose rates (< 9 e-/pixel/s), the cumulated intensity output every 4 s (Fig. 1a) so that the progression could be monitored. Automatic stabilisation also allows the choice of the exact position of the hologram fringes. Systematic errors were investigated by recording holograms with different initial phase values [4].

Results

The phase error, measured by the standard deviation in a region of vacuum, diminishes over time as expected by the theory (Fig. 1b). Indeed, direct detection provides a spectacular improvement in the precision of the phase. However, in both cases, the phase error reaches a plateau, with little improvement beyond a certain dose. We will show the cause of the systematic errors and how they can be corrected.

Conclusions

The theoretical limit for the phase precision can be obtained using dynamic automation and direct electron detection. We will show how systematic errors can be removed by controlling the incident illumination for an ultimate precision of 1 mrad at nanometre spatial resolution.

Acknowledgements

The authors acknowledge funding from the European Union under grant agreement no. 101094299 (IMPRESS). Views and opinions expressed are however those of the authors only and do not necessarily reflect those of the European Union or the European Research Executive Agency (REA). Neither the European Union nor the granting authority can be held responsible for them.

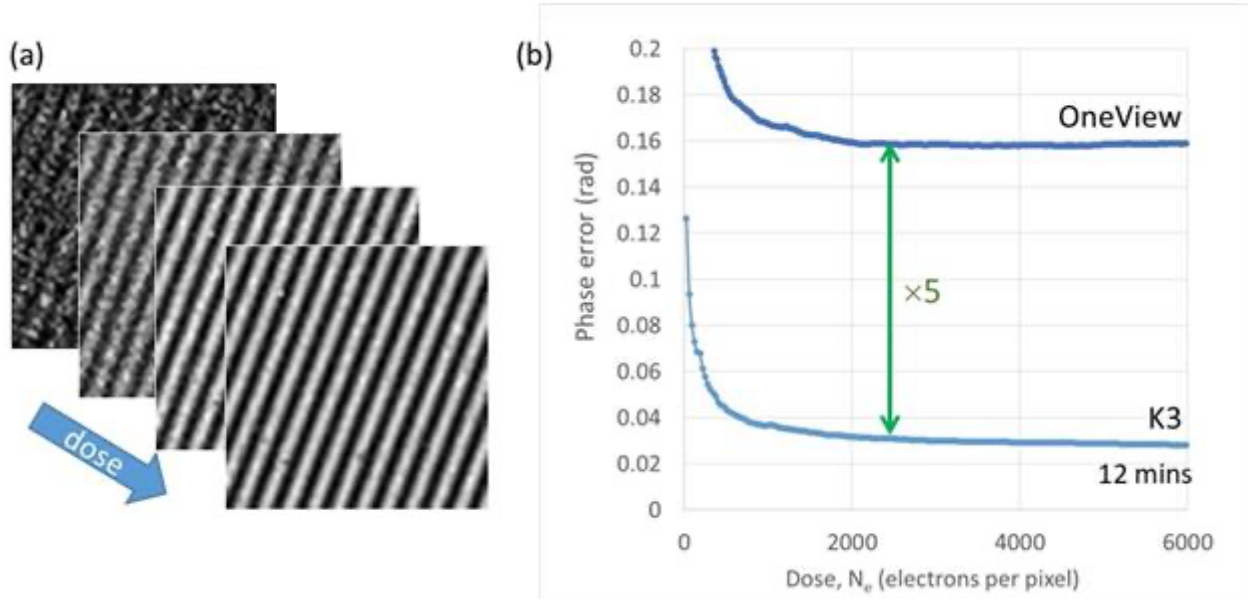

Keywords:

Electron Holography, Automation

Reference:

[1] T Denneulin, F Houdellier, MJ Hytch, Ultramicroscopy 160, 98 (2016).
[2] SLY Chang et al, Ultramicroscopy 161, 90-97 (2016).
[3] HoloLive! (HREM Research Inc.)
[4] C Gatel, J Dupuy, F Houdellier, MJ Hÿtch, APL 113, 133102 (2018).
[5] M.J. Hÿtch and C. Gatel, Microscopy 70, 47 (2021).

276

Holography with an Extended Reference in Transmission Electron Microscopy

Dr Wei Chao[1], Professor David Paganin[1], Dr Timothy Petersen[2], Professor Changlin Zheng[3], Professor Joanne Etheridge[1,2]
[1]School of Physics and Astronomy, Monash University, Clayton, Australia, [2]Monash Centre for Electron Microscopy, Monash University, Clayton, Australia, [3]Department of Physics, Fudan University, Songhu Road 2005, Shanghai, China

IM-03 (1), Plenary, august 28, 2024, 10:30 - 12:30

Background
Electron holography, first introduced in 1948 by Gabor [1], is one of the most widely used techniques for the retrieval of phase information in a transmission electron microscope (TEM). Conventionally a hologram is formed by interference between a scattered wave and a reference wave, for either an inline or off-axis experimental configuration. Holography is possible with an extended reference, arising from compact support in the specimen plane, for use in lens-less X-ray and laser applications as a dose-efficient method with a fast reconstruction process [2, 3]. In such approaches the reconstruction of the exit wave requires just one inverse Fourier transform of the recorded far-field diffraction pattern (Fig. 1a), with pre-weighted spatial frequencies. For a compact support defined by a polygonal aperture, sharp corners and edges provide innate scattered reference waves to interfere with the object wave (Fig. 1b), which can greatly simplify the mathematical form of the reconstruction process [2].
Methods
In this work, we experimentally implemented this method within a TEM operating at 300kV, choosing a square aperture as the compact support. To create effective reference waves, it is essential to ensure sharp edges and corners and to have a binary compact support defined by a sufficiently opaque aperture. To this end, a focused ion beam was used to accurately mill a micron sized square hole in an aluminum foil that was originally not electron-transparent at standard TEM operating voltages. Some residual material was left at the corner as an effective test object, the shape of which was imaged in the TEM by observing absorption contrast at low magnification. A diffraction pattern was recorded at the far field diffraction plane and used for the reconstruction.
Results
The shape of the test object was successfully reconstructed from the inverse Fourier approach using a single diffraction pattern, which provided six independent reconstructions (Fig. 1c-1d). Beyond that, we explored the possibility of applying a scanning parallel beam to overcome the limitations in the relative position and size of the object to the aperture. We also explored the comparative challenges against other instruments by considering the short wavelength of accelerated electrons, the quality of the fabricated corners, lens aberrations, centering of the diffraction patterns, far-field requirements, and detectors used. At this meeting, we will also discuss the use of a square probe forming aperture to provide optimum electron-optical configuration for this technique, as well as facilitating its implementation in a scanning mode.
Conclusions
To the best of our knowledge, this work is the first implementation of this deterministic extended reference Fourier holography method in TEM. Compared with other phase retrieval methods in TEM, the fast, real-time reconstruction process makes it promising for in-situ imaging techniques of magnetic materials. It also shows the feasibility of determining exit wave phases from just a single diffraction pattern, with potential applications in beam-sensitive materials and biological samples.

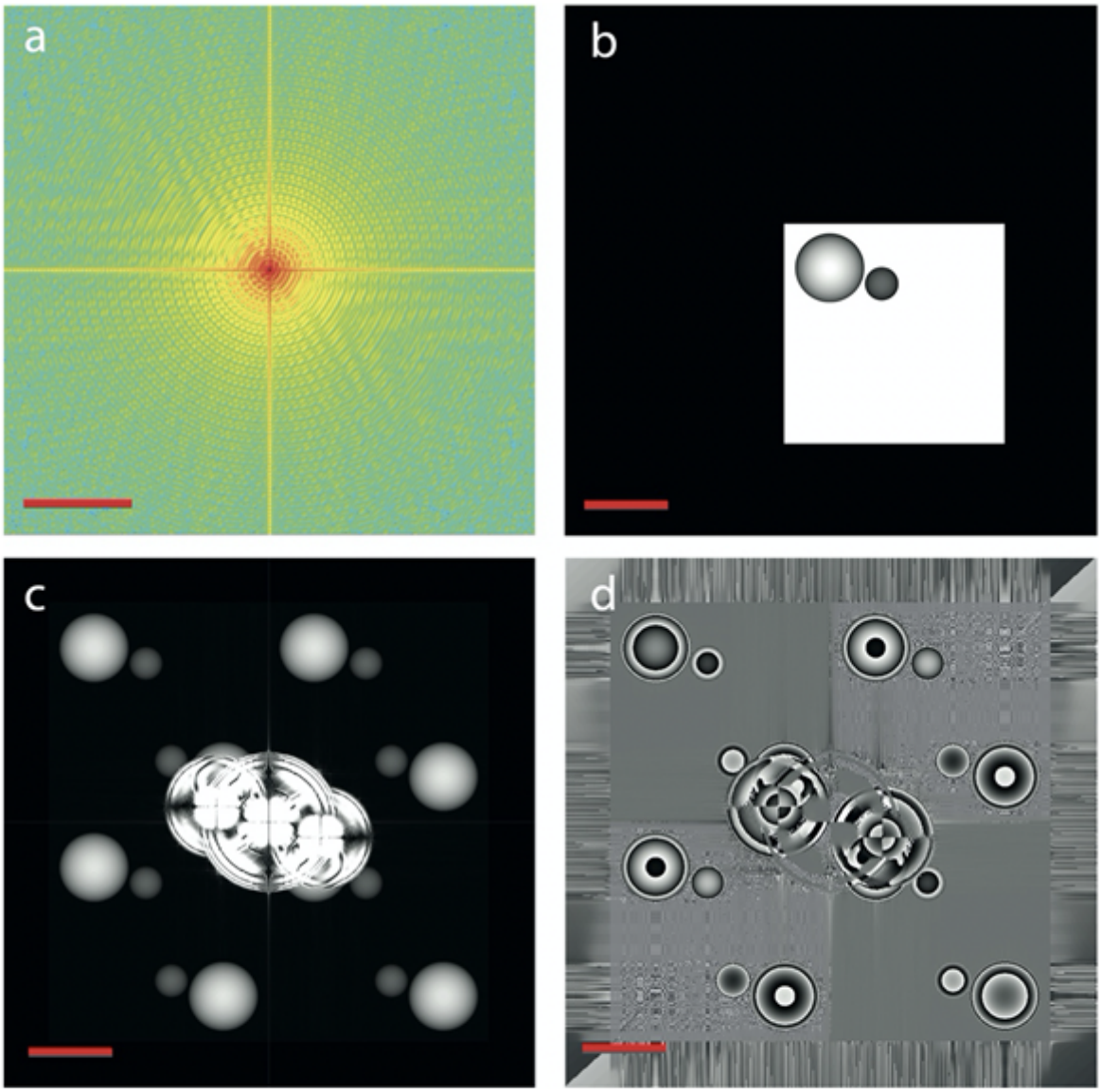

Fig. 1 The reconstruction results in simulation. (a) Diffraction pattern. The scale bar is 0.5nm^{-1}. (b) Object plane with nanoparticles (radius 200nm and 100nm) within the square aperture. The scale bar is 500nm. (c)-(d) Reconstructed amplitude (c) and phase (d) of the object. The scale bar is 500nm.

Keywords:

holography; phase retrieval; non-iterative reconstruction

Reference:

1. Gabor, D.,. Nature, 1948. 161: pp. 777-778.
2. Podorov, S.G., et al., Optics Express, 2007. 15(16): pp. 9954-9962.
3. Gauthier, D., et al.,. Physical Review Letters, 2010. 105(9), 093901.
4. This research used equipment funded by Australian Research Council grants LE0454166 and LE0882821 at the Monash Centre for Electron Microscopy (a node of Microscopy Australia).

346

Off-Axis Electron Holography of In-Situ-Biased Highly-Doped p-AlGaAs/n-GaInP Junctions for Solar Cell Applications

Vita Mergner[1,2], Malte Klitzke[2], Dr. Patrick Schygulla[2], Dr. David Lackner[2], Dr. András Kovács[1], Prof. Dr. Wolfgang Jäger[3], Prof. Dr. Rafal E. Dunin-Borkowski[1], Dr. David Cooper[4]
[1]Ernst Ruska-Centre for Microscopy and Spectroscopy with Electrons, Forschungszentrum Jülich, 52425 Jülich, Germany, [2]Fraunhofer Institute for Solar Energy Systems ISE, 79110 Freiburg, Germany, [3]Materials Science, Christian-Albrechts-University, 24143 Kiel, Germany, [4]Univ. Grenoble Alpes, CEA, LETI, F-38000 Grenoble, France

IM-03 (1), Plenary, august 28, 2024, 10:30 - 12:30

Introduction and motivation
Multi-junction solar cells that are based on MOVPE-grown III-V compound semiconductor layers achieve the highest solar cell efficiencies, as they absorb light from a large part of the solar spectrum. Tunnel junctions provide electrical interconnections to the device sub cells, while yielding high current capabilities and high optical transparency. As the tunnelling probability decreases exponentially with increasing depletion width, high dopant concentrations are required to achieve the narrowest junctions. Structural and electrical analysis with high spatial resolution is essential to provide feedback to optimize the growth process. Electrostatic potentials at p-n junctions can be measured quantitatively with nm spatial resolution using off-axis electron holography (EH).
Methods
Here, we combine EH with in situ electrical biasing and optimized TEM sample preparation to study electrically-contacted p-AlGaAs/n-GaInP tunnel hetero-junctions grown in upright and inverted configuration. First electron-transparent specimens of different thicknesses were studied to assess the influence on the measured electrostatic potentials of the presence of electrically-inactive specimen surface layers introduced during focused ion beam (FIB) milling. The crystalline thickness of each specimen was measured using convergent beam electron diffraction (CBED) in a scanning TEM (STEM) (Fig. 1B). The TEM specimens were prepared using dedicated chips for an electrical biasing TEM holder (Protochips Aduro 500). Reliable contacting was achieved by developing two different FIB milling procedures. First, conventional FIB milling was used to extract a region of interest, while preserving a pre-deposited Ohmic top contact (Fig. 1A). Tungsten was then deposited in the FIB workstation onto the bottom of the sample to provide a second electrical contact. The second approach involved the use of plasma FIB milling to extract slices of the wafer that contained the original top and bottom metal contacts. Electron hologram stacks were recorded from both junction configurations to improve the sensitivity and spatial resolution of the results. Measurements of depletion width were recorded as a function of both specimen thickness and applied external bias.
Results
Phase images (proportional to projected electrostatic potential) were reconstructed from the holograms as a function of applied electrical bias. Figure 1C shows a phase image recorded at zero bias and a corresponding line profile of the phase across the junction.
The inverted and upright junction configuration exhibit similar depletion widths measured at zero bias. Analysis under external bias is necessary to reveal differences in tunnelling performances occurring in the current regimes of operation under light. Our results demonstrate the importance of optimizing specimen preparation when performing in situ electrical biasing experiments. In particular, to create Ohmic electrical contacts, as opposed to the Schottky contacts that are normally formed using FIB metal deposition. By using an optimized specimen preparation approach, we could compare the electrostatic potential distribution across upright and inverted p-AlGaAs/n-GaInP junctions reliably.
Conclusions

This study demonstrates the progress that has been achieved in realizing successful in situ characterization of dopant potential distributions in III-V tunnel hetero-junctions in real solar cell devices.

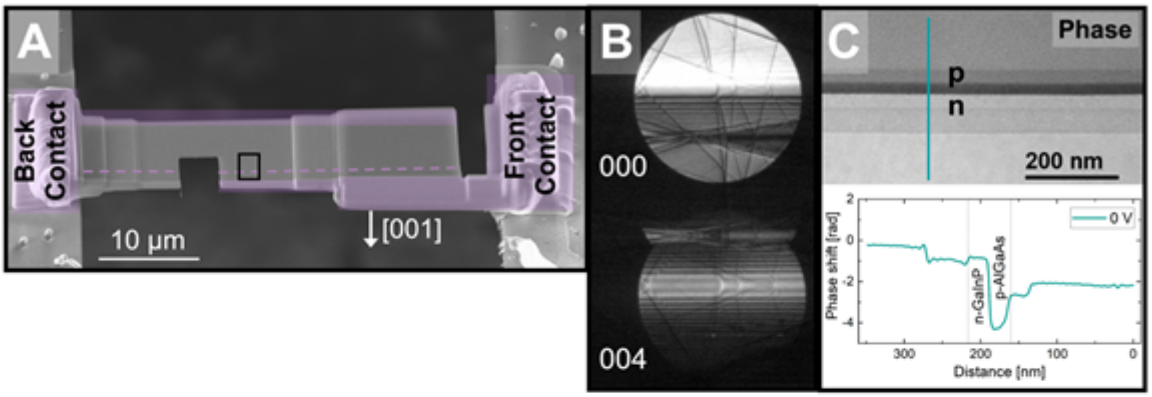

Fig. 1: A) Scanning electron micrograph of a TEM lamella of a multi-junction solar cell device that contains an upright-grown p-AlGaAs/n-GaInP tunnel hetero-junction (pink dashed line) prepared using a Ga-ion FIB backside-milling procedure. The lamella is mounted on a chip for *in situ* electrical biasing. B) STEM-CBED pattern recorded from the region marked in A to measure the crystalline specimen thickness. C) Electron optical phase image reconstructed from an off-axis electron hologram stack recorded at zero applied bias from the tunnel junction. A corresponding line profile of the phase shift (proportional to the projected electrostatic potential) is extracted from the phase image across the junction.

Keywords:

Electron Holography, III-V Multijunction PV

807

Minimising the distortive effects of diffraction on magnetic STEM-DPC imaging of monocrystalline thin films

Sivert Dagenborg[1], Andrea D'Alessio[2], Nikolas Vitaliti[2], Alessandro Palliotto[2], Eric Brand[2], Associate Professor Ingrid Hallsteinsen[3], Professor Nini Pryds[2], Assistant Professor Daesung Park[2], Associate Professor Felix Trier[2], Associate Professor Magnus Nord[1]
[1]Department of Physics, Norwegian University of Science and Technology, Trondheim, Norway, [2]Department of Energy Conversion and Storage, Technical University of Denmark, Kongens Lyngby, Denmark, [3]Department of Materials Science and Engineering, Norwegian University of Science and Technology, Trondheim, Norway

IM-03 (1), Plenary, august 28, 2024, 10:30 - 12:30

Development of state of the art electric and magnetic devices requires high resolution characterisation techniques, one such being scanning transmission electron microscopy – differential phase contrast (STEM-DPC), which gives quantitative magnetic information while allowing concurrent acquisition of structural and chemical information in the same sample area. Magnetic STEM-DPC characterization relies on detecting minute shifts of the electron probe, often in the range of a couple of microradians. At highly diffracting conditions, the electron probe can get heavily distorted, making it difficult to extract the small shifts caused by the in-plane magnetic field.
In this work, we acquired STEM-DPC datasets using a 4D-STEM detector on a monocrystalline magnetic freestanding La0.7Sr0.3MnO3 (LSMO) thin-film. We acquired several tilt orientations at a temperature of -150.0˚C, giving a systematic overview of diffraction induced distortions on probe shape and magnetic signal. Fig. 1 shows two STEM-DPC images from low- and high-diffraction conditions together with probes and line profiles as indicated on the figure, clearly demonstrating the distortive effects of diffraction. Tilt series were done at increasing angles away from the zone axis and with a constant off-axis angle but rotating around the zone axis. By examining the random variations in the STEM-DPC signal and comparing to the difference in signal between magnetic domains, a quantitative value for the signal to noise ratio was obtained.
This presentation will show which considerations and mitigation measures should be used to optimise STEM-DPC imaging in heavily diffracting samples, and how different data processing algorithms handle the distortions in the electron probe.

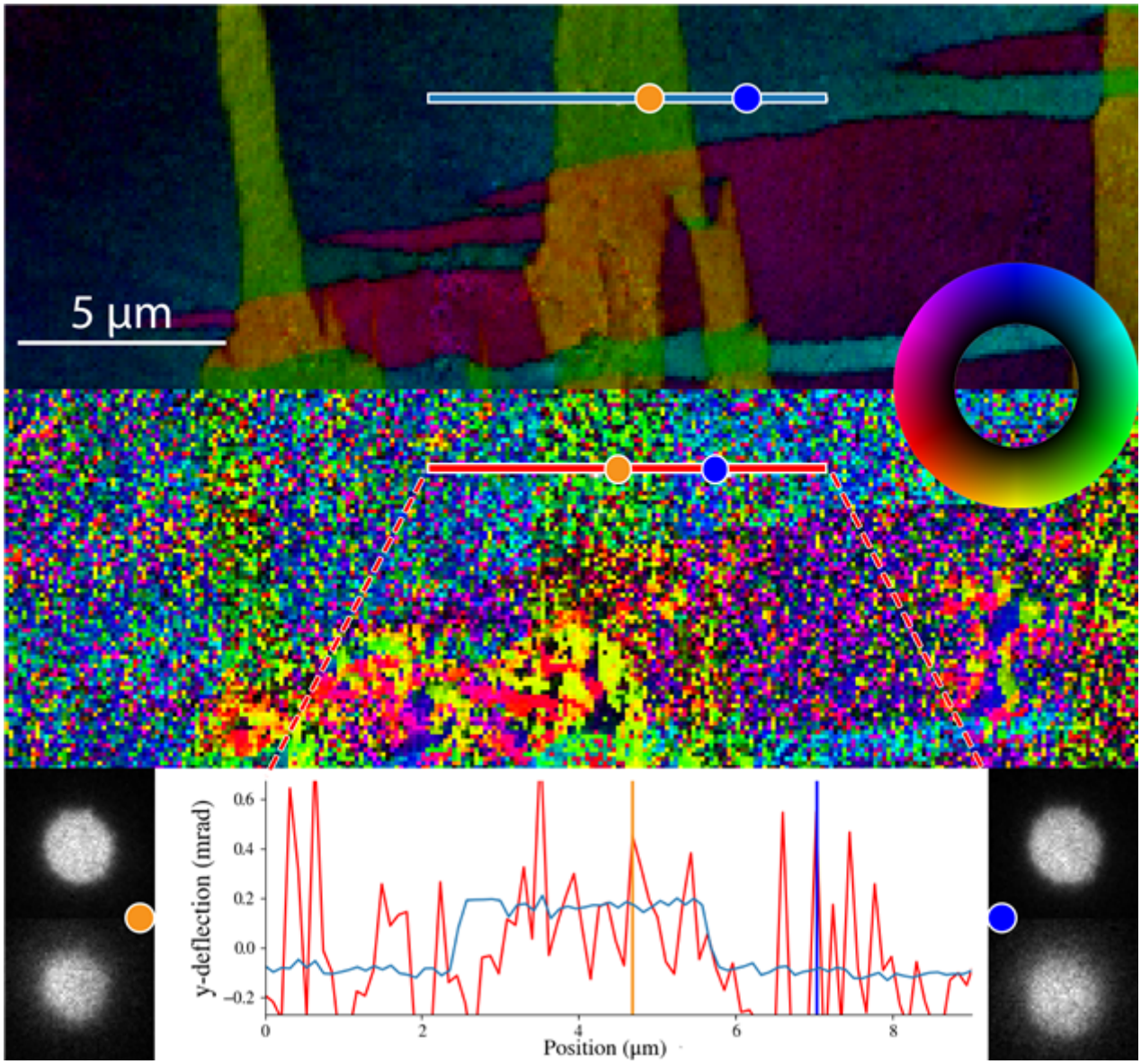

Keywords:

TEM STEM-DPC magnetism functional method

Reference:

J. Chapman, M. Scheinfein, Transmission electron microscopies of magnetic microstructures, J Magn Magn Mater 200, 729–740 (1999).
M. Nord et al., Strain Anisotropy and Magnetic Domains in Embedded Nanomagnets, Small 15, 1904738 (2019).
F. M. Chiabrera et al., Freestanding Perovskite Oxide Films: Synthesis, Challenges, and Properties, Ann. Phys. 534, 2200084 (2022).

1011

Sequential tilting 4D-STEM for reliable electric field mapping across junctions

Christoph Flathmann[1], Ulrich Ross[1], Andreas Beyer[2], Jürgen Belz[2], Kerstin Volz[2], Michael Seibt[1], Tobias Meyer[3]
[1]4th Physical Institute, Georg-August-University Goettingen, Göttingen, Germany, [2]Department of Physics and Materials Science CenterPhilipps-University Marburg, Marburg, Germany, [3]Institute of Materials Physics, Georg-August-University Goettingen, Göttingen, Germany

IM-03 (1), Plenary, august 28, 2024, 10:30 - 12:30

Background incl. aims
Momentum-resolved scanning transmission electron microscopy (MRSTEM) is an increasingly popular technique to map nanometer range electric fields [1]. Such measurements are of particular importance for device structures, for example pn-junctions [2], in order to understand functional properties of devices at the relevant length scales. To measure electric fields, MRSTEM determines the momentum transfer from an electric field to an electron beam via the deflection of the electron beam. However, relating the momentum transfer to the electric field is significantly complicated under dynamic diffraction conditions. Therefore, strategies are required to reliably determine electric fields from MRSTEM measurements under dynamic diffraction conditions. One such approach is tilting the incident beam relative to the sample in order to probe different diffraction conditions [3]. In this contribution, we explore how tilt patterns can be optimized and how MRSTEM based electric field mapping can be improved.

Methods
To get full control over the beam tilt, we use a custom developed beam tilt procedure. Here, we first calibrate the beam tilt and de-tilt coils of our microscope to allow us setting arbitrary beam tilts in STEM mode. In a second step, we calibrate the beam shift pivot points to obtain negligible beam shift at the sample for different beam tilts. These alignments enable us to repeatedly scan over the same sample region with different beam tilts, generating the data required for detailed MRSTEM analysis. We apply this acquisition technique to high quality lattice-matched AlAs/GaAs multi layers. These samples have the advantage that the mapped momentum transfer originates almost exclusively from a change of the mean inner potential across the materials interface, making assessment of the MRSTEM results easier.

Results
To analyze the effects of beam tilt on MRSTEM measurements, we scan across the AlAs/GaAs interface as shown in Fig. 1 a). We apply the scan patterns shown in Fig. 1 b), both consisting of 61 beam tilts, by sequentially scanning across the interface 61 times and collecting MRSTEM data for each tilt. Fig. 1 c) compares the measured electric fields for the annular and the full circle tilt patterns. The full circle pattern results in a sharp peak at the interface and an electric field close to zero away from the interface, as expected for AlAs/GaAs layers, while the electric field measured with the annular pattern shows stronger deviations from the expected behavior. In addition, we also have access to diffraction patterns of individual beam tilts. Fig. 1 d) shows the electric fields mapped with the beam tilts marked in Fig. 1 b). The strong differences for different beam tilts demonstrate that having access to this information is essential to improve MRSTEM measurements.

Conclusion
Our results show that full control over beam tilts and the capability to create arbitrary tilt patterns has a huge potential to improve the quality and reliability of MRSTEM measurements. Particularly,

the sequential acquisition of the data, giving access to individual beam tilts, is very beneficial for post-acquisition data examination and thus being fully consistent with the spirit of 4D-STEM of using as much information encoded in the data as possible.

Fig. 1: a) shows an annular dark field STEM image of the investigated AlAs/GaAs junction. The green line indicates the region scanned for field mapping. b) shows schematics of annular and full circle beam tilt patterns in reciprocal space, both consisting of 61 individual beam tilts with a maximum tilt angle of 7 mrad and a beam semi-convergence angle of 1 mrad. c) shows the electric field profiles obtained for the tilt patterns in b) scanned along the line indicated in a). d) shows electric field profiles of the same scan but for individual beam tilts. The corresponding beam tilts are indicated by colored circles in b).

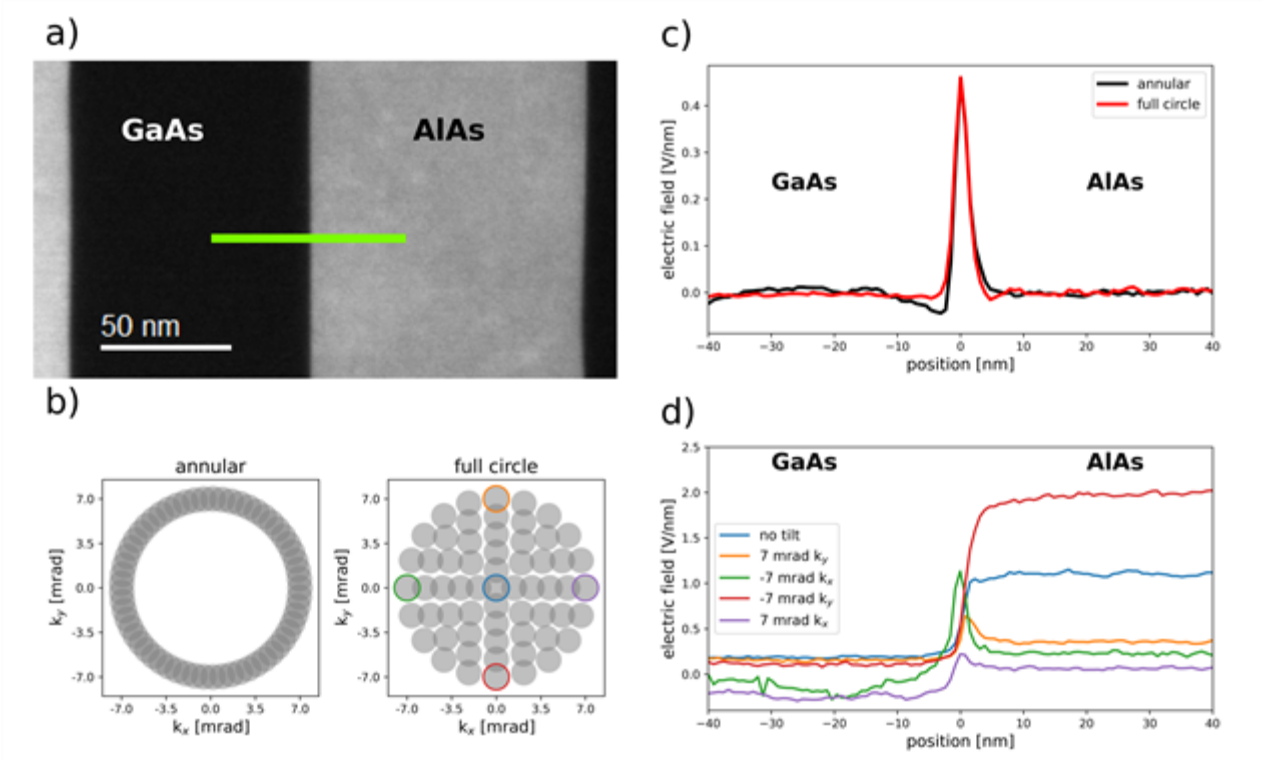

Keywords:

4D-STEM, momentum-resolved STEM, PED, heterojunctions

Reference:

[1] Chejarla, V. S., Ahmed, S., Belz, J., Scheunert, J., Beyer, A., & Volz, K. (2023). Measuring Spatially-Resolved Potential Drops at Semiconductor Hetero-Interfaces Using 4D-STEM. Small Methods, 7(9), 2300453.

[2] Beyer, A., Munde, M. S., Firoozabadi, S., Heimes, D., Grieb, T., Rosenauer, A., Müller-Caspary, K. & Volz, K. (2021). Quantitative characterization of nanometer-scale electric fields via Momentum-Resolved STEM. Nano letters, 21(5), 2018-2025.

[3] Mawson, T., Nakamura, A., Petersen, T. C., Shibata, N., Sasaki, H., Paganin, D. M., Morgan, M. J. & Findlay, S. D. (2020). Suppressing dynamical diffraction artefacts in differential phase contrast scanning transmission electron microscopy of long-range electromagnetic fields via precession. Ultramicroscopy, 219, 113097.

1083

Structured illumination near-field electron ptychography

Penghan Lu[1], Frederick Allars[2], Shengbo You[3], Thomas Schachinger[4], Rafal E. Dunin-Borkowski[1], Andrew M. Maiden[2,3]
[1]Ernst Ruska-Centre for Microscopy and Spectroscopy with Electrons, Forschungszentrum Jülich, Jülich, Germany, [2]Diamond Light Source, Harwell Science and Innovation Campus, Didcot, UK, [3]Department of Electronic and Electrical Engineering, University of Sheffield, Sheffield, UK, [4]University Service Centre for Transmission Electron Microscopy, TU Wien, Wien, Austria

IM-03 (1), Plenary, august 28, 2024, 10:30 - 12:30

Background incl. aims
Ptychography measures a correlated matrix of interference or diffraction patterns with sufficient overlap between adjoining illuminated area, and reconstructs both the object and the probe with their amplitude and phase components. For a ptychographically reconstructed image, its image pixel size is determined by the detector sampling in the Fourier space rather than the scanning step size in the real space [1]. This would allow a coarser scanning sampling and therefore a larger field of view with reasonable number of scan pixels or a lower dose with a practical probe current. In order to boost the sampling efficiency further, which would enable much larger field of view phase contrast imaging (e.g. weak contrast cellular structures) or fast time-resolved phase contrast movies (e.g. electromagnetic field dynamics), we developed a new ptychography imaging mode called near-field electron ptychography [2]. This is based on the classic ptychography principle but adopts a full-field parallel beam illumination and measures Fresnel (near-field), instead of Fraunhofer, diffraction patterns. In this case, structured illumination is of vital importance. Otherwise, each near-field diffraction image carries the same information except for laterally shifted, and therefore the ptychography reconstruction reduces to a single phase retrieval loop. In addition, a properly structured illumination will bring in a mixed range of spatial frequency to the diffraction patterns and open up the contrast transfer function over a wider range of frequencies.
Methods
A variety of diffuser designs and optical setups have been tested for the structured illumination near-field electron ptychography. A silicon nitride-based phase plate with patterned local thickness variation were firstly used as a phase diffuser. This can introduce almost arbitrary phase patterns to the illumination but the profuse inelastic scattering from the silicon nitride thin film will add an incoherent background to the measured diffraction patterns, which becomes more severe when working with lower energy electrons. An amplitude mask diffuser, consisting of a few narrow but opaque, random oriented, curved lines within a round aperture (see the enclosed figure), was found to be also very effective for this application [3] because in the near-field “ptychograms”, the Fresnel fringes, which comes from the hard edges of those lines, carry exactly the additional frequencies that are required for structured illumination. In this case, the inelastic scattering from the diffuser becomes negligible. Such a diffuser can be placed in either selected area aperture plane or condenser aperture plane. The latter is preferred because then only the area that is going to be measured will be illuminated, and also this will allow variable size of structured parallel illumination if three condenser lenses are available on the microscope. In order to realise the “shift invariance” principle of ptychography, the stage shift was originally used, which is flexible enough for large distance travel but suffers from jigging unless waiting enough time for stabilisation. In the latest development, we implemented a parallel beam 4D STEM acquisition mode that drives instant beam shift and synchronised fast detector readout for this application, which reduces the acquisition time by at least two orders of magnitude.
Results

We demonstrated, with as few as 9 diffraction patterns, near-field ptychography can already reconstruct micron square field of view phase images [2] and this can be easily extended to hundreds micron square field of view with a small number of diffraction patterns. Applying this method in magnetic field free TEM mode, we can visualise a permalloy magnetic domain structure using near-field ptychography [3] and the reconstructed phase image is almost equal to that measured by off-axis electron holography (see the enclosed figure). When switching to the parallel beam 4D STEM setup, ultralow dose phase reconstruction becomes possible (see the enclosed figure) with only second acquisition time and minutes reconstruction period.

Conclusion

A sampling efficient phase contrast imaging method is developed based on ptychography principle but with a bit adjusted optical setup including structured illumination and near-field diffraction measurement. It holds great promise to study large cellular structures with enhanced phase contrast or measure time-resolved dynamics of electronic or magnetic devices. Further discussions on how to push further its spatial resolution will be discussed in this presentation.

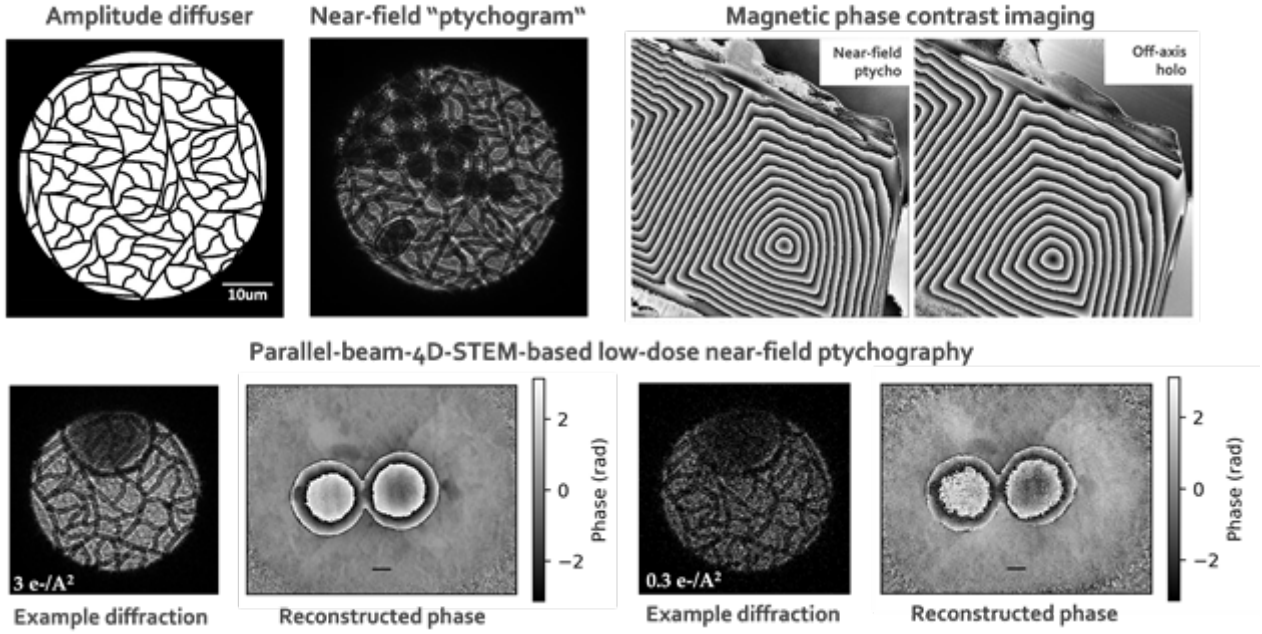

Keywords:

Structured illumination, near-field ptychography, diffuser

Reference:

[1] D. J. Batey et al., Physical Review A 89, 043812 (2014).
[2] F. Allars et al., Ultramicroscopy 231, 113257 (2021).
[3] S. You et al., Appl. Phys. Lett. 123, 192406 (2023).

74

Alternating-probe electron ptychography

Meng Zhao[1], Mr. Anton Gladyshev[1], Prof. Christoph Koch[1]
[1]Humboldt University of Berlin & Center for the Science of Materials Berlin,, Berlin, Germany

IM-03 (2), Plenary, august 28, 2024, 14:00 - 16:00

Background:
Ptychography has recently become a very powerful phase retrieval method and has been investigated by a number of groups in recent years. While applying a higher dose and a perfect electron microscope seems intuitively advantageous for maximizing the precision with which the unknown parameters can be determined in this process, the reality is constrained by various limitations. Different applications are required to push their limits in different aspects; there is still quite some potential for further optimization. Much effort has been directed towards refining physical models to incorporate more prior knowledge into reconstruction algorithms, such as adding different constraints [1], using multi-probe illumination to model partial coherence [2], and using mixed objects to model lattice vibrations [3].
Recent advances in the development of a low-noise, fast-response phase plate [4] present novel opportunities for adopting a different approach to increasing the number of known parameters in the reconstruction. Probe-diverse ptychography has been proven to be capable of overcoming the problem of converging to local minima inherent in the standard single probe scheme [5]. Initial tests in X-ray ptychography came to the conclusion that two different probes would be sufficient. In this abstract, we demonstrate, using simulated data, the use of a phase plate that adds different phase shifts to the probe at different scan positions. During reconstructions, we initialize and reconstruct a single probe, but incorporate an additional step within the algorithm to introduce phase changes to the wavefront that are induced by the phase plate.
Methods:
As a proof of principle for probe-diverse ptychography, we simulated 4D-STEM data of two hexagonal boron nitride (h-BN) crystals stacked with a 10° rotation between them (see Figure, (a)-(c))). (a) represents the projected potential of the complete sample, (b) shows the projected potential of the top half of the sample with no rotation, (c) depicts the projected potential of the second half of the sample with a rotation of 10°. For different electron doses, we simulated three distinct sets of data, each generated independently. These sets include data obtained from a probe without phase shift, a vortex beam, and a beam with phase shift of π applied to half of the elements of the phase plate [4]. The simulations were all conducted with a defocus of 9 nm, a scan step of 1 Å, and partial coherence implemented by convolving the 4D-STEM data set by a Gaussian with a full-width at half maximum (FWHM) of 0.7 Å. Subsequently, we generated two additional data sets. The first combined subsets of data were obtained from the normal probe and the vortex probe. The second data set combined data from all three previously mentioned sets. These simulations aimed to evaluate the effectiveness of probe-diverse ptychography in reconstructing the sample's structure with enhanced accuracy and resolution.
We performed reconstructions of all six simulated data sets using a multi-probe approach [2]. To estimate the quality of the reconstructions, we employed the Structural Similarity Index (SSIM) between the reconstructed phase object and the original potential utilized to generate the data.
Results:
In Figure(d)-(f), SSIM versus dose for different probe configurations is presented. (d) shows the sum of the SSIM of all reconstructed slices, reflecting the fidelity of the reconstruction for the entire structure. This plot indicates that reconstructions in extremely low-dose scenarios are not entirely successful, with relatively low SSIM values. In these cases, the benefit derived from applying diverse probes is overshadowed by noise. Upon reaching a moderate dose range (from 1×10^4 e/Å^2), despite

the larger probe size associated with the vortex and pi beams, probe-diverse ptychography still yields superior reconstructions. Additionally, the dataset comprising three distinct probe configurations exhibits further enhancement. (e) shows the sum of the SSIM for the first half of the potential slices, and similarly, (f) shows the sum of the SSIM for its second half. These results reveal that the reconstruction from the dataset containing three different probes captures more detailed information along the z-axis, especially at high doses.

Conclusions:

In this abstract, we have demonstrated a novel approach to diverse-probe ptychography and provided a proof of principle for its effectiveness in electron ptychography. Our findings suggest that applying more than two probes in ptychography leads to further enhancements in reconstruction quality. Additionally, the modification of the probe is not limited to phase plate adjustments. It's worth mentioning that the aberration corrector can also achieve similar outcomes, albeit with a limited number of configurable parameters.

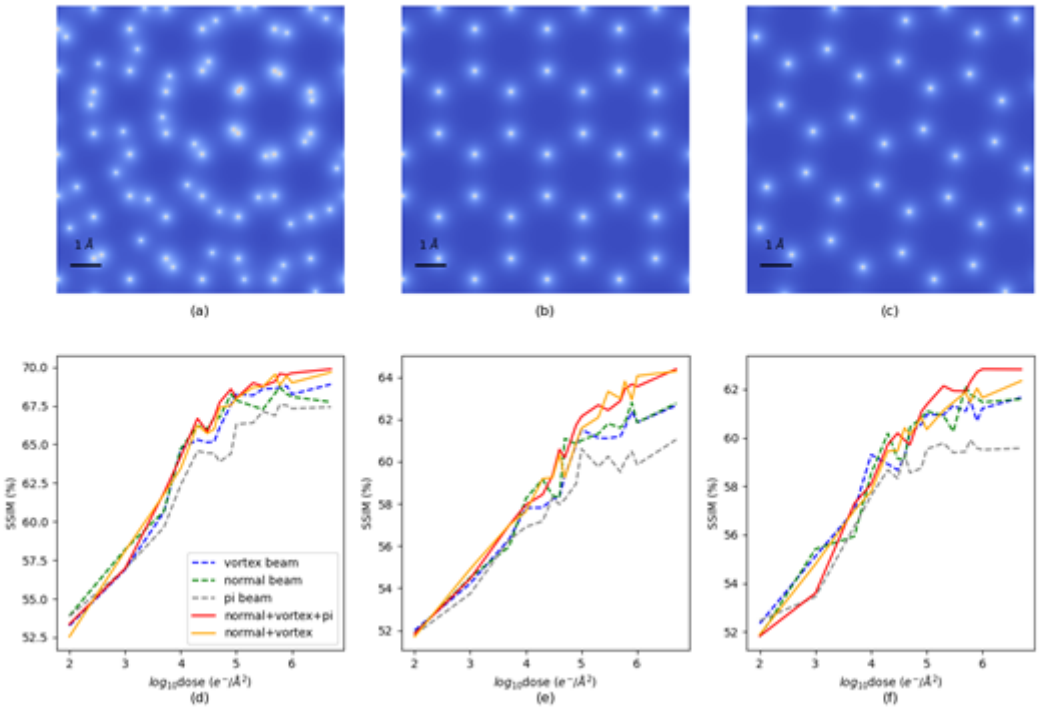

Keywords:

divers-probe ptychography, phase plate

Reference:

[1] M. Schloz et al., doi: 10.1364/OE.396925
[2] C. Zhen et al., doi: 10.1038/s41467-020-16688-6
[3] A Gladyshev et al., doi: arXiv:2309.12017
[4] Yu, C. P., et al., doi: 10.21468/SciPostPhys.15.6.223
[5] I. Peterson, et al., doi:10.1016/j.ultramic.2016.08.003

251

Full-field illumination ptychography with a structured electron beam

Hirokazu Tamaki[1,2], Dr. Koh Saitoh[3]
[1]Graduate School of Engineering, Nagoya University, Nagoya, Japan, [2]Research & Development group, Hitachi Ltd., Kokubunji, Japan, [3]Institute of Materials and Systems for Sustainability, Nagoya University, Nagoya, Japan

IM-03 (2), Plenary, august 28, 2024, 14:00 - 16:00

Background incl. aims
Coherent diffractive imaging (CDI) is a technique for reconstructing the complex wavefield from far-field diffraction pattern. CDI has advanced rapidly with the improvement of recent detectors and computing performances, and among them, ptychography has been attracting great interest. One of the key challenges in ptychography is accurate phase reconstruction for large structures. The diffraction intensity carrying the information of large structures is generally concentrated in the low scattering angle region and is often saturated beyond the dynamic range of the detectors. To overcome this obstacle, near-field ptychogrpahy [1][2], which utilizes the Fresnel diffraction pattern for the reconstruction, has been proposed in recent years. In this study, we propose a novel configuration for near-field ptychography with full-field illumination using a structured electron beam, aiming at the accurate and efficient observation of large structures.

Methods
The proposed method is configured on the conventional TEM setups. A series of in-line holograms observed in the Fresnel region below the specimen are obtained at different beam positions by scanning the illumination beam. Then, both the wavefield of the illumination beam and the complex transmission function of the specimen are reconstructed from the obtained holograms through a ptychographic procedure. This method does not require a spatial restriction on the specimen plane as a constraint, and instead introduces an irregular structure into the illumination beam that works as an alternative constraint. The structured beam is generated by using a film with random openings, placed in the condenser lens system above the specimen. The diameter of the incident beam is adjusted so that the entire field of view is always illuminated during the scanning. Full-field illumination prevents error accumulation when reconstructing a large field of view compared with conventional ptychographic reconstruction, which “concatenates” small patches of local structures. Full-field illumination provides uniform redundancy over the field of view since the entire field of view of each hologram is fully overlapped. These contribute to accurate and robust reconstruction of large structures. The use of random openings for beam structuring also suppresses coherence degradation of the illumination beam due to inelastic scattering, thereby improving the accuracy of phase determination.
The performance of the proposed method was first evaluated using simulated holograms. Then, its experimental feasibility was evaluated using MgO particles.

Results
Graphic 1a shows one of the in-line holograms obtained below the specimen. The wavefield of the illumination beam and transmission function of the specimen were reconstructed from the obtained holograms. The reconstructed amplitude (Graphic 1b) and phase (Graphic 1c) of the specimen transmission function show good agreement with the given structure. The phase reconstruction error was 1/12,097 and 1/3,485 of the wavelength for the fine (20 nm) and large (400 nm) structures, respectively. Both are comparable to other accurate phase measurement methods [3].
Graphics 2a and 2b respectively show the amplitude and phase components of the transmission function reconstructed from the experimental holograms of MgO particles. The reconstructed phase

component shows a periodic phase contour at the edge of the particle, and also shows a uniform phase in the constant thickness region of the particles with faces oriented toward the beam direction. These results are consistent with the particle shape, indicating the validity of the method.

Conclusion

In this study, we proposed a new configuration for near-field ptychography using full-field illumination with a structured electron beam. A simulation study demonstrated phase reconstruction with an accuracy of 1/3,485 of the wavelength, a performance comparable to other phase measurement methods. An experimental study using a MgO crystal also showed reasonable reconstruction consistent with the specimen structure. These results suggest that this method can be adopted for accurate and efficient observation of large structures.

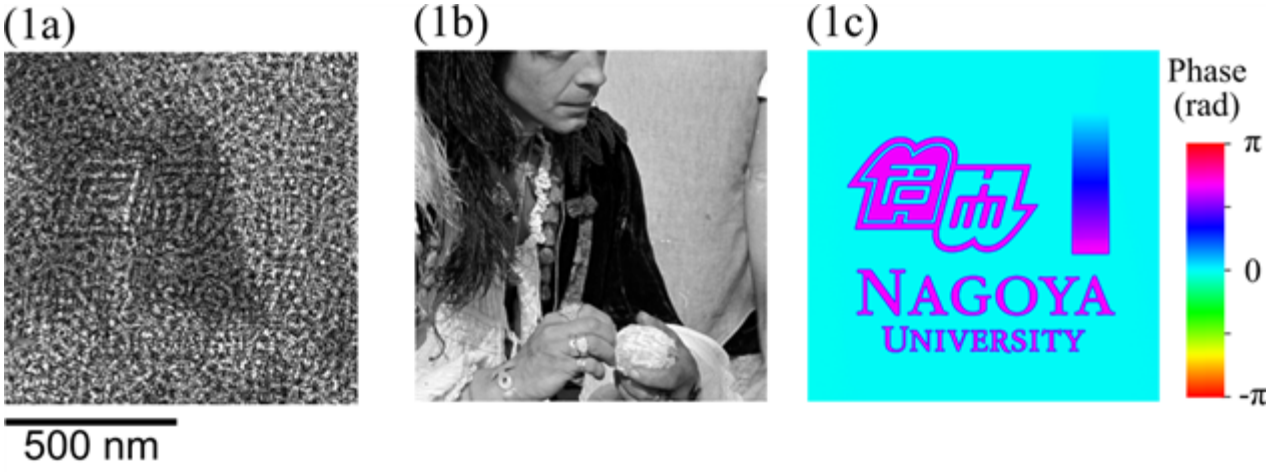

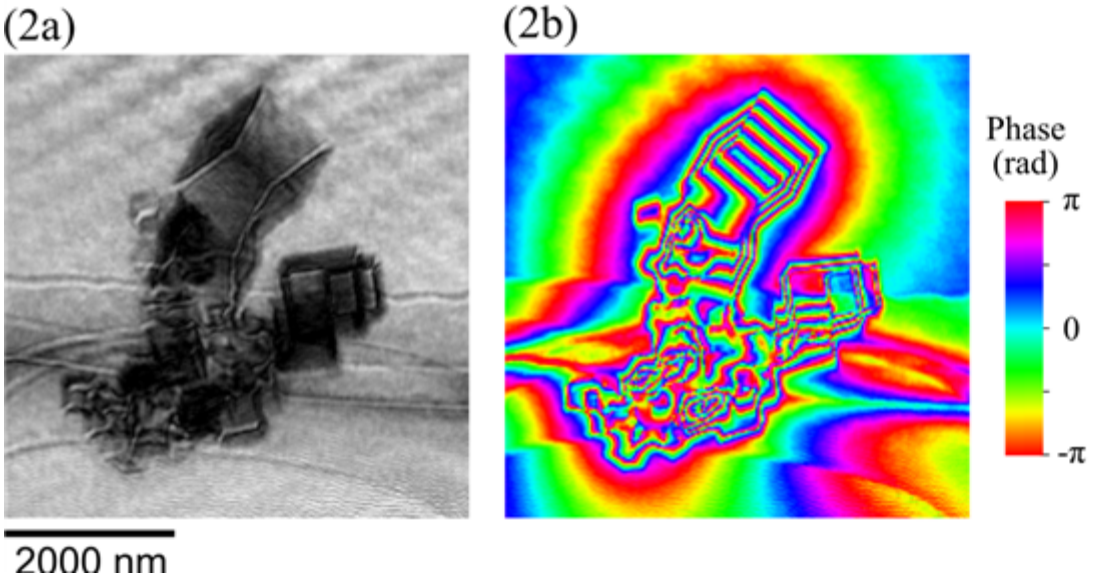

Keywords:

Wavefield reconstruction, Structured illumination, Ptychography

Reference:

[1] M. Stockmar, et al., Scientific reports, 3(1), 1927, (2013).
[2] F. Allars, et al., Ultramicroscopy, 231, 113257, (2021).
[3] K. Yamamoto, et al., Microscopy, 49, 31–39, (2000).

288

Quantitative comparison of HRTEM and electron ptychography

Felix Bennemann[1], Prof Peter Nellist[1], Prof Angus Kirkland[1,2]
[1]Department of Materials, University of Oxford, Oxford, United Kingdom, [2]Rosalind Franklin Institute, Harwell Science & Innovation Campus, Didcot, United Kingdom

IM-03 (2), Plenary, august 28, 2024, 14:00 - 16:00

Background incl. aims
Electron ptychography in the scanning transmission electron microscope (STEM) has been demonstrated to be capable of providing low-noise phase images of beam sensitive materials at low dose [1]. For such materials, in particular biological samples, conventional high-resolution transmission electron (HRTEM) is the most widely used approach - usually cryo-TEM. The question then arises of whether ptychography or HRTEM offers the most dose-efficient imaging approach. While resolution can be a useful measure for comparing imaging techniques, it is dependent on the electron dose. For some electron microscopy techniques, a phase contrast transfer function (PCTF) can be defined to quantify the technique's performance with respect to spatial frequency. However, the PCTF also does not account for the dose used and is not uniquely defined for common electron ptychography techniques like the Wigner distribution deconvolution (WDD) method. In this work we introduce the detective quantum efficiency (DQE), applied to electron microscopy as a dose independent and sample independent measure of technique performance.
Historically, the DQE has been used as the ultimate performance measurement of linear systems [2] ranging from electron detectors to medical imaging systems. If the incoming noise is pure Poisson noise, it can be calculated by dividing the signal to noise ratio of the system output squared ($SNRout^2$) by the signal to noise ratio of the system input squared ($SNRin^2$). SNRin also represents the signal to noise ratio of an ideal imaging system at the same dose. In this work the ideal TEM is defined as fully coherent HRTEM phase contrast imaging with an ideal Zernike phase plate. The SNRout represents the signal to noise ratio of the various electron microscopy techniques studied. Even though the signal to noise ratio is dose and sample dependent, the DQE is not. The DQE can be thought of as the fraction of incoming quanta contributing to the image.
Methods
For the calculation of the empirical DQE, simulations were performed using the MULTEM package [3]. All 4D-STEM simulations assumed an 80keV beam energy with a probe step size of 0.15 Å and a semi-angle of convergence angle α of 22.5 mrad on a 301 by 301 grid of probe positions. A detector size of 128 by 128 pixels was assumed. Reconstructions were performed using the single sideband (SSB) method, the Wigner distribution deconvolution (WDD) method and the integrated centre of mass (iCOM) method. As a comparison, simulations were also performed for high resolution transmission electron microscopy (HRTEM). The reconstruction methods were evaluated on coherent and partially coherent datasets containing 500 noise realisations each at a dose of 4.4M e/Å². Partial coherence was simulated through the introduction of a chromatic envelope with Cc = 1.1mm and an energy spread of 0.4eV leading to a defocus spread of 5.5 nm.
The ground truth was defined as the image from a fully coherent, aberration free HRTEM phase contrast image. For the purpose of calculating the empirical DQE of the different methods, a single carbon atom served as a sample because it provided a continous Fourier transform.
Results
The SSB and WDD electron ptychography methods reach a maximum DQE of around 23% as shown in the figure. The HRTEM reaches a maximum DQE of 100% at low spatial frequencies. However, through the introduction of a defocus spread of 5.5 nm, a rapid decay in the DQE of the HRTEM is observed. The DQE of the HRTEM decays to almost 0% at spatial frequencies above 1α while the DQE of SSB and WDD remains substantial up to 2α.

It can also be observed that the DQE of both SSB and WDD shows almost no change through the introduction of the chromatic envelope.
The DQE of iCOM follows the same shape as that of SSB and WDD. However, across all spatial frequencies it is 3-5% below that of SSB reaching its maximum at around 18%. It is interesting to note that even with partial incoherence introduced SSB outperforms fully coherent iCOM.
Conclusion
In this work we have successfully defined a dose and sample independent framework in which HRTEM and electron ptychography can be compared against each other using the DQE. We showed that in the absence of partial incoherence, an HRTEM can achieve a DQE of 100% while SSB and WDD ptychography have a maximum of around 23%. However, the introduction of partial coherence shows the weakness of the HRTEM. Considering a defocus spread of 5.5 nm the DQE of HRTEM remains close to 100% at low spatial frequencies but decays rapidly at higher spatial frequencies.

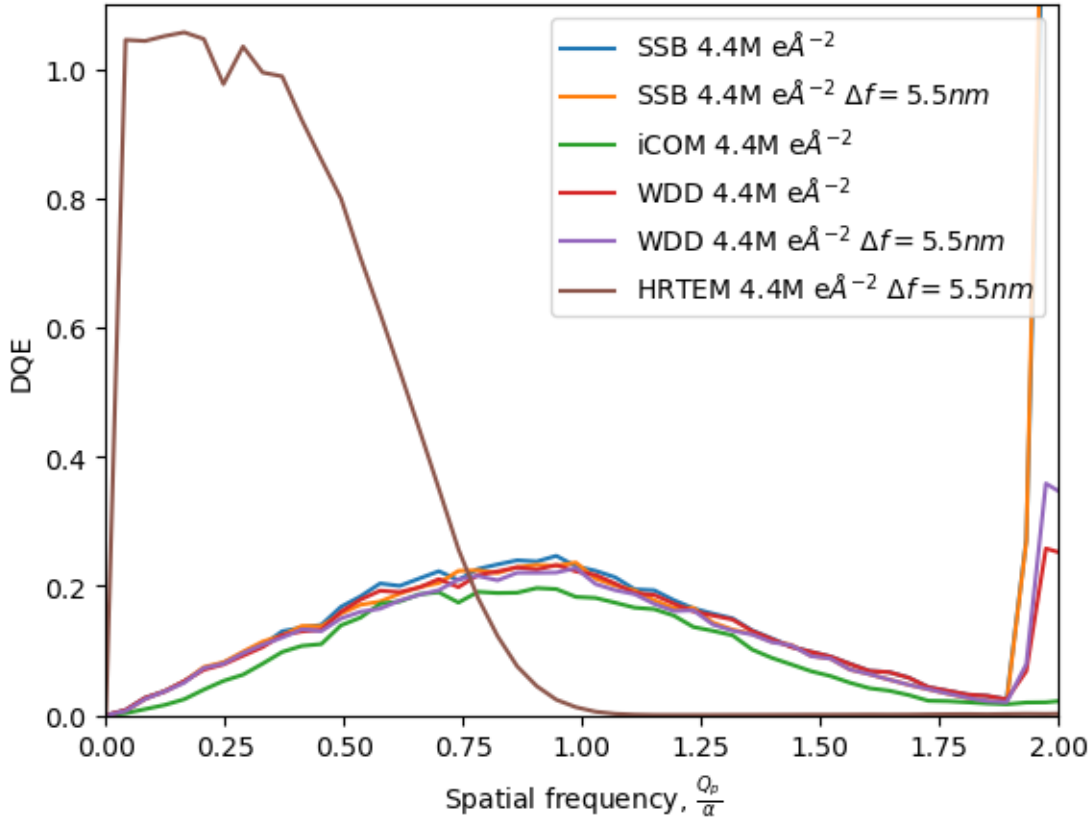

Keywords:

Ptychography, HRTEM, 4D-STEM

Reference:

[1] Colum M. O'Leary, Gerardo T. Martinez, Emanuela Liberti, Martin J. Humphry, Angus I. Kirkland, & Peter D. Nellist (2021). Contrast transfer and noise considerations in focused-probe electron ptychography. Ultramicroscopy, 221, 113189.
[2] R. C. Jones. Advances in Electronics and Electron Physics XI (Academic Press. Inc., New York, 1959, p. 121.)
[3] I. Lobato, & D. Van Dyck (2015). Ultramicroscopy, 156, 9-17.

315

Electron single pixel imaging enabled by ultrafast optical modulation of the illuminating wavefunction

Dr. Cameron Duncan[1], Beatrice Ferrari[1], Irene Ostroman[1], Maria Giulia Bravi[1], Sang Tae Park[2], Daniel Masiel[2], Jean Christophe Olaya[3], Paolo Rosi[4], Enzo Rotunno[4], Vincenzo Grillo[4], Giovanni Maria Vanacore[1]
[1]Unversità degli Studi di Milano-Bicocca, Milan, Italy, [2]JEOL-IDES, Pleasonton, United States of America, [3]Holoeye Photonics, Berlin, Germany, [4]Istituto Nanoscienze, Consiglio Nazionale delle Ricerche, Modena, Italy

IM-03 (2), Plenary, august 28, 2024, 14:00 - 16:00

Background incl. aims

Transmission electron microscopy (TEM) provides sub-angstrom imaging resolution unmatched by alternative modalities, but cumulative radiation damage to soft-matter specimens can pose an obstacle to applying TEM in the life sciences. Electron Single Pixel Imaging (ESPI) is a computational imaging technique with the potential to dramatically reduce the electron dosage needed to produce high-resolution images [1]. The key idea behind ESPI is to carefully imprint patterns onto the illuminating wavefunction and record the dependence of total scattering on pattern choice [2]. Controlling the illumination in this way ensures that every scattering event contributes useful information toward image reconstruction [3]. The outstanding instrumentation challenge when implementing ESPI is to modulate the electron probe. Here we report a novel, versatile method for imprinting arbitrary patterns onto the electron wavefunction that allows new patterns to be selected several times per second. We show proof-of-principle experimental results demonstrating image reconstruction of a MAX-phase nanoparticle.

Methods

Our modified JEOL TEM, shown in Fig. 1. is operated in pulsed mode: we drive electron emission via femtosecond laser pulses at repetition rates up to 600 kHz. Our column includes a secondary sample holder with a view port located directly below the acceleration section and above the primary specimen holder. In this secondary location, an electron-transparent, optically reflective metal film intercepts both the probe electron pulse and a control laser pulse, mediating an interaction between probe electrons and optical near fields. A Spatial Light Modulator (SLM) imprints a pattern onto the control laser, and the near fields at the metallic film transfer the SLM pattern to the electron beam. The patterned electron beam then scatters off the principal specimen, and diffraction-mode electron optics at long camera length enable detection of the total scattering of the modulated beam.

Results

Figure 2.a. shows a specimen of Ti3Al0.4Sn0.6C2 imaged with conventional TEM. Figure 2.b. shows a representative set of near-field modulated probe illumination patterns, while Fig. 2.c. shows the result of the image reconstruction algorithm applied to this basis set of patterns.

Conclusion

We are actively developing the ESPI technique, in particular, improving the coupling efficiency between control laser and electron probe pulses to provide sensitivity on the level of single-photon exchange. Simulation results suggest that by placing the specimen in the fourier plane of the

electron-laser interaction point, we can achieve beam patterning with nanometer feature sizes given a sufficiently coherent probe. We anticipate performing experiments on Li-based electrochemical samples and biologically embedded gold nanoparticles to demonstrate this capability.

This work is part of the SMART-electron Project that has received funding from the European Union's Horizon 2020 Research and Innovation Programme under Grant Agreement No. 964591.

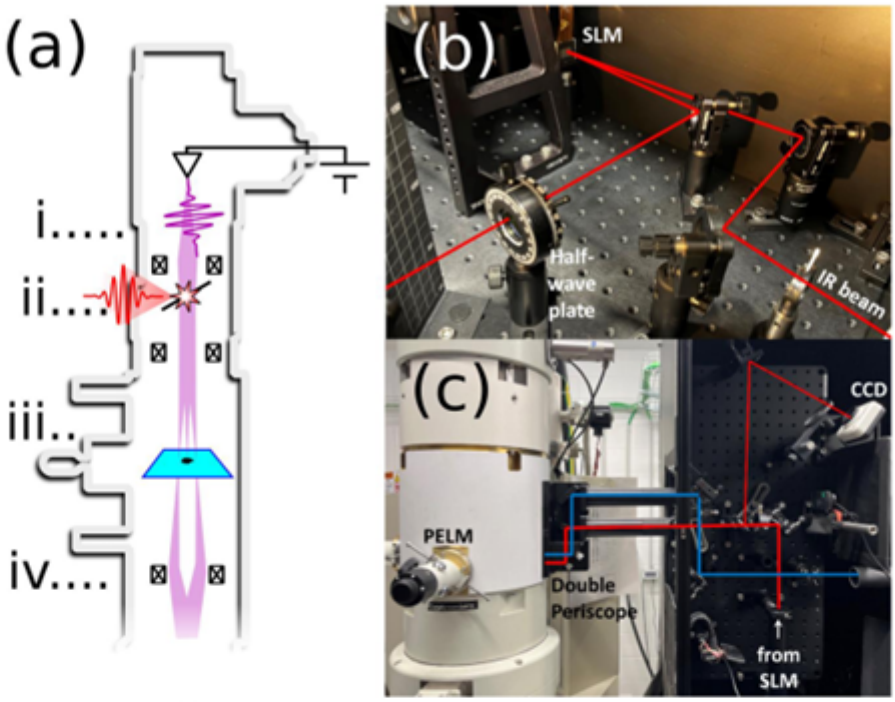

Figure 1. Experimental method. (a) Modified TEM column, showing i. photoexcitation of electron pulses via UV light, ii. optical modulation of electron pulses at a metallic interface, iii. patterned illumination of the specimen, iv. electron optics to collect the total scattering. (b) Optical path of the control laser, showing the spatial light modulator (SLM). (c) Photoemission laser (purple) and control laser (red) enter the microscope column through a viewport.

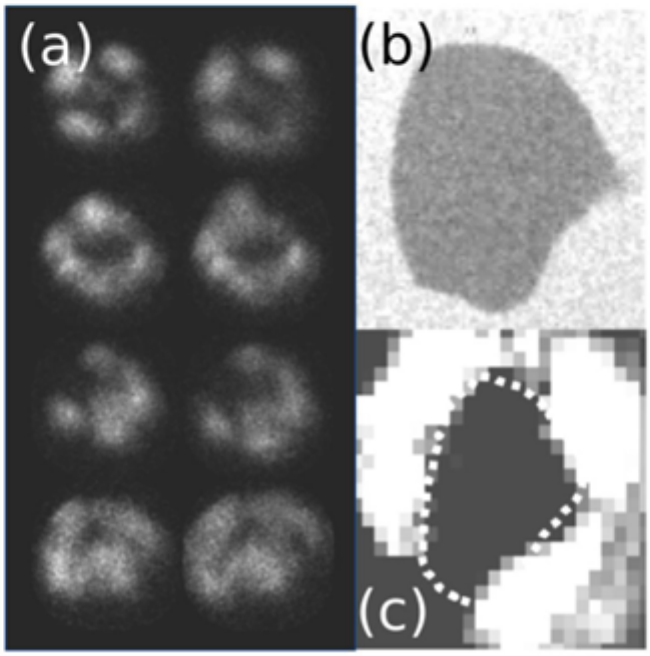

Figure 2. (a) Illumination patterns for Electron Single Pixel Imaging, (b) test specimen view under conventional TEM illumination. (c) Reconstructed image using the basis patterns in panel (a).

Keywords:

Ultrafast electron microscopy, single-pixel imaging

Reference:

[1] A. Konečná, et al. "Single-Pixel Imaging in Space and Time with Optically Modulated Free Electrons," ACS Photonics 10, 1463-1472 (2023)

[2] M. F. Duarte, et al. "Single-pixel imaging via compressive sampling." IEEE Signal Process. Mag. 25, 83-91 (2008).

[3] J. H. Shapiro, "Computational ghost imaging," Phys. Rev. A 78, 061802 (2008).

375

Atomic transitions analogue in phased-shaped electron energy-loss spectroscopy

Simon Garrigou[1], Mr. Arnaud Arbouet[1], Mr. Hugo Lourenço-Martins[1]
[1]CEMES-CNRS, Université de Toulouse, CNRS, Toulouse, France

IM-03 (2), Plenary, august 28, 2024, 14:00 - 16:00

Background incl. aims
Electron energy-loss spectroscopy (EELS) has proven its efficiency in probing nano-optical excitations down to the atomic scale e.g. plasmonic resonances, excitons or plexcitons. However, EELS being directly proportional to the magnitude of the electric field, it is unsensitive to a plethora of important properties of nano-optical excitations - such as e.g. their phase, chirality, field lines symmetry.
Over the last decade, several routes have been explored to enhance the EELS scheme and enable the detections of these so-far hidden properties. One solution – first proposed in 2014 [1] – consists in shaping the amplitude and phase of the electron beam before its interaction with the sample and sorting the final electron states after. This EELS scheme based on state preparation-selection is generally called phase-shaped EELS (PSEELS) and has attracted both a strong theoretical [2,3] and experimental interests [1,2]. Most of these efforts have been focused on the measurement of the chirality of matter through dichroic PSEELS measurements [1,2] and several other properties of matter remain to be explored through the prism of this technique.
In this conference, we will present our latest work on PSEELS aiming at giving a different physical perspective on this technique as well as exploring its application to the probing of multipolar resonances.
Methods
In a first part, we will show that most of the theoretical results found in the literature [1,2,3] can be demonstrated using a different approach treating the shaped and post-selected electron beam in an analogue way to an electron bounded to an atom. More precisely, we will demonstrate that PSEELS is physically equivalent to a spontaneous transition between two bounded electron states - known as Purcell effect – where the initial and final state are in our case shaped and post-selected electron states. This reformulation of the problem provides an elegant and intuitive derivation of the standard result of PSEELS [1,2,3], without the need of complex derivations.
Results
In a second part, we will focus on PSEELS transition between Hermite-Laguerre-Gauss states, which have drawn a strong experimental interest over the last years [4,5]. For this family of states, our formalism enables an exact formal analogy between PSEELS and transitions in a two-dimensional harmonic oscillator – a standard textbook problem. This enables us to express the PSEELS problem in a 2nd quantization language (using ladder operators) and derive closed-form expressions for the PSEELS transition probabilities. This approach has the benefit of directly highlighting the conservation rules of physical quantities such as the linear and angular momentum, thus giving an intuitive interpretation of PSEELS.
Conclusions
In a last part, we inject a multipolar development of the electromagnetic field into the previous formalism. Thus, we demonstrate that, by carefully selecting the in and out free electron states, one can directly measure the different multipolar moment of the electromagnetic field in PSEELS. We numerically illustrate our finding by simulating a PSEELS experiment on a plasmonic quadrupolar field using a boundary element method – as shown on figure 1. In particular, we show that simply by using 1st and 2nd order Hermite-Laguerre-Gauss beams (demonstrated experimentally [4]) one can selectively measure the in-plane quadrupolar field component, as well as the twist of the electric field lines, thus revealing the 3D field topology in EELS.

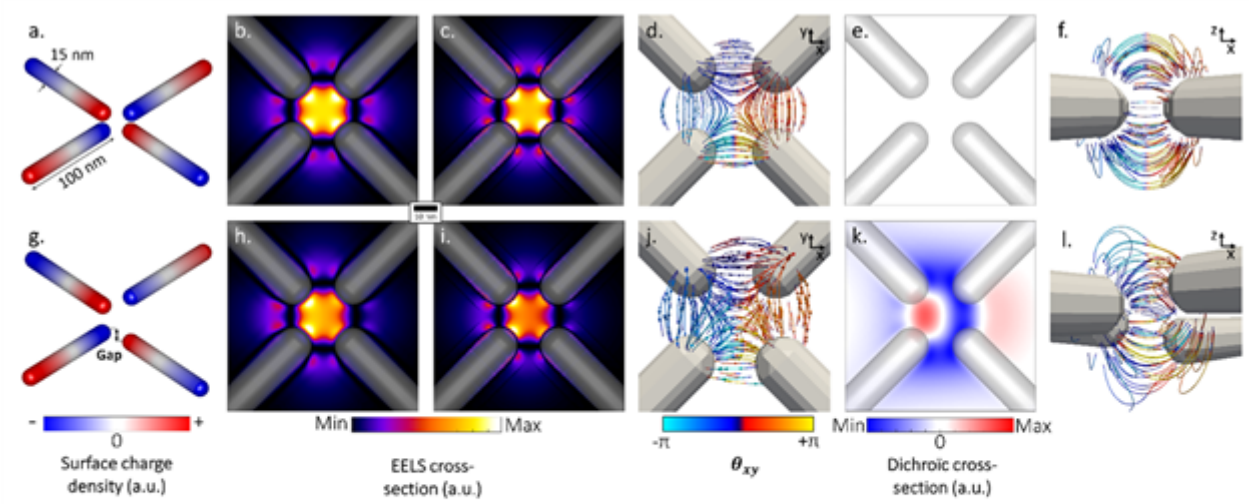

Figure 1 - (a,g) 3D representation of four coupled silver nanorods in **(a)** a flat disposition and **(g)** forming an helix. The colorscale represents the charge distribution of the lowest energy plasmonic mode. **(b,h)** Spatial distribution of the probability of scattering between a Hermite-Gauss (1,1) and a Gaussian state across the structure. **(c,i)** Intensity maps of the quadrupolar plasmonic field component showing a clear similarity with the previous EELS maps. **(d,f,j,l)** 3D representation of the electric field lines, color of the field line represent the orientation angle θ_{xy} of the electric field projected on the xy-plane. **(e,k)** Maps of the circular dichroism in EELS. As theoretically expected, the flat structure does not display any dichroism, while the 3D structured one does.

Keywords:

PINEM, Angular momentum, Numerical, nano-optics

Reference:

[1] Asenjo-Garcia and García de Abajo, Phys. Rev. Lett. 113, 066102 (2014)
[2] Lourenço-Martins et al., Nature Physics 17, 598–603 (2021)
[3] Bourgeois et al., Science Advances 9 (51) (2023)
[4] Guzzinati et al., Nature Comm. 8 14999 (2017)
[5] Tavabi et al., Phys. Rev. Lett. 126 094802 (2021)

557

Multi-Convergence-Angle Ptychography with Simultaneous Strong Contrast and High Resolution

Mr. Wei Mao[1,2], Mr. Weiyang Zhang[2], Dr. Chen Huang[3], Prof. Liqi Zhou[1,2,5], Dr. Judy Kim[3,4], Prof. Si Gao[2,6], Mr. Yu Lei[1], Mr. Xiaopeng Wu[1], Mr. Xudong Pei[2], Prof. Yuefeng Nie[2], Prof. Angus Kirkland[3,4], Dr Peng Wang[1,2]

[1]Department of Physics, University of Warwick, Coventry, UK, [2]National Laboratory of Solid-State Microstructures, Jiangsu Key Laboratory of Artificial Functional Materials, College of Engineering and Applied Sciences and Collaborative Innovation Centre of Advanced Microstructures, Nanjing University, Nanjing, China, [3]The Rosalind Franklin Institute, Harwell Campus, Didcot, UK, [4]Department of Materials, University of Oxford, Oxford, UK, [5]Institute of Materiobiology, College of Science, Shanghai University, Shanghai, China, [6]College of Materials Science and Engineering, Nanjing Tech University, Nanjing, China

IM-03 (2), Plenary, august 28, 2024, 14:00 - 16:00

Structural biology, which primarily focuses on the tertiary structure of biological molecules, has played a pivotal role in disease research, drug development, and the investigation of fundamental biological processes. Recently, the growing demand for more precise determination of three-dimensional biological structures using single particle analysis (SPA) or electron tomography (ET) necessitates high-quality two-dimensional projection images with both strong contrast and high resolution. Nevertheless, due to the fact that unstained biological samples are primarily composed of light elements and their structures are extremely radiation sensitive, which means that the electron dose used for imaging is limited, the contrast of biological samples in electron microscope images is very weak. To address this issue, phase contrast imaging at high defocus or novel phase plates is commonly employed. However, using high defocus corrupts information transfer at high spatial frequencies and the applications of phase plate attenuate signals from biological samples at high frequencies. Therefore, there is currently no technological means available to achieve imaging of non-stained biological samples with both strong contrast and high resolution simultaneously.
Electron ptychography has gained considerable interest in materials science and bioimaging, which has been recently reviewed1. However, the contrast transfer function of electron ptychography strongly relies on the selected convergence angles. In materials science, by employing a large convergence angle, ptychography has been demonstrated to achieve deep sub-angstrom resolution, whereas in the field of bioimaging, a small convergence angle tends to be used to enhance contrast of unstained biological samples at the expense of resolution2,3. In other words, conventional electron ptychography still fails to provide images with simultaneous strong contrast and high resolution.
Here, we introduce a novel ptychographic method, Multi-Convergence-Angle (MCA) Ptychography4. Our research addresses the current limitations of conventional ptychography and presents a promising approach for achieving high-quality two-dimensional images with improved clarity and precision.

The schematic experimental setup of MCA-ptychography is illustrated in Fig. 1(a). In contrast to conventional electron ptychography, which employs a single convergence angle (hereafter referred to as single-convergence-angle ptychography or SCA-ptychography), MCA-ptychography utilizes multiple condenser apertures with varying diameters to modify the convergence angles of the electron probe during the scanning process. However, such a device with the aperture-switching capability is not currently available for electron microscopes. Therefore, as a proof of concept, we performed MCA-ptychography in series by acquiring the first dataset with one aperture for the entire scanning area and subsequently switching to the other aperture to acquire the second dataset for

the same area. The two SCA-ptychographic datasets are mixed before reconstructing the object wavefunction via MCA-ptychography reconstruction algorithm.

A model of GroEL protein (PDB: 2eu1) suspended on a monolayer graphene substrate was simulated using the multislice method5. Two ptychographic datasets were generated at an accelerating voltage of 300 kV and convergence semi-angles of 3 mrad and 15 mrad, respectively. These two datasets were combined into a single dataset (mixed-angle dataset) and subsequently subjected to MCA-ptychographic reconstruction. The SCA-ptychographic reconstructed results at 3 mrad and 15 mrad, together with the MCA-ptychographic reconstructed result at different electron doses, are presented in Fig. 2. It is evident from the graph that SCA-ptychography at a smaller convergence angle provides strong contrast but limited resolution, while SCA-ptychography at a larger convergence angle achieves higher resolution albeit with weaker contrast. In contrast, MCA-ptychography not only provides strong contrast but also achieves high resolution. Furthermore, we found that even when the electron dose drops to as low as 11 e-/Å2, MCA-ptychography still maintain its robustness while providing simultaneous strong contrast and high resolution.

In conclusion, we propose a novel ptychographic method, MCA-ptychography, which incorporates multiple convergence angles during the data acquisition process and demonstrate its capability to provide simultaneous strong contrast and high resolution. Our research addresses the current limitations of conventional ptychography and in the future, we anticipate the integration of MCA-ptychography with cryo-electron microscopy, which will further enhance 2D projection images, leading to improved 3D reconstruction methods.

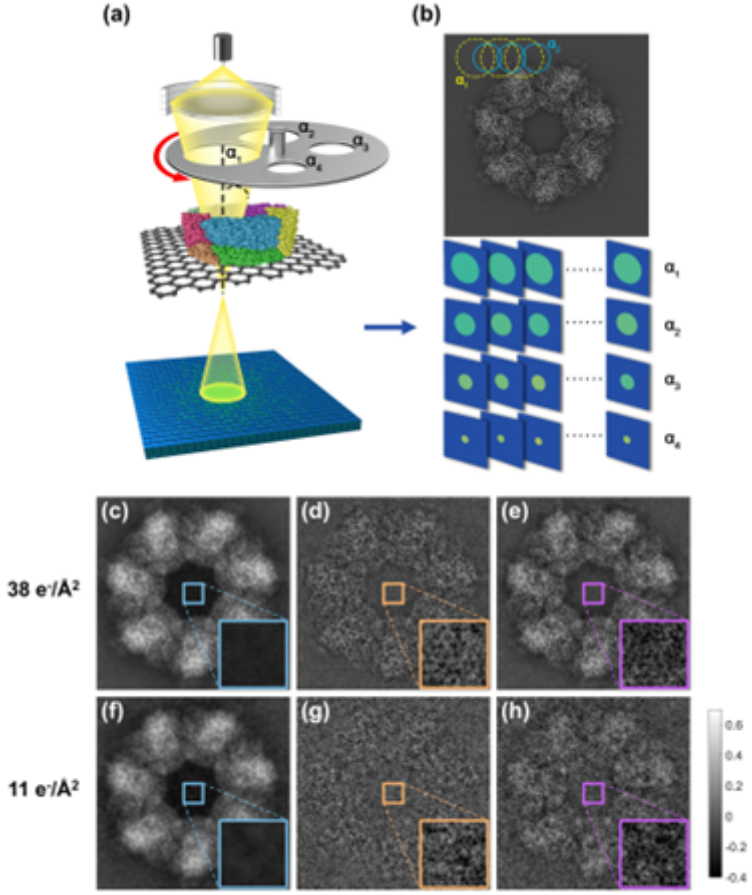

Keywords:

electron-ptychography, structural-biology, contrast-and resolution-enhancement

Reference:

1. Mao, W., Zhou, L., Gao, S. & Wang, P. Electron ptychography. in Encyclopedia of Condensed Matter Physics (Second Edition) (ed. Chakraborty, T.) 71-94 (Academic Press, Oxford, 2024).
2. Zhou, L. et al. Low-dose phase retrieval of biological specimens using cryo-electron ptychography. Nature Communications 11, 2773 (2020).
3. Pei, X. et al. Cryogenic electron ptychographic single particle analysis with wide bandwidth information transfer. Nature Communications 14, 3027 (2023).
4. Mao, W. et al. Multi-Convergence-Angle Ptychography with Simultaneous Strong Contrast and High Resolution. arXiv [physics.optics] (2024).
5. Kirkland, E.J. Advanced computing in electron microscopy, (Springer, 1998).

681

Mean inner potential change of latex sphere with temperature measured using off-axis electron holography

Dr. Yan Lu[1], Peng-Han Lu[1], Dominik Biscette[2], Denys Sutter[2], Prof. Giulio Pozzi[3], Prof. Rafal E. Dunin-Borkowski[1]
[1]Forschungszentrum Juelich, Juelich, Germany, [2]CondenZero AG, Zurich, Switzerland, [3]University of Modena and Reggio Emilia, Modena, Italy

IM-03 (2), Plenary, august 28, 2024, 14:00 - 16:00

Background incl. aims
Electron-beam-induced specimen charging is frequently encountered in transmission electron microscopy (TEM), in particular when studying insulating or biological materials. Polystyrene latex is a widely-used material for immunodiagnostic reagents and is often studied using cryo-TEM. Both a highly energetic electron beam and a low specimen temperature can change the intrinsic properties of materials. The mean inner potential (MIP) is an intrinsic parameter of a material, which is defined as its volume-averaged electrostatic potential with respect to a distant vacuum reference. The MIPs of many materials have been measured at room temperature using off-axis electron holography [1]. However, few low temperature measurements of MIPs and charging phenomena have been performed.
Methods
The TEM mode of off-axis electron holography involves the use of an electron biprism to overlap a reference electron wave that has passed through vacuum with an electron wave that has passed through a sample. Analysis of the resulting interference fringe pattern can be used to recover both amplitude and phase information. In the absence of dynamical diffraction and magnetic fields, the projected phase shift of the electron wave that has passed through the sample can be expressed in the form $\phi(x,y)=C\,V(x,y)\,t$, where C is a constant that depends on the microscope accelerating voltage (6.53×10^6 rad/Vm at 300 kV), V(x,y) is the total projected potential (including the MIP V_o and the electrostatic potential V_1 induced by electron-beam-induced charge redistribution) and t is the sample thickness. For a spherical solid of radius R, $\phi_o(x, y)=2C\,V_o\,(x,y)\,\sqrt{(R^2-(x^2+y^2))}$. The contribution to the phase from the electron-beam-induced charging outside and inside the sphere are $\phi_1(x,y)=C\,Q/(4\pi\varepsilon_o)\,\ln(((x-x_o)^2+y^2)/(x^2+y^2))$ $(r \geq R)$ and $\phi_1(x,y)=2C\,Q/(4\pi\varepsilon_o)\,(\ln(\sqrt{((x-x_o)^2+y^2)}/\sqrt{(R^2-(x^2+y^2))}+\sqrt{(R^2-(x^2+y^2)}/R+(\sqrt{(R^2-(x^2+y^2))^3}/3R^3)$ $(r < R)$, respectively [2], where ε_o is vacuum permittivity, $(x_o, 0)$ is the position of image charge. In order to quantitatively measure the charge on a latex sphere, we applied a model-independent (MI) approach [3, 4], which involves the measurement of the total charge enclosed by a chosen contour (Figs 1a and 1b). In this way, the contribution to the phase shift from the MIP and charge redistribution can be separated.
Off-axis electron holograms were recorded at 300 kV on an FEI Titan G2 TEM equipped with a 4K Gatan K2 camera. Each hologram was acquired by using a total exposure time of 6 s sub-divided into 30 frames of 0.2 s. Phase reconstruction was performed using HoloWorks software. Reduced specimen temperatures were reached by using a liquid helium holder from CondenZero (down to 5 K) and a liquid nitrogen cooling holder from Gatan (98 K).
Results
Figures 1a and 1b show a reconstructed phase image of a latex sphere with a diameter of ~220 nm attached to the end of a W tip. The hologram was recorded at room temperature (RT) and the charge was measured by performing a loop integral (marked using a yellow frame). The black arrow in Fig. 1a indicates the calculation direction. The total amount of charge on the latex sphere is calculated to be ~273 e. Figure 1c shows phase images of a latex sphere with a diameter of ~430 nm on a 50-nm-thin Au film recorded at RT and 5.3, 29 and 70 K. Figure 1d shows equiphase contours generated from differences between the RT and lower temperature phase images. The total amount of charge is

calculated to be 705, 633, 600 and 555 e, respectively. The differences result from both a change in electron-beam-induced charging and a change in MIP with temperature. In the surrounding vacuum region, phase changes are present due to the charge on the sphere and the substrate. By using this approach, 20 sets of data were recorded from spheres with sizes of 220, 430 and 604 nm at temperatures of 5.3, 23, 26, 29, 70, 98 and 298 K. The MIP value at each temperature was measured from these results. Figure 1e shows the relationship between temperature and MIP, with the measurements shown as black squares and error bars and a blue curve showing a parabolic fit with an R-squared value of 0.95732. The fitted parabola gives an intercept of 5.96 ± 0.16 V. The change in MIP from RT (5.17 ± 0.18 V) to that extrapolated to 0 K is ~16%.

Conclusions

Electron phase images of latex spheres of different sizes have been recorded at different specimen temperatures using off-axis electron holography. A model-independent approach has been used to measure the charge on each sphere. The MIP is also found to change, especially at the lowest specimen temperature.

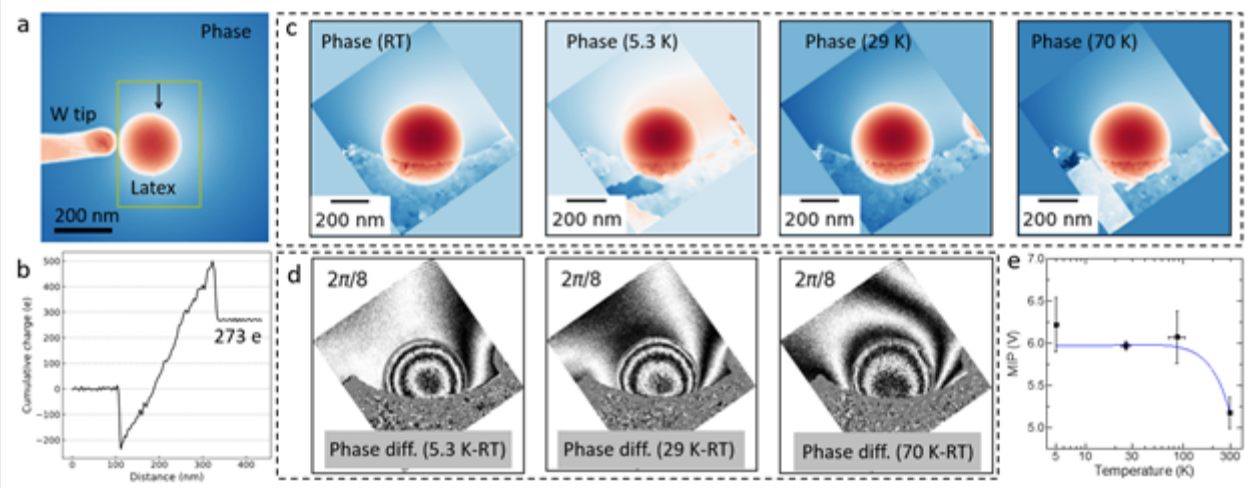

Keywords:

Mean-inner-potential, e-beam-induced charging, nanoparticle

Reference:

[1] M. Yesibolati, S. Laganà, H. Sun et al., Phys. Rev. Lett. 124, 065502 (2020).
[2] F. Zheng, J. Caron, V. Migunov et al., J Electron Spectros. Relat. Phenomena 241, 146881 (2020).
[3] M. Beleggia, T. Kasama, R. E. Dunin-Borkowski et al., Appl. Phys. Lett. 98, 243101 (2011).
[4] C. Gatel, A. Lubk, G. Pozzi et al., Phys. Rev. Lett. 111, 025501 (2013).

707

Coherent inelastic scattering probed by holographic scanning transmission electron microscopy

Dr. Nora Bach[1], Tim N. Dauwe[1], Dr. Murat Sivis[1], Prof. Dr. Claus Ropers[1]
[1]Max Planck Institute for Multidisciplinary Sciences, Göttingen, Germany

IM-03 (2), Plenary, august 28, 2024, 14:00 - 16:00

In today's nanoscale technology, a detailed understanding of the structures and induced fields is fundamental. Electron microscopy has proven a powerful method for quantitative phase-contrast imaging of electric fields in nanostructures. One successful approach is based on off-axis holography which employs the interference of a complex object wave with a reference wave. However, this technique requires a wide, coherent electron beam emitted from a highly coherent electron source, and cannot be transferred straightforwardly to access ultrafast dynamics in the femtosecond-nanometer range.
Nonetheless, phase-resolved measurements of local optical responses have recently been revealed using Lorentz microscopy [1] and free-electron homodyne detection [2]. These measurements rely on the inelastic scattering of electrons off optical near-fields in so-called Photon-Induced Near-field Electron Microscopy (PINEM) [3,4]. Pulsed electrons generated in an ultrafast transmission electron microscope (UTEM) gain or loose energy upon interaction with the optical field of the driving laser pulse. While both approaches for phase-resolved measurements have proven powerful in terms of resolution, sensitivity and robustness, their stringent requirements on electron beam coherence or a designated sample holder, respectively, render the general experimental implementation challenging.
In this contribution, we present a method based on scanning transmission electron miscroscopy (STEM) with spatially separated coherent probes [5], that yields holographic information on inelastic interactions at reduced electron beam coherence requirements. Specifically, we insert an amplitude grating in the electron microscope condenser system and can, thereby, prepare a tailored electron probe composed of a coherent superposition of spatially separated STEM foci corresponding to given diffraction orders. The far field of these probes interferes to form an image of the grating pattern. Distinct elastic and inelastic interactions experienced by the separate probes will modify the interference condition and affect the recorded far field distribution.
Experiments are carried out in a UTEM based on a Schottky field-emission JEOL JEM-F200 instrument, which we modified to allow for a laser-triggered photoelectron mode and optical sample excitation. As a first application of STEM holography, we perform 2D-raster scans at nm-scale spatial resolution to visualize elastic and inelastic interactions at an optically excited heterostructure.
In the simplest case of only elastic interactions, a difference in, for example, sample thickness between the separate probes would lead to a translation of the interference pattern for different scanning positions. Imaging of inelastic scattering processes is achieved by employing a single-electron-sensitive hybrid pixel detector behind an energy filter. Moreover, by adjusting the electron microscope imaging spectrometer to collapse one of the momentum space dimensions on the detector and adding energy dispersion along this direction, we anticipate recording two-dimensional images simultaneously, encoding holographic information both on relative phases between the probes and on the energy spectrum.
In conclusion, we demonstrate STEM holography adapted to the characterization of coherent inelastic scattering. A particular advantage of this technique is the relaxed coherence requirements, which could be central to overcoming common challenges in ultrafast transmission electron microscopy and improving time-resolved imaging of electric and magnetic fields on the nanoscale.

Keywords:

STEM-holography, inelastic scattering, optical near-fields

Reference:

[1] J. H. Gaida et al., Nature Communications 14, 6545 (2023)
[2] J. H. Gaida et al., Nature Photonics (2024)
[3] B. Barwick et al., Nature 462, 902-906 (2010)
[4] A. Feist et al., Nature 521, 200-203 (2015)
[5] F. S. Yasin et al., J. Phys. D: Appl. Phys. 51, 205104 (2018)

54

Vibration-Corrected Electron Ptychography

Anton Gladyshev[1,2], Mr. Johannes Müller[1,2], Dr. Benedikt Haas[1,2], Prof. PhD Christoph Koch1[1,2]
[1]Humboldt-Universität zu Berlin, Berlin, Germany, [2]Center for the Science of Materials Berlin, Berlin, Germany

IM-03 (3), Plenary, august 29, 2024, 10:30 - 12:30

Background incl. aims

Far-field electron ptychography is considered to be one of the most powerful phase retrieval techniques currently available for electron microscopists. Recently it was shown that ptychography is capable to surpass the Abbe resolution limit [1] and resolve specimens features as fine as the blurring due to the vibrations of the atoms [1]. A rather simple mathematical model of coherent diffraction pattern formation standing behind conventional algorithms [2,3] does not account for any motion or superposed states [1,2,3]. In order to overcome the resolution limit caused by the lattice vibrations we utilize the mixed-object formalism initially proposed in 2013 for X-rays [3], but never applied to electron microscopy data without assuming explicit atom positions [4]. In contrast to conventional ptychography [1,2,3] that treats a single transmission function of a specimen, mixed-object ptychographic reconstruction considers a sequence of superposed transmission function states, each producing a coherent diffraction pattern via a multislice simulation [1,2]. The total diffraction pattern corresponding to the entangled system is formed as an incoherent sum over the states [2,3,4].

Methods

For the tests of mixed-object ptychography we used a 4D-STEM dataset [1,2] of a monolayer MoS2 acquired in the Nion Hermes microscope at an accelerating voltage, convergence semi-angle, scan step and electron dose of 60 kV, 33 mrad, 0.2 Å and 5.3*10^6 e-/Å^2, respectively. To evaluate the resolution of the ptychographic reconstructions we propose a novel approach, akin to the Young fringe resolution test widely applied in TEM imaging [5]. We perform two ptychographic reconstructions with random initial guess for the object, e.g. uniform prior. Then the two independent results are shifted with respect to each other and the Fourier intensity of the difference is computed. The arising interference fringes indicate the range of spatial frequencies identical in the two results, allowing to conclude how deterministic a particular reconstruction is. Further, in contrast to conventional resolution tests, e.g. visibility of the Fourier peaks [1], the proposed approach allows to include aperiodic features that are crucial for a moving specimen.

Results

Assuming a single illumination mode [1,2,3] we conducted pairs of ptychographic reconstructions in two scenarios: one involving a single-state and the other involving 10 states of the transmission function. After 500 iterations of the gradient-descent [2] the achieved resolution was estimated. As a result, two independent pure-state reconstructions appear to produce identical information up to 1.9 Å^-1, while the mixed-object reconstructions contain deterministic information up to 2.3 Å-1. Figure 1 shows a comparison between pure- and mixed-state psychographic reconstructions.

Figure 1. Comparison of pure-state (upper row) and mixed-state (lower row) ptychographic reconstructions. Panels an and d show phases of a single-state reconstruction and an average over 10 states, panels b) and e) show the Fourier intensities (averaged over the states). The panels c and f show the results of Young fringe resolution test. The information limit of 2.3 Å^-1 denoted by the white circle was surpassed only by the mixed-state ptychographic reconstruction. The colorbar on the left side of the figure refers to the values of the phase in a) and d), the colorbar on the right refers to the Fourier intensities in b), c), e) and f).

Conclusions

Even with a monolayer specimen that is not supposed to produce a noticeable amount of incoherent scattering, we show that considering multiple entangled states of the transmission function makes the underlying model more realistic and improves the quality of the ptychographic fit. Thus, we liberate model-free ptychography from atomic vibrations, its last known resolution limit [1,2].

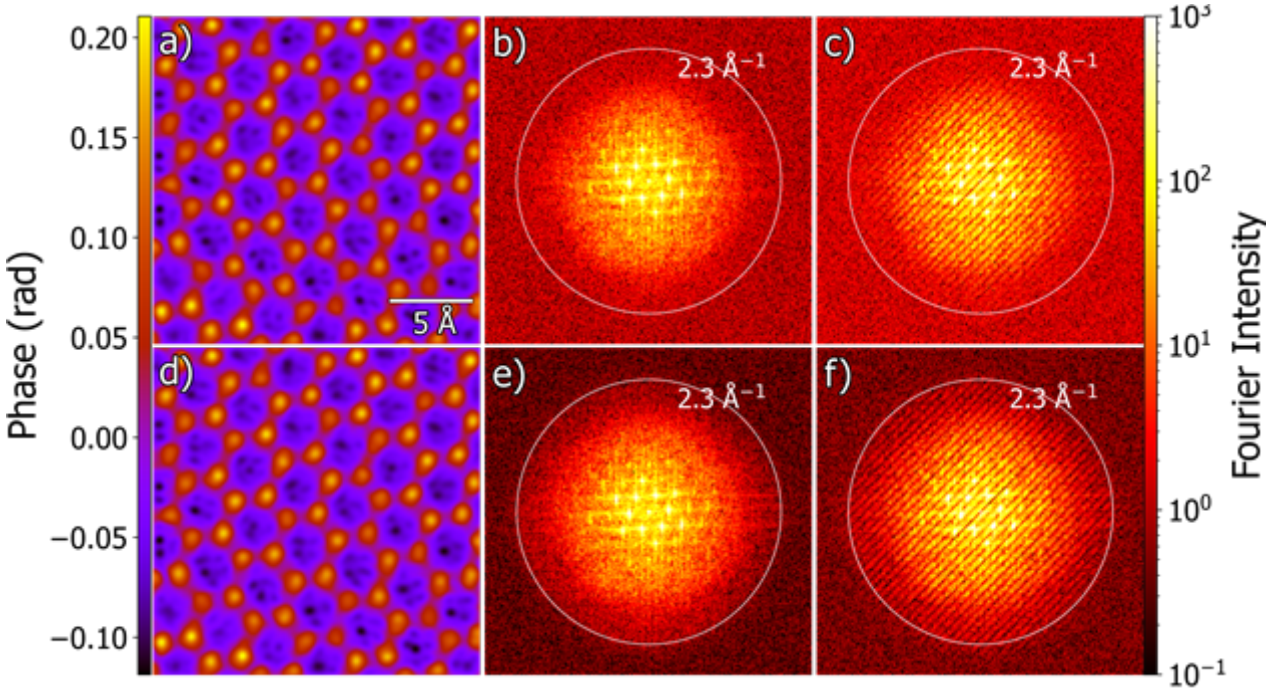

Keywords:

Ptychography, TDS, lattice vibrations

Reference:

[1] Chen, Z., et al. (2021). Science. doi: 10.1126/science.abg2533
[2] Gladyshev, A., et al. (2023). arXiv. doi:arXiv:2309.12017
[3] Thibault, P., & Menzel, A. (2013). Nature. doi:10.1038/nature11806
[4] Diederichs B. et al. (2024). Nature Communications. doi: 10.1038/s41467-023-44268-x
[5] Kisielowski, C., et al. (2008). Microscopy and Microanalysis. doi: 10.1017/S1431927608080902

103

End-to-end learning of atomic resolution phase-contrast volumes from 4D-STEM measurements

Shengbo You[1], Dr Andrey Romanov[1], Dr Philipp Pelz[1]
[1]Institute of Micro- and Nanostructure Research (IMN) & Center for Nanoanalysis and Electron Microscopy (CENEM), Friedrich Alexander-Universität Erlangen-Nürnberg,, Erlangen, Germany

IM-03 (3), Plenary, august 29, 2024, 10:30 - 12:30

Background incl. aims
Ptychography has been proven to have the ability to efficiently recover phase information of the specimen in the Transmission Electron Microscope (TEM). However, with traditional single slice ptychography, the multiplication assumption requires the specimen to be thinner than a few atomic monolayers. Otherwise, multiple scattering becomes significant, and the algorithm fails to recover even the basic structure. To accurately reconstruct the phase information of a thick sample, we combine electron ptychography and tomography into a single algorithm directly reconstructing a 3D electrostatic potential volume from 4D-STEM tilt-series measurements.
Ptychographic atomic electron tomography was experimentally demonstrated to be capable of imaging atoms in 3D volume, together with contrast improvements[1]. Another successful demonstration to image bulk materials was to combine the multi-slice algorithm with ptychography. This powerful combination is capable of imaging individual atoms at a resolution set by the intrinsic size of the atoms. The combination of the multi-slice algorithm and tomography have also been demonstrated using High Resolution TEM. Even with plane-wave illumination, the atoms were precisely located. Hence, with all the successful demonstration, our aim is to develop a joint reconstruction algorithm, combining the multilisce, tomography, and ptychography for bulk materials with atomic resolution. Our experimental realization is an end-to-end reconstruction process, the 3D structure of the material is recovered directly from the 4D-STEM dataset. In the result, the 3D atom positions can be clearly viewed in all 3 dimensions.
Methods
In the collection process, our method is similar to the ptychographic electron tomography experiment, a focused electron beam raster scan through the bulk specimen with adjacent scan positions overlapped. The electron beam passes through the specimen and then propagates through the vacuum. The detector, which is placed in the far-field with respect to the specimen, collects one diffraction pattern for each scan position. In the reconstruction process, we recover the electrostatic potential of the atoms, which multiplying an electron-charge interaction constant is the projected phase information of the specimen. A series of thin slices of the specimen are reconstructed for each tilt angle. The updates from all the tilt angles are applied to the same 3D volume, instead of integrating after the reconstruction. In other words, the updated volume in the current angle is used in the forward path of the reconstruction of the next angle. In Figure 1 a), the calculated volume is rotated and shifted using affine alignment (A), and then binned (B). The electron beam, with 3 modes and their exit wave shown, passes through the model and forms a diffraction pattern at each scan position. In Figure 1 b), the 4D-STEM datasets update the exit wave at the backward path at each angle, and eventually recover the potential of our model. A regularization kernel is used to reduce the binning effect. Butterworth filter and a modified L1 normalization are used to erase the noise.
Results
We used modal decomposition method to model the partial coherence of the illumination wave. The complex wave transfer function and their positions were reconstructed together with the 3D sample volume. The sample in our experiment was ZrTe2. The reconstructed electrostatic potential of our sample clearly imaged the individual atoms. The algorithm yielded a high contrast of the core structure, which helped us separate the atoms from the vacuum. A series of hyper-parameters were

tuned to test their effects. We also tested the performance of our system under low-dose condition by skipping part of the diffraction patterns.

Conclusion

In summary, we experimentally demonstrated end-to-end reconstruction for ptychographic multi-slice electron tomography is capable of 3D structure determination with atomic resolution. With a series of fine-tuned regularization tools, our joint reconstruction algorithm yields a high SNR volume with contrast improvements. With the low-dose test, the algorithm shows promising potential for imaging beam-sensitive materials such as polymers, battery materials, and biological molecules.

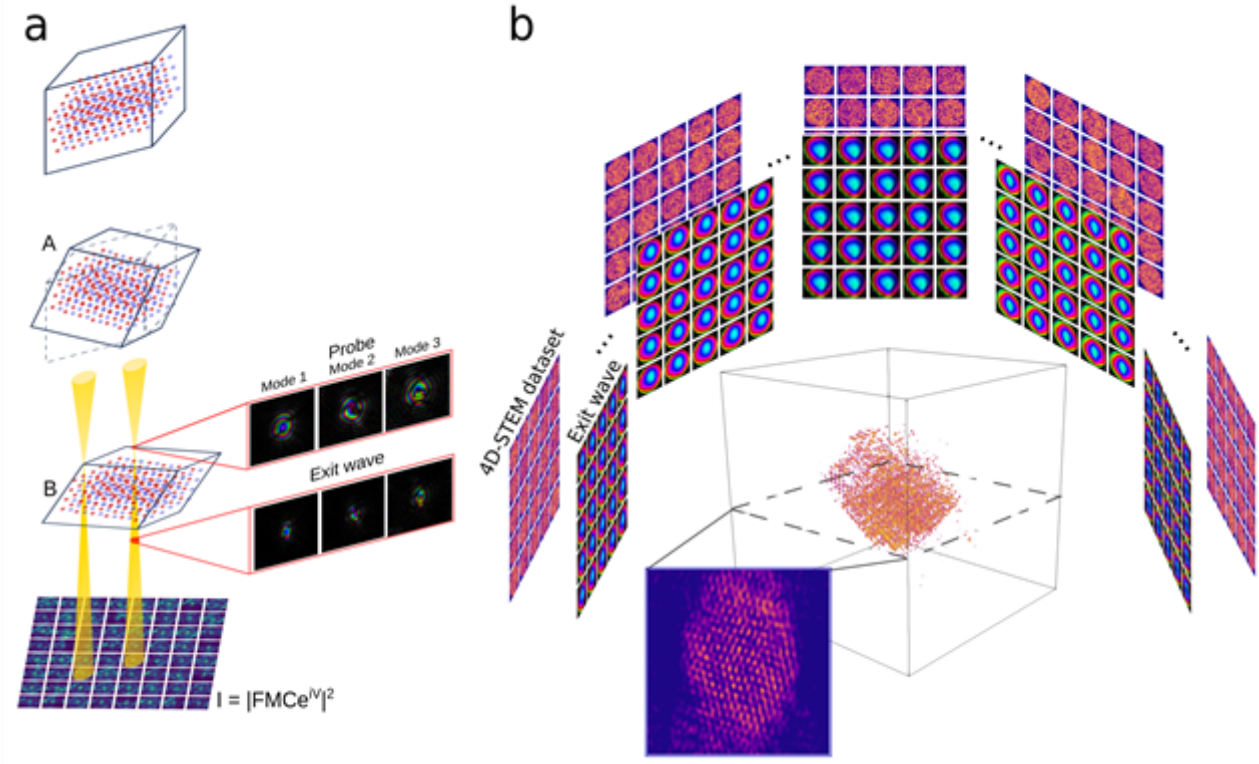

Keywords:

4D-STEM, multi-slice ptychography, tomography, reconstruction

Reference:

[1] Philipp M. Pelz, Sinéad M. Griffin, Scott Stonemeyer, Derek Popple, Hannah DeVyldere, Peter Ercius, Alex Zettl, Mary C. Scott, and Colin Ophus. Solving complex nanostructures with ptychographic atomic electron tomography. Nature Communications, 14:7906, November 2023.

352

Ptychographic imaging of nanoscale 3D objects with soft x-ray synchrotron and EUV table-top sources

Dr Vitaly Krasnov[1], Dr Kevin Dorney[2], Dr Esben Larsen[2], Prof. Igor Makhotkin[3], Dr Jeroen Scheerder[2], Dr Victor Soltwisch[4], Dr Paul van der Heide[2], Prof. Claudia Fleischmann[1]
[1]imec / KU Leuven, Department of Physics and Astronomy, Quantum Solid-State Physics, Leuven, Belgium, [2]imec, Leuven, Belgium, [3]University of Twente, Enschede, Netherlands, [4]PTB, Berlin, Germany

IM-03 (3), Plenary, august 29, 2024, 10:30 - 12:30

X-ray/Extreme ultraviolet (EUV) coherent diffraction imaging (CDI) is an efficient technique for the characterization of nano-structures. Unlike conventional microscopy, CDI does not rely on complex high-quality X-ray/EUV optics. However, in order to obtain a reconstructed image of the object, generally, a large amount of diffraction data is required. To reach the necessary level of oversampling, ptychography is often utilized. It is a form of CDI in which a focused light beam is scanned over the sample, obtaining a unique diffraction pattern at each scan position. This allows to reach the necessary amount of over-sampled data. The technique enables reconstruction of both amplitude and phase distributions, much like holography, via advanced iterative phase retrieval algorithms. Utilizing information about both absorption and phase shift in every pixel of the object's image yields chemical sensitivity. In addition, the relative transparency of many materials in the EUV/soft x-ray range allows buried structures and interfaces to be imaged that would otherwise be opaque in electron or probe-based microscopies.
Given the high spatial resolution that can be achieved with ptychographic CDI, we recently proposed [1] its exploitation to image atom probe samples. Atom probe tomography (APT) is highly complementary to transmission electron microscopy (TEM), as it enables nano-scale compositional analysis on 3D objects, which has triggered lots of attention in the semiconductor industry [4]. For APT analysis, the sample is shaped into a nano-sized object that resembles a tomography pin [2] but with much tighter aspect ratio and dimensions, i.e. the tip's endpoint has a radius of less than 100 nm, the length can be several hundreds to thousands of nanometer while the thickness of the sample changes along its z-axis with typical tapper angles around 5˚ to 10˚.
While APT is capable of atom-level resolution, the fidelity, and the resolution in APT is sample dependent. The reason is, in an atom probe microscope, the sample itself acts as the ion optics and thereby its shape and properties define the magnification during analysis.
Knowledge of the tip's actual shape, and the ability to monitor it during APT measurement is expected to provide substantial improvement in resolution and fidelity of APT reconstructions.
So far, most high-resolution EUV/X-ray ptychographic images were taken from thin film samples with imprints or holes, showing spatial resolution below 10 nm [3]. In this work we show the results of ptychographic imaging of APT tips with two distinct sources: soft x-ray produced by a synchrotron radiation at 800 eV (1.5 nm), and tabletop EUV light at 92 eV (13.5 nm). The shape of a typical APT tip significantly differs from both a typical thin planar sample for which the ptychography resolution is studied, and the more arbitrary 3D samples like grains or cells. The APT tip represents a conical needle with radius from 150 nm down to ~50 nm, where both the internal and surface structure of the top few hundred nm is of interest [4]. This leads to several challenges, on the one hand, the typically deployed planar approximation of the object is no longer valid, which leads to a decrease of resolution in the lower, and thus thicker part of the tip. On the other hand, the apex of the tip is very small both in lateral and axial dimensions. This leads to a miniscule change in the absorption and the phase shift resulting in low contrast and, consequently, also lower resolution, and higher requirements for the detector's dynamic range.

We demonstrate capabilities for quantitative analysis of chemical composition, shape determination and resolving of embedded structures. The imaging test was performed with two types of tips: Si fin and Mo/Si Multilayer, as the first one represents a 3D low-contrast structure and the second – a high-contrast layered structure. The fin-type tips analysis allows to study and demonstrate 3D imaging while the characterization of high-contrast layer structure allows analysis of the dependency of ptychography resolution on the thickness of the sample.

Using 800 eV light produced by a synchrotron together with a CDI setup with a 0.07 detection NA, on the example of the first needle we here demonstrate the ability to image buried interfaces with sub-30 nm resolution, while simultaneously determine the exterior geometry with 11 nm resolution as shown in Fig. 1 a,b.

Using the tabletop EUV source with 0.5 detection NA, we determine the exterior geometry of the second APT needle with 15 nm resolution, see Fig.1d. For comparison scanning electron microscope images of the two needles are presented in Fig. 1c, e, respectively. Please note that since the angle between the impinging SEM beam and the tip axis is 52 degrees, the SEM images are vertically elongated by 27% The EUV imaging clearly suffers from rather low signal-to-noise ratio due to large focal spot size (~20 µm) and sub-optimal EUV flux at our current setup compared to the synchrotron source. Nevertheless, we were able to resolve the needle exterior geometry in the colour-phase brightness-amplitude image (Fig 1.d) which perfectly matches SEM image (Fig 1.e).

Our first experimental results prove the feasibility of ptychographic imaging of APT tips using both synchrotron soft x-ray and tabletop EUV light sources. Ultimately, this might be a potential path forward to establish relevant information to feed into APT data reconstruction schemes to improve the spatial accuracy of reconstructed atom probe data [5].

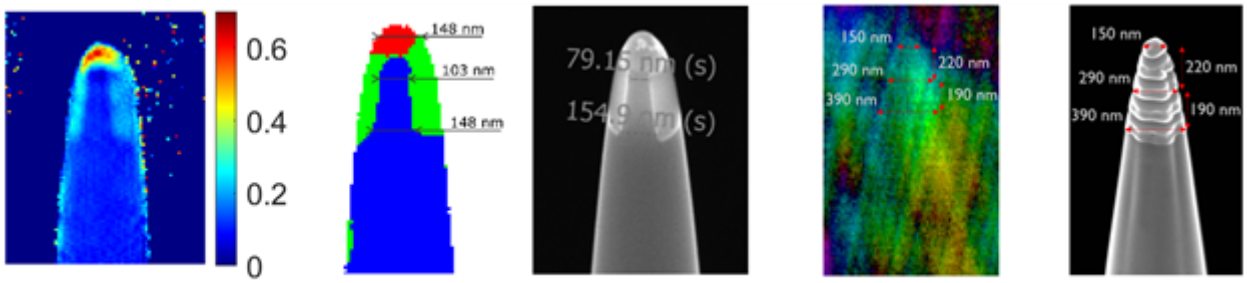

Keywords:

CDI, ptychography, EUV, x-ray, APT

Reference:

[1] P. van der Heide, I. Mathotkin, W. Vandervorst, and C. Fleischmann, “APT Tip Shape Modifications During Analysis, Its Implications, and the Potential to Measure Tip Shapes in Real Time via Soft-X-Ray Ptychography,” Microscopy and Microanalysis, vol. 25, no. S2, pp. 2504–2505, 2019

[2] M. Dierolf et al., “Ptychographic X-ray computed tomography at the nanoscale,” Nature 2010 467:7314, vol. 467, no. 7314, pp. 436–439, 2010

[3] J. Vila-Comamala et al., “Characterization of high-resolution diffractive X-ray optics by ptychographic coherent diffractive imaging,” Optics Express, Vol. 19, Issue 22, pp. 21333-21344, vol. 19, no. 22, pp. 21333–21344, 2011

[4] B. Gault et al., “Atom probe tomography,” Nature Reviews Methods Primers 2021 1:1, vol. 1, no. 1, pp. 1–30, 2021

[5] J. Op De Beeck et al., “The Prospect of Spatially Accurate Reconstructed Atom Probe Data Using Experimental Emitter Shapes,” Microscopy and Microanalysis, vol. 28, no. 4, pp. 1141–1149, 2022

583

Iterative Phase Retrieval Methods for Weakly Scattering Signals: Transfer of Information and Efficient Regularization

Georgios Varnavides[1,2], Dr Stephanie Ribet[2], Mr Reed Yalisove[2,3], Dr Mary Scott[2,3], Dr Colin Ophus[2]
[1]Miller Institute for Basic Research in Science, University of California, Berkeley, USA, [2]National Center for Electron Microscopy, Lawrence Berkeley Laboratory, Berkeley, USA, [3]Department of Materials Science and Engineering, University of California, Berkeley, USA

IM-03 (3), Plenary, august 29, 2024, 10:30 - 12:30

When a converged electron probe is scanned across a thin sample, it acquires phase-shifts due to sample interactions which scatter the incident electron wavefunction. Reconstructing these various scattering sources from phase-less measurements of the intensity at far-field detectors is a high-dimensional, non-convex, inverse scattering problem. Iterative electron ptychography is a phase-retrieval technique which attempts to solve this inverse problem using the redundant information in a set of converged-beam diffraction intensities with sufficient real-space illumination overlap [1], e.g., using defocused-probe 4DSTEM measurements [2].

We have recently introduced a general computational framework, implemented in the open-source analysis toolkit py4DSTEM [3], to reconstruct common coherent scattering sources using physically inspired forward and adjoint operators as-well as a suite of regularization constraints robust against common experimental artifacts. Here, we present recent experimental results using the ptychographic framework on a number of materials-science samples, including atomic defects in few-layer hBN, post-acquisition aberration correction on Au nanoparticles, few-layer twisted SrTiO3 moirés, and strain measurements in upconverting core-shell nanoparticles [4], as-well as biological samples, including single-particle analysis of frozen hydrated proteins at sub-nanometer resolution [5].

Moreover, we present simulated results on how the depth-resolution of these phase-retrieval methods can be extended by solving a joint inverse problem for orthogonal tilt-series directly to obtain the three-dimensional nature of scalar and vector scattering sources such as electrostatic (Figure 1a) and magnetic vector potentials (Figure 1b), respectively [3]. In contrast to "serial" ptychographic-tomography, where one performs 2D ptychographic reconstructions for each tilt projection before reconstructing the 3D object using standard tomographic methods, "joint" ptychographic tomography leverages the ability of multislice-ptychography to capture non-linear propagation, together with three-dimensional regularizations, to recover some information inside the "missing-wedge" due to sample-geometry limitations.

Finally, we discuss the transfer of information of iterative electron ptychography and derive various analytical expressions and numerical results for a white-noise model. We compare the results against other common iterative phase retrieval methods, notably differential phase contrast and tilt-corrected BF-STEM [3], to arrive at experiment design recommendations as a function of electron fluence and defocus (Figure 1c).

Phase-retrieval methods in STEM offer particular promise due to their remarkable dose-efficiency, enabling the observation of otherwise imperceptible signals, such as fields inside materials, and of radiation-sensitive materials, such as hybrid organic materials and biological samples.

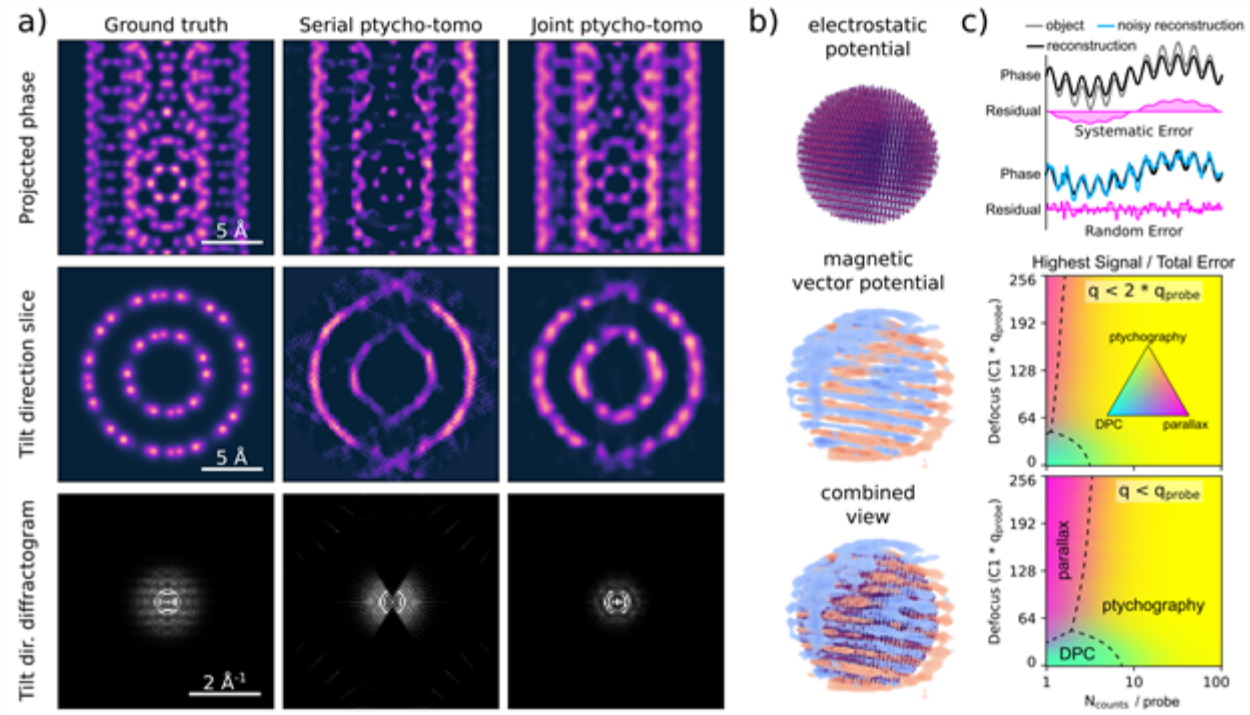

Keywords:

phase-retrieval, ptychography, tomography, single-particle analysis

Reference:

[1] J Rodenburg, A Maiden, Springer Handbook of Microscopy, (2019), doi: 10.1007/978-3-030-00069
[2] C Ophus, Microscopy and Microanalysis, 25 (2019), doi: 10.1017/S1431927619000497
[3] G Varnavides, S Ribet et al. arXiv:2309.05250 (2023), doi: 10.48550/arXiv.2309.05250
[4] S Ribet, G Varnavides et al. arXiv:2402.10084 (2024), doi: 10.48550/arXiv.2402.10084
[5] B Küçükoğlu et al., bioRxiv (2024) doi: 10.1101/2024.02.12.579607

633

Consistency and reliability of ptychographic deconvolution approaches

Tizian Lorenzen[1], Dr. Benedikt Diederichs[1,2], Charles Ogolla[3], Prof. Benjamin Butz[3], Prof. Knut Müller-Caspary[1]
[1]Ludwig-Maximilians-Universität, Munich, Germany, [2]Institute of Biological and Medical Imaging, Helmholtz Zentrum Munich, Neuherberg, Germany, [3]Micro- and Nanoanalytics Group, University of Siegen, Siegen, Germany

IM-03 (3), Plenary, august 29, 2024, 10:30 - 12:30

Background incl. aims
Control over and knowledge of the electron probe is important in all scanning transmission electron microscopy (STEM) techniques. This is emphasized even more in ptychography where the exact electron probe is required to deconvolve its effects from that of the specimen. Here the introduction of probe retrieval into iterative schemes has greatly increased their capability [1] and today iterative optimization of the electron probe is standard in most ptychographic schemes such as the extended ptychographic iterative engine (ePIE) [2]. However, in most cases the electron probe is reconstructed on a pixelated grid and thereby not limited to solutions physically realizable by the optical system. Here we present a method to characterize reconstructed probes by conventional lens aberrations. The fitted aberrations are then used to investigate the quality of the retrieved probes and their consistency is examined in a systematic study using 4D-STEM focal series recorded for a thin SnS2 2D-flake. Additionally, the influence of partial coherence and limited electron dose on the retrieved probes is analysed and the usefulness of the retrieved probes for different ptychographic methods, such as single sideband ptychography (SSB) and gradient descent-based schemes, is elucidated.

Methods
As a basis for the study 4D-STEM focal series were chosen as these datasets should only differ in defocus with the specimen and other aberrations being constant. 4D-STEM focal series were recorded of a thin SnS2 2D-flake using a Medipix3 detector and a probe corrected FEI Titan Themis STEM. ePIE reconstructions were performed using a GPU accelerated implementation in the pytorch framework. A probe fitting procedure was developed to fit axial lens aberrations up to third order by minimising the mean square error between the fitted probe and the ptychographic probe.

Results
The reconstructed phase gratings and the obtained probes are shown in Fig. 1. All phase gratings show the hexagonal atomic structure of the 2D-material with the heavy tin and lighter sulphur columns. Direct comparison is however hindered by specimen drift. The probes all show a strong contribution of coma. The excellent agreement between fitted and ptychographic probe is visible in both the real space amplitude and the reciprocal space phase plate (Fig. 1, bottom left). Here fitting against the complex wave function proved to be more successful than fitting the unwrapped reciprocal space phase plate. While fitting against only the real space intensity also worked it can result in the complex conjugate wave function i.e. a probe with opposite defocus.
Plotting the fitted defocus versus the defocus applied at the microscope shows the expected linear relationship (Fig. 1, middle). The other aberration coefficients are in very good agreement with each other (Fig. 1, right). The standard deviations for the mean aberration coefficients throughout the series are comparable to the ones obtained using a conventional Zemlin-tableau.
The obtained aberration coefficients are then applied to other ptychographic methods e.g. single-sideband ptychography, where only the correction of higher order aberration allowed the imaging of the atomic structure, or as a start for gradient-based maximum likelihood methods where multiple scattering and partial coherence are considered (Fig. 2).

Despite the good match between fitted and ptychographic probe some deviations appear, in comparison with the fitted probe the fine oscillations of the ptychographic probe vanish earlier into a noise background. Additionally, the reciprocal space amplitude deviates from theory, it is not flat inside and contains amplitude outside the apparent aperture. Simulations show that in our experiment these deviations are mainly produced by the limited electron dose while the effect of partial coherence is less important (Fig. 3). Experiments using CsPbBr3 nanocubes and gold nanoparticles additionally showed that the fitting procedure also performs well for thicker, strongly scattering specimen.

Conclusion

The successful fitting and good agreement of the aberration coefficients with each other indicate that the ptychographic deconvolution was effective and that the retrieved probes are physically meaningful. The good agreement of the aberration coefficients throughout the focal series suggests the use of the fitted aberrations to correct the alignment of the microscope during a session without requiring a dedicated alignment grid.

K.M.-C. and T.L. acknowledge funding from the DFG, contract EXC 2089/1-390776260 (Excellence Cluster e-conversion).

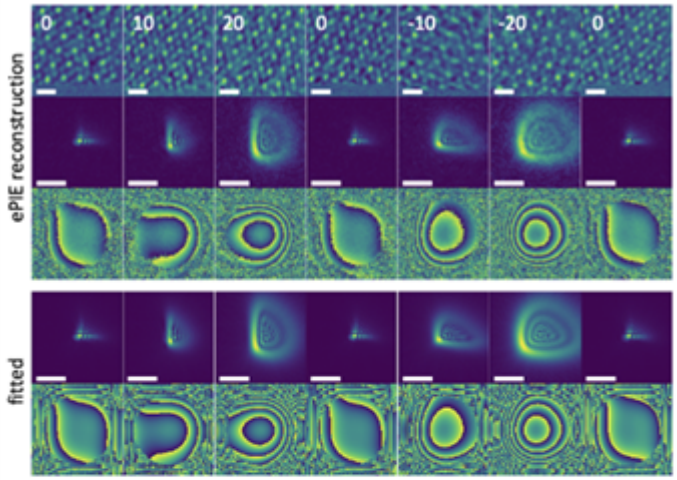

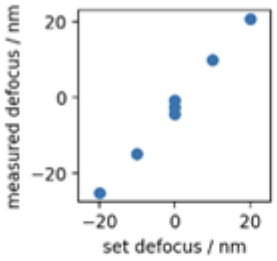

aberration	mean / nm
A_1	2.3 ± 0.5
A_2	106.9 ± 11.7
B_2	223.9 ± 11.4
C_3	-530.5 ± 3239.9
S_3	146.4 ± 370.2
A_3	392.6 ± 371.3

Fig. 1: **Top Left:** Phase grating (top) with foci (nm), probe (middle), aberration function (bottom) from ePIE. **Bottom Left:** Probe fit. **Middle** Plot of the fitted defocus vs. the one set at the microscope. **Right** Average aberration coefficients and their standard deviations calculated from the complete focal series.

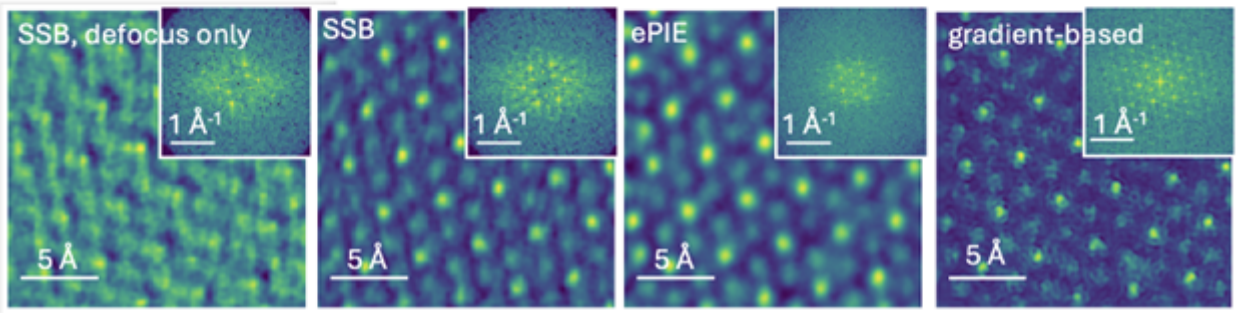

Fig. 2: Ptychographic reconstructions obtained using the fitted aberration coefficients. The inclusion of higher order aberrations significantly increases the quality of the SSB (**Left, Middle Left**) making it comparable to the specimen retrieved using ePIE (**Middle Right**). The same aberration coefficient can then be applied to more complex reconstructions such as maximum likelihood methods. Single slice from a gradient-based three-slice inverse multislice reconstruction including the effect of partial coherence performed using the fitted aberration coefficients (**Right**). The insets show the power spectra.

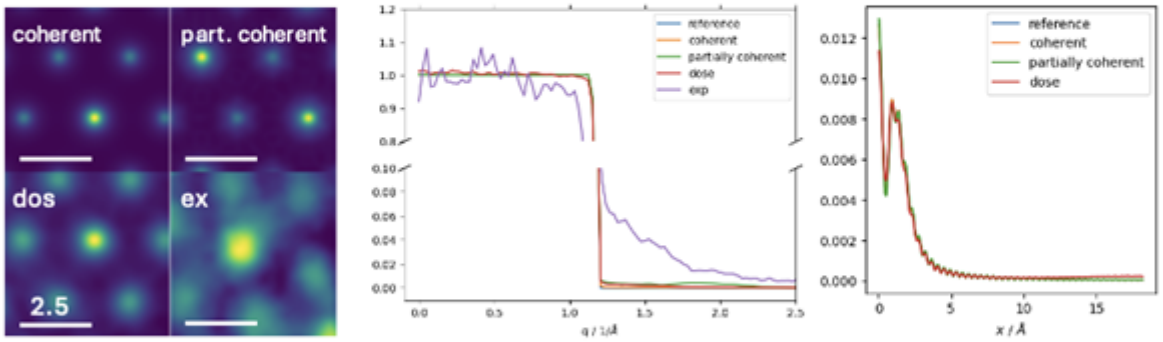

Fig. 3: **Left** Phase gratings obtained using ePIE for simulated data assuming perfect coherence, including the effects of partial spatial and temporal coherence, including Poisson noise with a dose comparable to the experiment and a phase grating obtained using experimental data. **Middle** Radial averages of the reconstructed reciprocal space apertures show a loss of sharpness when including partial coherence and electron dose, an effect that is even more pronounced in the experiment. **Right** Radial average of real space probe intensities reconstructed using ePIE for simulated data. Particularly the inclusion of dose effects suppresses the oscillations of the probe amplitude.

Keywords:

Ptychography, 4D-STEM, Aberrations

Reference:

[1] Thibault et al. Ultramicr. 109, 338 (2009).
[2] Maiden et al. Ultramicr. 109, 1256 (2009).
[3] Rodenburg et al. Ultramicr. 48, 304 (1993).
[4] Diederichs et al. Nat Commun. 15, 101 (2024).

1164

Quantum Measurements using Interferometric STEM-EELS

Professor Benjamin McMorran[1], Dr. Cameron Johnson[1,2], Dr. Amy Turner[1]
[1]Department of Physics, University of Oregon, Eugene, USA, [2]Molecular Foundry, Lawrence Berkeley National Laboratory, Berkeley, USA

IM-03 (3), Plenary, august 29, 2024, 10:30 - 12:30

Background incl. aims
Nanoscale amplitude beamsplitters for electrons enable flexible electron interferometry in STEM instruments. Nanofabricated materials phase gratings provide a way to coherently diffract electron wavefunctions into different paths, and can easily be placed in probe-forming apertures of unmodified TEM instruments. These tools provide a way to manipulate both the phase, amplitude, and momentum of electrons [1]. This lends itself to the implementation of new interferometric methods in electron microscopy [2-4], with the ultimate goal of performing quantum measurements in the TEM.

Methods
We used a pair of nanoscale phase gratings as diffractive amplitude beamsplitters to provide a Mach-Zehnder electron interferometer inside an unmodified TEM [2]. One phase grating beamsplitter coherently divides the electrons into separated probes before the specimen, and the second beamsplitter recombines the paths after the specimen, creating a set of discrete interfering outputs. This enables several new imaging and measurement modalities. For example, phase contrast imaging can be provided if one of the probes transmits through a specimen region while the other passes through vacuum, acquiring a relative phase shift that can be recorded by monitoring a discrete electron beam output.
The setup also enables quantum-inspired measurements, such as interfering electron paths that have lost energy to the specimen. If the interferometer is tuned to provide destructive interference at the detector, blocking one of the probe paths with an object eliminates the destructive interference, allowing a non-zero probability current to be incident on the detector. This is a quantum interrogation method sometimes called “interaction-free” measurement, because a detection event in a dark detector indicates the presence of an absorbing sample; the electrons that did not scatter from the sample indicate its presence.

Results
We demonstrated using the 2-grating electron interferometer for STEM phase imaging of nanostructures [2], even using only inelastically scattered electrons [3]. We used this to determine that fast electrons passing on either side of a metallic nanoparticle that excite a plasmon acquire a relative π phase difference, corresponding to the symmetry of an optical dipole excitation. We also used the setup to demonstrate a quantum “interaction-free” measurement of the presence of an opaque object [4]. In this case, single electron events recorded at the detector indicate the presence of an object without scattering from or transmitting through it.

Conclusion
We used nanoscale phase gratings to implement electron interferometry in STEM without modifying the instrument other than an aperture change. Potential advantages of the techniques this enables relative to other methods will be discussed.

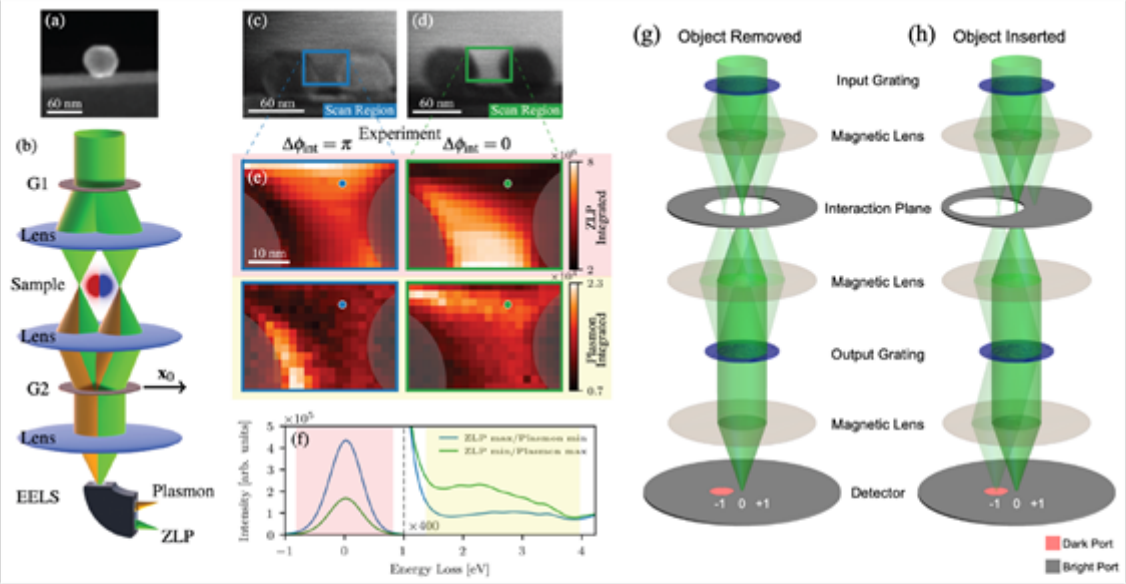

Figure 1 – (a-f) Adapted from [4]. (a) ADF-STEM image of a 60 nm gold nanoparticle (NP) isolated on the edge of a carbon substrate. (b) A two-grating electron Mach Zehnder interferometer consisting of a STEM with two gratings used as beamsplitters. The first grating (G1) divides electrons in a superposition of two separate paths, each of them interacting with the NP sample, with some probability of losing energy to an excitation such as a plasmon resonance (orange). (c,d) The electron paths are then recombined using the second grating (G2), which can be positioned for (c) destructive (blue borders) and (d) constructive (green borders) interference, conversely modifying the elastic and inelastic signals. (e,f) For both alignment schemes, we integrate over the plasmon (yellow-shaded) and ZLP (red-shaded) regions of the energy loss spectra (f) at every scan location to create the spectral images shown in (e). The raw spectra in (f) correspond to the dotted positions in (e). (g) and (h), borrowed from [5], illustrate the interaction free measurement.

Keywords:

Electron interferometry, electron holography

Reference:

[1] Johnson, C. W., Bauer, D. H. & McMorran, B. J. Improved control of electron computer-generated holographic grating groove profiles using ion beam gas-assisted etching. Appl. Opt. 59, 1594–1601 (2020).
[2] Johnson, C. W., Turner, A. E. & McMorran, B. J. Scanning two-grating free electron Mach-Zehnder interferometer. Phys. Rev. Research 3, 043009 (2021).
[3] Johnson, C. W., Turner, A. E., García de Abajo, F. J. & McMorran, B. J. Inelastic Mach-Zehnder Interferometry with Free Electrons. Phys. Rev. Lett. 128, 147401 (2022).
[4] Turner, A. E., Johnson, C. W., Kruit, P. & McMorran, B. J. Interaction-Free Measurement with Electrons. Phys. Rev. Lett. 127, 110401 (2021).
[5] The author gratefully acknowledges collaboration with Pieter Kruit (Delf University) and Javier García de Abajo (ICFO). This material is based upon work supported by the National Science Foundation under Grant No. 2012191.

85

Near-Ideal Direct-Electron Focused-Probe 4D-STEM Data for Open-Source Phase Reconstructions

Prof. Toma Susi[1], Niklas Dellby[2], Russ Hayner[2], Christoph Hofer[3], Jani Kotakoski[1], Tracy Clark Lovejoy[2], Clemens Mangler[1], Andreas Mittelberger[2], Timothy J. Pennycook[3], Benjamin Plotkin-Swing[2]
[1]University of Vienna, Faculty of Physics, Vienna, Austria, [2]Nion Co. R&D, Kirkland, USA, [3]EMAT, University of Antwerp, Antwerp, Belgium

IM-03 (4), Plenary, august 29, 2024, 14:00 - 15:00

Background incl. aims
The availability of direct-electron cameras with high dynamic ranges and very fast detection speeds is revolutionizing the ability of scanning transmission electron microscopy (STEM) to make use of every electron for virtual imaging and advanced computational phase reconstructions. State of the art detectors can now acquire four-dimensional (4D) data at STEM pixel dwell times of over 100,000 diffraction patterns per second while counting each electron.

At the same time, the proliferation of open software packages to make use of this data has made such analyses widely accessible, and due to a convergence to the Python programming language, easy to compare in terms of computational efficiency and reconstruction quality.

Methods
The first commercially available Dectris ARINA detector [1] has been installed in the Nion UltraSTEM100 instrument in Vienna, where an ultra-stable sample stage and flexible electron optics are ideally suited to 4D-STEM. For our initial comparisons, we use an atomically focused probe (34 mrad convergence semi-angle) and choose a camera length optimized for maximum signal in the bright-field and the first-order Bragg disks.

In this contribution, we present some of the first data acquired on this new detector, namely convergent-beam electron diffraction maps of pristine monolayer graphene, which is a near-ideal dose-robust uniform atomic phase object. The ability to reliably count electrons at such speeds (the detective quantum efficiency is 0.85 at 60 keV [1]) also enables the variation in beam current to be easily measured and, if desired, corrected for, which we find has an appreciable impact on the bright-field signal and reconstructions that make use of it (most notably parallax imaging [2]).

Results
A pixel exposure time of 100 µs provided a high signal for phase reconstructions without needing to resort to multi-frame averaging. The ARINA is able to bin the native 192×192 detector array in hardware for faster acquisition, and we find that further software binning up to four times does not harm reconstructions, whereas a dense real-space sampling below 0.08 Å per pixel (512×512 px scan over the 2×2 nm² field of view) was noticeably helpful.

The graphic shows the concurrently acquired high-angle annular dark-field (HAADF, 80–300 mrad) and virtual ADF images (~40–80 mrad), as well as a range of open-source phase reconstructions from the binned 4D dataset: single-sideband (SSB) and Wigner distribution deconvolution (WDD) [3], as well as iterative differential phase contrast (DPC), parallax-corrected bright-field imaging, and batched iterative gradient descent single-slice ptychography [2]. Apart from modest scan distortions, visual inspection of the phase images reveals deviations from the expected uniform atom contrast, and notable differences in phase magnitudes. Computational times also vary greatly depending on the algorithm and the binning.

Conclusion

The quality of the phase images is assessed by evaluating the variation of atomic phase shifts using a robust parameter-based quantification method [4] and compared to data simulated with the abTEM code [5] and reconstructed with the same algorithms. These quantitative comparisons will be presented at the meeting, where the data and code will also be provided. Further results on defocused-probe datasets and the prospects for live reconstructions will be discussed.

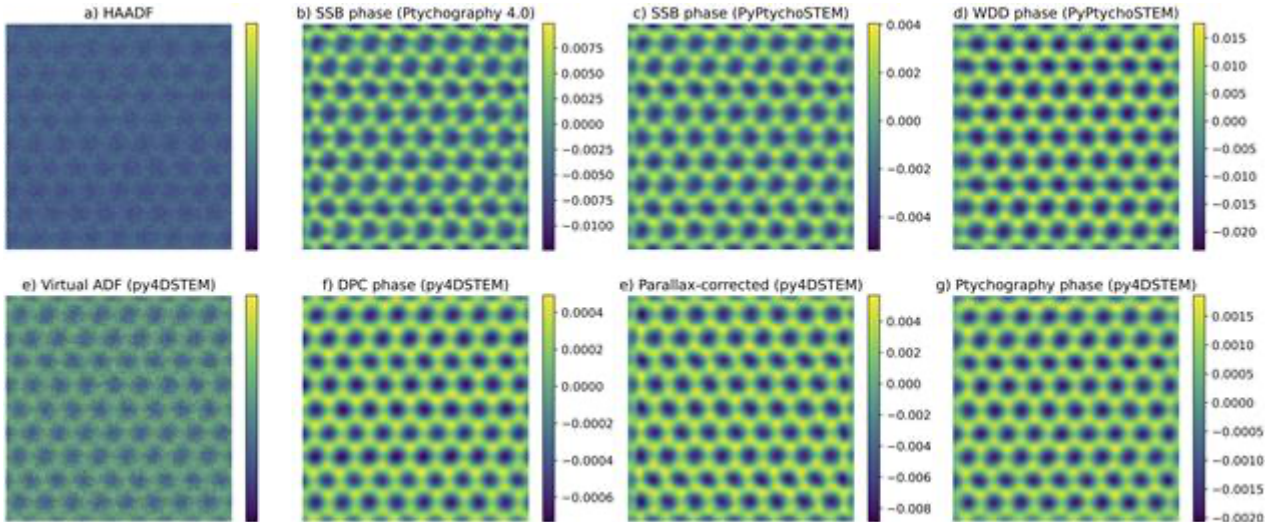

Keywords:

4D-STEM, graphene, direct-electron-detection, ptychography, phase-reconstruction

Reference:

1. P. Zambon et al., Front. Phys. 11 (2023), p. 1308321
2. G. Varnavides et al., arXiv:2309.05250 (2023)
3. T.J. Pennycook et al., Ultramicroscopy 151 (2015), pp. 160–167
4. C. Hofer and T.J. Pennycook, Ultramicroscopy 254 (2023), p. 113829
5. J. Madsen and T. Susi, Open. Res. Europe 1:24 (2021)

390

Thermal vibrations in inverse dynamical electron scattering

Ziria Herdegen[1], Dr. Benedikt Diederichs[2], Prof. Dr. Knut Müller-Caspary[1]
[1]Depart. Chemistry, Ludwig-Maximilians-Universität München, Munich, Germany, [2]Institute of Biological and Medical Imaging, Helmholtz Zentrum München, Neuherberg, Germany

IM-03 (4), Plenary, august 29, 2024, 14:00 - 15:00

Background incl. aims
Inverse multislice (IM) schemes have enabled structure retrieval in the presence of dynamical scattering, extending the applicability of electron ptychography assuming single scattering. This allows structure determination for thick specimens with super-resolution, to date only limited by the thermal atomic vibrations [1]. These thermal vibrations cause thermal diffuse scattering (TDS) which becomes partly dominant at elevated specimen thickness. Since the TDS governs the darkfield in diffraction patterns (DP) which contains crucial information about the atomic structure and chemical composition, its correct consideration in IM is a prerequisite for accurate specimen retrieval. Because various IM approaches evolved, differing by their implicit or explicit consideration of TDS, studying the impact on specimen structure reconstructions suggests itself. For this purpose different slicing concepts are studied as to the effect of TDS on the reconstruction and on the capabilities to yield atomic types and thermal mean square displacements, thus local temperature, quantitatively [2].
Methods
The multislice approach calculates momentum-resolved STEM data by propagating an electron wave through a set of slice transmission functions (STF), mathematically performed by iteratively multiplying the wave function with one STF and then propagating it to the next slice, e.g., formulated as an artificial neural network [3]. The inverse model then applies a loss function to the calculated DPs and those of the reference data set and minimizes the loss by optimizing the STF to reconstruct the specimen structure. To this end the home-built, gradient-based TorchSlice program utilizing the PyTorch framework was used [4]. We discuss the influence of TDS on three different optimization models performing reconstructions of simulated momentum-resolved STEM data for an SrTiO3 crystal as the ground truth. To incorporate TDS in the simulation we used the frozen phonon (FP) model which incoherently averages multiple diffraction patterns calculated from different phonon ensembles. First we optimize one slice transmission function pixel-wise which is reused to describe the interaction in each slice, precluding any ensemble averages thus being incapable to incorporate TDS correctly. Second, 50 slices are optimized pixel-wise and individually, providing the opportunity of incorporating TDS by allowing displacements of atomic potential maxima from their equilibrium position from slice to slice [5]. Third, a parameterized approach [4] is used which constrains the STF to be a sum of atomic potential functions, and a set of specimen parameters characterizing the STF is optimized every iteration. This model incorporates a full FP simulation ensuring physically correct inclusion of TDS within the FP approximation using the Einstein model.
Results
Optimizing wrapped slices pixel-wise the STF's phase grating (PG) shows stripe-like artefacts superimposed to the atomic structure (Fig. 1a), not being physically reasonable but reproducing the diffuse intensity in the corresponding DPs (Fig. 1b). It is shown that the strength of the artefacts and the cutoff angle up to which the loss is calculated are directly correlated. Restricting the solid angle such that TDS is excluded from the loss calculation, or using different regularization methods was found to successfully suppress the artefacts in the PG, however, suppressing the diffuse intensity in the DPs, too (Fig. 2). Optimizing each STF individually, the diffuse intensity was reconstructed very accurately (Fig. 3a). The phase maxima at the atomic sites are displaced from their equilibrium position, following a slightly narrowed Gaussian function (Fig. 3b) having, however, a standard deviation of only 28% and 12% of the theoretical values for the Sr and the O columns, respectively.

Still showing artefacts in the PG, the diffuse scattering within this model is produced via both, physically reasonable but too small thermal displacements and artificial phase noise to achieve numerical consistency with the ground truth. The parameterized optimization approach achieved the smallest DP error compared to the other optimization methods, and could retrieve the atomic phases very accurately which has been observed case-dependent for pixel-wise approaches. Also the mean thermal displacement could be received with an accuracy of at least 89%. The accuracy of both parameters is shown to increase with increasing number of phonon ensembles underlining the importance of incorporating TDS correctly. A final simulation study examining the sensitivity of the loss to the atom type and the mean thermal displacements clarifies the observed accuracy of these parameters and is used to outline the capability of IM to map the local chemistry by including TDS-affected Z-contrast in the inverse FP multislice model.

Conclusions

Different IM slice optimization concepts show a varying accuracy of reconstructed parameters among the models i.e. maximum atomic phases and mean thermal displacement and, when explicitly precluding thermal displacements from the model, the occurrence of physical unreasonable phase artefacts. We show various ways for suppressing these artefacts to achieve a smooth PG. In particular, we also demonstrate that for retrieving quantitative information on temperature and chemical composition, including TDS in IM within the FP approach is essential.

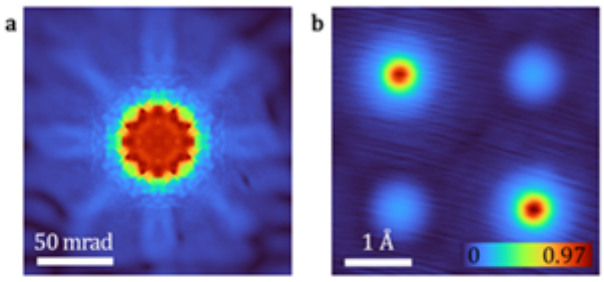

Fig. 1: a. Position-averaged convergent-beam electron diffraction (PACBED) pattern (square root scale) and **b.** PG of the IM reconstruction optimizing one repetitively used STF pixel-wise.

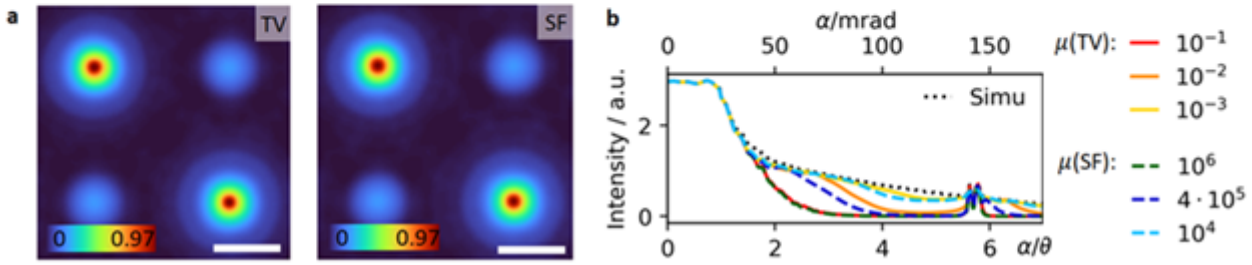

Fig. 2: a. PG with suppressed artefacts using total variation (TV) and sparse frequency (SF) regularization. **b.** Radially averaged PACBEDs of reconstructions using both regularization methods weighted with different factors μ showing a suppression of the diffraction intensity at high angles as μ increases.

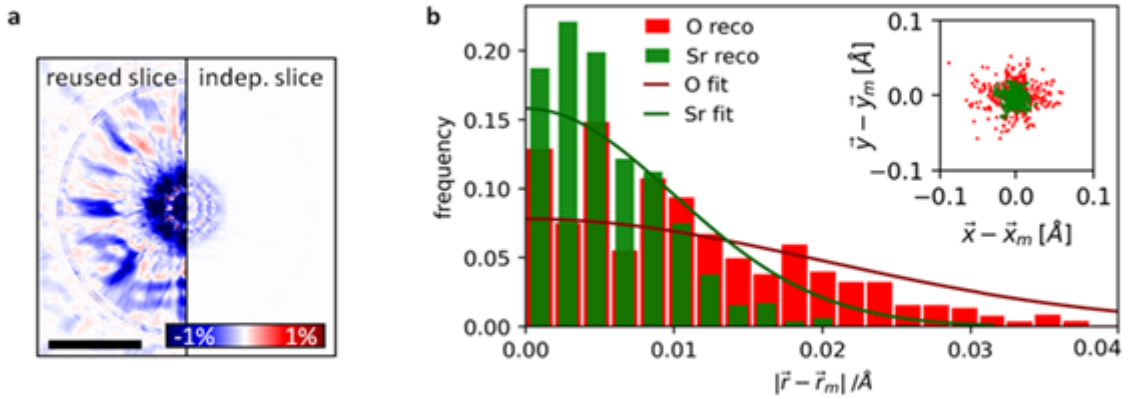

Fig. 3: a. Relative error of the PACBED images of the reconstruction to the simulation for the reconstruction optimizing one repetitive used STF pixel-wise (left) and optimizing 50 STFs independently (right). **b.** Histogram and scatter plot of too small atomic displacements received by the latter model following a slightly narrowed Gaussian function.

Keywords:

STEM, Inverse Multislice, Thermal Vibrations

Reference:

[1] Chen, Z. et.al. Science, 372(6544), 826–831 (2021).
[2] Herdegen, Z., Diederichs, B., Müller-Caspary, K., Thermal vibrations in inverse dynamical electron scattering, submitted.
[3] Van den Broek, W., Koch, C. Phys. Rev. Lett. 109, 245502 (2012).
[4] Diederichs, B., Herdegen, Z., et al. Nat Commun 15, 101 (2024).
[5] Gladyshev, A., et.al. arXiv:2309.12017 (2023).

555

Influence of the loss function on gradient-based iterative ptychographic reconstructions in 4D-STEM

Max Leo Leidl[1,2], Carsten Sachse[2,3], Knut Müller-Caspary[1,2]
[1]Ludwig Maximilian University of Munich, Munich, Germany, [2]Ernst Ruska-Centre, Forschungszentrum Jülich GmbH, Jülich, Germany, [3]Heinrich Heine Universitöt Düsseldorf, Düsseldorf, Germany

IM-03 (4), Plenary, august 29, 2024, 14:00 - 15:00

Background incl. aims
The noise model of a detector's counting process is known as Poisson shot noise. However, direct reconstruction algorithms like single-sideband (SSB) or Wigner-distribution deconvolution (WDD) do not assume a specific noise model. This is not the case for gradient descent-based iterative methods that allow the free choice of the loss function and, therefore, the underlying noise model. In practice the mean square error (MSE), also known as L2 loss, is often used, which assumes Gaussian white noise. This is a good approximation for the Poissonian statistics for high counts.
In contrast, the (extended) iterative engine (e)PIE assumes no specific noise model. However, Melnyk showed that ePIE can be seen as a particular case of stochastic gradient descent using the MSE Loss on the amplitudes instead of the intensities [1], which we will call the Amplitude loss function in the following. The amplitude loss can be derived from the Poisson loss function via a Taylor expansion, assuming that the specimen guess is close to the original specimen [2] and, therefore, an approximation of the Poisson loss.
The interest in using STEM for low-dose applications has grown in recent years, e.g., to examine dose-sensitive, weakly scattering specimens like covalent or metal organic frameworks (COFs/MOFs), or 2D materials. Moreover, the interest rises to explore STEM for imaging proteins and lamellae of cells [3, 4, 5], which are very dose-sensitive. Therefore, we perform a detailed analysis of the influence of the loss function on the reconstruction accuracy using a gradient descent approach for the L1, MSE, amplitude and Poisson losses.
Methods
We used a MoS_2 monolayer as a test case to perform STEM simulations and experiments. Simulations were conducted with an acceleration voltage of 60 kV and 300 kV with a convergence semi-angle of 18 mrad, in focus with a dose of 10^6 electrons per diffraction pattern. The high-dose case is of particular interest because the dark field (DF) contains very few counts.
To better understand the loss functions, we compare different virtual detector geometries. Firstly, we compare the results of the full pixelated detector for 300 kV and 60 kV. Subsequently, only an acceleration voltage of 300 kV is used. Secondly, we use the pixelated bright field (BF) disc in combination with virtual ring detectors for the dark field. Thirdly, we use only the BF disc. The results suggest that the choice of the loss function makes a difference if a wide dynamic range of electron counts is measured. Therefore, we explore the BF disc again, but this time with more features in the BF disc introduced by an under-focused electron probe of 25 nm. Finally, we go back to the first case using 300 kV and stepwise reduce the dose to 10000 and 100 electrons per diffraction pattern for sparse-count dark field studies.
Results
Figure 1 depicts reconstruction results using different loss functions and high (left) as well as low (right panels) dose. The differences between the reconstructed objects using various loss functions are significant if the signal involves a wide dynamic range of electron counts. This applies to the high-dose case (left) in which the signal levels of the BF disc and the DF differ significantly. It is best seen in the power spectra (c) where Poisson and Amplitude losses lead to reconstructed object transmission functions containing the highest spatial frequencies, followed by the L1 loss result. Note that only the

Poisson loss leads to a flat spatial frequency transfer, whereas the other methods pronounce Fourier coefficients within a band of twice the probe-formin aperture radius. The line profile in (d) exhibits the sharpest peaks for the Poisson loss. Chemical contrast between a Mo monomer and S dimer is only represented in the phase of the Poisson and amplitude loss functions, respectively.
An electron dose of 100 electrons per diffraction pattern on the right of Fig. 1 appears as a limiting case for all losses considered here, with the Poisson loss still performing best. However, the difference to the MSE loss becomes smaller than for the high-dose case.
The counts in the DF are sparse, so we used virtual ring detectors for the DF to perform an azimuthal integration to get a more robust measurement. In this case, the differences between the loss functions became smaller and the chemical contrast accessible. Excluding the dark field counts and only using the BF, all loss functions lead to comparable reconstructions because the dynamic intensity range in the BF itself is rather small. Moreover, the introduction of more features into the BF disc by an under-focus increases the dynamic range slightly, but the variation is too small to pronounce one of the loss concepts against others.

Conclusion

Our results show that the differences between the loss functions become large for a broad dynamic range of electron counts, which is the case for high-dose measurements when the BF and DF are of interest at the same time, is relevant for chemical contrast found accurately represented in the phase of the Poisson loss based reconstruction. The MSE loss assumes a constant Gaussian noise distribution and the same standard deviation for all pixels. In contrast, the standard deviation of the Poisson loss scales with the square root of the number of counts. This makes a difference for a wide dynamic range in measurements and is consistent with our results. Our results suggest that the differences between the MSE and Poisson loss become small for dose-sensitive materials because sparse counts are measured and, as a result, a very low dynamic range. However, the Poisson loss is still beneficial at high frequencies and shows a lower variance of the reconstruction. In addition to the simulations, our study includes dose-dependent MoS_2 measuremts as well, which will be used to demonstrate the reliability of the theoretical findings in practice.

Funding

Funding from the European Research Council under Grant Agreement 101118656 (ERC Synergy project 4D-BioSTEM) is kindly acknowledged.

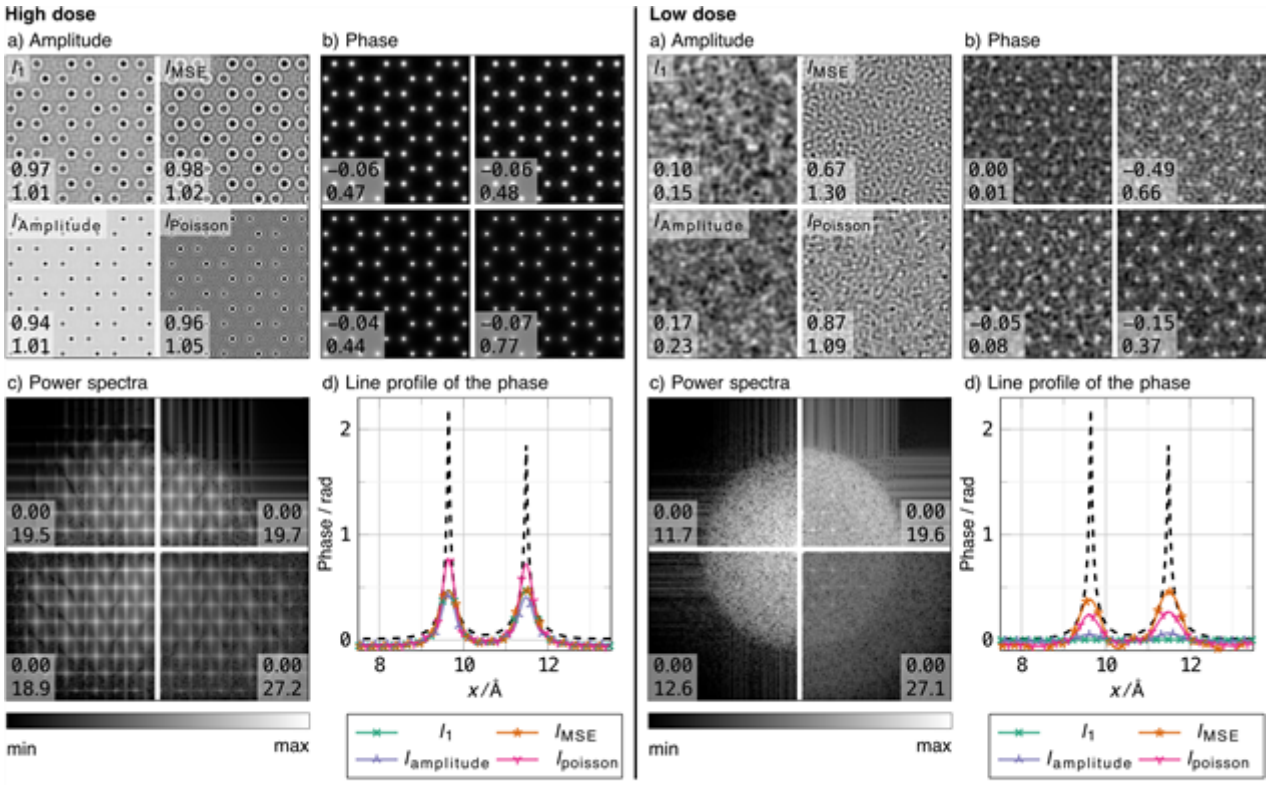

Figure: Left/right reconstruction for the different loss functions as annotated in (a) for the high/low dose case with 10^6/100 electrons per diffraction pattern. (a) - (c) Amplitude, phase and power spectrum for the different loss functions the values indicated in the image are the min and max values. (d) Average line profile of the phase trough a Mo and two S atoms. The phase of the ground truth is shown as a black dashed line in the background.

Keywords:

Loss functions, low-dose, gradient descent

Reference:

[1] Melnyk, Oleh. "Convergence properties of gradient methods for blind ptychography." arXiv preprint arXiv:2306.08750 (2023).
[2] Thibault, Pierre, and Manuel Guizar-Sicairos. "Maximum-likelihood refinement for coherent diffractive imaging." New Journal of Physics 14.6 (2012): 063004.
[3] Lazić, Ivan, et al. "Single-particle cryo-EM structures from iDPC–STEM at near-atomic resolution." Nature Methods 19.9 (2022): 1126-1136.
[4] Zhou, Liqi, et al. "Low-dose phase retrieval of biological specimens using cryo-electron ptychography." Nature communications 11.1 (2020): 2773.
[5] Leidl, Max Leo, Carsten Sachse, and Knut Müller-Caspary. "Dynamical scattering in ice-embedded proteins in conventional and scanning transmission electron microscopy." IUCrJ 10.4 (2023).

969

Transport of Intensity Phase Retrieval in the Presence of Intensity Variations and Unknown Boundary Conditions

Daniel Wolf[1], Radmila Kyrychenko[1], Max Herzo[1], Oleksandr Zaiets[1], Axel Lubk[1]
[1]Leibniz Institute for Solid State and Materials Research, Dresden, Germany

IM-03 (4), Plenary, august 29, 2024, 14:00 - 15:00

Background incl. aims

The so-called Transport of Intensity Equation (TIE) phase retrieval technique is widely applied in light, x-ray and electron optics to reconstruct, e.g., refractive indices or electric and magnetic fields in solids [1,2]. The TIE method reconstructs the phase from two or three mutually slightly defocused microscopy images by solving an elliptic partial differential equation – the TIE. Here, we present a largely improved TIE reconstruction algorithm, which properly considers intensity variations as well as unknown boundary conditions in a finite difference implementation of the Transport of Intensity partial differential equation. [3] That largely removes reconstruction artifacts encountered in state-of-the-art Poisson solvers of the TIE, hence significantly increasing the applicability of the technique. Notwithstanding, its widespread proliferation the TIE method in its predominantly employed form suffers from a number of fundamental challenges that often introduce reconstruction artifacts and hence degrade the information obtained from the phase: (I) Intensity variations of the wave functions are frequently either neglected or considered in an incomplete way, e.g., by equating the phase with the scalar "potential" pertaining to irrotational (particle) currents. (II) The boundary conditions (BCs) required to solve the TIE are often not known and strongly deviate from homogeneous Dirichlet, Neumann, or periodic Bcs, used in TIE solvers. (III) The reconstruction of small spatial frequencies in the phase is mildly (i.e., algebraically) ill-conditioned and, hence, requires regularization to suppress error amplification. Indeed, the above three challenges are intertwined in practical applications, because, e.g., erroneous long-range phase variations due to erroneous BCs or neglected amplitude variations are suppressed by regularization at the expense of introducing a regularization error. Here, we report on a TIE reconstruction algorithm that properly considers intensity variations, allows retrieving the correct BCs through a variational scheme, and can be additionally regularized, if necessary.

Methods

We numerically solve the TIE using a finite difference scheme: the equidistant x and y sampling points of the 2D image intensity are interlaced so that the phase and intensity at the sampling points may be represented as vectors. Subsequently, the directional derivatives along x and y are approximated by the left- and right-sided difference to the nearest neighbors, which can be written as a multiplication with bidiagonal matrices. With these building blocks, the whole TIE may be written as a system of linear equations, which can be inverted numerically to yield the phase. In order to suppress error amplification, the linear equation system may be additionally regularized by a Tikhonov scheme. In order to incorporate arbitrary inhomogeneous Dirichlet BCs, the discrete phase image is embedded in a frame comprising one pixel. The values of the phase on this frame (i.e., the unknown Dirichlet BCs) are retrieved through a variational scheme that minimizes the difference between the experimental defocused image intensities and the numerically defocused intensities obtained from the TIE reconstruction. To facilitate sufficiently fast convergence only a small number of Fourier coefficients of the BC function are retrieved in practice. The values on this frame are then assigned to Dirichlet BCs. The above system of equations is solved in a numerically efficient way by exploiting sparse representations and sparse equation solvers.

Results

We demonstrate the improved performance of the TIE reconstruction algorithm at a set of simulated and experimental image intensities arising from magnetic structures investigated in TEM, focusing on Landau domain pattern in geometrically confined permalloy thin films. They consist of magnetic vortices and antivortices and are suited to demonstrate the main features of the enhanced TIE reconstruction (Fig. 1), namely consideration of intensity variations (Figs. 1a-c), automatic determination of nontrivial BCs (Figs. 1d-f), and its application on an experimental example (Figs. 1g-i).

Conclusion

We have demonstrated that solving the TIE with the help of a finite difference scheme incorporating a variation of the boundary conditions largely mitigates reconstruction artifacts encountered with the previously used Poisson reconstruction schemes. The reconstruction algorithm reduces or even removes the need for additional regularization and mostly improves the reconstruction of long-range variations of the phase. That opens new avenues for TIE reconstructions, where intensity variations cannot be avoided, and long-range fields are important (e.g., vector field electron tomography). Further improvements of the algorithm hinge on further optimization of the optimization algorithm employed for determining the boundary conditions, faster sparse matrix solvers, and transition from a finite difference to a finite elements scheme (that allow adaptive meshing), amongst others.

Fig. 1. TIE reconstructions for specific cases of magnetic Landau domain patterns. a) Simulated amplitude variation of a vortex configuration at the position of the vortex core. b,c) Magnetic induction reconstructed using conventional (Poisson) (b) and improved TIE (c) algorithm including the amplitude variations (a). d) Simulated magnetic induction of Antivortex pattern. e,f) Magnetic induction reconstructed of (d) using Poisson algorithm (e) and improved TIE (f) algorithm in the presence of unknown boundary conditions. g) Lorentz TEM image of a permalloy film with vortex-antivortex pair taken at an underfocus of 1mm. The scalebar corresponds to 1.5 µm. h,i) Magnetic induction reconstructed of (g) using Poisson algorithm (h) and improved TIE (i) algorithm.

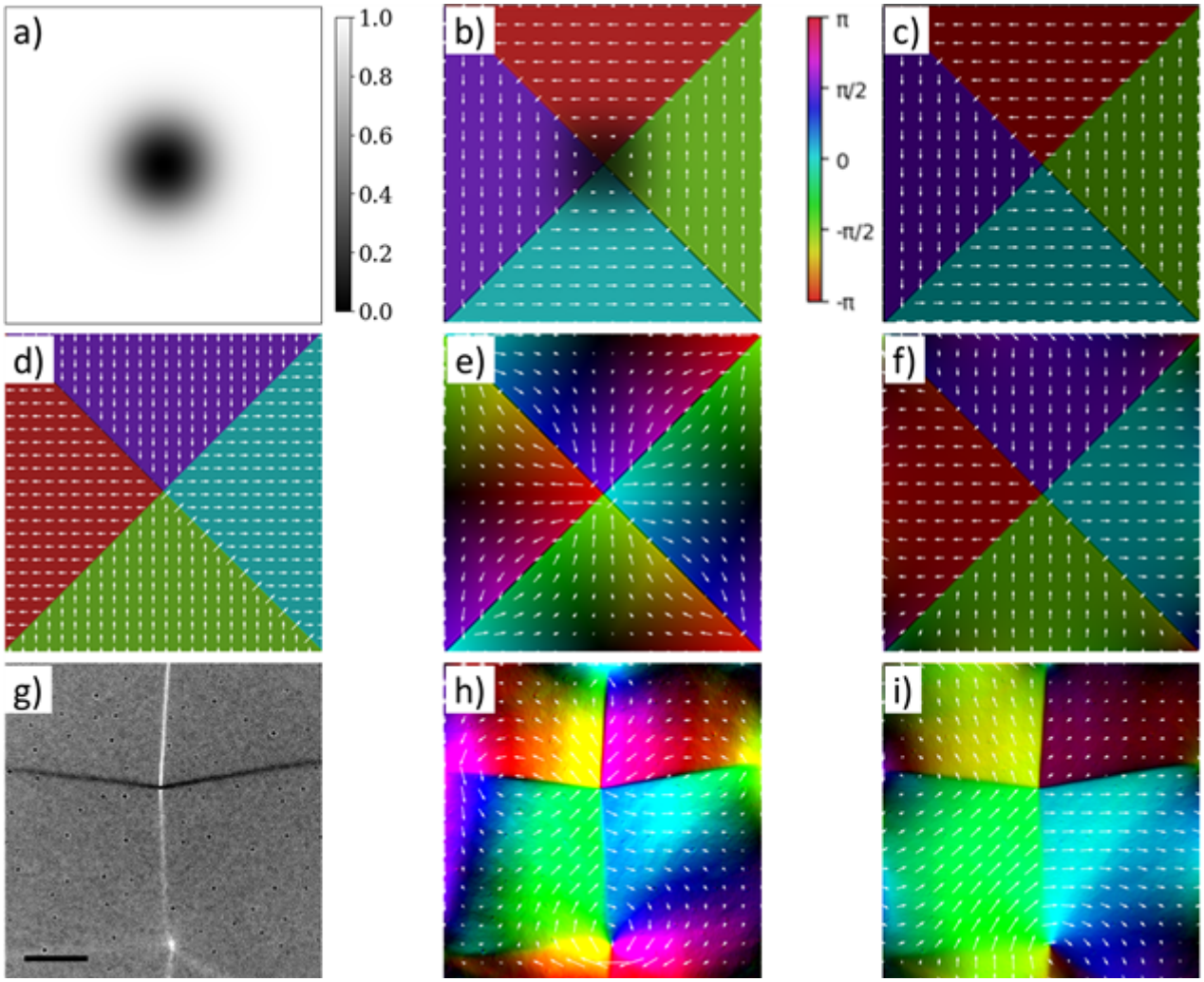

Keywords:

Holography, Phase Retrieval, Magnetic Imaging

Reference:

[1] M. R. Teague, J. Opt. Soc. Am. 73 (1983) 1434
[2] C. Zuo et al., Optics and Lasers in Engineering 135 (2020) 106187
[3] A. Lubk et al., arXiv:2401.03744 (2024)
[4] We acknowledge financial support by the Collaborative Research Center SFB 1143 (project-id 247310070).

50

Electron holography for electrostatic potential measurement and contrast enhanced imaging of biological samples

Dr Elio Karim[1,2,4], Mr. Bumsu Park[1], Mr. Christophe Gatel[1], Ms. Amélie Le Forestier[3], Ms. Vanessa Soldan[2], Ms. Stéphanie Balor[2], Ms. Célia Plisson-Chastang[2], Mr. Pierre-Emmanuel Gleizes[2], Mr. Etienne Snoeck[1]

[1] Centre d'élaboration de matériaux et d'études structurales (CEMES) - CNRS, Toulouse, France, [2]MCD and METi, Centre de Biologie Intégrative, Université de Toulouse, CNRS, Toulouse, France, [3] Laboratoire Physique des Solides (LPS) - Université Paris-Saclay, CNRS, Orsay, France, [4]Institut de Biologie Structurale (IBS) – University Grenoble Alpes, CEA, CNRS, Grenoble, France

Poster Group 2

Background

Transmission electron microscopy (TEM), especially at cryogenic temperature, is largely used for studying biological macromolecules at high resolution and for 3D reconstruction. The main difficulty of TEM imaging of biological samples is the weak amplitude contrasts due to electron diffusion on light elements. Achieving 3D high-resolution reconstructions implies the acquisition of a huge number of TEM micrographs followed by a time-consuming image analysis. This TEM constraint could be overcome by imaging the phase shift of the electron beam resulting from its interaction with the sample.

Methods

In our work, we developed two TEM techniques, off-axis electron holography and in-line electron holography, for phase image extraction of biological samples. We mainly used unstained T4 and T5 bacteriophages as model samples which were deposited on graphene grids provided by Sara Bals's team (Antwerp University, Belgium) for room temperature experiments, while we used lacey grids for cryogenic temperature experiments.

Results and Conclusions

Thanks both to recent developments carried out at CEMES on off-axis holography [1,2] and to the direct electron detectors performances, we show on one hand that off-axis holography enables us to retrieve the phase shift information that the electron undergoes when interacting with the low-Z biological samples (figure 1 a-d). On the other hand, thanks to the in-line holography capability to be performed on any microscope, as well as the automation of a cryogenic electron microscope equipped with a direct electron detector, we show the ability of this technique to resolve high-resolution structural details (figure 1 e-f) with very low noise levels at low electron dose. We thus demonstrate the possibility of both techniques to obtain highly contrasted phase images of unstained samples both at room and cryogenic temperatures, in addition to an improved signal-to-noise ratio. Furthermore, since a change in electric charges affects the phase shift and can be detected by electron holography, we show a novel potential application using both off-axis and in-line electron holography methods, to measure electrostatic variations on biological specimens. This was evidenced in off-axis holography by measuring the phase shift changes at the capsid between phages treated with spermine, a multivalent cation that diffuses inside the capsid and neutralizes the DNA, and a non-treated T5 phages (Figure 1d). This electrostatic change was also observed locally by in-line holography by studying at high resolution the phase shift pattern of the tail, and globally by studying the phase shift signal around a full capsid and comparing it to the one around an empty one (figure 1f). More work is needed to fully take advantage of these microscopy phase imaging techniques

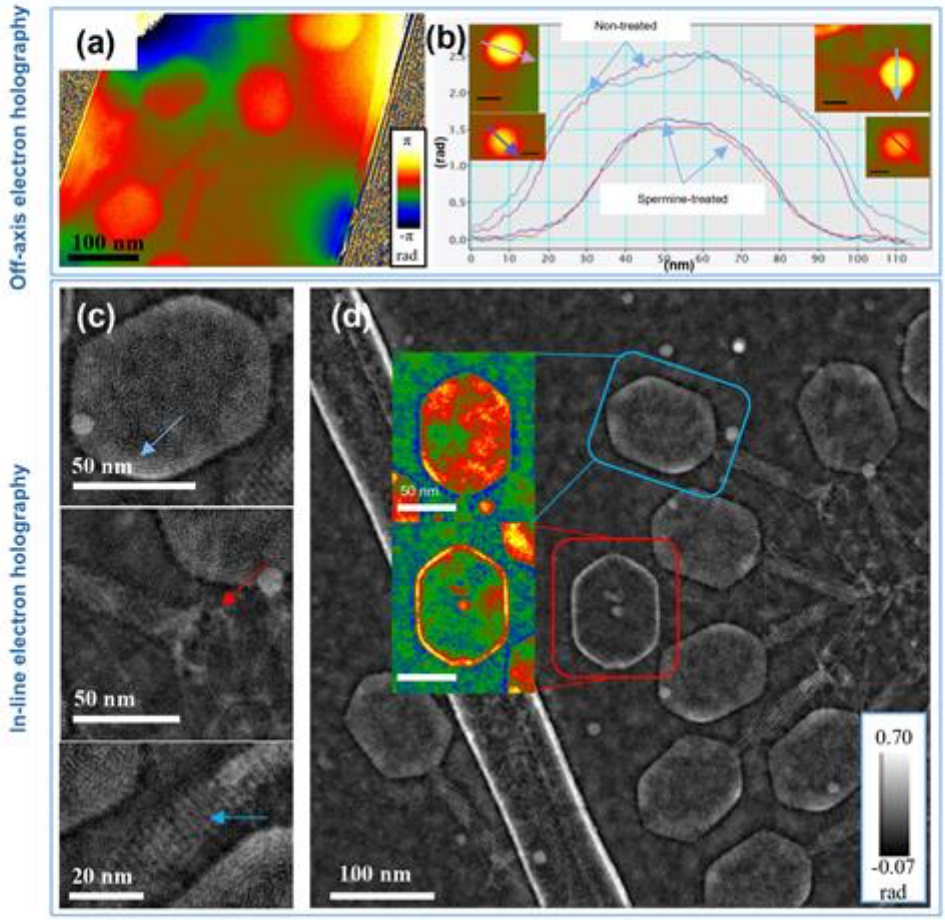

Figure1. (a-b) Cryogenic off-axis electron holography of the T4 bacteriophage. (a) Raw phase image. (b) Phase shift profile showing the difference between phase shifts measured across the capsid of non-treated T5 bacteriophages (light blue and purple profiles) compared to the ones measured across capsids of spermine-treated T5 phages (dark blue and red profiles). The selected phages are shown in the inserts. (c) Crop of raw phase images of T4. The orange arrow points at the DNA stacked at the periphery of the capsid. The red arrow points at the T4 baseplate. The blue arrow points at the tail rings. (d) Raw phase image with a zoom on two bacteriophages (colored phase signal) showing the difference in the phase signal surrounding a full and empty capsid.

Keywords:

Electron Holography
Electrostatic potential
Cryo-EM

Reference:

[1] C Gatel et al, Applied Physics Letters, 113 (2018), p. 13. https://doi.org/10.1063/1.5050906
[2] M Hÿtch & C Gatel, Microscopy, 70 (2021), p. 47. https://doi.org/10.1093/jmicro/dfaa044

51

Investigating the potential variation of in-operando semiconductor nanostructures in electron beam direction

Hüseyin Çelik[1], Mr. Robert Fuchs[2], Dr. Dirk Berger[3], Dr. Christian M. Günther[3], Mr. Simon Gaebel[4], Dr. Tolga Wagner[5], Prof. Dr. Michael Lehmann[1]
[1]Technische Universität Berlin, Institute of Optics and Atomic Physics, , Germany, [2]Technische Universität Berlin, Institute of Theoretical Physics, , Germany, [3]Technische Universität Berlin, Center for Electron Microscopy (ZELMI), , Germany, [4]Max-Born-Institut für Nichtlineare Optik und Kurzzeitspektroskopie, , Germany, [5]Humboldt-Universität zu Berlin, Department of Physics, , Germany

Poster Group 2

Off-axis electron holography is a well-established method for the investigation of projected potential distributions down to atomic spatial resolution. However, in the case of in-operando (electrical biasing) investigations of externally controlled semiconductor nanostructures, parasitic modulations of the electron wave occur due to long-range electrostatic stray fields [1]. In addition, a well-known problem is the alteration of the sample during preparation using a focused ion beam (e.g. ion implantation, surface amorphization or generation of conducting surfaces), which also severely influences the potential distribution within the sample [2]. Both effects have a particular impact in the direction of the electron beam as well, which makes a quantitative analysis particularly difficult. Standard approaches to resolve the entire potential distribution involve projective tilt series and their tomographic reconstruction [3], which entail a significant measurement effort (e.g. sample tracking or long-time stability) and instrumentational limitations (e.g. limited tilt angle (i.e. missing wedge), interior Radon transform or parallax displacement), in addition to extensive simulations (e.g. FEM or DEM), which are highly computationally intensive and require rarely given knowledge of the microscopic charge carrier distribution.
Here, a simple and intuitive model (SIMP) for the approximation of such potential distributions inside and outside nanostructured FIB-prepared samples of a p-n junction, requiring a limited set of parameters, is presented. The model uses only independent convolutions of an initial potential distribution (e.g. analytic textbook models) with a Gaussian kernel (see attached figure), allowing the reconstruction of the entire potential distribution from only one measured projection (electron hologram). In addition, various contacted semiconductor nanostructure samples (TEM-lamellae) are produced in a systematic approach using FIB under varying preparation parameters (i.e. currents and acceleration voltages of the ions) to evaluate the proposed model.
In comparison with FEM-simulations, representing an established simulation method, it can be shown that the self-developed model is able to accurately approximate the 3D electrostatic potential distribution of various contacted TEM-samples, whereby the computational complexity can be significantly reduced with respect to FEM-simulations (i.e. ~1000x faster with ~1/1000th of the memory usage at ~5000x more nodes). An excellent agreement can likewise be observed in comparison with electron holographic and tomographic investigations considering experimental restrictions, revealing the real potential distribution in propagation direction of the electron beam. By this, a significant reduction of the required computational power as well as a drastically simplified measurement process is achieved, paving the way towards quantitative electron holographic investigation of electrically biased semiconductor nanostructures. In particular, the latter can in turn also be used to understand the exact effects of the FIB-preparation (e.g. implantation concentration or implantation depth) on the sample, thus leading to improved preparation strategies.

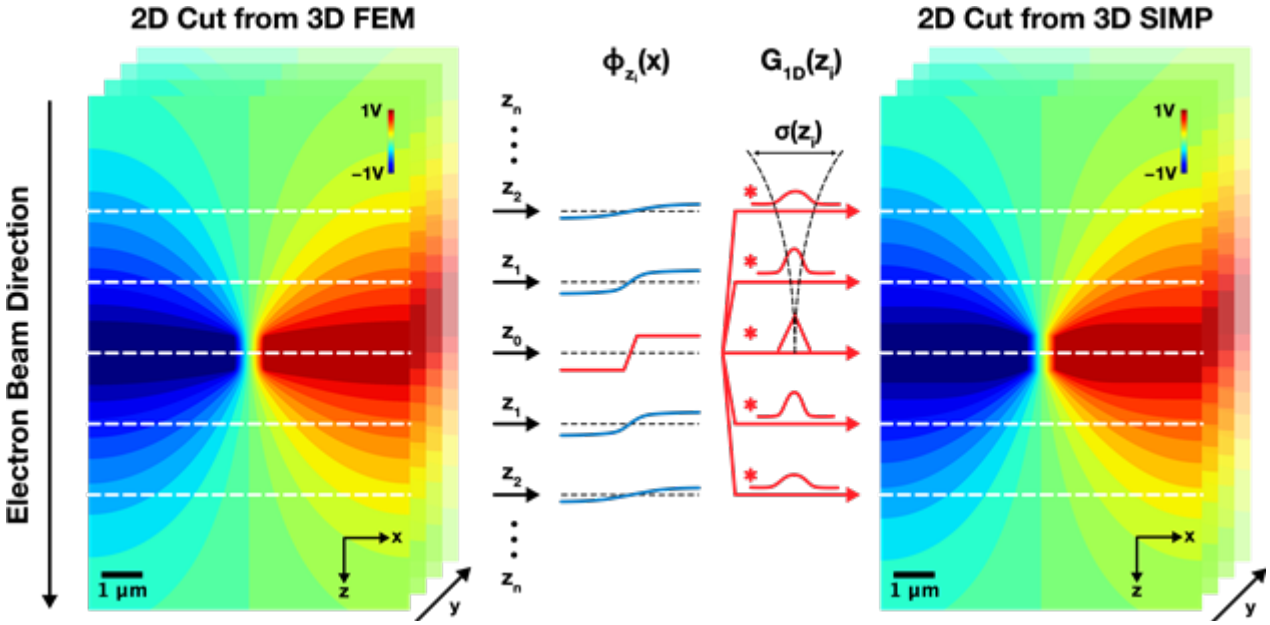

Keywords:

Electron-Holography, Semiconductor-Nanostructures, 3D-Potential-Distribution, Surface-Effects, Computational-Optimization

Reference:

[1] S. Yazdi et. al., Ultramicroscopy 152, 10 (2015).
[2] D. Cooper et. al., Journal of Microscopy 233, 102 (2009).
[3] A. C. Twitchett-Harrison et. al., Nano Lett. 7, 2020 (2007).

62

Optimized Bright Field STEM Imaging for Detecting Molecules absorbed within Zeolite Pores

Yu Xia[1], Mr. Tom WIllhammar[1]
[1]Department of Materials and Environmental Chemistry, Stockholm University, Stockholm, Sweden

Poster Group 2

Background incl. aims
Zeolites, characterized by their large and regular pores, are utilized to filter target molecules from mixtures, purify effluent by removing pollutants and in catalysis. Atomic resolution imaging of small molecules in pores will contribute to elucidate host-guest interactions between small molecules and porous structures and understand diverse molecular absorption/desorption behaviors in pores. Scanning transmission electron microscopy (STEM) is a powerful technique to capture interpretable atom-scale images, facilitating localized structural analyses. Recognizing the inherent sensitivity of zeolites and molecules to electron beam exposure, low electron dose imaging techniques, including the differential phase contrast (DPC) employing segmented detectors and 4D-STEM using pixelated detectors, have been developed. Pixelated detectors employed by 4D-STEM offer superior electron collection efficiency with fine resolution and high signal-to-noise ratio (SNR) at probe positions[1]. However, pixelated detectors entail higher costs and longer dwell time compared to segmented counterparts. The integrated DPC (iDPC) technique has shown its power in imaging light elements with low-dose conditions. Recently, a newly developed optimum bright-field (OBF) STEM technique demonstrates enhanced SNR relative to iDPC[2 3]. OBF images are reconstructed by combining the images captured by segmented detectors. Each segmented image is weighted by a frequency filter for the contribution to the Fourier component of the reconstructed OBF image, where the frequency filters are built using phase contrast transfer functions (PCTFs) for the segmented detector[2]. Here, the OBF-STEM technique with a custom-made python package is utilized for the efficient detection of molecules within the pores of ZSM-5 zeolite using a four-segmented detector.
Methods
The theoretical framework of the OBF STEM image can be derived from the single side band (SSB) ptychography[2], where the specimen is weakly electron scattering. The exit wave function M(k ,Q) is given by the convolution of the entrance probe wavefunction ψ(k)·ψ* (k-Q) on the specimen with the pupil function A(k) A* (k+Q) , where Q is the spatial frequency of the probe at spaced position r on the specimen in Fourier space. Therefore, the PCTF can be calculated by T* (k)T(k-Q)-T(k) T* (k+Q), where T(k) is the aperture transfer function defined as the multiplication of the aperture function with the probe wave function in reciprocal space. In a segmented detector, the STEM image intensity of the i-th segment I_i (r) is described mathematically as ∫I(k, r) D_i (k)𝑑k, where D_i (k) is the i-th segmented detector response function in reciprocal space and I(k, r) is the inverse Fourier transform of the diffraction pattern (|M(k, Q)|^2). The OBF STEM image is reconstructed by combining the segmented images weighted by frequency filters in reciprocal space, or combining the convolution of each segmented image with a corresponding point spread function (PSF) in real space[2]. For maximizing the SNR of the reconstructed OBF image, the PCTFs in the segmented detector are optimized by incorporating real-valued functions, such as high/low pass filters[2]. In this work, a custom-made python package is developed to calculate the PCTFs and the corresponding real-valued functions for OBF STEM image reconstruction. The specimen of ZSM-5 zeolite absorbed pollutants was imaged with the convergence semi-angle of 21 mrad on an aberration-corrected FEI Titan Cubed Themis Z microscope operated at 300 kV. A four-segmented detector was employed to capture images using a beam current around 4.7 pA and a dwell time of 2 µs per pixel within a collection angle range of 8-42 mrad, with a camera length of 185 mm.
Results

The ZSM-5 with pollutants in pores was imaged along the [0 1 0] direction under a dose rate of 856 e-/Å². iDPC image (Figure a) and OBF image (Figure b) were reconstructed using the same dataset. Compared with the iDPC image, OBF image demonstrates clearer structural details due to its higher contrast and SNR, evident in line profiles and the cropped image (Figure d) from the same area in iDPC and OBF images. The superior contrast and finer resolution of OBF image enable more distinct observation of pollutants (marked by arrows in the line profiles) within pores than that of the iDPC image.

Conclusion

OBF-STEM images were reconstructed using the custom-made python package. This package implements algorithms to compute the PCTFs and the corresponding real-valued filters for image reconstruction. The reconstructed OBF image demonstrates enhanced contrast and SNR, giving clearer discernment of structural features. Importantly, features within the pores of ZSM-5 were distinctly distinguished in the OBF images compared to those reconstructed iDPC images. These findings imply that the OBF technique, employing a high-speed segmented detector, represents a promising approach for low-dose imaging of molecules encapsulated within the pores of zeolites.

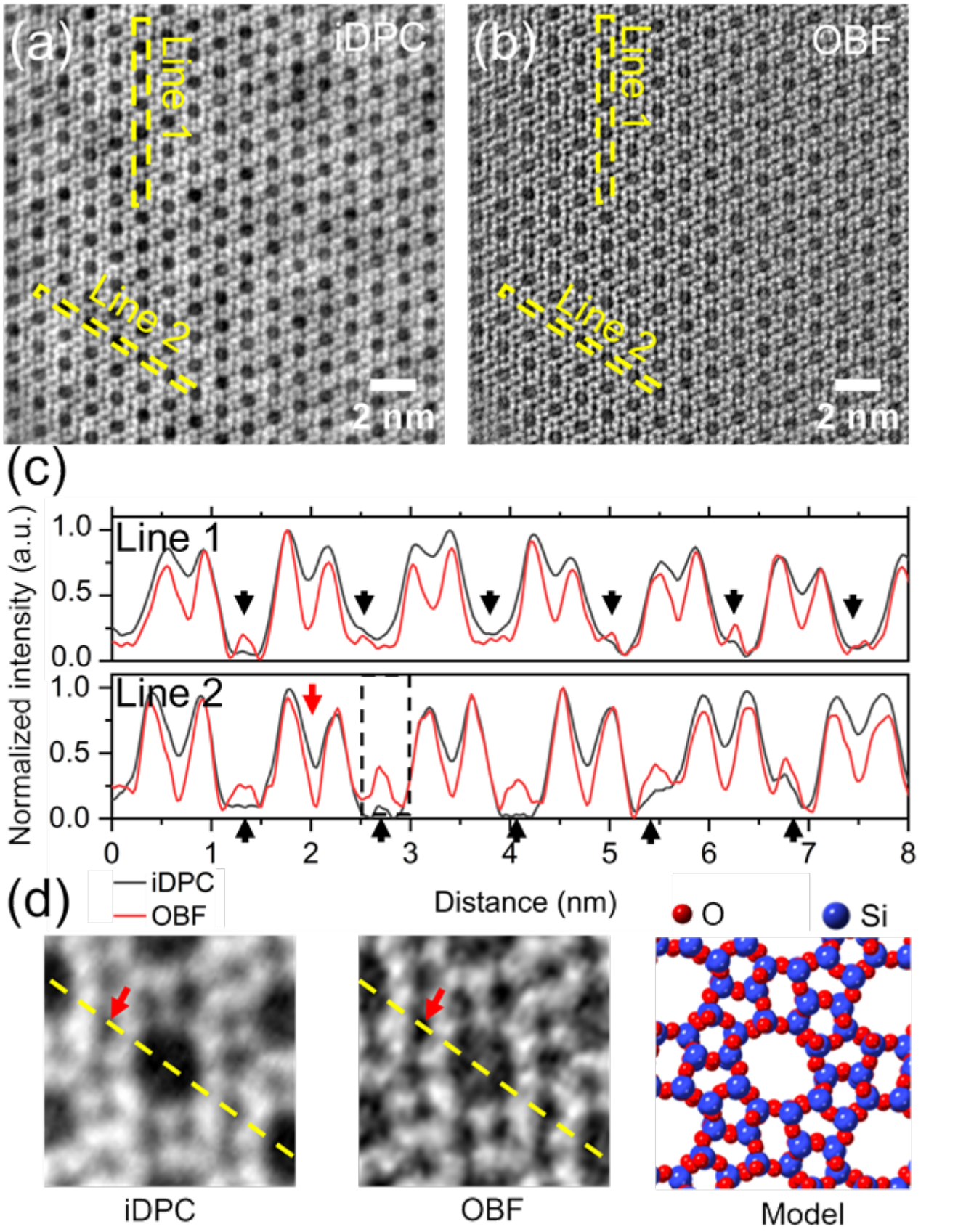

Keywords:

STEM, segmented detectors, low-dose imaging

Reference:

1. O'Leary, C. M. et al.. Ultramicroscopy 221, (2021).
2. Ooe, K., Seki, T., Ikuhara, Y. & Shibata, N. Ultramicroscopy 220, 113133 (2021).
3. Ooe, K. et al. Sci. Adv. (2023) doi:10.1126/sciadv.adf6865.

4. Rodenburg, J. M., Mccallum, B. C. & Nellist, P. D. Ultramicroscopy 48 (1993).

162

Liquid Phase Transmission Electron Microscopy

Mads Søndergaard Larsen[1], Mr Ebrahim Chalangar[1], Mrs Sofie Tidemand-Lichtenberg[1], Mr Murat Nulati Yesibolati[1], Mr. Emil Jensen[1], Mr. Kristian Speranza Mølhave[1]
[1]DTU Nanolab, Kgs. Lyngby, Denmark

Poster Group 2

Background
Liquid phase transmission electron microscopy (LPTEM) is a small field in the realm of microscopy. However, its significance appears in understanding various scientific domains. However, measuring the main driving force in many liquid-based processes, e.g., in electrochemistry, is still yet to be fully explored. Similarly, understanding the liquid itself is key in quantum mechanical models for our understanding of how liquids behave.
Electron holography (EH) has emerged as a new tool to measure both the electrostatic- and magnetic potentials of a specimen. As the electrons from the incoming electron beam undergo elastic scattering, a phase shift is presented in the exit wave [1]. In EH, the phase shift is measured by measuring against a reference wave, which has not been shifted in phase. By computing the phase shift between the two waves, the object and reference wave, the electrostatic and magnetic potential are retrieved by post-mortem analysis.
It, therefore, begs the question if it is possible to combine EH with LPTEM in order to measure those potentials, which may be used in more delicate systems in order to study liquids and liquid-based processes where the potential is the main driving force, e.g. in any electrochemical experiment. We coin the new method of Liquid Phase Transmission Electron Holography (LPTEH).
Methods
In LPTEH, we make use of two primary chips, which have previously been used in LPTEM to examine nanoscale liquid-based processes. The first type of chip used, the nanochannel chip, is a chip comprised of two bonded silicon wafers with nitride as the window material, see Figure 1(a). The thickness in the nanochannel chip is much better defined, given that the channels have a width of < 2 µm, where bulging is less compared to the clamped liquid cell with a width of > 100 µm. However, these chips have not yet been fabricated with electrodes. Thus, the nanochannel chip is primarily used via LPTEH to determine the intrinsic properties of the liquids.
The other type of chip, the clamped liquid cell, is an LPTEM cell where the liquid is squeezed between two electron transparent windows, see Figure 1(b). The thickness of the liquid is defined by how thin a liquid can be squeezed by squeezing on the surrounding O-ring. Additionally, we have in our clamped liquid cell fabricated Au electrodes, where we start to examine how to use those chips for any electrochemical experiments. Lastly, EH itself is done using a TEM. There are two main methods for EH, namely in-line and off-axis EH. For our experiments, we use off-axis EH, since the TEM at DTU (the FEI 80-300 kV E-TEM) has a standard ThermoFisher biprism (a quartz filament) installed in the SAD plane. We carry out experiments on a single biprism setup, where the biprism voltage determines both the interference width and the fringe spacing.
Alignment of the object and reference wave can be done in different ways for both chips. For instance, if one were to examine the liquid itself on the nanochannel chip, the reference wave is usually passed through the bonded nitride between the channels, as that defines a common 0 rad phase shift. If features in the liquid are instead studied, the reference wave can be passed through the liquid, thus only the phase shift elastic scattering with the feature is measured.
Results
We show our latest results of both systems and some of the features studied with LPTEH. First and foremost, we extend an earlier paper on the study of the mean inner potential (MIP) of water [2], where our updated results show how the MIP can be understood as a refractive index for high energy

electrons by studying the change in MIP of glycerol:water mixture, see Figure 1(c). By increasing the volume fraction (f_g) of glycerol, it can be seen that the MIP of the mixture increases linearly shown by the dashed black line in Figure 1(c). This linear increase with solute concentration can be thought of as an analogy to how the optical refractive index increases linearly with solute concentration, which was also how the MIP was first described by H. Bethe [3]. We compare our experimental results to a first-order approximation of the MIP, known as the independent atom model, shown as the dashed red line in Figure 1(c), and compare our results of pure MQ water with [2] shown as the blue data point. Evidently, it can be seen that the MIP is the refractive index of high-energy electrons, and it behaves similarly to the optical refractive index.

In our second example, we show how LPTEH can be used to measure the potential from the solid-liquid interface, see Figure 1(d). This study shows how LPTEH can be used to measure the potential of the electric double layer, which is key in any electrochemical process. Its potential profile indicates that of a screened potential, which is understood as the screening of free ions in the liquid. Such a measurement of the potential is the first of its kind, as most techniques use an almost ideal non-polarizable reference electrode. However, the e-beam used for EH/LPTEH is ideally non-polarizable, as it does not create its own double layer contrary to any solid reference electrode. It could, therefore, be speculated that the e-beam can be used in the future as an ideal reference electrode and be able to measure the driving force in any electrochemical experiment.

Conclusion

In summary, we have shown two studies of how LPTEH can be used to measure the driving force and intrinsic properties of a liquid. By combining two TEM-based methods, LPTEM and EH, we have shown how we may start to use LPTEH as a new tool to understand liquids in a deeper understanding. We note that this is the first of its kind, and thus, there is still much to improve in terms of spatial resolution to better capture the innermost layer of the double layer, where our results only provide evidence of the outermost layers of the double layer.

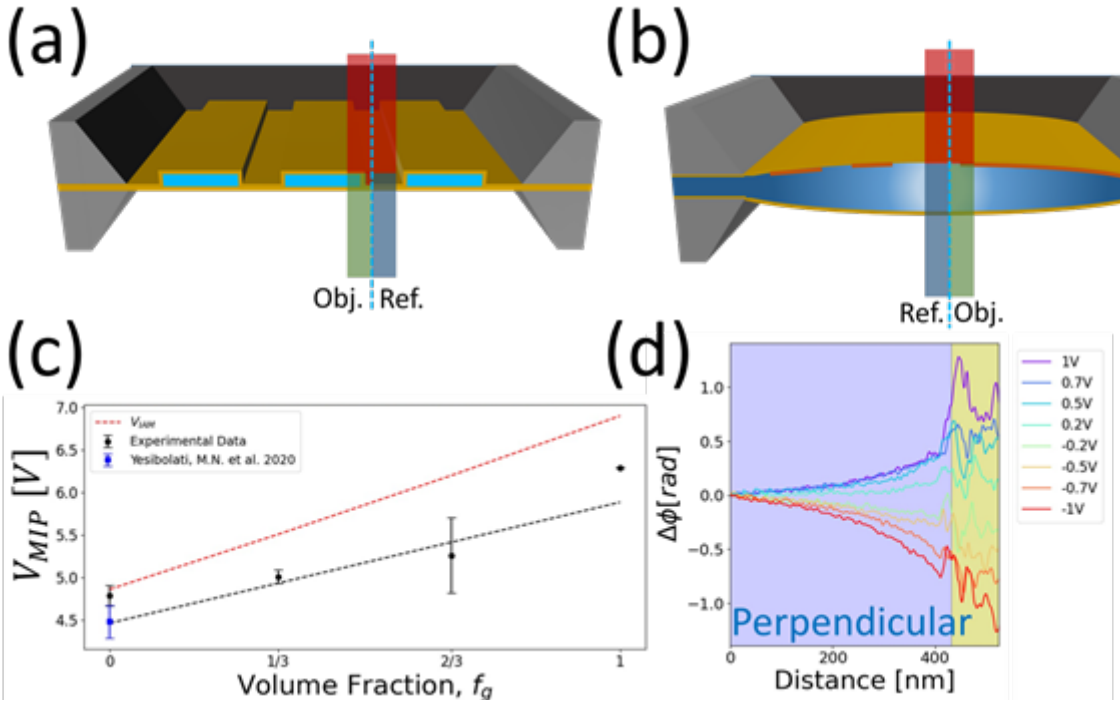

Keywords:

LPTEM, Electron Holography, MIP, EDL

Reference:

[1] F. M. Ross, Liquid Cell Electron Microscopy, New York: Cambridge University Press, 2016.
[2] Microscopy and Microanalysis, vol. 8, pp. 447-466, 2002

[3] Ultramicroscopy, vol. 64, no. 1, pp. 79-86, 1996.
[4] Phys. Rev. Lett., vol. 124, no. 6, p. 065502 , 2020.
[5] Annalen der Physik, vol. 392, no. 17, pp. 55-129, 1928.

165

Assessing the sensitivity of 4D-STEM measurements for electric field mapping at the sub-micrometer scale

Pierpaolo Ranieri[1], Dr. Reinis Ignatans[1], Dr. Victor Boureau[2], Prof. Vasiliki Tileli[1]
[1]Institute of Materials, École Polytechnique Fédérale de Lausanne, Lausanne, Switzerland,
[2]Interdisciplinary Centre for Electron Microscopy, École Polytechnique Fédérale de Lausanne, Lausanne, Switzerland

Poster Group 2

Four-dimensional scanning transmission electron microscopy (4D-STEM) can provide quantitative information about electric fields in materials and it is currently a technique of choice for such measurements. However, mapping electric fields over large (micrometers) field of view with a very high sensitivity and a nanometer spatial resolution remains challenging [1]. Herein, we perform a systematic study to evaluate the expected achievable precision of 4D-STEM measurements for electric field mapping in vacuum.
All experiments were performed on a Thermo Fisher Scientific Titan Themis TEM operated at 300 kV in micro-probe configuration and equipped with a MerlinEM detector. First, the effect of microscope parameters was investigated by acquiring 4D-STEM maps in vacuum while varying one parameter at a time such as convergence semi-angle, electron beam current, dwell time or camera length. To assess the accuracy of the electric field mapping, a coplanar capacitor was fabricated by focused-ion beam (FIB) deposition of Pt on a MEMS biasing chip (DensSolutions). The center of mass (COM) method was used to analyze the shift of the transmitted beam, which was achieved by subtracting the COM map obtained at an applied voltage (object map) from a COM map in free field conditions (reference map) [2]. The reconstructed electric field was then compared with the results of finite element method (FEM) simulations using COMSOL [3].
The electric field sensitivity was evaluated in terms of measurement error. The results show that reducing the convergence semi-angle increases linearly the sensitivity but has a negative effect on the spatial resolution. Electron beam current and dwell time are also shown to have a direct effect on the field sensitivity, as directly controlling the electron dose. In practice, low electron dose values mean low sensitivity, which follow the root square behavior of the Poisson noise. Finally, the camera length study shows that this parameter has no influence on the sensitivity except for extremely small values when it strongly deteriorates. Overall, the experimental trends are in good agreement with previous theoretical studies [4]. The microscope parameters that optimize the measurement, including a convergence semi-angle of 370 µrad, dwell time of 2 ms, electron beam current of 150 pA and camera length of 1.45 m, were then used to quantify the stray electric field of the capacitor induced by an applied difference of potential between the plates. The integral of the in-plane component of the stray electric field over the electron path was directly compared with a FEM model where the simulated electric field was integrated along the z direction, assumed to be the direction of electron propagation. This comparison revealed good agreement for applied voltages in the range of 1 to 10 V, corresponding to a maximal projected field in the capacitor gap of 2 to 25 V, respectively. Finally, the electric field reconstruction was repeated using the template matching (TM) method and the results showed that proper choice of template is essential for comparable trends.
In conclusion, this study highlights the effects of microscope parameters on the sensitivity of large field of view electric field measurements using 4D-STEM and provides guidelines for optimized measurements. The full quantification of the electric stray field induced by an applied external potential is demonstrated as an example.
This work was supported by the Swiss National Research Foundation (SNSF) under award number 200020_204240.

Keywords:

4D-STEM
Electric_field_mapping
Finite_element_simulations

Reference:

[1] D. Cooper, L. Bruas, M. Bryan, V. Boureau, Micron 2024, 179, 103594.
[2] V. Boureau, M. Staňo, J.-L. Rouvière, J.-C. Toussaint, O. Fruchart, D. Cooper, J. Phys. D: Appl. Phys. 2021, 54, 085001.
[3] J. F. Dushimineza, J. Jo, R. E. Dunin-Borkowski, K. Müller-Caspary, Ultramicroscopy 2023, 253, 113808.
[4] S. Pöllath, F. Schwarzhuber, J. Zweck, Ultramicroscopy 2021, 228, 113342.

173

Mean inner potential variation with strain in III-nitrides studied by off-axis electron holography

Lou Denaix[1], Dr Jing Li[1], Dr Benoît Scklenard[1], Dr David Cooper[1], Dr Eva Monroy[2]
[1]Univ. Grenoble Alpes, CEA, Leti, F-38000 Grenoble, France, [2]Univ. Grenoble Alpes, CEA, Grenoble INP, IRIG, PHELIQS, F-38000 Grenoble, France

Poster Group 2

Background incl. aims
Wurtzite III-nitride semiconductors are well known for their intense spontaneous and piezoelectric polarization fields. A deeper understanding of these properties is relevant for applications in various fields such as optoelectronic or power electronic devices. Off-axis electron holography is a powerful tool to measure directly and with a nanometer resolution the total electrostatic potential in these materials. However, to be able to study the polarization fields in III-nitrides, we need to remove the contribution from mean inner potential (MIP), which corresponds to the volume average of the Coulomb potential in the specimen. In the literature, MIP is traditionally derived for bulk materials within density functional theory (DFT).1,2 Evaluating the MIP using electron holography, we noticed disparities with values from the literature. One explanation that we propose is that the calculation for bulk material does not reflect the reality of heterostructures that are used in devices, with for instance the importance of strain. We propose here a deep analysis of the MIP evaluation for III-nitrides, comparing electron holography results with DFT calculation of the MIP that include the variation of strain.

Methods
MIP was computed through ab-initio simulations performed using GPAW code with plane wave basis-set of 300 eV cutoff energy, PBE functional, and 8x8x1 k-point sampling. The calculations were performed in a slab containing 11 atomic layers terminated in nonpolar m-{10-10} facets, centered in a 6.2-nm-long vacuum region with periodic boundary conditions. The MIP was obtained by averaging the Coulomb potential in the center 7 atomic layers, to prevent surface effects. The effect of strain has been modelled considering a biaxial strain configuration for layers grown along the <0001> direction.
From the experimental point of view, we study here 4 different samples. The first structure consists in a 6-period non-polar AlN/GaN (13nm/16nm) on 60 nm of AlN deposited on a (1-100) SiC substrate. The second sample is a 10-period polar AlN/GaN (20nm/20nm) superlattice grown by plasma-assisted molecular beam epitaxy (PAMBE) on 100 nm of GaN deposited on 1-µm-thick AlN-on-sapphire templates.3 The third and fourth samples consist in 5-period GaN/InGaN multi-quantum wells (MQWs) grown on a 2 µm-thick GaN layer that is itself grown on a 220-nm thick AlN buffer layer on patterned Si(111) templates using low-pressure metal organic vapor phase epitaxy (MOVPE). In one of the samples, the MQW consists in 5 periods of In0.13Ga0.87N (2 nm)/GaN (12 nm). In the other one, the indium content in the barriers is higher, between 14 and 16%.4 These samples have been studied using off axis electron holography performed in a double corrected FEI Titan Ultimate TEM operating at 200kV. Electron holograms were recorded on a Gatan One View 4k camera. TEM specimen were prepared by in-situ lift-out focus ion beam (FIB) using a FEI Strata 400.

Results
III-nitride heterostructures are usually grown along a polar axis, resulting in strong polarisation-induced internal electric fields that contribute to the total potential measured in electron holography. Additional contributions come from dopants, which can partially screen the internal electric fields, and from the MIP. Our first experiment consist in an attemp to measure MIP in an

AlN/GaN heterostructure. To avoid the presence of internal electric fields, the heterostructure was grown along a non polar axis, and we verified that the lattice was fully relaxed. We obtained a difference of MIP between GaN and AlN of 1.53 V which is very different from the generally accepted 1.01 V, calculated by Schowalter et al. [1], and the 2.77 V that we obtain from our DFT calculations for relaxed materials. This opens a question about the real value of MIP for these compounds.
We used then a polar superlattice of AlN/GaN (second sample) to repeat the same measurement. In this case, the MIP difference between GaN and AlN, extracted from the electron holography result, was 1.3 V, i.e. slightly lower than in the non polar sample. We assumed that the difference could be attributed to a different strain in the structure. However, keeping in mind that AlN is under tensile strain and GaN is under compressive strain, the expected result is rather an increase of the MIP difference, which might reach up to 3 V. In summary, we conclude that current uncertainties in the AlN MIP value make it extremely difficult to extract precise information about the potential profile field in GaN/AlN heterostructures.
We have extended this work to InGaN/GaN, now obtaining more reliable results. The TEM specimen from the third sample was prepared with a gradient of thickness, so that there is a different degree of surface-induced relaxation in the 5 quantum wells. In this sample, we can show experimentally the variation of MIP with respect to strain, with the MIP of GaN and InGaN being almost equal for a completly relaxed sample. The experimental results match closely our DFT computation, including the strain dependence.
In the last sample, also InGaN/GaN but with different indium concentration, we could further confirm the effect of strain on the MIP, including a clear evaluation of the MIP difference between GaN and In0.16Ga0.84N.

Conclusion

The understanding and computation of MIP is highly important for a correct interpretation of the potential profiles measured in electron holography. In this work, we provide a theoretical and experimental evaluation of the MIP in III-nitrides. We outline the important disagreement between theory and experiments in the case of AlN/GaN heterostructures, even taking the strain into account. In contrast, we were able to provide reliable values of MIP for InGaN/GaN, showing excellent agreement between experimental and theoretical estimations, and confirming the effect of strain predicted by the calculations.

This work, carried out on the Platform for Nanocharacterisation (PFNC), was supported by the “Recherche Technologique de Base” and "France 2030 - ANR-22-PEEL-0014" programs of the French National Research Agency (ANR).

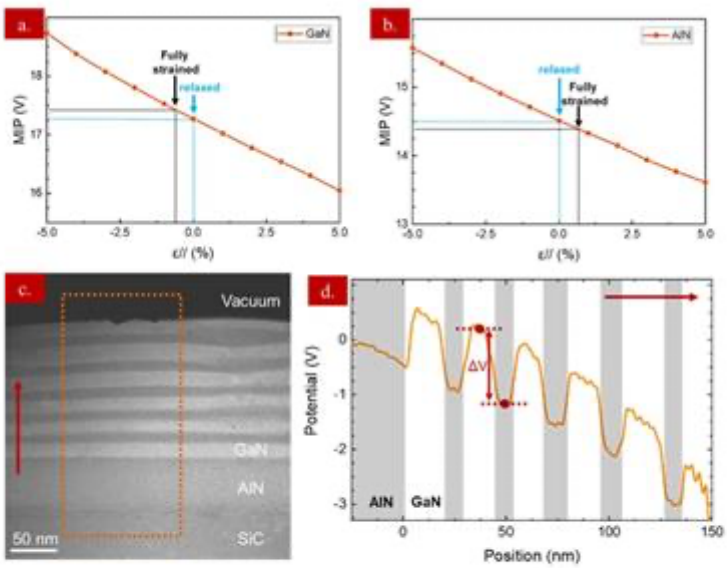

Fig.1: The red arrow represents the [0001] growth direction. [a] MIP computation of GaN and [b] AlN as a function of the biaxial strain. [c] Phase image of the non-polar AlN/GaN mutlilayer sample and [d] resulting potential profile. The difference of MIP between AlN and GaN is estimated as represented in [d], taking the difference of potential between the middle of AlN and GaN layers.

Keywords:

Holography, III-nitride, Mean inner potential

Reference:

[1] M. Schowalter et al. Appl. Phys. Lett. 88, 232108 (2006).

[2] P. Kruse et al. Si and Ge by Density Functional Theory and Electron Holography, Ultramicroscopy 106, 105 (2006).

[3] D. Cooper, J. Phys. Appl. Phys. 49, 474001 (2016).

[4] L. Denaix et al. ACS Appl. Mater. Interfaces 15, 11208 (2023).

185

New paradigm for ultra-low-dose high-resolution imaging through a dedicated event-driven analytical ptychography methodology

Dr. Hoelen L. Lalandec-Robert[1,2], Prof. Dr. Jo Verbeeck[1,2]
[1]Electron Microscopy for Materials Science (EMAT), University of Antwerp , Antwerp, Belgium,
[2]NANOlab Center of Excellence, University of Antwerp, Antwerp, Belgium

Poster Group 2

Recently, significant advances in scanning transmission electron microscopy (STEM) have made it a viable solution for the high-resolution imaging of beam-sensitive specimens such as 2D materials, ordered nanoporous particles, viruses or protein crystals. In particular, the development of dose-efficient computational imaging approaches such as analytical ptychography, e.g. in the form of the Wigner distribution deconvolution (WDD) and side-band integration (SBI) methods, have permitted the direct retrieval of the projected electrostatic potential with the highest achievable signal-to-noise ratio [1]. Furthermore, with the introduction of event-driven detectors (EDD), the ultra-low-dose measurement (<100 e-/Å2) of the far-field electron intensity was enabled as well [2].

In this work, we present developments of WDD and SBI aiming to improve their performances in imperfect recording conditions, e.g. by including geometric aberrations, partial coherence and the modulation transfer function (MTF) of the camera. We also introduce a scan-frequency partitioning algorithm permitting the computationally heavy implementation of those methods in a RAM-limited device, such as a commercial graphics processing unit (GPU). Moreover, we evaluate the capacities of analytical ptychography to transfer a range of frequency information, with dependence on both the scan sampling and the illumination parameters, on the basis of the Cramér-Rao lower bound [3]. As such, an updated metric for the probe overlap requirement of electron ptychography is presented.

Additionally, we establish the guided progressive reconstructive imaging (GPRI) method, which constitutes a new framework to perform WDD and SBI through the direct treatment of a stream of electron events provided by an EDD. This process is purely cumulative, as each count leads to the addition of a single contribution to the result, selected from a set of pre-calculated libraries. GPRI should thus permit reaching the best achievable dose-efficiency and processing speed in live ptychography, in particular through a direct implementation in the field-programmable gate array (FPGA) unit of the EDD and thus with no need for a prior transfer of the event data to a separate computer, which currently represents the main bandwidth limitation in other approaches. This method can be furthermore supplemented with recording strategies optimized for damage mitigation [4,5].

The methods developed in this work are tested by means of multislice frozen phonon simulation, allowing the exploration of different experimental parameters, such as dose, probe focus, specimen thickness, source size and focus spread. Preliminary experimental demonstrations are carried out as well.

Figure: examples of analytical and iterative ptychography results to recover the projected potential μ or a transmission function T (complex exponential of μ). The simulated STEM scan was performed on a single-layer MoS2 specimen. The chosen semi-convergence angle α was 30 mrad and the acceleration voltage U was 60 kV. Two cases were investigated: the use of a perfectly focused probe and of an overfocused probe, with focus f equal to 50 nm. Dose limitation was included by realistic representation of single counts, whose total number per frame was determined by Poisson statistics.

Note that, for the focused probe case, an average number of 4 counts per scan position leads to a dose of about 164 e-/Å2 (i.e. ratio of total electrons used by scanned surface).

This work received funding from the Horizon 2020 research and innovation programme (European Union), under grant agreement No 101017720 (FET-Proactive EBEAM).

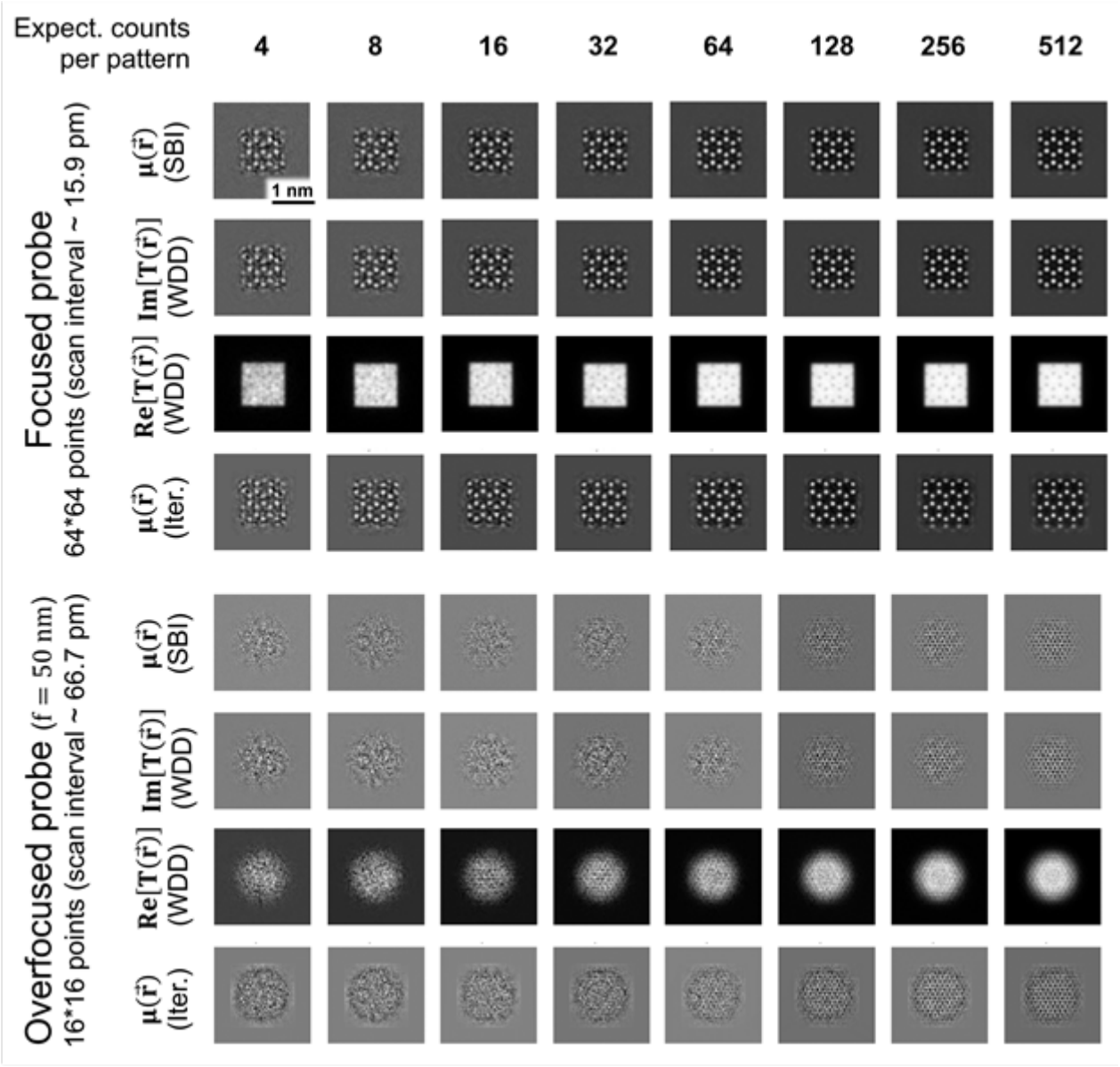

Keywords:

Ptychography, Low-dose imaging, Event-driven detection

Reference:

[1] C. O'Leary et al. ; Ultram. 221, 113189 (2021)
[2] D. Jannis et al. ; Ultram. 233, 113423 (2022)
[3] C. Dwyer and D. M. Paganin ; arXiv:2309.04701v2
[4] A. Velazco et al. ; Ultram. 232, 113398 (2022)
[5] D. Jannis et al. ; Ultram. 240, 113568 (2022)

196

High Spatio-Temporal Resolution Differential Phase Contrast Imaging via Detector Signal Digitisation

Julie Marie Bekkevold[1,2], Dr. Jonathan J. P. Peters[1,2], Prof. Ryo Ishikawa[3], Prof. Lewys Jones[1,2]
[1]School of Physics, Trinity College Dublin, Dublin, Ireland, [2]Advanced Microscopy Laboratory, Dublin, Ireland, [3]University of Tokyo, Bunkyo, Tokyo, Japan

Poster Group 2

Imaging of the functional properties of materials using phase contrast techniques is increasingly in-demand. The high sensitivity of phase techniques to weak phase objects makes them excellently equipped to study weakly scattering and beam sensitive materials in STEM. To study beam sensitive materials, the beam current must be significantly reduced to avoid damaging the sample. However, this often means that high dwell times are used to collect a high enough signal for the image to be interpretable. This requires the sample to be stable and unchanging over the significant time needed to acquire the frame. A different approach to collect enough signal is acquiring many subsequent frames as a lower dwell time and then later average the signal to get the final interpretable image. This has the added benefit that it fractionises the dose resulting in lower beam damage to the sample[1]. However, at fast scan speeds a scintillator detector is often too slow to keep up, resulting in streaking artefacts in the image due to single electron events lasting longer than the pixel dwell time[2].
In this work we investigate the practicability of in-hardware digitisation of scintillator detector signal in the ABF region for differential phase contrast (DPC). Digitisation retains the precision of electron detection events in time, such that every electron is detected in the correct pixel only[3]. Still, the occurrence of two electrons too close in time to be separated into two digitised events increases at collection angles within the semi-convergence angle because the arrival rate of electrons to the detector is high. This coincidence loss problem reduces the practicable beam current for digitisation imaging in the ABF region. Using segmented detectors for DPC imaging reduces the coincidence loss, since each segment is digitised separately.
Experimentally using live digitisation of four segments from an annular segmented detector, we demonstrate that atomic position precision can be retained at incredibly high scan speeds. With a low beam current of 5.2pA, to reduce loss of signal due to coincidence loss, and multi-frame imaging, the atomic column positions in an STO sample have been recorded at dwell time as low as 50 ns. The analog images captured with the same parameters show significant loss of information in the fast scan direction due to image streaking. At this high-speed scanning, binning of the multi-frame data stacks allow us to gain time-resolution as well. Thus, we may sacrifice some of our spatial resolution for time-resolution – paving the way for in-situ materials characterisation with DPC.

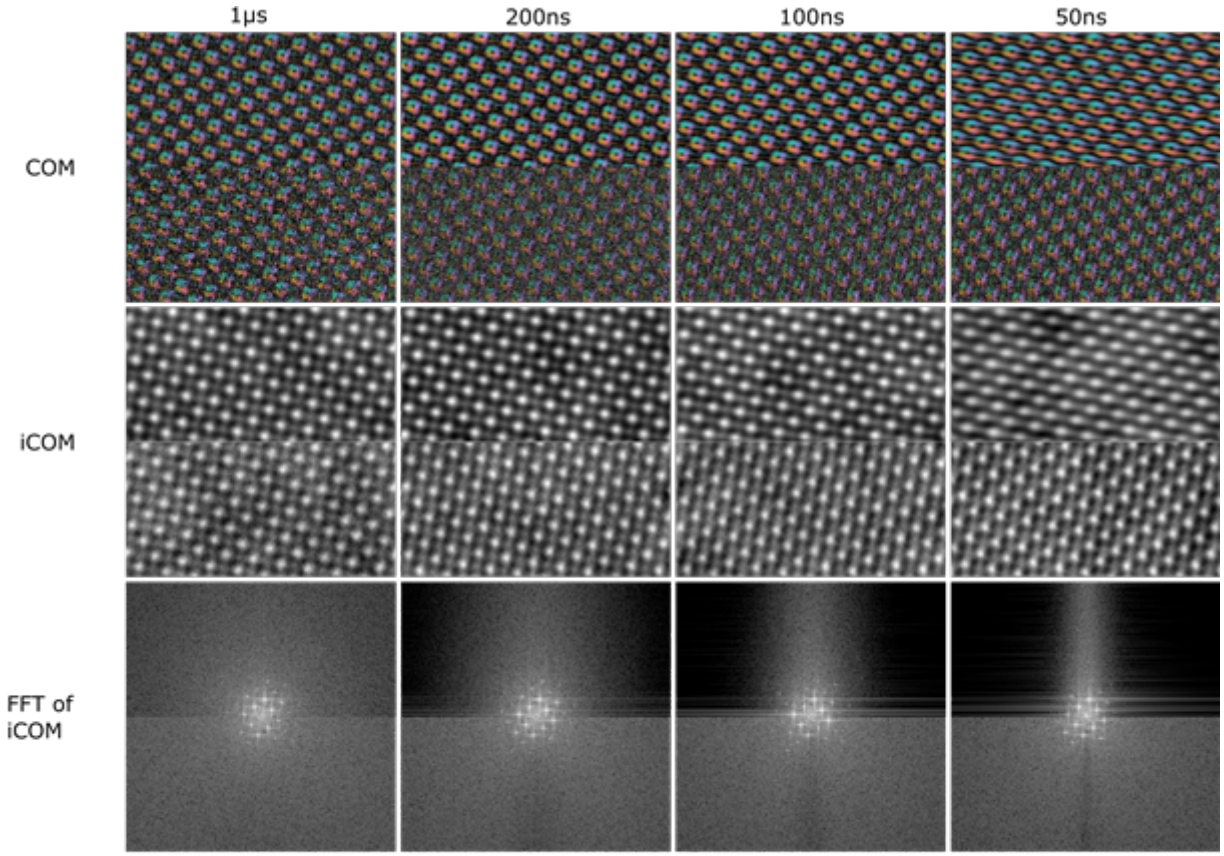

Figure 1: Analog (top) and digitised (bottom) images acquired at beam current 5.2pA and with increasingly (towards the right) fast scan speeds. The analog images lose information in the fast scan direction due to signal streaking, whereas the digitised images retain the precision even at the fastest scan speed.

Keywords:

DPC, scintillator digitisation, multi-frame imaging

Reference:

1. Jones, L. et al. Microscopy 67, i98–i113 (2018).
2. Buban, J. P., Ramasse, Q., Gipson, B., Browning, N. D. & Stahlberg, H. Journal of Electron Microscopy 59, 103–112 (2010).
3. Peters, J. J. P. et al. Nat Commun 14, 5184 (2023).

204

Distortions correction in HR-(S)TEM and low resolution TEM images: absolute size, strain and polarization measurements

Dr. Nikolay Cherkashin[1], Mrs Sylvie Schamm-Chardon[1]
[1]CEMES-CNRS, Toulouse, France

Poster Group 2

Background incl. aims
TEM and STEM imaging are widely used techniques for visualizing and quantifying shape, size, density, composition, strain and structure in solid state materials at micro-, nano- and subnanometer scales. Such images are subjected to different types of distortions and calibration errors. For the purpose of fully quantitative analysis, these distortions should be removed. We propose here several methods for the correction of low magnification TEM, high-resolution TEM (HR-TEM) and STEM (HR-STEM) images, followed by their quantitative analysis.
Methods
For the correction of low magnification images taken at a basic conventional TEM we apply the technique named “Moiré by specimen design” (MoSD) [1] which allows to measure deformation and displacement in single-crystal structures, in cross-sectional and plan view geometries, with nanometric resolution over a micrometer field of view. The method is based on a specific sample preparation of a stack of two superimposed rotated lamellas of known single crystal that provides the formation of “controlled” moiré images. The deviation of experimentally obtained pattern from the anticipated one can be quantitatively mapped in form of a displacement field by reciprocal space treatment. We developed a method which allows to correct any other image for these distortions.
For HR-(S)TEM images, we present a method named “Absolute strain” (AbStrain) [2]. It allows for quantification and mapping of interplanar distances and angles, displacement fields and strain tensor components with reference to a user-defined Bravais lattice and with their corrections from the image distortions. AbStrain goes beyond the restriction of the existing method known as geometric phase analysis by enabling direct analysis of the area of interest without the need for reference lattice fringes of a similar crystal structure in the same field of view.
For the case of a crystal composed of two or more types of atoms, we also present a method named “Relative displacement” [2] for measuring relative atom displacements of the sub-structures in the unit cell, the quantity being in link to the intrinsic polarization.
Results
We applied the first method for the correction of low-magnification TEM images taken with old generation Jeol2010 TEM. The images contain layers of different thickness, nanoparticles and dislocations, which require a statistical analysis of their size, density and volume fraction. Before correction, the relative errors in the measured values are estimated of 5%, 10% and 60%, respectively. The correction allowed a drastic enhancement in the accuracy of measured values by an order of magnitude.
We demonstrated a successful application of AbStrain and Relative displacement to HR-STEM images of functional oxide and semiconductor heterostructures. BaTiO3/SrTiO3 ferroelectric heterostructure grown on silicon and InGaN 2D layers and 3D islands embedded in GaN will be of particular concern.
Conclusion
The first method proposed here enhances the precision in quantification of nanomaterials dimensions by using low magnification TEM images, that paves the way for elucidating their growth laws based on justified numbers. The 2 other methods extend the range of possible crystalline materials that can be analyzed by the treatment of their HR-(S)TEM images. For example, nanoparticles embedded within different types of matrices, free-standing nanowires, high-angle grain boundaries, multiple stacks of heterostructures of complex oxides and semiconductors, anti-

phase domains and defects inducing long range displacements, constitute just a part of the list of such materials.

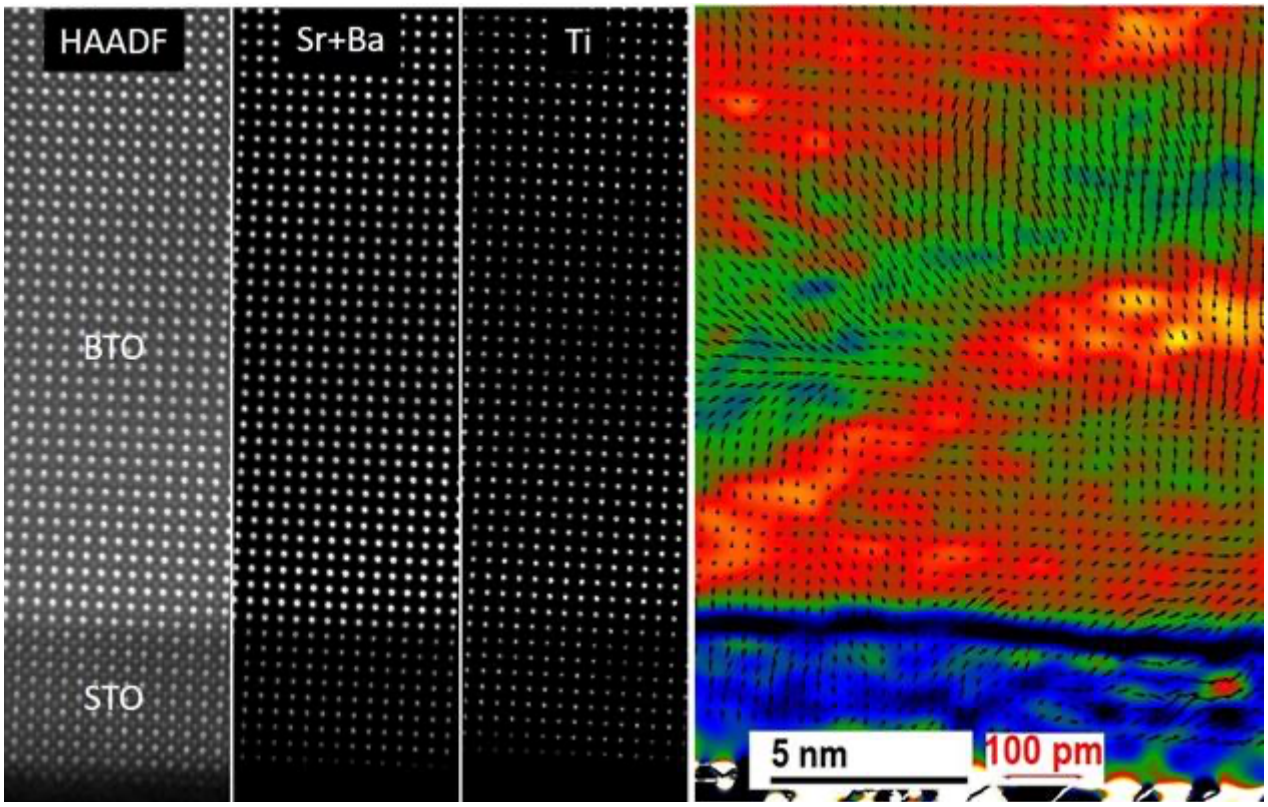

Keywords:

HR-(S)TEM, distortions, strain, polarization, Abstrain

Reference:

Figure: Abstrain corrected HR-STEM-HAADF image of the BaTiO3/SrTiO3/Si structure decomposed into images of Ba+Sr and Ti atoms; out-of-plane strain with reference to the BTO Bravais lattice (colored background) and the relative displacement between the Ti and Sr+Ba atoms (arrows).

[1] N. Cherkashin et al, Scientific Reports 7 (2017), p. 12394.
[2] N. Cherkashin et al, Ultramicroscopy 253 (2023), p. 113778.

241

Information Transfer Improvement by Parallax Correction and Ptychography Reconstruction Applied to Large-Area 4D STEM Experiments

Daniel Stroppa[1], Dr. Stephanie Ribet[2], Dr. Georgios Varnavides[2], Dr. Colin Ophus[2], Dr. Philipp Pelz[3]
[1]DECTRIS, Baden-Daettwil, Switzerland, [2]NCEM, Molecular Foundry, Lawrence Berkeley National Laboratory,, Berkeley, USA, [3]Institute of Micro- and Nanostructure Research (IMN) & Center for Nanoanalysis and Electron Microscopy, Erlangen, Germany

Poster Group 2

Scanning Transmission Electron Microscopy (STEM) is currently a reference technique for high spatial resolution imaging, with wide adoption in the characterization of material science samples and with growing use in life science studies. 4D-STEM [1] approach presents a more detailed recording of the electron scattering pattern using pixelated electron detectors and extends the imaging possibilities by combining the real-space scanning and reciprocal-space scattering components. Recent improvements in the direct electron detector technology allow 4D-STEM experiments at similar speeds to STEM imaging [2], and motivates its exploration as a possible substitute to conventional imaging.

This study addresses the information retrieval from 4D STEM datasets using virtual bright field imaging, parallax-corrected phase imaging, and ptychography reconstruction. Large fields-of-view (> 500 nm) of reference samples were measured with fast 4D-STEM (10 µs dwell time), moderate defocus (~100 nm), and scanning sampling between 0.3 and 2.4 nm/pixel. The 4D STEM datasets were processed with the open-source python-based py4DSTEM package [3, 4], including the preliminary assessment and subset selection by virtual STEM images. Defocused probe parallax imaging and a ptychographic gradient descent method were used to correct probe aberrations, particularly defocus. These methods resulted in reconstructed images with effective upsampling, due to the information retrieval from both real and reciprocal spaces.

While the 4D STEM reconstruction with a virtual BF approach resulted in an image with spatial resolution limited by either probe aberration or sampling, equivalent to conventional BF STEM imaging, both parallax-corrected phase imaging and ptychography reconstruction allowed for information retrieval down to lattice level (< 0.2 nm). The findings indicate that 4D STEM reconstruction methods can yield resolution beyond real-space sampling, possibly limited by the effective electron dose used in fast 4D STEM experiments. A current challenge is to extend and optimize these image reconstruction methods to recover resolution from the full field of view of such large-area scans. However, with the increasing efficiency and accessibility of 4D STEM data analysis, the calculation and display of (near-) real-time super-resolution images is foreseen.

Fig. 1. Comparison of (left) Virtual DF image and (center) parallax-corrected phase image from a cropped 128x128 pixels region from a standard gold nanoparticles sample. scale bar = 10 nm.(right) Detail of up-sampled crop region and respective Fourier Transform indicating transfer of lattice information. scale bar 5 nm.

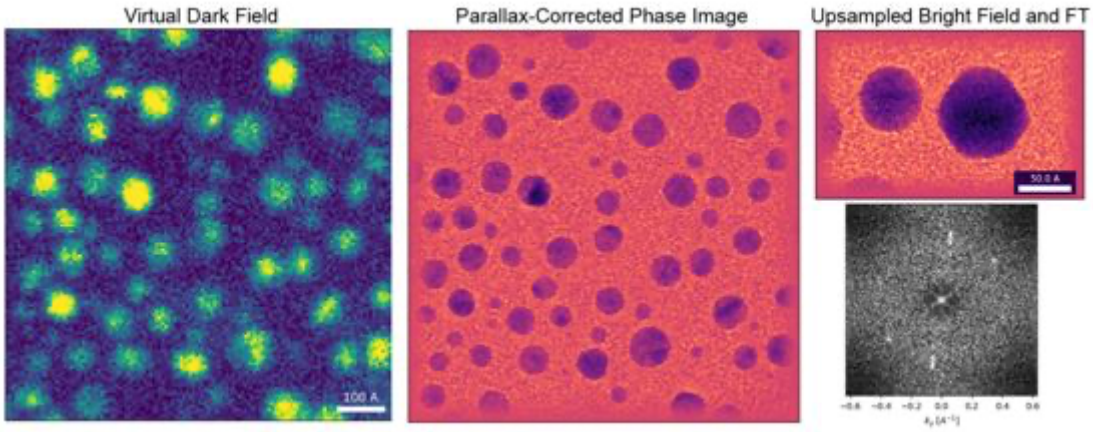

Keywords:

4D STEM, ptychography, parallax

Reference:

1. C. Ophus, Microsc. Microanal. 25-3 (2019) 563-582. DOI: 10.1017/S1431927619000497
2. M. Wu et al., J. Phys. Mater. 6 (2023) 045008. DOI: 10.1088/2515-7639/acf524
3. B. H. Savitzky et al., Microsc. Microanal. 27-4 (2021) 712-743. DOI: 10.1017/S1431927621000477
4. G. Varnavides et al., arXiv preprint: https://arxiv.org/abs/2309.05250

246

Depth sensitivity of atomic resolution secondary electron imaging

Professor Koh Saitoh[1]
[1]Institute of Materials and Systems for Sustainability, Nagoya University, Nagoya, Japan, [2]Department of Applied Physics, Nagoya University, Nagoya, Japan, [3]Hitachi High-Tech Corporation, Hitachinaka, Japan

Poster Group 2

Background incl. aims
Recent advances in spherical aberration-corrected electron microscopes have enabled us to observe not only the projected structure of a sample using transmission electrons but also the surface structure with atomic resolution using secondary electrons (SE) emitted from the sample [1,2,3]. Atom-resolved SE imaging of surface structures is one of the key challenginges. The first attempt was made by Ciston et al. for 2 x 6 reconstruction on the surface of SrTiO3 (001) [4]. This report showed that SE signal has a potential capability to detect surface structures uniquely formed only on the topmost surface of the material with a high spatial resolution. In this study, the depth resolution of the SE imaging is investigated using twisted layers of MoS2, which are the thinnest system composed of a surface layer and substrate. The spatial resolution and elemental contrast of the SE images are also evaluated.
Methods
Monolayer MoS2 was grown on SiO2 thin film formed on a silicon substrate by chemical vapor deposition (CVD). The monolayers were peeled off from the substrate and transferred to a carbon support film for TEM observation. Some of the MoS2 monolayers were stacked on the other monolayer MoS2 by rotating 30 deg. to fabricate twisted bilayer MoS2. An aberration-corrected scanning transmission electron microscope equipped with a cold field emission gun and Everhart-Thornley SE detector (Hitachi High-Tech HF-5000) was used to acquire atom-resolved SE and ADF-STEM images at an acceleration voltage of 200 kV. The convergence semi-angle of the incident beam was set to 23 mrad, and the acceptance angle of the ADF detector was set to 40-200 mrad.
Results
Figures 1(a) and 1(b) show ADF-STEM and SE images simultaneously taken from a region containing both monolayer (upper left) and bilayer (lower right) MoS2, respectively. The ADF-STEM image of the monolayer region shows Mo and S sites as bright spots with different intensity, or Z-squared contrast, confirming the projected structure of MoS2 [0001] incidence shown in Fig. 1(c). The SE image of the monolayer region is noisier than the ADF-STEM image, but shows signals at positions corresponding to the locations of Mo and S atoms, forming the six-membered rings of the MoS2 structure. Mo and S show a similar intensity, indicating that the observed signal is not due to the backscattered electrons but due to SEs emitted from the illuminated atoms and their surrounding regions. The spatial resolution of the ADF-STEM and SE images, which are estimated by the outermost peaks in the FFT patterns, are 0.1 nm, and 0.16 nm, respectively.
The ADF-STEM image of the bilayer region shows wheel-shaped atom clusters with 12-fold symmetry as indicated by the white circle in Fig. 1(a). The 12-fold wheel-shaped clusters are formed by stacking two MoS2 monolayers rotated by 30 deg. to each other. Figure 1(d) shows an atomic arrangement of the projection structure of the wheel-shaped cluster. The central bright dot of the wheel-shaped cluster corresponds to the superposed two Mo atoms and surrounding 12 dots correspond to 12 Mo atoms in the surface and second layers, 6 Mo atoms are in the surface layer and the other 6 Mo atoms are in the second layer. SE images of the bilayer region do not show the projection structure of bilayer MoS2 but show the six-membered rings as observed in the SE image of the monolayer region. In other words, SE images selectively visualize only the surface monolayer. This result indicates that

atomic-resolution SE imaging has an extremely high surface sensitivity and is very effective for the determination of the surface structure.
The SE image of the bilayer region is about 1.5 times brighter than the monolayer region. An FFT pattern of the SE image of the bilayer region shows 12 spots around the central spot, which are composed of 6 intense spots alternate with 6 weak spots. The FFT pattern can be understood as an overlap of two 6-fold patterns rotated by 30 degrees with different intensities. This confirms the fact that the SE image visualizes one of the monolayers more intensely than the other. The reason why the second layer is not visualized in SE imaging is considered to be because SEs emitted from the second layer and directed toward the detector are significantly attenuated as they pass through the surface layer.
Conclusion
In the present study, we found that high-resolution SE imaging selectively shows atomic arrangement of a surface monolayer, even though the monolayer is located on other materials. The present results indicate that high-resolution SE imaging has a high surface sensitivity of a monolayer level. We also confirmed that the transverse spatial resolution of the SE images does not differ significantly between the monolayer and bilayer MoS2, achieving at less than 0.2 nm. The thickness dependence of the SE yield should also be examined to clarify whether the SE production by energy transfer of excited states produced by primary electrons leads to the enhancement of the SE production beyond volume effects. A further study will be conducted on the formation mechanism of layer-number-contrast in SE imaging of atom layer materials.

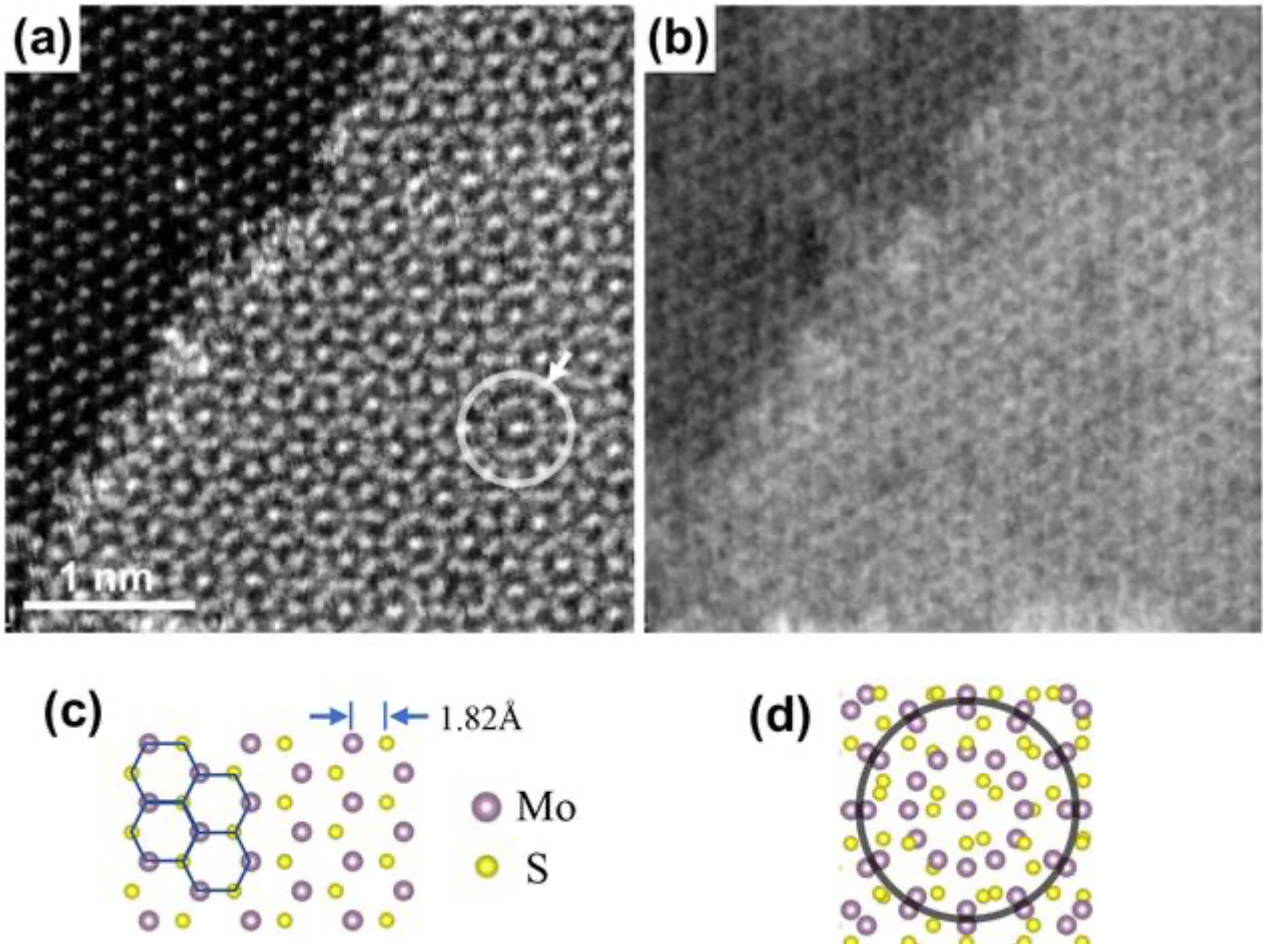

Keywords:

atomic resolution secondary electron imaging

Reference:

[1] H. Inada, L. Wu, J. Wall, D. Su, Y. Zhu Y (2009) J. Elec. Microsc. 58: 111.

[2] Y. Zhu, H. Inada, K. Nakamura, J. Wall (2009) Nat. Mater 8: 808.
[3] H. Inada, et. al. (2011) Ultramicrosc. 111: 865.
[4] J. Ciston, et. al. (2015) Nat. Commun. 6: 7358.

255

Investigation of electron-beam-induced charging in a dolomite needle using off-axis electron holography

Dr. Fengshan Zheng[1], Mrs Ingrid McCarroll[4], Dr Vadim Migunov[3], Dr Marco Beleggia[5], Prof Giulio Pozzi[6], Prof Julie Cairney[4], Prof Rafal Dunin-Borkowski[2]
[1]South China University of Technology, Guangzhou, China, [2]Forschungszentrum Jülich, Jülich, Germany, [3]RWTH Aachen University, Aachen, Germany, [4]The University of Sydney, Sydney, Australia, [5]Technical University of Denmark, Denmark, Denmark, [6]University of Modena and Reggio Emilia, Modena, Italy

Poster Group 2

The phenomenon of electron-beam-induced charging of specimens in the transmission electron microscope (TEM) is attracting increasing attention, both for fundamental reasons and because it has a strong influence on image contrast and quality, in particular when studying insulating and (cryo-)biological specimens [1], in which it is responsible for the bee-swarm or Berriman effect [2-4]. Electron-beam-induced charging is generally believed to result from secondary electron emission from specimen surfaces as a result of primary electron bombardment. However, the underlying physics is not yet fully understood.

Recent developments in off-axis electron holography in TEM offer the possibility to directly map charge density distributions in materials in real space [5, 6] as a function of parameters such as dose (rate), applied voltage and specimen temperature.

Figure 1 shows a measurement of electron-beam-induced charging of a needle-shaped specimen recorded at 300 kV using off-axis electron holography in the TEM at an electron dose rate of approximately 0.9 e-/Å2/s. The needle contains an apex of insulating dolomite (CaMg(CO3)2) and a W base. These two regions are separated from each other by Pt, which was deposited in a focused ion beam scanning electron microscope. The phase contour map shows that the needle is charged at its apex. The contours suggest the presence of a dipole-like charge distribution along the length of the needle. Asymmetry in the phase contour map results primarily from the influence of the perturbed reference wave. There is neither a dose-rate nor a total dose dependence of charging in this needle (not shown).

Surprisingly, a decrease in the reconstructed amplitude is visible in the vacuum region around the apex region. Although this observation is suggestive of a time-dependent charging and discharging process, no double exposure effects are visible in the recorded holograms in the form of Moiré fringes. Secondary electron emission alone may not be sufficient to interpret this result. Coincidence measurements between secondary electrons and electron energy-loss spectra may help to determine the physical origin of secondary electron emission in such samples. Parameters that include the distance to surrounding regions of the specimen and microscope, the presence of surface contamination, the specimen temperature, the presence of residual gas in the TEM column and the voltage applied to the specimen should be varied systematically in such experiments, in order to understand their influence on electron-beam-induced charging and to unravel the underlying physics of charging during illumination by high-energy electrons (and photons) [7].

References:
[1] Russo, CJ. et. al., Ultramicroscopy 187, 43-49 (2018).
[2] Dove, DB, Journal of Applied Physics 35, 1652-1653 (1964).
[3] Drahoš, V. et. al., Czech J Phys 15, 760–765 (1965).

[4] Berriman, JA. et. al., Ultramicroscopy 116, 106–114 (2012).
[5] Zheng, F. et al., Journal of Electron Spectroscopy and Related Phenomena 241, 146881 (2020).
[6] Zheng, F. et al., Ultramicroscopy 241, 113593 (2022).
[7] The authors acknowledge the European Union for funding through the Marie Curie Initial Training Network Grant No. 606988 under FP7-PEOPLE-2013-ITN) and National Natural Science Fund (No. 52373226).

Figure 1 Electron-beam-induced charging of a needle-shaped specimen recorded using off-axis electron holography. The needle contains dolomite (CaMg(CO3)2) in the apex region, a W base and Pt in between. The electron dose rate is 0.9 e-/Å2/s. Upper panel: Electron holographic phase contour map obtained from reconstructed phase images. The phase contour spacing is 2π radians. Lower panel: Amplitude image reconstructed from off-axis electron holograms. Each image is stitched together from results obtained from 5 aligned off-axis electron holograms.

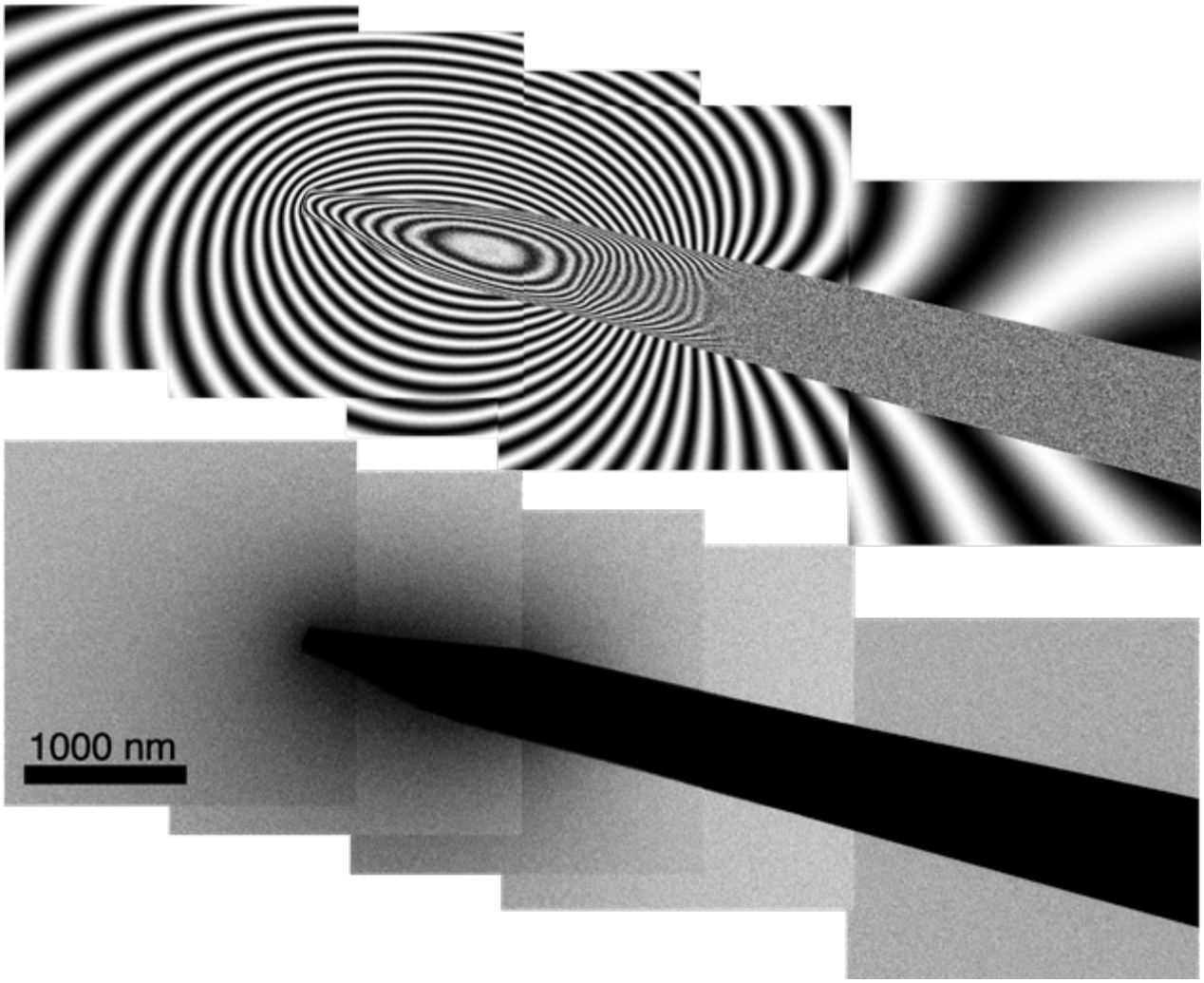

Keywords:

Electron holography, specimen charging

293

Improving Control Signals for Interference Gating

Simon Gaebel[1,2], Hüseyin Çelik[2], Dr. Christian M. Günther[2], Dr. Tolga Wagner[3], Prof. Dr. Michael Lehmann[2]
[1]Max-Born-Institut, Berlin, Germany, [2]Technische Universität Berlin, Berlin, Germany, [3]Humboldt-Universität Berlin, Berlin, Germany

Poster Group 2

Background incl. aims
Time-resolved methods in transmission electron microscopy have become increasingly important in recent years. For off-axis electron holography, one of the most established phase-resolved methods in electron microscopy, interference gating (iGate) [1], has proven to be the most effective implementation for dynamic studies, achieving a time resolution of 25 ns [2]. It is based on the targeted elimination of interference patterns for a large part of the period, synchronized with a periodic process to be investigated. By disturbing the interference pattern with uniformly distributed phase shifts between object and reference wave, the interference pattern is smeared, while the measurement remains undisturbed for a short time (gate), allowing a time-resolved interference pattern to build up.

Methods
Based on theoretical approaches to describe the contrast-influencing properties of gating signals, a novel approach for square-wave-based control signals is developed and presented. The basic idea is that to cancel the interference it is sufficient to superimpose two identical interference patterns, which are shifted only by a constant phase shift of exactly pi to each other. This can be realized by simple square wave-based signals, thus avoiding the signaling problems associated with complex signal shapes (e.g. noise-based control signals) as used so far. The main advantages of this approach are, on the one hand, that such signals can be realized with common electronics (e.g. fast square wave generators) and, on the other hand, that the improved control signal requires a significantly lower amplitude to cancel the interference pattern. The presented adaptations are tested by means of time-resolved electron holography on a nanostructured coplanar capacitor at the FEI Titan 80-300 Berlin Holography Special.

Results
Compared to the noise-based control signal, the developed square wave-based control signal provides matching results when sampling a sawtooth signal applied to the capacitor at a time resolution of 100 ns. Due to the advantages mentioned above, it is already possible to achieve a time resolution of less than 2 ns using a conventional digital pattern generator (DG2040). With this it is possible to investigate the switching behavior of the capacitor at a repetition rate of 50 MHz. The attached figure shows the slope of the time-resolved phases (orange). Compared to the expected switching behavior (dashed green line), these reveal overshooting, which is most likely caused by signal reflections.

Conclusion
According to the results, the square wave-based control signal proves to be superior to the previous noise-based control signals and will be indispensable in future implementations of interference gating, particularly due to its ease of implementation. Time resolutions in the picosecond range are now within reach thanks to this innovation.

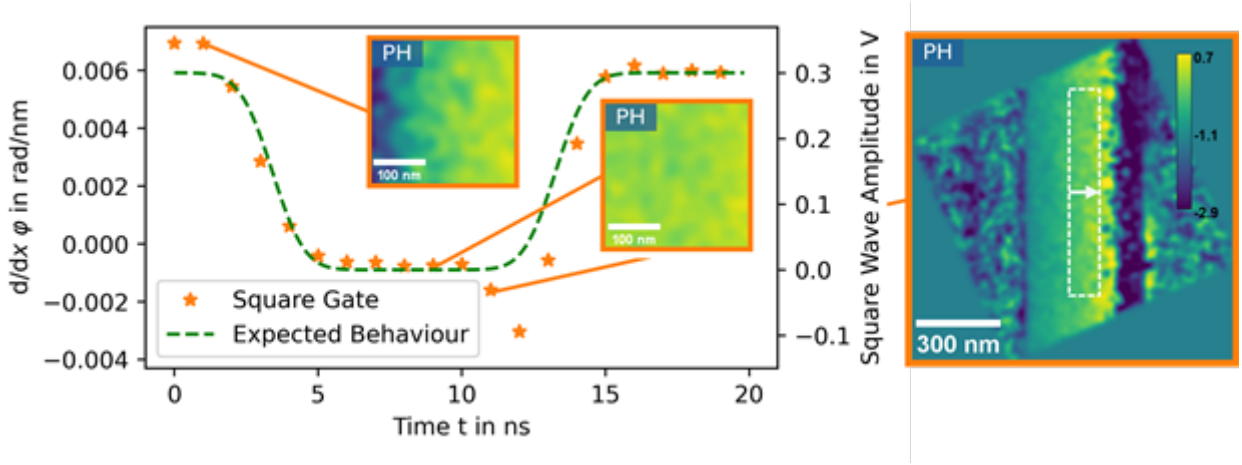

Keywords:

Electron Holography, Temporal Resolution, iGate

Reference:

[1]: Tolga Wagner et al. “Nanosecond Electron Holography by Interference Gating”. In: Ultramicroscopy 206 (Nov. 2019), p. 112824. doi: 0.1016/j.ultramic.2019.112824.

[2]: Tolga Wagner et al. “Imaging localized variable capacitance during switching processes in silicon diodes by time-resolved electron holography”. In: Phys. Rev. B 109 (Feb. 2024), p. 085310 doi: 10.1103/PhysRevB.109.085310

304

Influential factors affecting the quantification accuracy of magnetic moments with electron magnetic chiral dichroism technique

Dr Xiaoxiao Fu[1], Mr Zhixin Zeng[1], Miss Qiwen Hu[1], Dr Xiaoxu Huang[1]
[1]International Joint Laboratory for Light Alloys (MOE), College of Materials Science and Engineering, Chongqing University, Chongqing , China

Poster Group 2

Background:
Electron magnetic chiral dichroism (EMCD), a transmission electron microscopy (TEM) technique based on electron energy-loss spectroscopy (EELS), allows quantitative measurements of element-selective spin and orbital moments at a high spatial resolution [1-2]. Since EMCD was first demonstrated in 2006 [1], the investigation of the influencing factors of quantitative determination has always been fundamentally important. The influencing factors of asymmetrical diffraction condition, plural scattering effect and signal-to-noise ratio (SNR) have been mostly discussed in the literature, and some data treatment methods have been correspondingly proposed. However, more questions are open. First, deconvolution has been routinely applied to EMCD spectrum to remove the plural scattering, but how effective the deconvolution of momentum-resolved spectra can be? Second, how the universal problem of electron damage can affect the EMCD quantification? Third, what is relationship between SNR and quantification accuracy? We explored our answers to these questions.

Method:
For the first question, TEM experiments were performed on a wedge-shaped area in a plane-view TEM specimen of Fe/MgO(001) thin film. A series of low-loss EELS, conventional in-axis core-loss EELS with Fe-L2,3, and pairs of q-resolved core-loss EELS with Fe-L2,3 edges at two chiral positions were acquired from areas of different thicknesses, using spectrum imaging in the scanning TEM mode (STEM-SI), as in Figure (a). The in-axis EELS and q-EELS before and after deconvolution with changing thickness were then compared.
For the second question, TEM experiments were performed on a cross-sectional TEM specimen of Co/MgO(001) thin film. The surface oxidation layer and amorphous layer were damaged under continuous electron irradiation, as in Figure (a). The changes in shape and intensity of EELS spectrum Co-L2,3 edges under continuous electron irradiation were followed and its influence on the shape of EMCD spectrum was discussed.
For the third question, a pair of EELS spectra at Co-L2,3 edges were mathematically constructed. The background, L3 edge, L2 edge and continuum background of each spectrum were respectively described by one inverse power exponent function, two gaussian functions and one double arctan step function. Various degrees of white gaussian noise were added to the EELS spectra. EMCD spectra with different SNR were thus obtained, and quantification results were compared.

Results and Conclusions:
(1)The q-resolved spectra after deconvolution still contain residual plural scattering, which is more significant in thicker areas than thinner ones, as shown in Figure (c-d). It is then derived that the existence of such residual plural scattering would bring artifacts to ml/ms value. The thicker the detected area is, the higher the ml/ms value would be obtained even after deconvolution. We suggest that even deconvolution would be performed, EMCD spectra should be acquired from sufficiently thin samples for minimizing the plural scattering effect in originally detected spectra before any deconvolution [3-4].

(2) Under sustained electron irradiation during spectra acquisition, a gradual removal of the thin surface oxidation layer, rather than a simple continuous thickness reduction that changes the diffraction and plural scattering conditions, can lead to notable residual nonmagnetic components in EMCD spectra and may make the quantified result of the orbital-to-spin moment ratio remarkably higher than the actual value, as in Figure (f-g). It was thus proposed to pay great attentions to the surface oxidation and to minimize the effect of oxidation layer by performing electron irradiation on the target area prior to EMCD experiments, for improving the quantification accuracy [5].
(3) For quantitative measurement of orbital-to-spin moment ratio of Fe, Co, Ni with an error range within about 50% of actual value, the minimum noise degree should be smaller than 0.01.

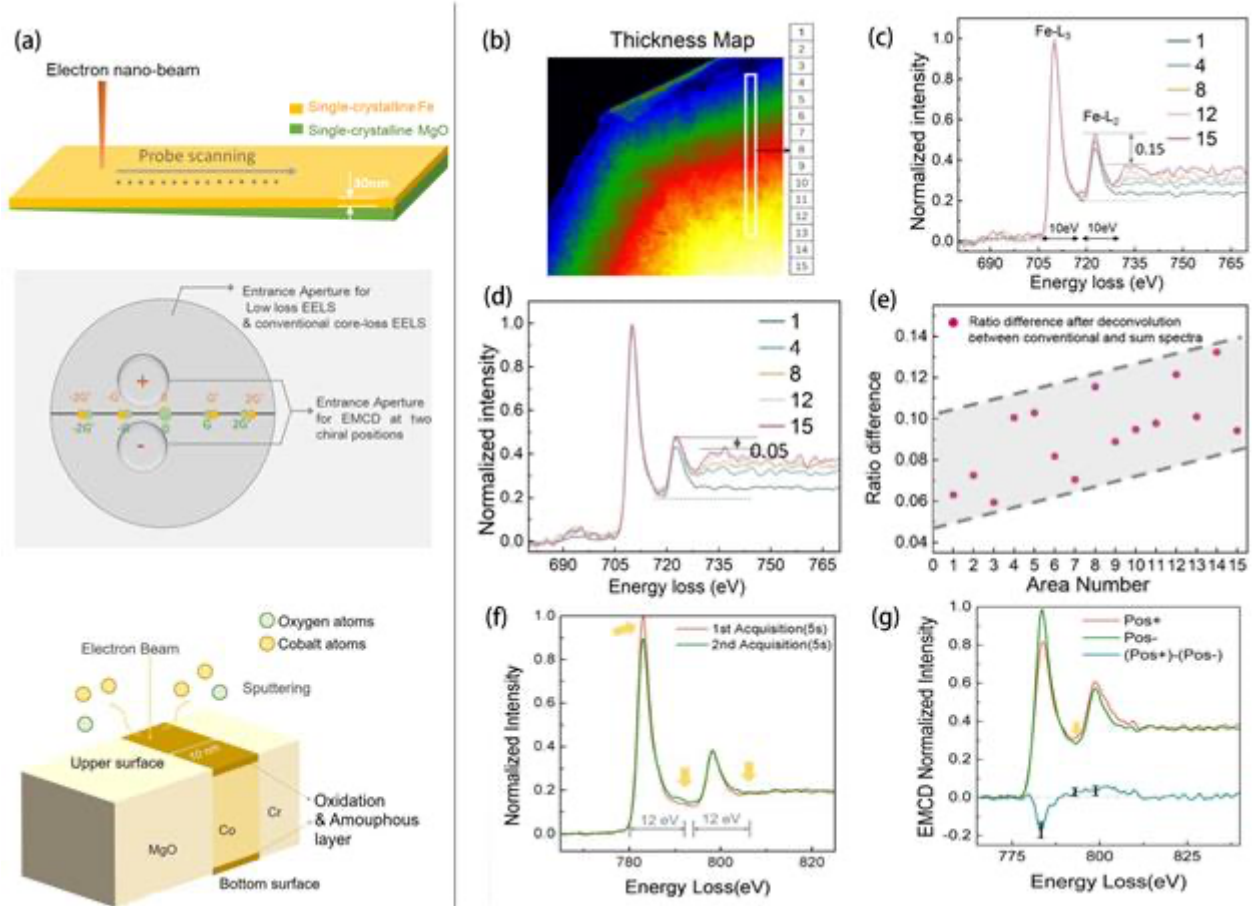

Keywords:

TEM, EMCD, quantification, magnetic moment

Reference:

[1] P. Schattschneider, S. Rubino, et al., Detection of magnetic circular dichroism using a transmission electron microscope, Nature 441 (2006) 486–488.
[2] D. Song, Z. Wang, J. Zhu, Magnetic measurement by electron magnetic circular dichroism in the transmission electron microscope, Ultramicroscopy 201 (2019) 1-17.
[3] Z. Zeng, X. Fu, et al., The influence of residual plural scattering after deconvolution in electron magnetic chiral dichroism, Ultramicroscopy, 2023, 253: 113860.
[4] X. Fu, K. Wu, V. Serin, B. Warot-Fonrose, et al., Electron energy-loss magnetic chiral dichroism of magnetic iron film affected by an underlayer in a double-layer structure, Applied Physics Letters, 2019, 115: 112401.
[5] Q. Hu, X. Fu, et al., Electron knock-on damage effects on electron magnetic chiral dichroism of magnetic metals using cobalt as a model, Applied Physics Letters, 2024, 124(9): 092407.

312

3D atomic-resolution imaging of nanomaterials based on exit wave reconstruction

Sophie Kargo Kaptain[1], Mr. Joakim Kryger-Baggesen[1], Mrs. Rikke Egeberg Tankard[2], Mr. Fu-Rong Chen[3], Mr. Dirk van Dyck[4], Mr. Joerg R. Jinschek[1,5], Mr. Jakob Kibsgaard[2], Mr. Christian Danvad Damsgaard[1,5], Mr. Stig Helveg[1]
[1]Center for Visualizing Catalytic Processes (VISION), Department of Physics, Technical University of Denmark, Kgs. Lyngby, Denmark, [2]Surface Physics and Catalysis, Department of Physics, Technical University of Denmark, Kgs. Lyngby, Denmark, [3]Department of Materials Science and Engineering, City University of Hong Kong, Kowloon, Hong Kong, [4]Departments of Physics, EMAT, University of Antwerp, Antwerp, Belgium, [5]National Center for Nano Fabrication and Characterization, Technical University of Denmark, Kgs. Lyngby, Denmark

Poster Group 2

Breakthroughs in transmission electron microscopy (TEM) have opened for visualizing nanomaterials with atomic resolution and uncovering the surface terminations that are governing e.g. catalytic properties. In a TEM experiment, the most informative outcome is the recovery of the electron wave function exiting the nanomaterial. While different experimental and mathematical reconstruction schemes exist to recover the underlying exit wave, the transformation of exit waves into a three-dimensional (3D) structural model is still being debated. Recently, our group presented an analytical model to describe the 3D atomic-scale arrangement in an excited 2-dimensional Co-Mo-S nanocrystal [1]. The model was based on channeling theory and made for the first time use of the full shapes of the atomic columns in the exit wave. Extending this model to an arbitrary 3D nanomaterial is challenged by the role of extinction distance in relation to the sample thickness as well as the irregular surface both at entrance and exit of the nanomaterial. Here, we will outline the development of this analytical approach to investigate arbitrary nanomaterials at 3D atomic-resolution.

We examine nanometer-sized metal nanoparticles with a focus on their terminating surface structure. The exit waves are reconstructed from experimental focal series of bright-field TEM images, which carries most signal pr. electron. This is vital for investigating surfaces of nanomaterials since under coordinated atoms at the surface are particularly prone to beam-induced alteration compared to the bulk. Imaging is therefore done with low electron dose rates using direct electron detectors (DED) to establish sufficient SNR for the reconstruction while maintaining the pristine structure of the material.

With the complex exit wave, we use the channeling approaches in [1,2] to determine the 3D atomic position and stoichiometry of atomic columns of a carbon supported Pt nanoparticle with a diameter of 5 nm. We present a strategy to counteract the influence of extinction and show how this drastically reduces the elongation of the 3D tomogram along the beam direction. Furthermore, we also present a strategy for the non-uniform entrance and exit surface of the nanoparticles.

In this work, we present an approach to reconstruct 3D structural information about nanoparticles from electron wave functions exiting the sample. Based on channeling theory, an analytical model is outlined to establish the location and stoichiometry of the atomic columns and approaches to counterbalance the role of extinction and irregular entrance and exit plane surfaces are demonstrated. The present work therefore build a foundation to recover a 3D atomic model of a nanoparticle and thereby uncover its exposed surface structure. The present approach should be generally applicable to any nanomaterial even under exposure to reactive environments and should

thus aid the understanding of gas-surface interaction is diverse fields such as crystal growth, corrosion, and catalysis.

Keywords:

Holography, exit waves, 3D atomic-resolution

Reference:

[1] Chen, F. R., Van Dyck, D., Kisielowski, C., Hansen, L. P., Barton, B., & Helveg, S. (2021). Probing atom dynamics of excited Co-Mo-S nanocrystals in 3D. Nature communications, 12(1), 5007.
[2] Chen, F. R., Van Dyck, D., & Kisielowski, C. (2016). In-line three-dimensional holography of nanocrystalline objects at atomic resolution. Nature communications, 7(1), 10603.
[3] The Center for Visualizing Catalytic Processes is sponsored by the Danish National Research Foundation (DNRF146)

326

Identification of inorganic fibres in workplace air by SEM-EDS

Dr. Markus Mattenklott[1], Dennis Kaiser[1], Bianca Gasse[1]
[1]Institute for Occupational Safety and Health (IFA), Sankt Augustin, Deutschland

Poster Group 2

When assessing fibre dusts in the air at workplaces, it is crucial to identify and classify the type of fibre in order to distinguish carcinogenic fibres from others from an occupational health and safety perspective. Up to now, this has been done using an error-prone method of product fibre identification. The aim of the project is to create a database for determining the type of fibre independently of reference materials from the sampled work areas and, based on this, to define identification criteria.
Using available reference materials from the synthetic inorganic fibres used in work areas (synthetic mineral fibres, high temperature wool, micro glass fibres, textile glass fibres, etc.), the range of element composition of the fibre types is determined by means of EDS analysis. In addition, systematic investigations are used to determine the quality of these analyses of fibres with diameters in the micrometre range, identify systematic problems and derive possible differentiation criteria. This database is supplemented by information from publications and manufacturer data, which have been structured for comparison with EDS analyses
A scheme was established that allows fibres in airborne dusts to be classified largely independently of reference materials. It is important not only to look at individual particles separately, but also to classify the fibres found on the basis of previous grouping.
The presented solution to the problem of identifying fibres shows the limits of manual classification. A further step will be the establishment of self-learning neural networks, which have already achieved successful results in initial tests in this area and provide constructive support for identification.

Keywords:

fibres, workplace air, SEM/EDS, identification

445

Assessing Ptychographic Methods for Maximum Low Dose Performance

Tamazouzt Chennit, Ph.D Christoph Hofer[1], Ph.D Biao Yuan[1,2], MS.c Songge Li[1], Ph.D, MEng Andrew Maiden[3,4], Prof. Dr. Timothy Pennycook[1]
[1]EMAT, University of Antwerp, 2020, Belgium, [2]Electron Microscopy Center, University of Technology, South China, China, [3]EEE. Dept, University of Sheffield, S13JD, UK, [4]Diamond Light Source, OX110DE, UK

Poster Group 2

For beam sensitive materials, the dose that can be applied and the dose efficiency of the imaging method often sets the achievable resolution, rather than just the capabilities of the optical system. This is crucial in biology but also for many materials science samples such as metal organic frameworks (MOFs), zeolites, and organic perovskites. While scanning transmission electron microscopy (STEM) has come to dominate high resolution materials science, for the most beam sensitive materials TEM [1] has remained predominant due to the dose efficiency of its phase contrast imaging. Recent technological advances have, however, started to challenge this status quo for low dose imaging, through the combination of fast 4D STEM and ptychography. Ptychography can exceed the dose efficiency of TEM but has been limited until very recently by the relatively slow speed of cameras, which makes 4D STEM exceedingly slow for high probe position count datasets. This bottleneck has recently been overcome using event driven camera technology [2], and conventional framing cameras are also increasingly closing the gap between 4D STEM scan speeds and high-speed conventional STEM, greatly facilitating drift-free and low dose 4D data acquisition.

However, there are many forms of ptychography and so far, sufficient broad comparison of the low dose performance of the various ptychographic methods has been lacking. Ptychographic methods can be grouped into iterative and direct algorithms. Iterative methods are most often performed with a defocused probe, as the higher signal per diffraction pattern facilitates convergence, but with a careful choice of reconstruction parameters they can also produce useful phase images in a low dose focused probe configuration. Here, we present a comparison of a broad spectrum of these algorithms, both iterative and direct, for reconstructing low dose data sets.

Figure 1 compares ptychographic reconstructions of 2.5 nm thick Methylammonium lead iodide (MAPbI3) at a dose of 50 e-/A², using a convergence angle of 13 mrad, with a focused probe. The iterative gradient descent (GD) algorithm converges, but to a relatively poor quality image showing very little atomic structure. The rPIE, ePIE [3], ER and WASP [4] iterative and direct SSB algorithms, all perform better under these conditions, revealing relatively similar atomic structures from which the iodide and the Pb sites can be located. On the heavy Pb atomic sites, contrast reversals are present. These reversals can be easily corrected using our new phase offset method [5], which can greatly improve the interpretability of ptychographic data.

Switching to a defocus of 20 nm, as shown in Figure 2, improves the GD result significantly, however it remains dominated by low frequency features of limited utility, with high resolution information still less clear than the other iterative methods. Although the SSB becomes blurred when the probe is defocused, as expected due to the optical sectioning effect, this can be corrected post collection as we show in the figure.

In addition to the choice of algorithm, the parameters used are critical to obtaining the best solutions. For iterative schemes, probe step size and defocus are linked in their importance to the amount of overlap of adjacent illuminated regions. The convergence angle determines which

frequencies will be transferred most strongly and sets the upper limit on conventional image resolution. Although ptychography can provide super-resolution and exceed this limit, at very low doses there is insufficient scattering to higher angles for super-resolution to provide significant benefits; rather, at low doses, correction of residual aberrations is expected to play a greater role.

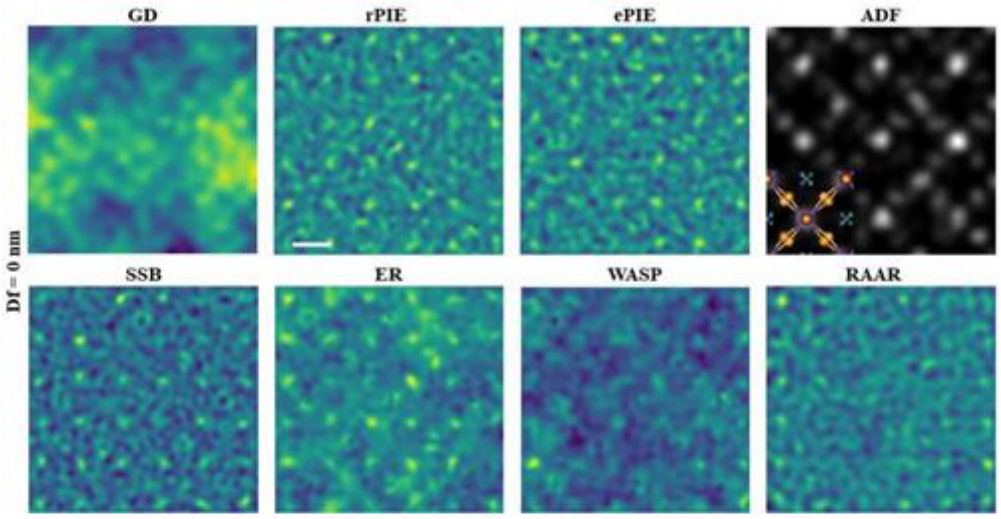

Fig. 1. GD, rPIE, ePIE, ER, WASP and SSB reconstructions at 50 e^-/A^2 dose using a 13 mrad convergence angle shown alongside the annular dark field (ADF) images using a focused probe. Scale bar is 3 Å.

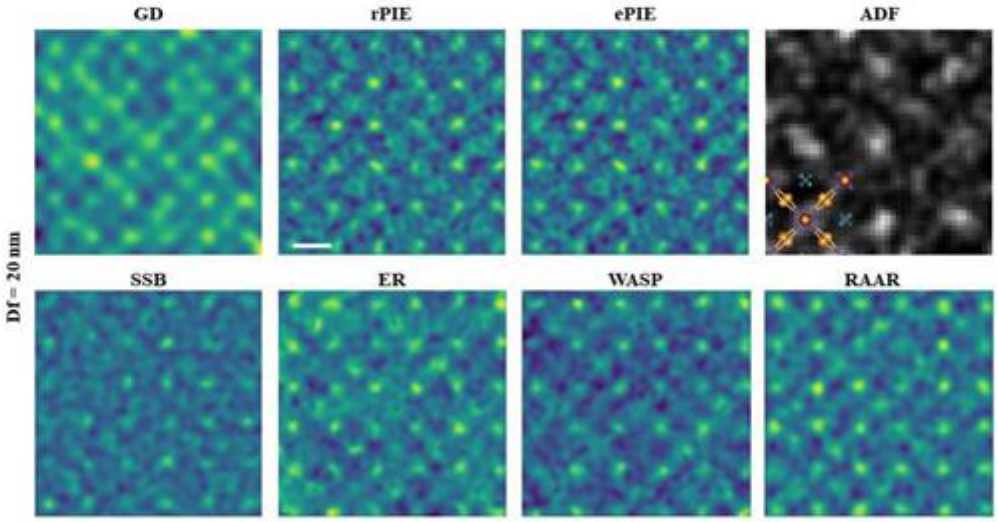

Fig. 2. GD, rPIE, ePIE, ER, WASP and SSB reconstructions at 50 e^-/A^2 dose using a 13 mrad convergence angle shown alongside the annular dark field (ADF) images using a defocused probe of 20 nm. Note that the SSB image for the defocused probe has had the defocus corrected post collection. The iterative methods produce noticeably stronger atomic contrast with the defocus. Scale bar is 3 Å.

Keywords:

Ptychography, Low-dose, 4D STEM

Reference:

[1] T. J. Pennycook et al., Ultramicroscopy 196 (2019), p. 131-135.
https://doi.org/10.1016/j.ultramic.2018.10.005

[2] D. Jannis et al., Ultramicroscopy 233 (2022), 113423.
https://doi.org/10.1016/j.ultramic.2021.113423

[3] A. M. Maiden and J M. Rodenburg., Ultramicroscopy 109 (2009), p. 1256-1262.
https://doi.org/10.1016/j.ultramic.2009.05.012

[4] A. Maiden et al., (2024), 10.1364/opticaopen.24894489.

[5] C. Hofer et al., Ultramicroscopy 258 (2024), 113922.
https://doi.org/10.1016/j.ultramic.2024.113922

447

Towards atom-counting from first-moment STEM images

Dr. Yansong Hao[1], Dr. Annick De Backer[1], Prof. Scott David Findlay[2], Prof. Sandra Van Aert[1]
[1]EMAT, University of Antwerp, Antwerp, Belgium, [2]School of Physics and Astronomy, Monash, Australia

Poster Group 2

Background incl. aims
Over the past few years, a model-based approach has been established to extract quantitative measurements from atomic resolution HAADF STEM images. In this approach, the image is modelled as a superposition of 2D Gaussian peaks from which unknown structure parameters, such as atomic column positions, peak intensities and scattering cross-sections, can be estimated. This approach has been used to achieve accurate and precise determination of the chemical composition of materials and to count the number of atoms with single atom sensitivity. Atomic column intensities in HAADF STEM scale with the square of the atomic number and so light columns are easily hidden by the stronger intensity from heavier columns, making simultaneously estimating structural parameters for both light and heavy atomic columns challenging. However, this limitation might be overcome by quantifying other types of STEM image via a model-based method.
Methods
Recent advances in pixelated detectors, along with the capability to collect 4D STEM datasets, offers significant flexibility in generating diverse STEM imaging modes. One example is first-moment STEM images, in which the center of mass (COM) of convergent beam electron diffraction (CBED) patterns is recorded at each scan position. Typically, the COM is determined in two perpendicular directions, generating COMX and COMY images. Within the phase object approximation, the COM is proportional to the gradient of the projected potential, which is expected to scale linearly with the number of atoms in atomic columns as well as atomic number. Therefore, COMX(Y) images are expected to narrow down the signal difference between light and heavy atomic columns. By means of simulations, our study has explored the possibilities to estimate structure parameters and to perform atom counting based on COMX(Y) images. The precision of counting atoms with COMX(Y) images is also evaluated and compared to that using the traditional HAADF regime.
Results
We have performed model-based quantification on simulated COMX(Y) images of aluminum crystals. The integrated-intensities of atomic columns have been determined as a function of thickness by fitting a parametric model of a superposition of X(Y) derivatives of 2D Lorentzian-functions. For aluminum, a monotonic increase is observed up to a thickness of 30 atoms (~12nm), suggesting these intensities can be used as a quantitative measure for atom counting. Based on repetitive noise realizations of both COMX(Y) and HAADF images, it is possible to estimate the precision with which intensities can be measured. Furthermore, examining the overlap of the integrated-intensity distribution between atomic columns with consecutive thickness offers a means to evaluate the atom counting precision. This overlap can be quantified in terms of its relative width. The reduction of the relative width suggests the possibility to attain more precise atom counts when using COMX(Y) images as compared to the use of HAADF STEM images. Finally, the integrated-intensities from an aluminum wedge, whose thickness ranges from 5 to 15 atoms, is compared to those values from the aluminum crystals. The excellent agreement demonstrates the robustness to use bulk crystal simulations as a library, where the atom counting for samples with different shapes can be achieved by comparing to those library values.
Conclusions
In this study, a model-based quantification approach for COMX(Y) images has been developed. Unknown structure parameters, especially the integrated intensities of atomic columns, can be

estimated, which enables us to perform atom-counting. As a comparison to traditional HAADF STEM imaging, atom-counting based on COMX(Y) images shows better precision and has great potential for further use in materials where both light and heavy elements are present.

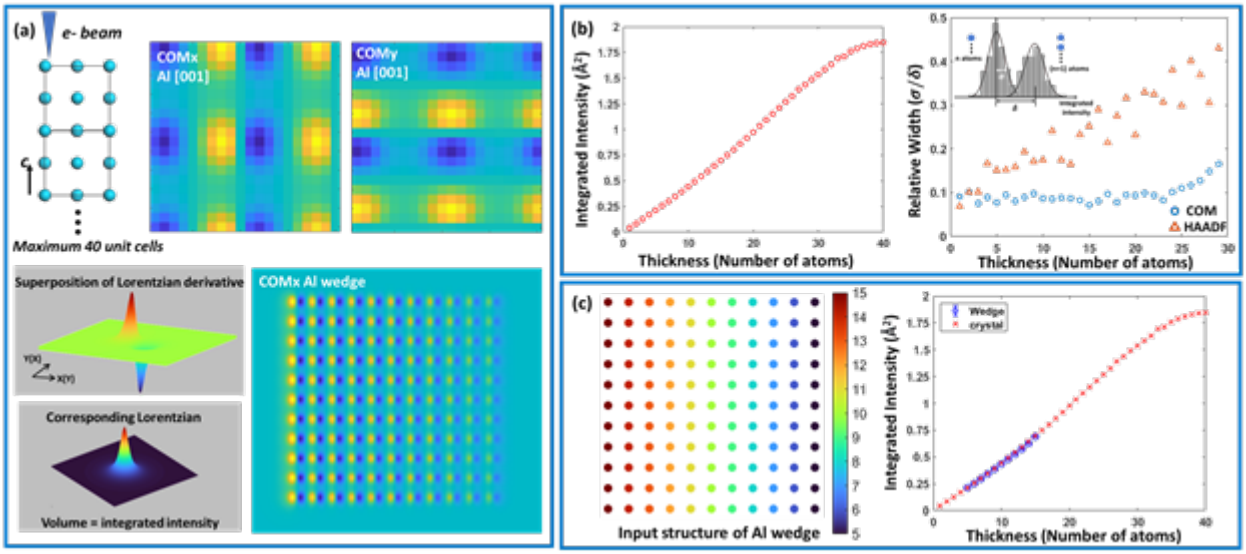

Keywords:

Quantitative 4D-STEM, atom counting,

Reference:

[1] S. Van Aert et al, Nature 470 374-377 (2011).
[2] S. Van Aert et al, Ultramicroscopy 109 1236-1244 (2009).
[3] S.J. Pennycook, Ultramicroscopy 30 58–69 (1989).
[4] C. Ophus, Microscopy and Microanalysis 25 563–582 (2019)
[5] R. Close et al, Ultramicroscopy 159 124–137 (2015).

459

Overcoming the aberration-limit of a non-corrected Transmission Electron Microscope with computational ghost imaging

Paolo Rosi[1,2], Lorenzo Viani[2], Dr Enzo Rotunno[1], Prof. Stefano Frabboni[2], Dr Amir Hossein Tavaby[3], Prof Rafal E. Dunin-Borkowski[3], Dr Alberto Roncaglia[4], Dr Vincenzo Grillo[1]
[1]CNR-Institute for Nanoscience, Modena, Italy, [2]University of Modena and Reggio Emilia, FIM department, Modena, Italy, [3]Ernst Ruska-Centre for Microscopy and Spectroscopy with Electrons, Forschungszentrum Jülich, Jülich, Germany, [4]CNR - Institute for Microelectronics and Microsystems, Bologna, Italy

Poster Group 2

Background incl. aims

The invention of aberration correctors at the end of the 20th century has made modern Transmission Electron Microscopes (TEMs) one of the most sought-after scientific instruments in modern material science and life science laboratories since they now allow to image and characterize samples with the highest lateral (spatial) resolution. [1,2] The most important technological advancement which further increased the interest in TEMs was the invention of spherical aberration correctors. [3,4] Unfortunately, aberration correctors are quite costly and are reaching performance limitations: this has prompted some research groups to work on computational imaging methods to increase the lateral resolution in TEMs.
Here we present the results from a simulated computational ghost imaging (CGI) scheme for TEMs where we demonstrate numerically that it's possible to overcome the resolution limit imposed by aberrations using well-characterized structured probes and a bucket detector.

Methods

In computational ghost imaging the image of the sample (and its spatial information) is computationally recovered by illuminating the sample with a series of known structured beams and collecting the integrated transmitted intensity via a single-pixel bucket detector positioned after the sample. In fact, if the measurement is linear we can see that it can be described in matrix notation with the equation $I = P \hat{} T$ where I is the array containing the N signals recorded by the single pixel detector, P is the array containing the intensity pattern of the N probes and T is the sample transfer function. By knowing both P and I it is possible to recover T and many algorithms exist to this end [5]. We have developed a custom python-based algorithm that allows us to simulate the generation of structured patterns, provides us with the value of the signal measured by a virtual bucket detector (even in presence of noise and realistic coherence effects) and recovers T with three different reconstruction algorithms: the traditional one, the alternated projection algorithm and the conjugate gradient descent algorithm.

Results

For the generation of the simulated structured patterns we assumed a 300kV microscope with Cs=2.7mm, a 15.4 mrad probe convergence angle and as defocus four times the Scherzer STEM defocus. All other aberrations were neglected since we had such a large value of Cs. The electron modulator is assumed to be in the last condenser aperture, while the sample of choice (a twisted bilayer of MoS2 – Figure1a) is conventionally positioned in the sample plane. As single pixel detector we used the annular dark field detector, but in principle we could use other single pixel detectors

such the bright field detector or those used for energy dispersive X-Ray imaging, electron energy loss spectroscopy or cathodoluminescence.
As it is possible to appreciate from figure 1, our CGI scheme is able to overcome the aberration limit imposed by the instrument (figure 1e) with a two-fold increase in spatial resolution compared to an aberration-limited STEM image (figure 1c) as confirmed by the analysis of their FTTs (figure 1f and d, respectively).

Conclusion

Here we have demonstrated that, if the optical system is well characterized and the aberrations that act on the illumination are known and quantified, it is possible via a computational imaging technique to overcome the aberration-limit.
We are already working on an experimental implementation where the phase plate for structuring the beam has been realized using MEMS technology. As a next step for further improvements, we are working on the possibility to use machine learning (ML) to further optimize our electron modulator and the pattern that it can generate, with should enhance both our simulated results and more importantly the future experimental ones. Moreover, we are also working on a mixed scheme where we also control the scan coil of the TEM to optimize the illumination, increases reliability and acquisition speed, and should allow for the reconstruction of the probe.

Figure 1 Caption: a) schematic of the electron-optical setup, (b,d,f) comparison between the sample atomic potential, the aberration-limited STEM image, and CGI reconstruction and their corresponding FFT (c,e,g). For the CGI reconstruction reported here no noise and no realistic coherence effects (temporal or spatia) were considered, but we have also performed simulations in those scenarios. In the FFT images the yellow inner circle corresponds to 2α, while the red outer circle corresponds 4α, where α=7.3 mrad. Scalebar in b,d and f is 0.5nm. In h) is shown an example of a structured pattern utilized for the CGI reconstruction and in i) is shown complex image of its FFT.

The authors acknowledge support from the European Union's Horizon 2020 Research and Innovation Programme (grant agreement no. 964591 "SMART-electron" and no. 101094299 "IMPRESS") and the Italian Ministry of research (PRIN Project no. 2022249HSF "AI-TEM")

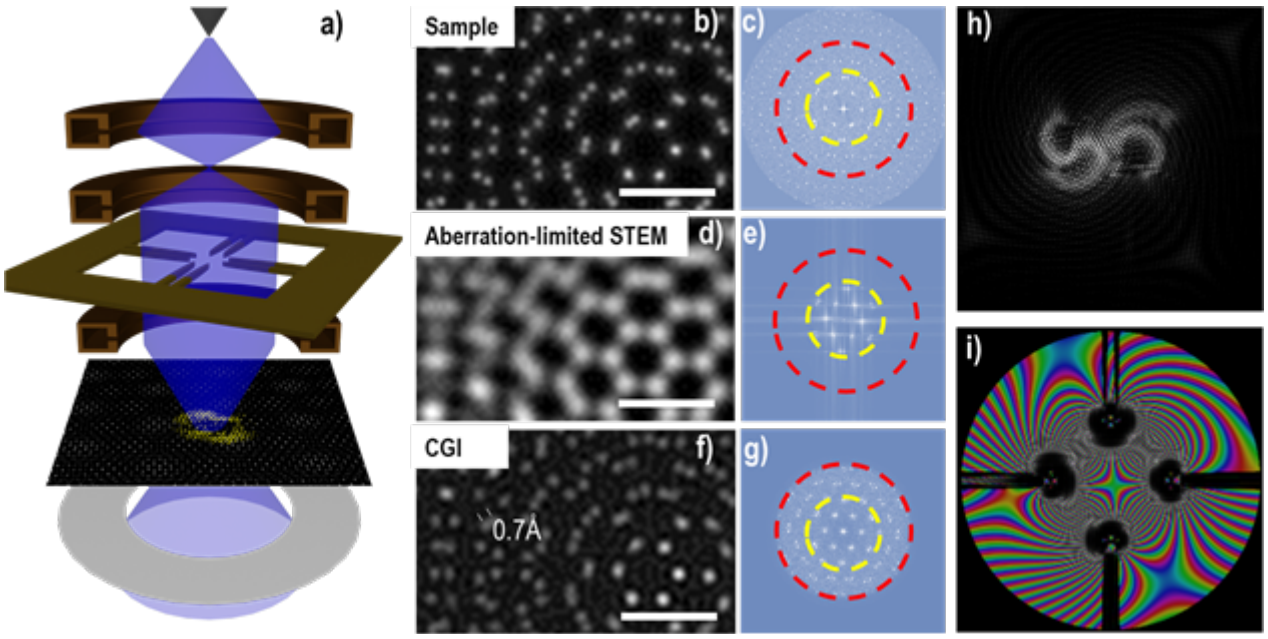

Keywords:

Phase-plates, electron-beam-shaping, single-pixel-imaging, high-resolution, MEMS

Reference:

[1] M. Haider, H. Müller, S. Uhlemann, J. Zach, U. Loebau, and R. Hoeschen, Prerequisites for a Cc/Cs-Corrected Ultrahigh-Resolution TEM, Ultramicroscopy 108, 167 (2008).
[2] H. H. Rose, Historical Aspects of Aberration Correction, J. Electron Microsc. (Tokyo). 58, 77 (2009).
[3] M. Haider, H. Rose, S. Uhlemann, B. Kabius, and K. Urban, Towards 0.1 Nm Resolution with the First Spherically Corrected Transmission Electron Microscope, J. Electron Microsc. (Tokyo). 47, 395 (1998).
[4] M. Haider, S. Uhlemann, E. Schwan, H. Rose, B. Kabius, and K. Urban, Electron Microscopy Image Enhanced, Nature 392, 768 (1998).
[5] L. Bian, J. Suo, Q. Dai, and F. Chen, Experimental Comparison of Single-Pixel Imaging Algorithms, J. Opt. Soc. Am. A 35, 78 (2018).

481

Largely improved momentum resolution in STEM-DPC imaging of Si(110) with a segmented detector

Julius Bürger[1], Maja Groll[1], Aladin Ullrich[2], Manfred Albrecht[2], Jörg K. N. Lindner[1]
[1]Paderborn University, Paderborn, Germany, [2]University of Augsburg, Augsburg, Germany

Poster Group 2

Differential phase contrast (DPC) imaging in scanning transmission electron microscopy (STEM) is one of the promising methods to precisely characterise the electric field and the charge density distribution in solids at atomic resolution. DPC measurements are based on the detection of the lateral shift in the centre of mass (CoM) of intensity distribution in the detector plane. This shift of the CoM is detected by a position-sensitive detector such as a segmented or pixelated detector and can be related to the transferred momentum, which is imposed on the electron beam by the electrostatic potential of the specimen via the Coulomb force [1]. Besides the sensitivity to electric fields, DPC measurements are influenced by many factors such as residual lens aberrations, specimen thickness and tilt [2], as well as the detector response function. For segmented detectors the latter is determined by the polar and azimuthal detection angle intervals of the detector segments. Due to the small number of segments and their comparably large detection angle intervals, segmented detectors have a much lower momentum space resolution than pixelated detectors. This significantly influences the measurable DPC signal [3]. The detection intervals of a segmented detector can intentionally be modified: The polar detection intervals can be varied via the camera length; the azimuthal detection angle intervals can be set via the detector rotation. It is mandatory to know how and to what extend the detector response function of a segmented detector influences the features in a DPC image. For quantitative DPC imaging, it is therefore in the best interest to give methods for identification of artefacts and optimisation of the detector response function. This is presented in this contribution, including a comparison of DPC measurements of Si(110) acquired with segmented and pixelated detectors.

Experimental DPC images of a 30 nm thick Si(110) specimen are acquired with two probe-side corrected microscopes, a JEOL JEM-ARM200F and a JEOL JEM-ARM200F NEOARM, both operated at 200 kV. For DPC imaging, the former is equipped with a rotatable eight-fold segmented detector, the latter with a fast GATAN OneView camera for 4D-STEM imaging. To evaluate the DPC signal of the pixelated detector, the CoM determined from the complete intensity distribution and from intensities of virtual detector segments, which are projected onto the pixelated detector in post-processing, are utilised. While a thickness of 30 nm is ill-suited for quantitative DPC, it is appropriate to reveal and study the influence of the detector response function. Analogous image simulations are obtained using the software Dr. Probe [4], which is based on a multislice algorithm.

Comparative DPC investigations of Si(110) acquired with the segmented and the pixelated detector (Fig. 1 a-d) reveal that measured electric field and charge density distributions match in the order of magnitude. However, a strong influence of the segmented detector can be seen from significantly different image features, e.g. resulting in unexpected positive charge densities at interatomic pixels (Fig. 1b) which are not detected with a pixelated detector (Fig. 1d). To study the influence of the segmented detector's response function, series of measured and simulated DPC images are compared for different detector rotations. This is facilitated with the so-called scattergram, which is a 2D histogram of the transferred momentum distribution of the DPC image. The scattergrams exhibit characteristic intensity distributions depending on the detector rotation. A good agreement between experimental and simulated scattergrams is observed. In addition, a method is presented to find the optimum polar and azimuthal collection angles of a segmented detector to obtain a DPC image with high similarity to the one of a pixelated detector. This is achieved by comparing the DPC images extracted from the full intensity distribution of the measured 4D-STEM data set with the DPC image

acquired by projecting virtual detector segments on the same 4D-STEM data set. In case of a 30 nm thick Si(110) specimen the optimum detector response function is achieved when the direct beam illuminates the complete detector at a detector rotation of 45° to the Si dumbbell axis (inset in Fig. 1b). Ultimately, a novel method to increase the azimuthal momentum space resolution of segmented detectors is presented which uses a series of DPC images of equidistant detector rotations. Using this method, artefacts such as the positive charge density at interatomic pixels are minimised even for such large specimen thicknesses (Fig 1.f).
The results show a strong influence of the detector response function of segmented detectors and emphasise the importance of minimising this influence on DPC images for correct image interpretation. In particular, the here presented method for increasing the azimuthal momentum space resolution of segmented detectors enables to obtain equally good DPC measurements with a segmented detector as with a pixelated detector.

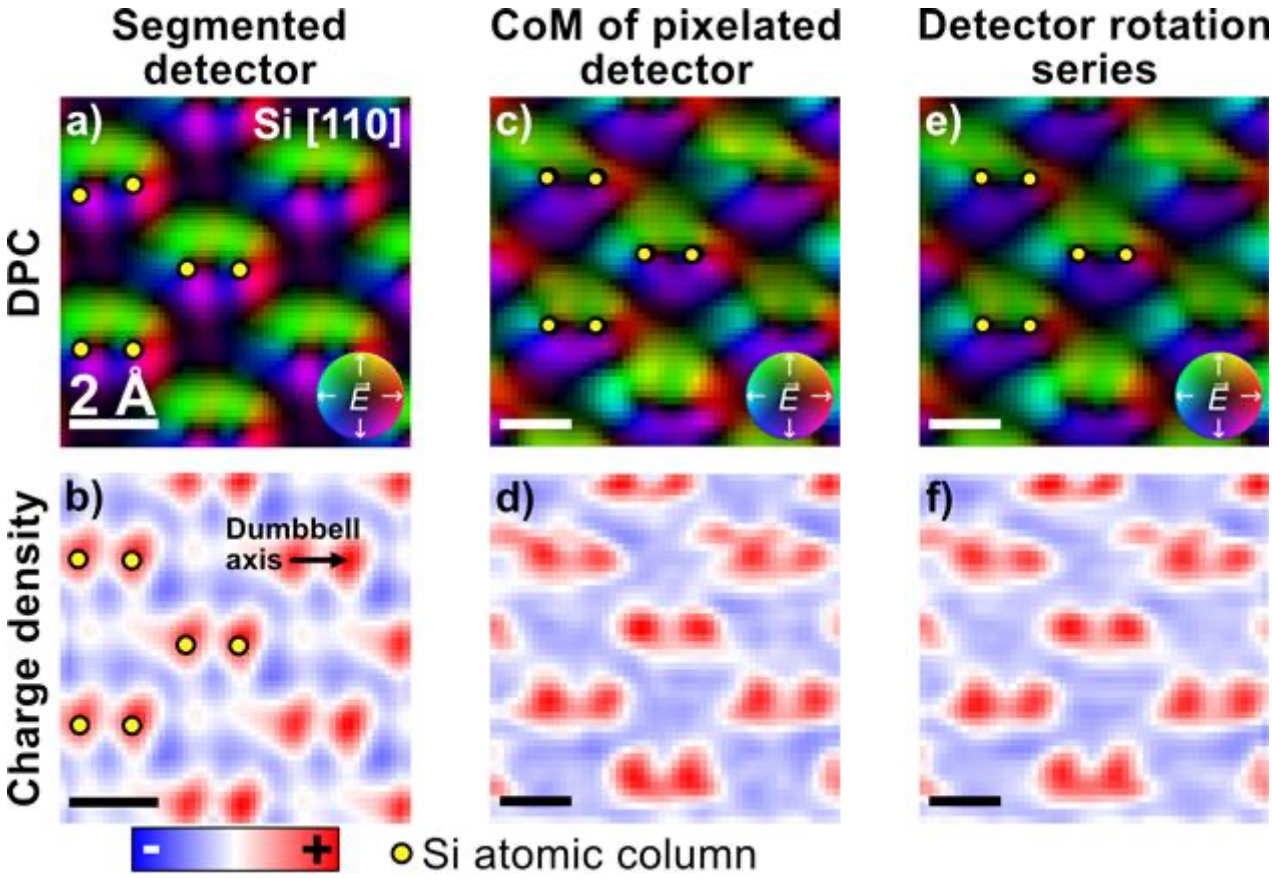

Keywords:

DPC, detector response function

Reference:

[1] Müller-Caspary, K., et al., Ultramicroscopy 178 (2017), 62-80.
[2] Bürger, J., et al., Ultramicroscopy 219 (2020), 113118.
[3] Mawson, T., et al., Ultramicroscopy 233 (2022), 113457.
[4] Barthel, J., Ultramicroscopy 193 (2018), 1-11.

emc2024 COPENHAGEN

486

Influence of dynamical diffraction on DPC measurements of 2D materials

Maja Groll[1], Julius Bürger[1], Prof. Dr. Jörg K. N. Lindner[1]
[1]Paderborn University, Paderborn, Germany

Poster Group 2

Dynamical diffraction effects in (scanning) transmission electron microscopy often hamper direct image interpretation. While dynamical diffraction effects are commonly neglected in conventional STEM investigations, they are crucial in quantitative phase retrieval techniques as multiple coherent scattering events alter the intensity distribution during the interaction of the electron wave with the specimen. One of these phase retrieval techniques is differential phase contrast (DPC) imaging, which is based on the detection of the center of mass in the post specimen intensity distribution and is promising for the precise quantification of atomic electric field and charge density distributions in solids. It is commonly accepted that qualitative DPC imaging is only feasible for specimen thicknesses below 20 nm [1] due to the influence of dynamical effects resulting in beam broadening and intensity redistribution within the specimen. For quantitative DPC imaging, the maximum specimen thickness is estimated to be about 2 nm, depending on the atomic species [2].
Due to their inherently low thickness, 2D materials are therefore of great interest for DPC measurements and are intensively investigated also by other phase retrieval methods [3,4]. Among the 2D materials there is the class of transition metal dichalcogenides (TMD) which consist of molecular layers with the stoichiometric form MX2 (M: transition metal, X: chalcogenide). The molecular layers are bound to each other only by weak van-der-Waals interactions. This allows for a comparatively simple preparation of specimens that are only one or a few molecular layers thick and are therefore suitable for quantitative DPC imaging. However, the possibility that dynamical effects may influence the measurable electric field distribution even in 2D materials, has only been rudimentarily investigated.
Since slight changes in the intensity distribution along the propagation of the electron wave through the specimen alter the measurable electric field and charge density distributions measured by DPC, it is important to understand the influence of dynamical effects on DPC measurements in a few-layer 2D TMDs.
In this contribution, we present investigations on the influence of dynamical diffraction effects on the DPC images of mono- and multilayers of tungsten diselenide, which is a 2D TMD. This is achieved using multislice simulations performed with the software Dr. Probe [5] and a comparison with experimental DPC images. For the acquisition of the latter, an eight-fold segmented bright-field detector installed at a probe-side Cs-corrected microscope is used and the same configuration is assumed in the simulations. In addition to simulations for 2D WSe_2, image simulations are also conducted for isolated atomic columns to investigate the obtainable DPC images in dependence of the atomic species, the atomic spacing and the acceleration voltage. By comparison with the DPC image of a single atom, the influence of dynamic effects is revealed. Furthermore, the propagation of the electron beam in the vicinity of different atomic columns is investigated by analyzing the real space probe intensity as a function of the specimen thickness.
The DPC measurements and simulations of WSe_2 [0001] are in good qualitative agreement. However, they show an unexpected ratio of electric field magnitudes and charge densities at W and Se atomic columns, even for a monolayer: despite their lower projected atomic number, Se atomic columns exhibit an increased electric field and positive charge density magnitudes compared to W. This can be explained by dynamic diffraction effects superimposed with other influences such as lens aberrations. These findings are supported by simulations for the isolated atomic columns which reveal that the measurable mean DPC signal of W and Se atomic columns is always smaller than the mean DPC signal of a single atom multiplied by the number of atoms in the column. In addition, the

DPC image is significantly affected by the atomic spacings in beam direction and number of atoms in an atomic column. The behavior of the real space probe intensity for the interaction with different atomic columns is presented and related to the measurable DPC signal, again supporting the finding that the atomic species of the atomic columns strongly affect the influence of dynamical diffraction on the DPC image. The results highlight that for quantitative DPC measurements even on 2D materials a careful consideration of dynamic influences must be made.

Keywords:

2D materials, differential phase contrast

Reference:

[1] C. Addiego, et al., Ultramicroscopy 208 (2020).
[2] K. Müller-Caspary, et al., Nat. Commun. 5 (2014).
[3] S. Fang, et al., Nat. Commun. 10 (2019)
[4] K. Müller-Caspary, et al., Phys. Rev. B 98 (2018)
[5] J. Barthel, Ultramicroscopy 193 (2018)

500

Zernike Phase Plates for aberration-corrected TEM in Material Science

Simon Hettler[1,2], Raul Arenal[1,2,3]
[1]Instituto de Nanociencia y Materiales de Aragón (INMA), CSIC-Universidad de Zaragoza, Zaragoza, Spain, [2]Laboratorio de Microscopías Avanzadas (LMA), Universidad de Zaragoza. Zaragoza, Zaragoza, Spain, [3]Araid Foundation, Zaragoza, Spain

Poster Group 2

Background incl. aims
Aberration correctors are tools to manipulate the phase of the electron wave, which have strongly increased the resolution and the impact of transmission electron microscopy (TEM) studies in multiple scientific fields. However, the phase cannot be adjusted in a completely random way by such correctors. Specifically, although the aberrations can be corrected for a large range of spatial frequencies allowing to resolve almost all crystal lattices, the overall phase contrast in acquired images is low. In fact, for perfect aberration correction, phase-contrast transfer and thus phase contrast in the image would be zero. Physical phase plates (PPs), developed for life science specimens [1], potentially allow to obtain maximum phase contrast if combined with aberration correction [2]. The aim of this investigation [3] was to demonstrate the promising application of PPs in material science.
Methods
For this study, we fabricated a Zernike PP, consisting of a thin amorphous carbon film with a central hole milled by a focused ion beam. Figure (a) shows a sketch of the objective aperture stripe with mounted PP consisting in a conventional Cu TEM grid (SEM image in (a)), which was implemented in an aberration-corrected (image) transmission electron microscope (Titan3, Thermo Fisher Scientific). Figure (b) shows a SEM image of one of the grid frames showing the carbon film with central hole. The PP was applied to different nanomaterial samples, for example to Fe_3O_4 nanoparticles [4].
Results
Figure (c) shows an example TEM image of Fe_3O_4 nanoparticles at the edge of an amorphous carbon film acquired with PP. While the lattice-fringe contrast of the nanoparticles is clearly resolved, the PP causes a strong phase-contrast transfer also for intermediate spatial frequencies making the carbon film and the nanoparticle morphology visible. The power spectrum of the TEM image (d) shows that the phase contrast is increased for spatial frequencies larger than the cut-on frequency corresponding to the radius of the hole. The power spectrum also reveals the reflections linked to the crystalline nanoparticles. The application of the unheated Zernike PP is limited to thin samples with small crystalline structures as the PPs charges if hit by a diffracted beam with increased intensity [3].
Conclusion
The experimental results obtained with an unheated Zernike PP clearly prove the benefits of applying a PP for high-resolution TEM studies in material sciences allowing to image features at the atomic and nanometric scale at the same time [3]. The combination of aberration correction TEM with PPs is especially promising as it potentially allows to perform a wave-function reconstruction with only two images, containing pure amplitude and phase contrast, respectively. Further technological improvement, such as the implementation of a PP heating device to avoid charging, or the use of electrostatic PPs could overcome the limitations of the unheated Zernike PP used for the presented results.
Acknowledgments
Research supported by the DFG (HE7675/1-1) and by the Spanish MICIU (PID2019-104739GB-100/AEI/10.13039/501100011033).
Figure caption

(a) Sketch of objective aperture stripe with objective apertures and a Zernike PP. (b) SEM image of a frame of the PP grid. (c) Aberration-corrected TEM image of Fe_3O_4 nanoparticles acquired with PP and (d) corresponding power spectrum. Scale bars are (c) 6 nm and (d) 2 1/nm.

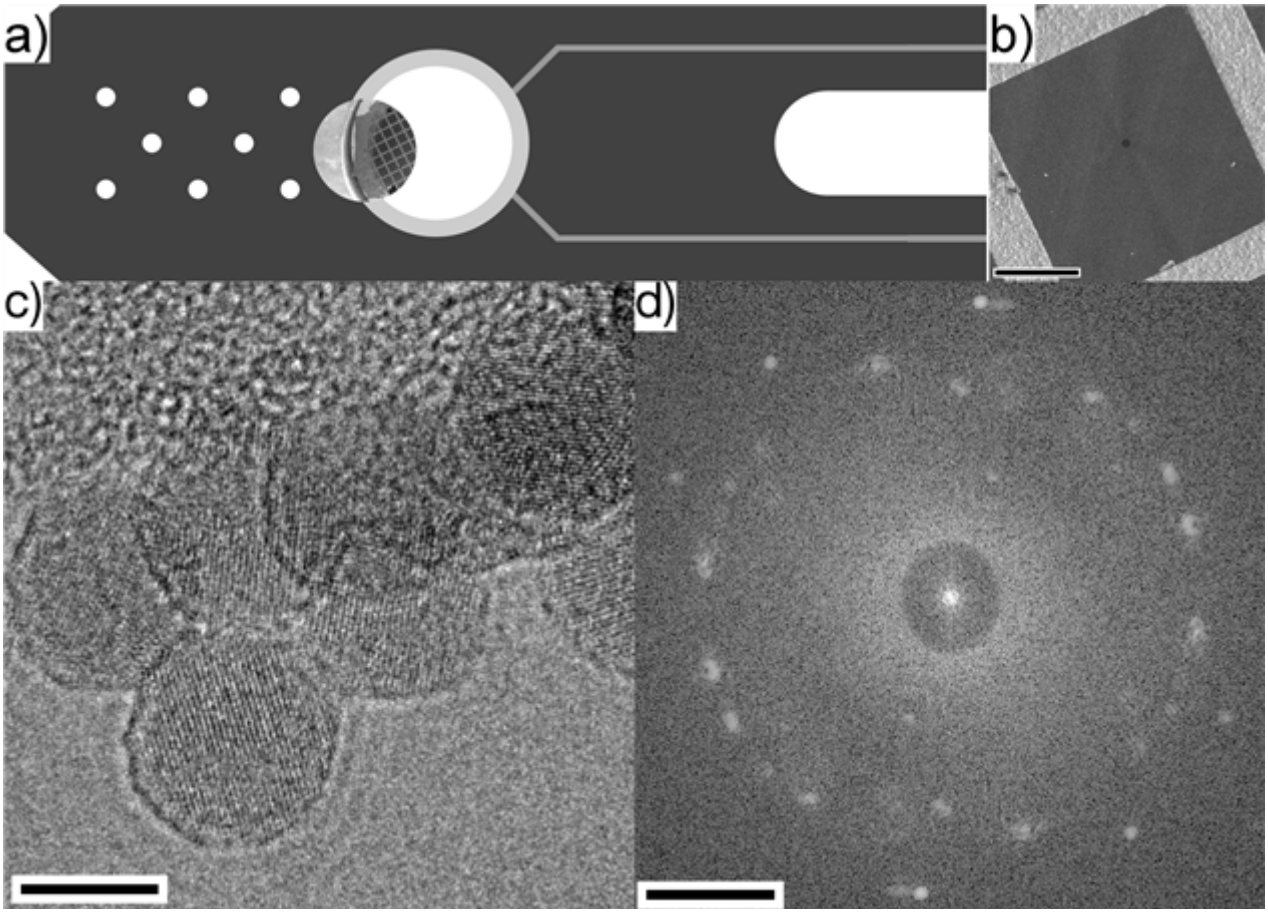

Keywords:

TEM, phase-plate, aberration-correction, phase-contrast, nanoparticles

Reference:

[1] M. Malac et al, Microscopy 70, 1, 75-115 (2020), http://dx.doi.org/10.1093/jmicro/dfaa070.
[2] B. Gamm et al, Ultramicroscopy 108, 9, 878–884 (2008), https://doi.org/10.1016/j.ultramic.2008.02.009.
[3] S. Hettler, R Arenal, Ultramicroscopy, 239, 113564 (2022), https://doi.org/10.1016/j.ultramic.2022.113564.
[4] K. Sartori et al, ACS Appl. Mater. Interfaces 13, 14, 16784-16800 (2021), https://doi.org/10.1021/acsami.0c18310.

551

4D-STEM Post measurement machine learning enhanced aberration correction for amorphous and magnetic samples

Maximilian Töllner[1], Xiaoke Mu[3], Di Wang[1], Christian Kübel[1,2]
[1]Institute of Nanotechnology - KIT, Karlsruhe, Germany, [2]KNMFi, Karlsruhe, Germany, [3]School of Materials and Energy and Electron Microscopy Centre, Lanzhou University, Lanzhou, China

Poster Group 2

High-resolution transmission electron microscopy is one technique to resolve the atomic structure of materials. However, the phase information of the exit-wave is lost. Therefore, 4D-STEM techniques such as ptychography were developed to retrieve the phase information and enhance the resolution. Even so electron ptychography is used frequently on different material systems, imaging the domain structure of magnetic samples remains challenging. This is due to the fact that for magnetic imaging the objective lens needs to be switched off and the aberration corrector becomes obsolete. This would decrease the resolution limit.
This work is a first step to achieve aberration free high-resolution imaging of magnetic domains in the field-free mode (objective lens is off). This is needed to avoid the interaction between the strong magnetic field of the objective lens with the magnetic sample.
It has been previously shown that 4D-STEM datasets can be used to remove residual aberrations in high resolution images of crystalline samples[1]. This work builds on the previous work and transfers it to objective lens free operations in which the probe corrector cannot be used. The largest issue in lens-free operations is that the spherical aberrations cannot be corrected. Additionally to field free measurements, this method can also be used for post processing 4D-data on amorphous samples like polymers or metallic glasses in which the probe correction was not ideal.
For the reconstruction of the aberrations, the Single-Side Band(SSB) ptychography method is used for gaining information about the aberrations. The SSB method is a direct reconstruction method, which is performed by making a Fourier transform of the real space. It should be noted that in the field-free mode, the Fourier transform of a brightfield image does not show sharp spots, but a more diffusely spread intensity distribution. As an example, a gold cross grating imaged at low magnification is shown in figure 1a and its Fourier transform in 1d. In order to remove the higher-order aberrations to improve the phase reconstruction, more SSB patterns need to be selected, in comparison to the method that relies on crystalline samples. This is due to the previously mentioned diffuse distribution of the intensity in the Fourier space which is then visible as noise in the SSB-patterns as shown in figure 1b. A minimum number of 20-30 patterns are needed to achieve good results. To index these patterns the knowledge of the position of the discs needs to be known see figure 1b. The position was accurately indexed by using artificial intelligence (AI), which measures the angle and the distance between the discs. The training data of the artificial intelligence was simulated to look as close as possible to real measurements. Since the amount of data for training an AI needs to be large and it needs a large amount of computational power to simulate thousands of 4D-STEM datasets. The SSB datasets have been calculated directly without running a full simulation. For this a list of object function was created, the distances, the angles between the discs and the aberrations were selected randomly. After the indexing of the patterns the aberrations are calculated in the same way as previously shown by Ning et al. in [1]. The resulting SSB phase images show that the aberrations have been corrected compare figure 1c and 1e. The resulting data can then be used to be further processed by an iterative ptychography method like the extended ptychographic iterative engine(ePIE).

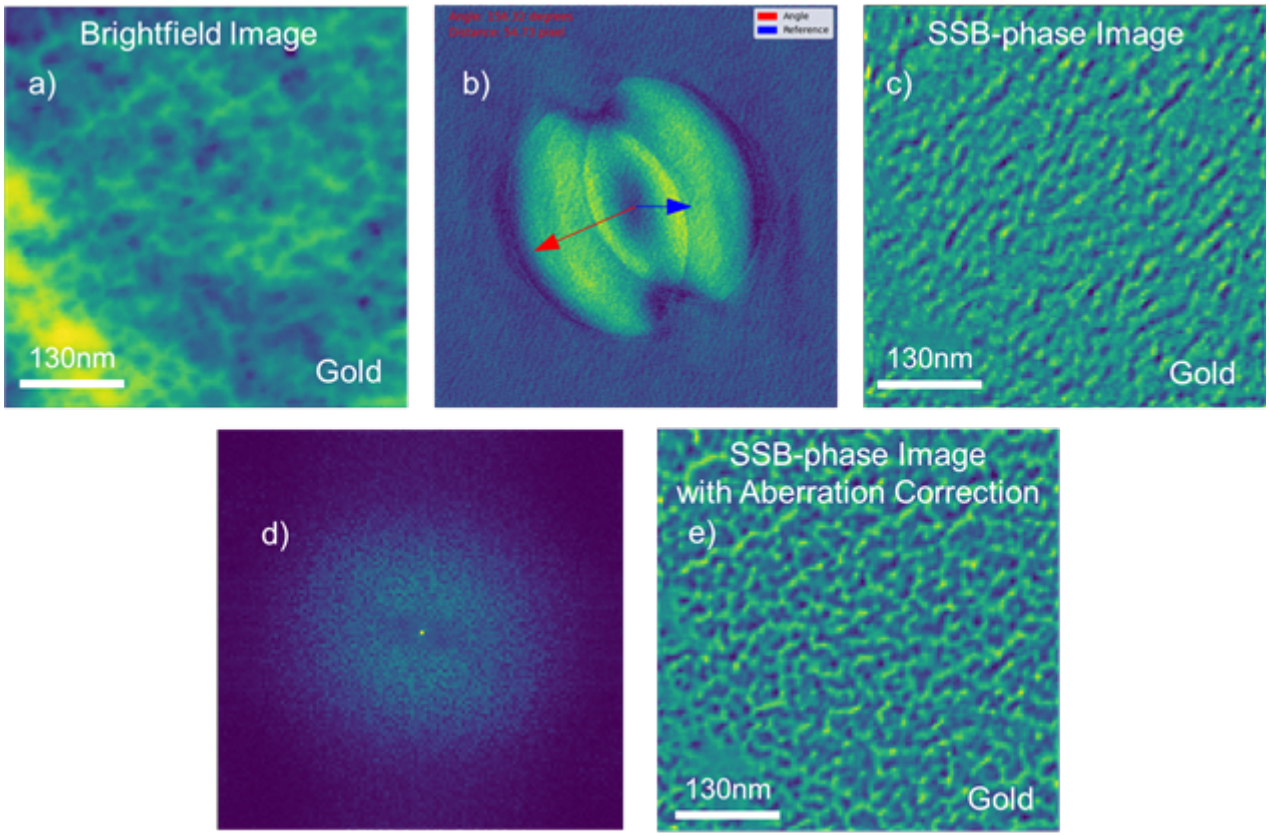

Keywords:

Ptychography, aberration correction, AI

Reference:

[1] Shoucong Ning et al., Accurate and Robust Calibration of the Uniform Affine Transformation Between Scan-Camera Coordinates for Atom-Resolved In-Focus 4D-STEM Datasets, Microscopy and Microanalysis, Volume 28, Issue 3, 1 June 2022, Pages 622–632, https://doi.org/10.1017/S1431927622000320

612

Simultaneous acquisitions and applications of DPC/OBF STEM, EDS and EELS

Dr. Yuhiro Segawa[1], Dr. Akiho Nakamura[1], Mr. Hiroki Hashiguchi[1], Mr. Yuji Kohno[1], Dr. Shigemasa Ohta[1], Senior Assistant Professor Takehito Seki[2], Professor Naoya Shibata[2]
[1]JEOL Ltd., Akishima-shi, Japan, [2]The University of Tokyo, Bunkyo-ku, Japan

Poster Group 2

Background incl. aims
The use of a segmented detector has become standard for various STEM observations, particularly for Differential Phase Contrast (DPC) STEM[1] and Optimum Bright Field (OBF) STEM[2]. DPC STEM can visualize weak electromagnetic fields such as p-n junction interfaces[3] and magnetic skyrmions[4]. In low-dose experiments with beam-sensitive materials, like zeolites and metal-organic frameworks (MOFs)[5], OBF STEM method achieves noticeably better contrast during live imaging. The applications of a segmented detector are further extending across a variety of material and life science fields. As an example, this research shows a combined analysis of these advanced imaging techniques with elemental analysis methods, EDS and EELS, simultaneously acquired in our new FEMTUS platform.
Methods
The sample was a semiconductor memory. The experiment was performed using JEM-F200, equipped with SAAF-Quad detector (an annular four-segmented detector), Dual SDD detector for EDS, CEOS Energy Filtering and Imaging Device (CEFID) with Dectris ELA hybrid-pixel electron detector, and integrated analysis platform FEMTUS developed by JEOL. In the FEMTUS platform, all detectors and cameras can be synchronized and simultaneous acquisition becomes possible with easy operation. For all experiments we chose an accelerating voltage of 200 kV, STEM mapping was performed with a dwell time of 10ms, convergence semi-angle of 6.6 mrad, and EELS collection semi-angle of 2.2 mrad limited by the central hole of SAAF-Quad detector.
Results
Figure 1 shows the result of DPC STEM and EDS/EELS elemental mapping, acquired simultaneously in a single scan. Fig. 1a shows the x-components of the center of mass (COM) DPC STEM derived from the signals of four SAAF-Quad detector channels. It can be seen that the COMx image reveals thin line contrasts around the regions indicated by the arrows. The DPC STEM method has better sensitivity for differences in projected potential, originating from both electromagnetic field and/or local chemical composition. Fig. 1b and 1c represent a magnified view of the EDS and EELS count maps, respectively. EDS mapping has an advantage in detecting heavy elements such as tungsten and titanium, which are difficult to access using the phase imaging method (DPC or OBF STEM) and EELS. As complementary information, the EELS mapping shows clear contrast for light elements (oxygen, nitrogen, and silicon) with higher S/N ratio compared to EDS. All of this information can be used to analyze the origin of DPC STEM contrast. Fig. 1d shows intensity profiles of COMx and EELS data extracted from the area indicated by the white square. The peaks of COMx intensity correspond to the increase of oxygen component, whereas the amount of nitrogen decreases in the interface region. Such combined information is very helpful to investigate the origin of phase contrast images, such as the composition difference between SiOx film and SiNx bulk region shown here.
Conclusion
In summary, we acquired DPC STEM, EDS, and EELS data of semiconductor samples simultaneously and revealed that the origin of DPC STEM signals was due to changes in the local chemical composition. Without the additional information from EDS and EELS, it was difficult to clarify whether the obtained phase contrast represents chemical composition, electromagnetic field, or just a difference in local thickness. Such simultaneous acquisition of DPC, EDS, and EELS enables us to directly understand the origin of the observed phase image contrast. Furthermore, since compared

to EDS and EELS mappings, DPC STEM is very sensitive to changes in the projected potential, it will be possible to clarify compositional differences by integrating the EDS and EELS signals of regions where phase contrast differences could be observed, even under low-dose conditions. This should also be useful for the composition analysis of electron beam-sensitive materials whose structures are destroyed with just a few scans. On the day of the presentation, we will show the details of the experimental results and additional instances of simultaneous data acquisition including OBF STEM.

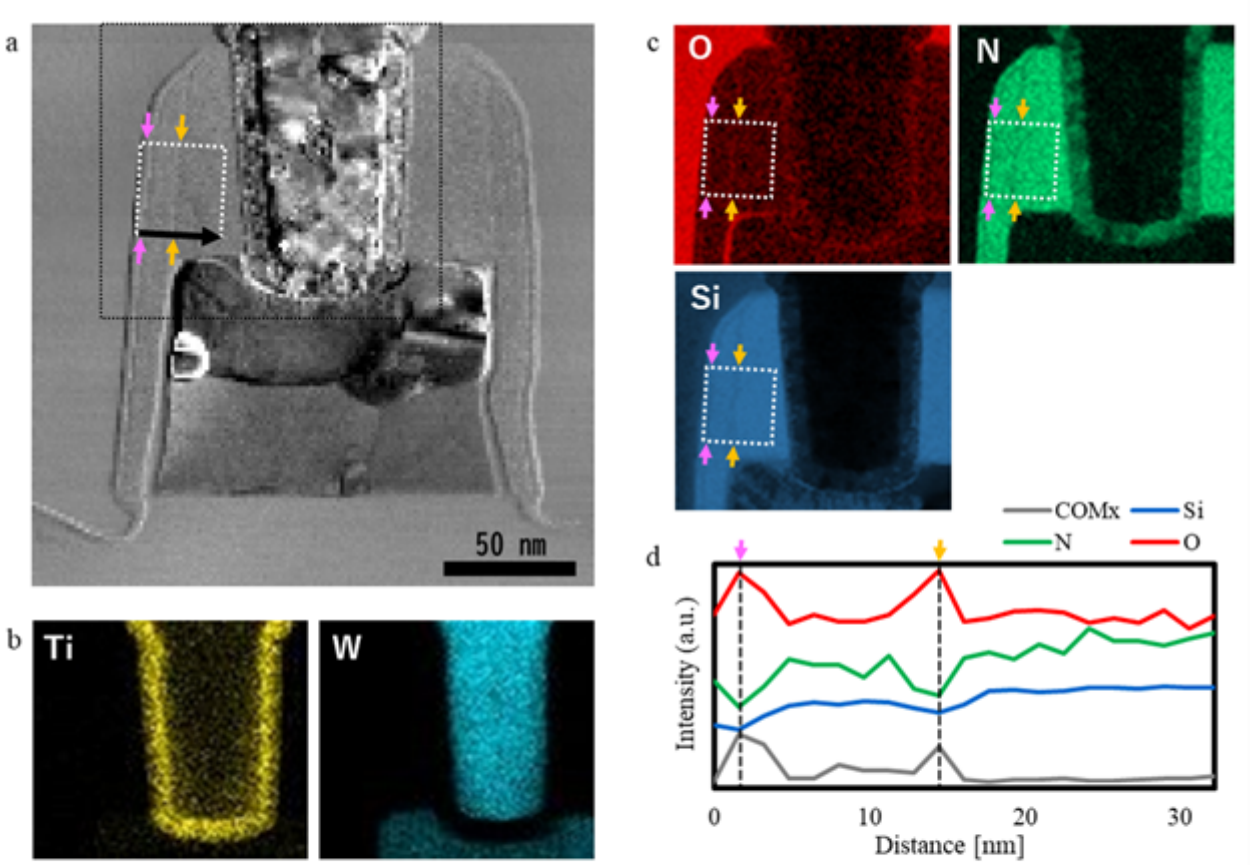

Figure 1. Semiconductor material observed by DPC, EDS and EELS
a: COMx image acquired using SAAF-Quad detector. b: EDS count maps of titanium (Ti) and tungsten (W) extracted from the area marked by the black square in a). c: EELS count maps of oxygen (O), nitrogen (N), and silicon (Si) extracted from the area marked by the black square in a) d: intensity profiles of COMx and EELS. These profiles were acquired in the direction of the black arrows, integration over the white dotted area shown in the COMx and EELS datasets.

Keywords:

Segmented-Detector, DPC-STEM, OBF-STEM, EDS, EELS

Reference:

[1] Naoya Shibata, Scott D. Findlay, Yuji Kohno, Hidetaka Sawada, Yukihito Kondo, Yuichi Ikuhara, Nature Physics, 8, 611 (2012).
[2] Kousuke Ooe, Takehito Seki, Yuichi Ikuhara, Naoya Shibata, Ultramicroscopy, 220, 113133 (2021).
[3] Yuji Kohno, Akiho Nakamura, Shigeyuki Morishita, Naoya Shibata, Microscopy, 71, 111 (2016).
[4] Takao Matsumoto, Yeong-Gi So, Yuji Kohno, Hidetaka Sawada, Ryo Ishikawa, Yuichi Ikuhara, Naoya Shibata, Scientific Reports, 6, 35880 (2016).
[5] Hiroki Hashiguchi, Akiho Nakamura, Vacuum and Surface Science, 66, 695 (2023).

635

Innovative Designs For Enhancing the Functionality of MEMS-Based Phase Plates through Numerical Simulation and Optimisation

Mr Payam Habibzadeh Kavkani[1,2], Dr Vincenzo Grillo[2], Professor Marco Beleggia[1]
[1]Universitá di Modena e Reggio Emilia, Modena, Italy, [2]CNRNANO - Istituto di Nanoscienze - Centro S3, Modena, Italy

Poster Group 2

Background incl. aims:
MEMS-based phase plates play an important role in shaping electron beams within transmission electron microscopes, opening avenues for diverse applications such as generating vortex beams [1], orbital angular momentum (OAM) sorter [2], aberration corrector phase plates, and more [3]. Despite their significance, designing and modeling phase plates pose challenges due to the difficulties encountered in obtaining analytical solutions. In the design process of phase plates, simulation using numerical methods such as Finite-Difference Time-Domain (FDTD) or Finite Element Method (FEM) stands as a crucial step. This capability allows us to compare numerical results with the expected phase shift produced by a phase plate. While simulation proves fundamental in designing phase plates, finding an optimal topology and parameters can often be challenging due to the complexity of the design space. Consequently, a significant portion of the potential of a MEMS phase plate remains unexplored. In recent years, the emergence of Machine Learning and computational tools has revolutionized design optimization processes. In this study, we leveraged the potential of utilizing numerical simulation alongside optimization tools to enhance the functionality of different types of phase plates. A crucial aspect of our investigation involved simulating, analyzing, and enhancing the proposed MEMS-based phase plate devices, scrutinizing the interaction of the generated field by the phase plate with the electron beam prior to fabrication and experimental testing.
Methods :
In our study, we utilized COMSOL Multiphysics software, a powerful FEM tool renowned for its versatile capabilities in simulating MEMS devices, complemented by other numerical methods such as Deep Neural Networks (DNN). COMSOL provides various Finite Element simulation techniques alongside optimization approaches such as Parameters, Topology, and Shape optimization. Moreover, we investigated alternative methods, including Inverse design using DNN, to explore new avenues for advancing phase plate design. In certain studies, to navigate the complexity barrier and enhance the design process, we employed a hybrid optimization method that combines inverse design of phase plates with additional forward optimization. In these specific instances, we utilized a Hybrid Machine Learning (HML) approach, leveraging the TensorFlow library in Python, coupled with forward optimization tools available in COMSOL.
Results :
In this paper, we present an analysis of three distinct phase plates, detailing their simulation and optimization methodologies.
In the first design, we investigated the performance of an Electrostatic Spiral Phase Plate. The primary objective of this phase plate is to generate a linear distribution of phase to produce a vortex beam. Upon optimizing the parameters, it was observed that the applied potential should take on the form of a rounded curve, with minimal bias variation in the direction facing the 'chopstick electrodes' and a steep gradient in their proximity. Forward optimization of parameters was employed, utilizing the absolute difference between simulation results and the aimed phase shift as the objective function (Fig a).
In the second example, we investigated the electrical and thermal properties of OAM sorter phase plates. Unlike the Spiral PP, which requires a linear phase distribution on the boundary, the boundary conditions in this case are more complex. We initialized our optimization study with a circular

symmetric design involving a needle and 42 boundary electrodes. However, due to the limitation of the number of bias connections in a real TEM holder, having 42 biases would not be feasible. Nevertheless, this optimization gives us a broad understanding of the possible design and can later serve as an initial guess for Topology Optimization. To reduce the number of electrodes, the design underwent topology optimization, which suggested a change in the geometry to a non-symmetric design. Additionally, we simulated the Joule Heating effect of the OAM sorter phase plate, as heating effect can help avoid contamination. Figure b illustrates the simulation results of the electrical and thermal response of the OAM sorter phase plate, along with the optimized boundary potential. Figure c showcases the simulation and optimization of an aberration corrector phase plate. This thin-film phase plate aimed to compensate for the aberration of the electron beam by imposing a continuous quartic function as a phase shift. In addition to precise simulation, we enhanced the optimization process with DNN machine learning. A HML approach using the TensorFlow library in Python was employed to determine the optimal set of electrode potentials that result in the desired quartic phase shift. A Convolutional Neural Network (CNN) was trained using over 100000 2D simulations with random bias voltages applied to six electrodes as inputs, and the resulting total phase shift as the output. The output of the HML model was subsequently used in a parameter optimization process within COMSOL Multiphysics® to address any inaccuracies in the machine's predictions.

Conclusion:

In this study, we demonstrated how numerical and computational methods can enhance the functionality of MEMS phase plates. Utilizing powerful simulation tools allowed us to predict results before fabrication and hands-on testing. By leveraging optimization tools, we were able to explore new design possibilities and optimize phase plate geometries to achieve enhanced performance and functionality. Our findings underscore the importance of employing advanced computational techniques in MEMS design and pave the way for further research in this field.

Figures Caption :

a) Model for Optimization of boundary conditions electrodes for spiral phase plate with a large number of adjustable electrodes. Simulation results show phase shift (left). Projected potential before and after optimization (right).

b) Optimized potential of boundary electrodes for the OAM sorter (left). Thermoelectric Simulation (right).

c) Bias potential of the phase plate and a 3D surface representing the corresponding phase shift (left). The outcome details the total phase shift (right).

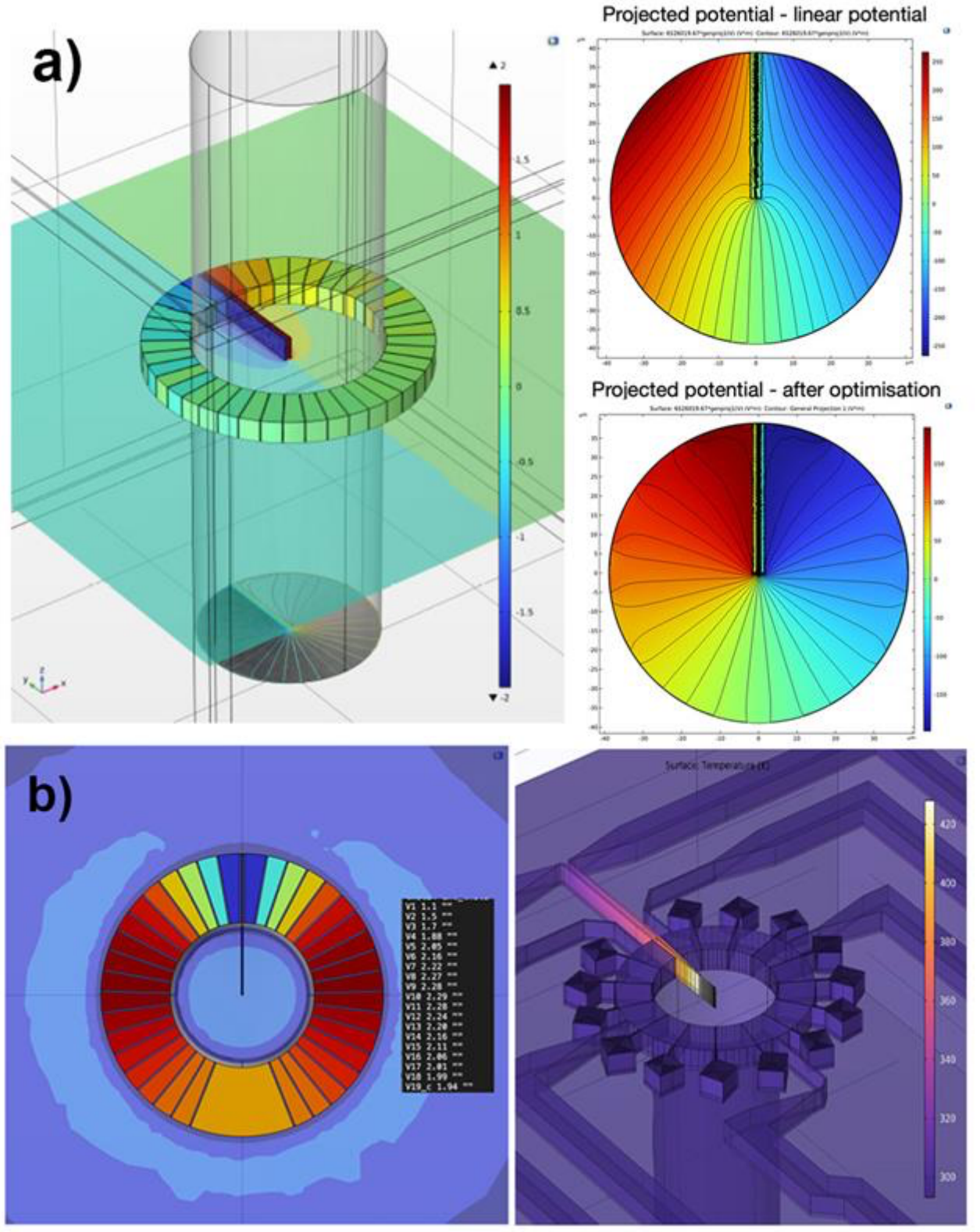
a)
Projected potential - linear potential
Projected potential - after optimisation
b)
c)
COMSOL
V(V)
ϕ(rad)
cos(ϕ)
y(µm)
+1
0.0

Keywords:

Electron_Microscopy Electron_beam_shaping Phase_plate Simulation Optimization

Reference:

[1] Tavabi, A. H., et al. Applied Physics Letters 121, 073506 (2022).
[2] Tavabi, Amir H., et al. Physical review letters 126, 094802 (2021)
[3] Hyllested, J.(PhD Thesis) Æ. Realisation of Gas Electron Holography. DTU Nanolab. (2020).

637

Accessible low-cost, open-source, single-shot phase imaging implemented on an openFrame-based microscope

Huihui Liu[1], Sunil Kumar[1,2], Edwin A Garcia Castano[1], Yasin Razak[3], William Flanagan[1], Jonathan Lightley[1], Ruiyang D Duan[1], Freen Liao[1], Xiaoyu Sun[1], Shanhe N Zeng[1], Brian D Robertson[4], Christopher W Dunsby[1,2], Paul (PHOT) M W French[1,2]
[1]Physics Department, Imperial College London, SW7 2AZ, London, United Kingdom, [2]Francis Crick Institute, 1 Midland Road, NW1 1AT, London, United Kingdom, [3]University of Cape Town, , South Africa, [4]Department of Life Sciences, Imperial College London, SW7 2AZ, , United Kingdom

Poster Group 2

Background incl. aims
We have previously presented polarisation-resolved differential phase contrast microscopy (pDPC) - a robust, low-cost single-shot open-source technique utilising "PolCam" (a polarisation-sensitive camera with a Sony Polarsens™ sensor) to simultaneously acquire 4 images from which semi-quantitative phase images can be calculated [1]. While pDPC microscopy can be easily implemented on a commercial microscope, as we have demonstrated with an automated multiwell plate fluorescence microscope (based on an Olympus IX-83 frame), the implementation of pDPC on an openFrame-based microscope [2] controlled by µManager [3] greatly widens access to phase imaging – with facile integration with fluorescence imaging modalities – at a whole system component cost below €20,000 (<€3000 for only the pDPC components). openFrame describes our specific open-source modular hardware for light microscopy that enables users to assemble a wide range of instruments with no constraints on software or other hardware components that can be self-built or commercial products. Examples of openFrame-based instruments and other open-source instrumentation can be reached through www.openScopes.com.
Here we present an improved pDPC software plug-in for µManager that performs analysis of pDPC data and provides real-time phase imaging. We also report the extension to higher magnification in a new condenser-less geometry that we have applied to imaging biological samples including mycobacteria.
Methods
An openFrame microscope stand is configured for brightfield transillumination imaging including a Köhler transillumination arm utilising a low-cost white LED and a condenser lens that provides a maximum illumination numerical aperture (NA) of 0.55. pDPC is initially implemented by mounting a diffuser and quadrant polariser (QP) mask at the condenser back focal plane. This QP utilises low-cost polarising polymer film and is implemented in a custom 3D-printed mount. Because differential phase microscopy requires a higher illumination NA relative to the imaging NA [4], this condenser-based pDPC system is limited to a spatial resolution of ~λ/1.1. To overcome this limit, we have developed a condenser-less geometry using a simple extended LED array that provides approximately uniform illumination. This approach is simpler and at lower cost compared to approaches based on electronically switched microLED arrays, e.g. [4] and enables the use of higher NA objective lenses.
The pDPC image data processing is managed by a new µManager plug-in (MM2_pDPC) that reads the four polarization resolved images from the PolCam raw images and uses a pre-determined calibration matrix to correct unbalanced illumination and crosstalk between the different polarising quadrants. The phase component of the optical transmission function of the sample is calculated, and a preview of the resulting phase image can be displayed in real time within the µManager graphical user interface (GUI).
The single-shot capability of pDPC makes it suitable for dynamic subjects including timelapse imaging of microbiology and we have extended the capabilities of openFrame-based microscopes by

developing a low-cost 3D-printed stage top incubator with temperature stabilization, which we have applied to support the long-term imaging of live mycobacteria.

Results

Our condenser-based pDPC implementation on openFrame provides robust and rapid (>60 frames/s) phase imaging up to ~0.5 NA. The condenser lens efficiently couples the LED radiation to the sample and the new pDPC µManager plug-in provides real-time phase images. We have applied this to extended time-lapse imaging of mycobacteria in a low-cost (<€500 components) stage-top incubator that provided stable operation at ~34°C over >4 hours with <3°C fluctuation and rapid (~30 minutes) warm-up time.

The condenser-less pDPC system can be realised at even lower cost – we initially used a domestic LED light panel (<€20) to provide 60x, 0.8 NA imaging of mammalian cells HEK-293 and (M. smegmatis) mycobacteria. The figure shows a phase image of a HEK-293 cell acquired with condenser-less pDPC at 60x magnification. However, the highly diffuse illumination of this set-up resulted in lower illumination intensity at the sample and therefore requires longer (~500 ms) image data acquisition times. We are currently upgrading this to a higher transillumination power and higher NA pDPC system that will be optimised for imaging mycobacteria and particularly for the study of M. tuberculosis.

Conclusion

We have demonstrated that research-grade semi-quantitative phase microscopy capabilities can be realised using open-source modular hardware and software to widen access to this important imaging modality. pDPC is particularly convenient to integrate with other modalities as it is wavelength agnostic (within the detection sensitivity range of the Polarsens™ camera). The modular openFrame microscope platform supports the straightforward integration of pDPC with other imaging modalities, including fluorescence microscopy and single molecule localisation microscopy (e.g., easySTORM [2]), which can also be open-source and cost-effective. The compact size, robust design and relatively low-cost of openFrame-based microscopes make them suitable for biosafety containment facilities, e.g., for the study of infectious diseases.

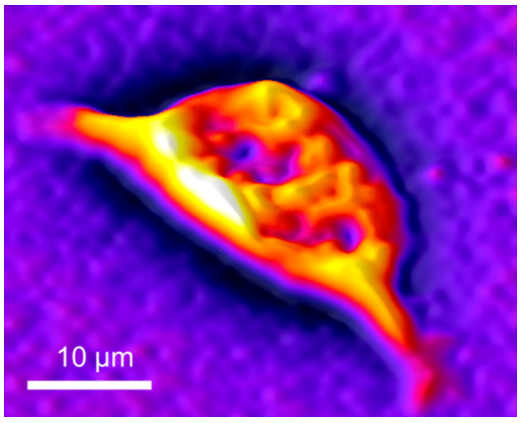

Keywords:

Polarisation differential phase contrast microscopy

Reference:

[1] R. Kalita et al, J. Biophotonics 14 (2021) e202100144 https://doi.org/10.1002/jbio.202100144
[2] J. Lightley et al., J Microsc, 292 (2023) 64, https://doi.org/10.1111/jmi.13219
[3] A. D Edelstein et al., J. Biological Methods (2014), https://doi.org/10.14440/jbm.2014.36
[4] L. Tian and L. Waller, Opt Express, 23 (2015) 11394, https://doi.org/10.1364/OE.23.011394

646

Analytical Phase-Shifting Electron Holography using Fresnel-corrected holograms

Augustin Nogier[1], Aurélien Masseboeuf[1], Kévin Garello[1]
[1]SPINTEC, Grenoble, France

Poster Group 2

Background incl. aims
Unlike conventional Transmission Electron Microscopy (TEM) techniques, Electron Holography (EH) gives an access to the phase of the electron wave, which makes it suited for imaging electromagnetic fields with fine sensitivity and a spatial resolution in the range of nanometers [1].
When performing a measurement, the complex wave contribution of the sample is contained in the object band of the Fourier transform of the recorded hologram. For this reason, the most common way of extracting the sample phase contribution consists in applying a circular mask around the object band [2]. This low-pass filtering cuts off excessive noise and undesirable Fresnel diffraction effects, but also limits the final spatial resolution of the recovered phase map. While this limit may not be an issue depending on the scale of interest, such a loss of precision can lead to artefacts in the phase maps realignment process when working with finer details, which remains a critical step in separating the electric and magnetic contributions.
Other approaches overcome this by combining two holograms to suppress the zero-order band [3], effectively doubling the maximum mask size available and typically getting the spatial resolution down to 2 - 3 nm. This may not be enough in some cases though. A solution to this problem is the Phase Shifting (PS) method, which uses linear combinations of a greater amount of holograms to mathematically isolate the object band [4], thus negating the necessity to apply a mask in Fourier space and allowing for a theoretical pixel precision. Implementations tend to use specific initial phase values in order to get back to an ideal diagonal matrix system, which greatly facilitates the calculation. When working with arbitrary initial phase values, it is still possible to avoid the complex matrix inversion by performing sine fittings in each pixel, using an even greater amount of hologram recordings [5]. Due to the absence of any filtering however, Fresnel modulation effects become a source of errors in the reconstruction process in both cases. However, this effect can be rendered ineffective by adjusting the hologram fringes spacing to match that of the modulation pattern [5].
In this work, we aim for the pixel-precise reconstruction of phase maps using a modification of the PS method, so that the recovered sharp atomic details can lead to better phase maps alignments. This study focuses primarily on a more general analytical solution to the PS equation in the case of arbitrary chosen initial phase values, which eliminates the need to conform to an ideal case. We also investigate the use of biprism voltage as a suitable way to minimize Fresnel modulation effects and related calculation errors. Finally, we apply these methods to both computer simulations and TEM measurements from specifically prepared magnetic samples.
Methods
The general analytic solution we derived to the PS matrix equation works for any set of non-redundant initial phases containing at least three elements. While more measurements ultimately yield less noise in the final phase map, we typically used 5 or 7 hologram recordings for each manipulation up to this point. As common as it is for this matter, we used beam tilting to tune each initial phase value. Under the small angle approximation and disregarding the Fresnel modulation pattern, this is equivalent to an overall phase offset in the fringe pattern. The experimental values can then be extracted for each hologram from the center of the object band in Fourier space and be used as parameters in the solution expression.

Since there is no requirement regarding the fringe spacing in the holograms, we also choose to tune the biprism voltage low enough to give a sufficiently good contrast while still cancelling out the Fresnel effect. Up to this point, all of our measurements have used this particular setting.

Results

Our computer simulations use artificially generated phase and amplitude maps from which holograms are calculated. We first tested our method on square-shaped phase maps with various apodizations, noise levels and Fresnel diffraction effects. Using our analytical method on Fresnel-free holograms, we see that the reconstructed phase maps show accurate reconstructions of the initial wavefront regardless of the spatial details [Fig.1].

Additionally, we measured the Fresnel modulation effect on holograms for various biprism voltage values in order to minimize this effect. So far, all of our experimental results have thus been using a voltage of 21 V instead of the usual 200V, which corresponds to 24nm-wide fringes for an image pixel resolution of 0.12 nm.

Conclusions

We were able to reconstruct phase maps using our generalized PS analytical method for reasonable noise and Fresnel modulation levels. While this method works best on perfectly generated holograms, we also have shown that it is possible to maximize the fringe contrast and correct the Fresnel modulation effect by adjusting the biprism voltage. Likewise, other parameters such as the initial phase do not need to match ideal values since our method takes the experimental measurements into account.

Using this modified phase shifting method, we expect that further testing done on specifically prepared samples can give satisfactory results with an effective spatial resolution approaching the theoretical pixel size.

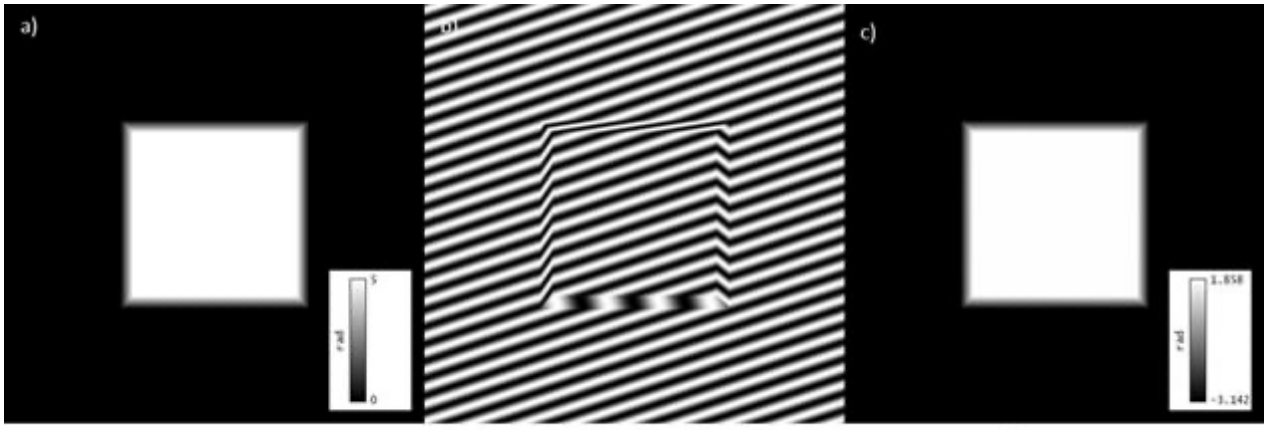

Fig.1 : Simulation result of the phase shifting process: a) Artificially generated phase map; b) One of the 7 simulated holograms with arbitrary initial phases; c) Recovered final phase map

Keywords:

Holography, phase-shifting, biprism, Fresnel, modulation

Reference:

[1] Martha R. McCartney, Rafal E. Dunin-Borkowski, David J. Smith: Quantitative measurement of nanoscale electrostatic potentials and charges using off-axis electron holography: Developments and opportunities, Ultramicroscopy 203 (2019) 105–118

[2] Qi Fan, Hongru Yang, Gaoping Li and Jianlin Zhao: Suppressing carrier removal error in the Fourier transform method for interferogram analysis, J. Opt. 12 115401 (2010)

[3] V.V. Volkov, M.G.Han, Y.Zhu: Double-resolution electron holography with simple Fourier transform of fringe-shifted holograms, Ultramicroscopy134 (2013) 175–184

[4] Q. Ru, G. Lai, K. Aoyama, J. Endo, A. Tonomura: Principle and application of phase-shifting electron holography, Ultramicroscopy 55 (1994) 209-220

[5] Kazuo Yamamoto, Yoshihiro Sugawara, Martha R. McCartney and David J. Smith: Phase-shifting electron holography for atomic image reconstruction, Journal of Electron Microscopy 59 S81–S88 (2010)

683

Ptychography at finite dose in SrTiO3

Dr Malcolm Dearg[1], Mr James Gilbert[1], Mr Nick Michaelides[1], Dr Laura Clark[1]
[1]School of Physics, Engineering and Technology; University of York, York, United Kingdom

Poster Group 2

Many important materials are unstable under the electron beam and easily damaged by high-dose imaging, leading to a blurred image of a damaged sample. Ptychography is one of the most dose-efficient electron microscopy techniques currently available, providing a route to high-resolution images of undamaged samples.

The aim of this research is to develop, implement and apply new dose-efficient 4D-STEM imaging methods, based around existing algorithms for electron ptychography to improve imaging of beam-sensitive materials. Here, we lay the groundwork for an in-depth discussion of finite dose ptychography, towards the development of new low dose algorithms for ptychographic imaging to improve achievable contrast at low electron dose.

Previous studies have explored ptychographic techniques theoretically for infinite dose (Clark et al. 2023). In this study, we are investigating the thickness dependence of ptychographic imaging methods, in particular we are interested in the dependence on varied electron probe dose to see just what the dose limits are for an accurate reconstruction.

We simulate a Strontium Titanate (STO) thickness series of 1-55 unit cells (3.905 – 215 Å) along the [1 0 0] axis with a 26.6 mrad electron probe at 300 keV with a midplane focus, using μSTEM (Allen et al. 2015). We then model a dose-series across the thicknesses, by applying Poisson statistics. The resulting 4D datasets were then used to form images via a range of algorithms, including central Bright-Field (cBF), Annular Dark-Field (ADF), integrated Center of Mass (iCoM), Single Sideband (SSB), Wigner Distribution Deconvolution (WDD), and extended Ptychographic Iterative Engine (ePIE).

With these data, we then find lowest-feasible dose limits for imaging samples in realistic imaging conditions, detecting image features and atomic column positions, to provide guidelines for successful experimental data collection, advice for expected most-successful imaging approaches, and data collection parameters.

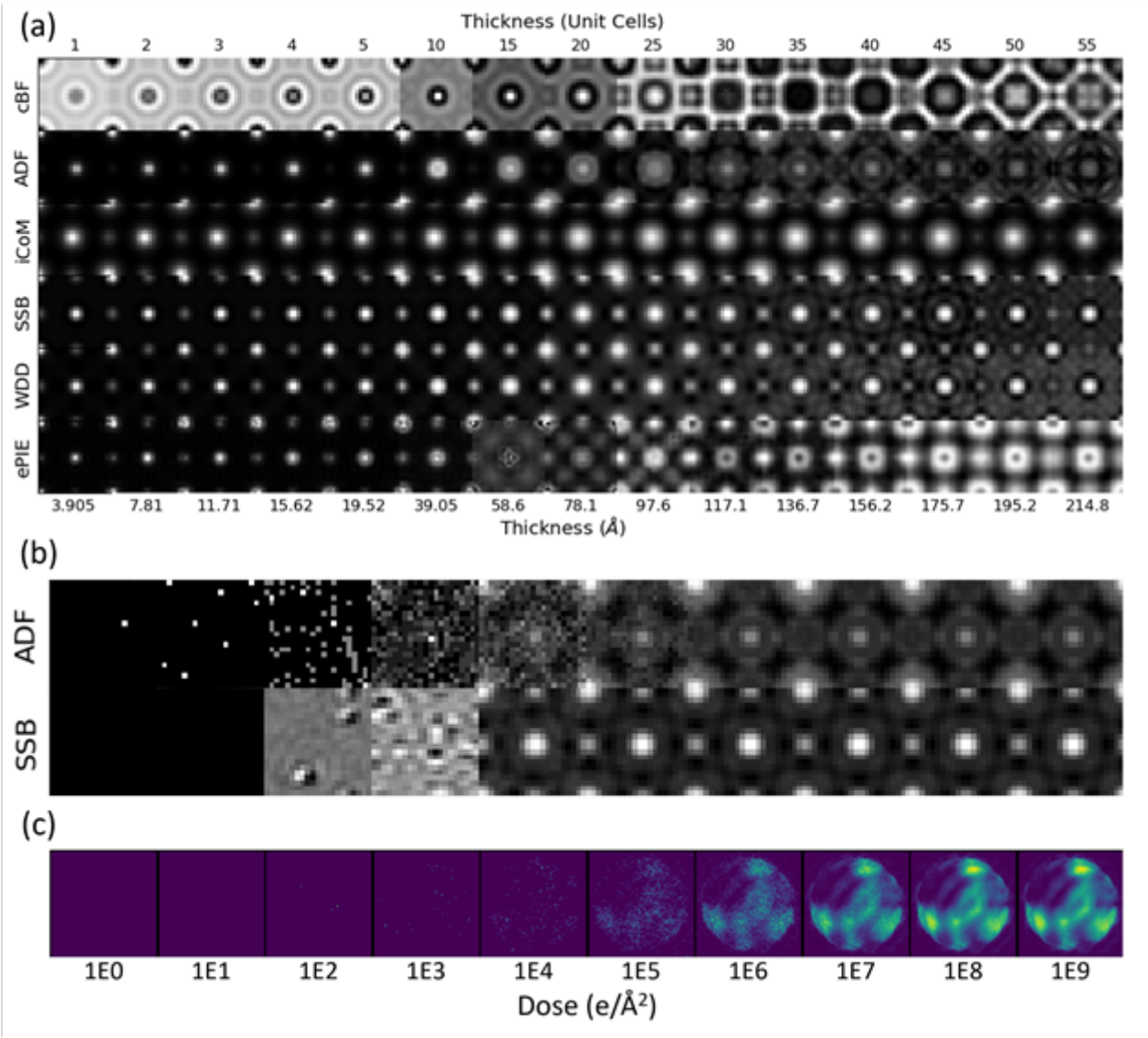

Keywords:

Low dose, Ptychography, 4D-STEM

Reference:

L. Clark et al., The Effect of Dynamical Scattering on Single-plane Phase Retrieval in Electron Ptychography, Microsc. Microanal., 29 1 (2023) 384–394, https://doi.org/10.1093/micmic/ozac022

L.J. Allen , A.J D'Alfonso & S.D. Findlay, Modelling the inelastic scattering of fast electrons, Ultramicroscopy, 151 (2015) 11–22. https://doi.org/10.1016/j.ultramic.2014.10.011

799

Towards Quantitative analysis of electrostatic potential of monolayer WSe2 using electron ptychography

Yiran Lu[1], Alexis Wartelle[1], Djodje Dosenovic[2], Matthew Bryan[3], Hanako Okuno[2], Julio-Cesar da Silva[1], Jean-Luc Rouvière[4], Martien I. den Hertog[1]
[1]Univ. Grenoble-Alpes, CNRS, Grenoble INP, Institut Néel, Grenoble, France, [2]Univ. Grenoble-Alpes, CEA, Grenoble INP, IRIG, PHELIQS, Grenoble, France, [3]CEA, LETI, Grenoble, France, [4]Univ. Grenoble-Alpes, CEA-IRIG, MEM, Grenoble, France

Poster Group 2

4D-STEM has thrived thanks to the emergence of fast pixelated detectors in the last few years. The latter enables recording the rich information of the diffraction patterns in STEM [1]. This also makes it possible to map magnetic and electric properties at microscopic scales using methods like Center-of-Mass (CoM) and electron ptychography. Compared to conventional imaging techniques in STEM, electron ptychography enables imaging of the materials beyond the aberration-limited resolution with an optimal use of electron dose. The resolution achieved by this technique was demonstrated to be as small as 20 pm [2], and the ability to recover the diffraction pattern outside the detector plane allows for super-resolution imaging [3]. Quantitative ptychography, where the potential change over an atom can be directly related to the present chemical species combined with the effect of bonding, will have many applications, but has yet to be demonstrated in literature. Since, to the best of our knowledge, no publication directly compares experimental ptychographic reconstructed phase/potential maps or profiles with simulated data, quantitative ptychography appears still challenging.

In this presentation, 4D-STEM diffraction maps of WSe2 were simulated using abTEM[5]. Then the datasets were reconstructed using electron ptychography on the simulated diffraction maps using different reconstruction algorithms, namely ePIE and difference map (DM), implemented in the PtyPy[4]. The reconstructed diffraction pattern as well as the object function were compared using the ground truth of the input to the simulation, to better understand the strengths and weaknesses of both algorithms. The influence of padding was evaluated on the reconstructed data. Finally, this study allows comparison with reconstructions on experimentally obtained 4D-STEM maps on WSe2 or other 2D materials, intending to develop a method of quantifying the electrostatic potential.

The simulations for the 4D-STEM dataset were done on monolayer WSe2 with focused and defocused probes working at 80 kV with abTEM. The convergence semi-angle is 20 mrad. The diffraction patterns were sampled at 0.41 mrad/pixel and then cropped to a size of 256x256 or 512x512. This results in a collection angle of 51.7 mrad and 103.4 mrad at the edge. The dataset of diffraction patterns of size 256x256 was then fed to the ptychography reconstruction using ePIE and DM in the python package PtyPy: One with added padded zeros around the diffraction pattern up to doubled collecting angle and one without. An extra reconstruction using padded diffraction patterns up to 1024x1024 was done to see if it affected the recovered diffraction pattern. An analysis of a random diffraction pattern generated from the reconstructed probe and the reconstructed object function is shown in Fig. 1. While the reconstructions without padding show a good agreement with the original diffraction pattern, the reconstructions with padding fit the original pattern even better. However, for padded reconstruction, ePIE failed to recover the signals while DM smoothly transits and continues to fit outside the detector region. Further analysis of the power spectrum of the object function exhibits a similar tendency that can be observed: until about 1.65 Å-1, padded ePIE reconstruction (orange dashed profile) matches the input simulation well, while DM matches up to a

cutoff at 1.75 Å-1. The same analysis with extra padding up to 1024x1024 shows no significant signal improvement, implying that the effect of padding has a limited reach.

This work presented a possible method to quantitatively analyze the electrostatic potential of the monolayer WSe2. Padding in the reconstruction can improve the resolution, however, is limited. Moreover, the comparison between low-pass-filtered ground truth and reconstructions with a simulated finite-sized detector shows quantitative agreement. Care must therefore be taken in experiments since this finite-size constraint is always present.

Acknowledgments: This project received funding from the European Research Council under the European Union's H2020 Research and Innovation programme via the e-See project (Grant No. 758385). Y.L. thanks the Ecole Doctoral de Physique de UGA for the PhD scholarship. Experiments have been performed at the Nanocharacterisation platform PFNC in Minatec.

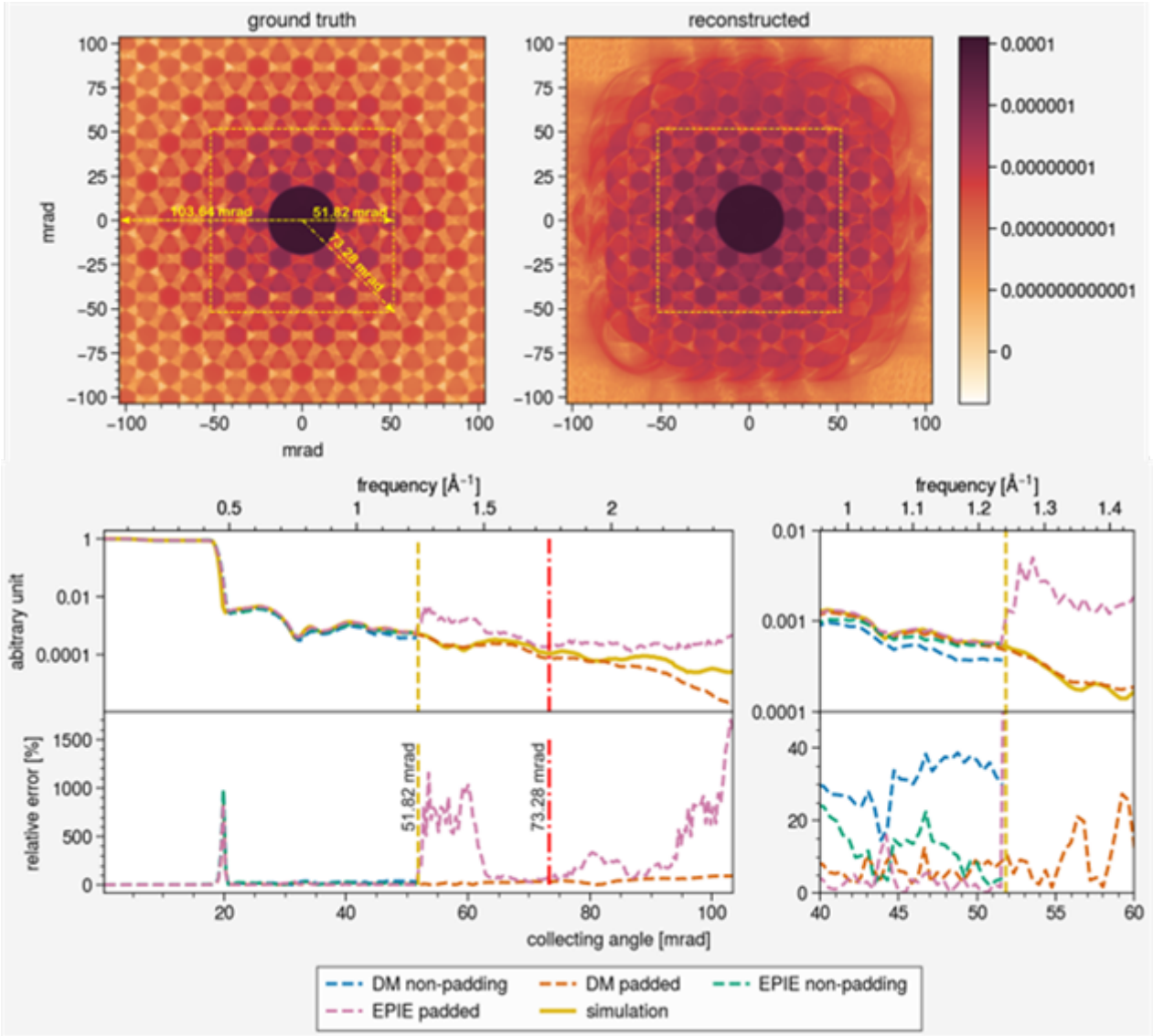

Keywords:

ptychography 2D material quantification

Reference:

[1] C. Ophus, Microsc Microanal, 2019, 25, 563–582.
[2] Z. Chen, Y. Jiang, Y.-T. Shao, M. E. Holtz, M. Odstrčil, M. Guizar-Sicairos, I. Hanke, S. Ganschow, D. G. Schlom and D. A. Muller, Science, 2021, 372, 826–831.
[3] A. M. Maiden, M. J. Humphry, F. Zhang and J. M. Rodenburg, J. Opt. Soc. Am. A, 2011, 28, 604.

[4] B. Enders and P. Thibault, Proc. R. Soc. A., 2016, 472, 20160640.
[5] J. Madsen and T. Susi, Open Res Europe, 2021, 1, 24.

814

An examination of exit-wave reconstruction algorithms for low dose imaging at atomic-scale resolution

Jacob Svane-Petersen[1], Andreas Nymand[1], Joerg R. Jinschek[1,2], Stig Helveg[1], Joakim Kryger-Baggesen[1], Sophie Kargo Kaptain[1]
[1]Center for Visualizing Catalytic Processes (VISION), Technical University of Denmark, Kgs. Lyngby, Denmark, [2]Nanolab, Technical University of Denmark, Kgs. Lyngby, Denmark

Poster Group 2

Electron microscopy is a technology which is used in many modern research fields and in cases relying on heterogeneous materials the only viable solution for achieving atomic scale resolution. High-resolution electron microscopy utilizes a parallel, broad beam of high energy electrons to probe a sample and images at high spatial resolution are obtained by measuring the intensity of the electron wave function with a loss of its phase. By acquiring a series of images at different focus values, both the amplitude and phase of the electron wave function can be retrieved at the exit of the sample surface. The reconstructed exit wave provides the maximal amount of structural information, and it also enhances signal-to-noise ratios and therefore represents powerful phase imaging technique in low-dose-rate regime for suppressing beam-induced sample alterations for chemical and biological sciences. However, several schemes are employed to reconstruct the exit wave functions and are often employed without reference to their basic assumptions. In this study we provide a quantitative comparison of the most commonly used algorithms and discuss their pros and cons. Using simulation of HRTEM images in abTEM we compare how these algorithms perform in the regime of low dose imaging. Furthermore, we implement and present an algorithm for exit-wave reconstruction using abTEM and Python based on the paper by Oxley, et al. [1].
To compare different exit wave reconstruction algorithms on an equal basis, we simulate focal series of high-resolution transmission electron microscopy (HRTEM) images of model structures. Specifically, we use the multislice algorithm included in the abTEM package for HRTEM image simulation of structures modelled with the atomic simulation environment (ASE) package. Optical parameters incudes a primary electron energy of 300 keV, spherical aberration coefficient of -12 µm, an image pixel size of 0.1 Å and a focal range of -10 to 10 nm in steps of 1 nm. The focal series were reconstructed by using the three different algorithms [1-3] as implemented in commercial and open accessible codes and the reconstructions are then compared both qualitatively and quantitatively using a sum of square error (SSE) measure. Also, for reference, we implemented our own version of the algorithm by [1].
While the three algorithms overall perform similarly, we find differences reflecting a dose-dependence. We present data showing how an increase in the length of the focal series increases the quality of the reconstruction and results indicating an optimal tradeoff between dose and focal series length.
We investigated exit wave reconstruction algorithms implemented in Python codes and commercial packages. The comparison of the reconstruction the exit wave from a simulated focal series of HRTEM image shows differences depending on the overall image signal-to-noise levels. The present finding indicates that careful optimizing of the focal series image acquisition is needed to capture the finest structural features under low dose and dose-rate imaging conditions.

Keywords:

Exit-wave reconstruction, low-dose-rate, atomic-scale resolution

Reference:

[1] L. J. Allen, W. McBride, N.L. O'Leary, M.P. Oxley. "Exit wave reconstruction at atomic resolution". Ultramicroscopy 100 (2004) 91–104. doi:10.1016/j.ultramic.2004.01.012.
[2] W.-K. Hsieh, F.-R. Chen, J.-J. Kai, A.I. Kirkland. "Resolution extension and exit wave reconstruction in complex HREM". Ultramicroscopy 98 (2004) 99–114. doi:10.1016/j.ultramic.2003.08.004.
[3] M. Op de Beeck, D. Van Dyck, W. Coene. "Wave function reconstruction in HRTEM: the parabola method". Ultramicroscopy 64 (1996) 167-183. PII: 0304-3991(96)00058-7.
[4] The Center for Visualizing Catalytic Processes is sponsored by the Danish National Research Foundation (DNRF146).

825

Entanglement in Bragg Scattering

Ao. Univ. Prof. Peter Schattschneider[1], Assoc.-prof. Stefan Löffler[1]
[1]TU Wien, Wien, Austria

Poster Group 2

Whenever two quantum systems interact and their state changes (in a non-separable way), they become entangled. In essence, they can no longer be seen as two separate systems, but rather as a single, large system (until they decohere). Since electron microscopy deals with elementary particles as well as structures and processes on the atomic scale – i.e., quantum objects – entanglement is fundamental. In inelastic scattering (EELS), this has been embraced fully for quite some time by the use of the mixed dynamic form factor (MDFF) [1,2]. To our knowledge, the same cannot be said for the much more widespread (and theoretically simpler) case of elastic scattering.
The strange effects of entanglement occur also in Bragg diffraction, as we are dealing with the two interacting quantum systems of the probe beam and the crystal. Take the two-beam case as an example: Measuring in the diffraction plane and detecting the probe electron in the 0 or in the g diffracted beam results in a momentum transfer of either 0 or -g ħ to the scatterer. On the other hand, measuring in the image plane leaves the scatterer in a quantum superposition of two states with different momenta like Schrödinger's cat. This shows that a measurement on one part of an entangled system can have an effect on the other [3]. Therefore, it is critical to include entanglement in the theoretical description of the process to get complete and accurate predictions.
In this work, the joint quantum state of the probe beam and crystal system is described by its density matrix [4] which captures all aspects of the state. It allows to predict the evolution of the state and the outcome of measurements on parts of the system (the beam electron in the present context) by virtue of the reduced density matrix. In the 1-dimensional case, the N degrees of freedom of the scatterer (the positions of the N atoms) can be rewritten as N-1 relative coordinates of a rigid lattice and the position of the center of mass (CM). It is shown that the diagonal elements of the density matrix in a momentum basis correspond to the well-known scattering distribution from conventional kinematic scattering theory. The relative coordinates define the amplitude whereas the CM position imprints a lattice periodic phase factor. Apart from the diagonal terms, the reduced density matrix features off-diagonal elements, which give insight into correlation and interference effects. Among other things, these can be used for determining the decoherence properties of the electron beam.
A rigorous treatment of the entangled system "probe electron/crystal" leads to the standard (reciprocal space) description of Bragg diffraction as scattering on a static periodic Coulomb potential. But on top of that, it also contains additional information on the quantum system, that is accessible in other bases (such as in position space). This work sheds light onto the quantum mechanical measuring process in the context of electron microscopy and therefore contributes to a better understanding on a fundamental level. [5]

Keywords:

scattering, entanglement, interaction, quantum mechanics

Reference:

[1] H. Kohl, H. Rose: Adv. El. El. Phys. 65 (1985) 173
[2] P. Schattschneider et al.: Micron 31 (2000) 333
[3] P. Schattschneider, S. Löffler: Ultramicroscopy 190 (2018) 39
[4] K. Blum: Density Matrix Theory and Applications. Springer 1996
[5] SL acknowledges financial support by the Austrian Science Fund (FWF) under grant nr. I4309-N36. PS thanks Helmut Kohl for valuable comments

887

Numerical study on high orbital angular momentum vortex electron beams in hafnium dioxide

Christian Bick[1], Dr. Dorothee Hüser[1]
[1]Physikalisch-Technische Bundesanstalt (PTB), Braunschweig, Germany

Poster Group 2

Background incl. aims
Electron vortex beams (EVB) are electron beams that have a quantized orbital angular momentum (OAM) along their propagation axis. These beams have found applications in electron magnetic circular dichroism (EMCD) and beam focusing, and have attracted new attention with the development of programmable phase plates [1, 2]. In this study we aim to improve our understanding of the behavior of vortex beams and their OAM in complex electronic materials.
Methods
We present a numerical study of vortex electron beams modeled as Bessel beams [3, 4]. The commonly used multislice algorithm is utilized to propagate the beam through crystalline material.
Results
We compare our results with previous work [3, 4] for OAM with quantum number l=1 and make predictions for higher angular momentum beams in new materials. The results indicate a reduction in the expectation value of the OAM with propagation depth inside the crystal potential, which depends on the initial value of l. We present simulation results for HfO_2 systematically investigating different beam shaping parameters. Furthermore, we investigate the numerical limits of our method.
Conclusion
Our method is capable of reproducing previously published work for low OAM. It shows physically conclusive results for higher angular momentum vortex beams.

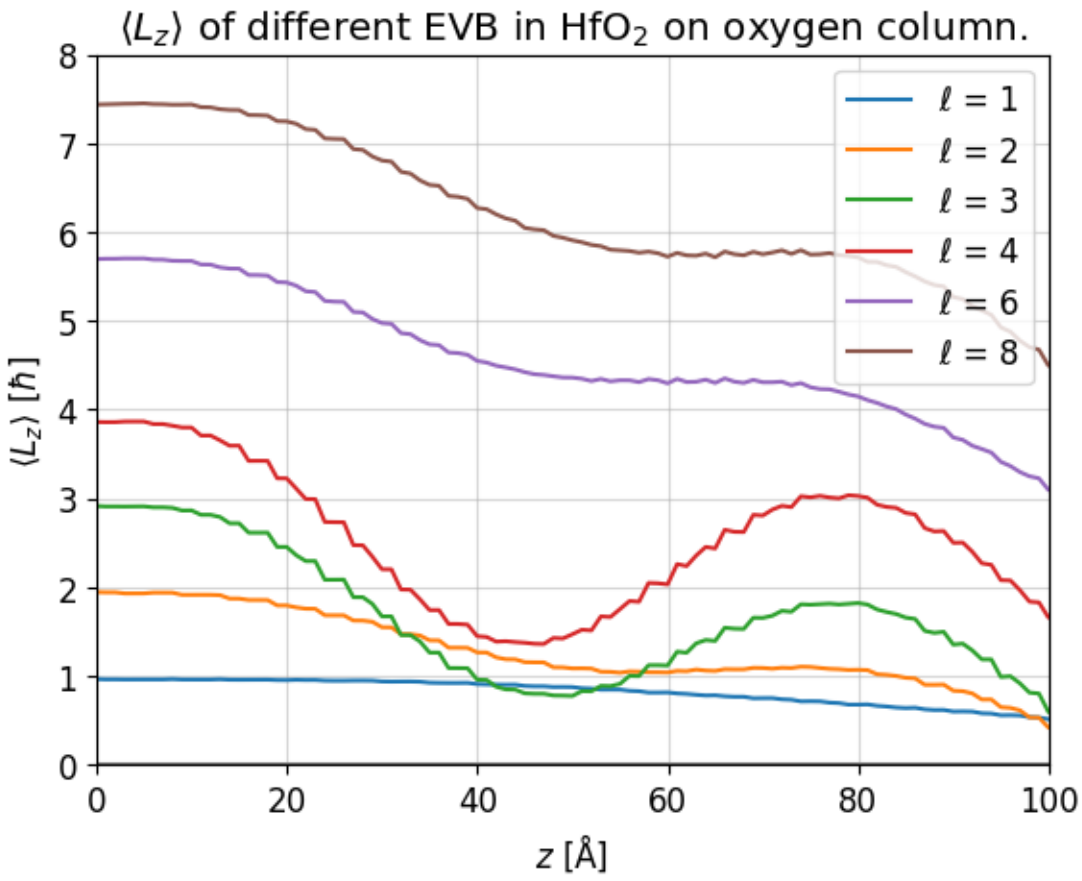

Keywords:

electron vortex beam; multislice simulation

Reference:

[1] S. M. Lloyd et al., Rev. Mod. Phys. 89, 035004 (2017).
[2] C.-P. Yu et al., SciPost Phys. 15, 223 (2023).
[3] S. Löffler and P. Schattschneider, Acta Crystallogr. A 68, 443 (2012).
[4] A. Lubk et al., Phys. Rev. A 87, 033834 (2013).

914

On the accuracy of atomic-resolution DPC-STEM measurements

Rafael V. Ferreira[1,2], Sebastian Calderon V.[3], Paulo J. Ferreira[1,2,4]
[1]INL – International Iberian Nanotechnology Laboratory, Braga, Portugal, [2]Mechanical Engineering Department and IDMEC, Lisbon, Portugal, [3]Department of Materials Science and Engineering, Carnegie Mellon University, Pittsburgh, USA, [4]Materials Science and Engineering Program, The University of Texas at Austin, Austin, Portugal

Poster Group 2

Background

The study of prevalent defects and their impact on functional properties is a critical issue for the successful implementation of 2D materials in next generation devices. However, the direct quantitative characterization of a specific defect is a challenging task, requiring atomic resolution measurements that are sensitive to the electronic structure of the material. The use of differential phase contrast (DPC) in scanning transmission electron microscopy (STEM) is particularly promising for this purpose, leveraging the natural coupling between the electron probe and the atomic-scale electric fields within a sample, which leads to a redistribution of intensity at the diffraction plane. For thin specimens, the centre of mass (CoM) of the diffraction disc is then directly related to the phase gradient, allowing for the mapping of electrostatic forces between atoms of the material structure, a capability which has already been demonstrated in the study of several 2D materials [1–4].

CoM-based measurements can be performed with pixelated detectors, capable of recording the entire diffraction disc, or with segmented detectors that integrate the intensity of the disk over independent quadrants. Pixelated detectors offer the greatest accuracy, but the faster processing times associated with segmented detectors allow for the generation of DPC-STEM images in real time, making it easier to identify interesting features and to correct electron lens aberrations. Additionally, series acquisitions and larger fields of view become more manageable, greatly aiding in the observation of easily damaged 2D materials. These benefits, along with the fact that segmented detectors are still the most accessible option, make it worthwhile to explore methodologies to manage their reduced accuracy. For this reason, it is essential to understand the precise effect of instrumental parameters on segmented-detector DPC STEM observations, such that their influence may be accounted for when analysing the results.

Methods

In this work, the influence of key instrumental parameters – probe convergence angle, defocus and detector orientation – on the retrieval of atomic-scale electrostatic field and potential configurations obtained from COM-based images is analysed, by determining the qualitative and quantitative changes induced by each of the parameters. This analysis is based on extensive multislice simulations of DPC- and COM-STEM images, in which the impact of each parameter under study is evaluated independently. Due to the complications of directly interpreting and comparing the vectorial electrostatic field images, these are analysed by representing the vector field in scattergrams [5] – polar graphs where the COM vectors associated with the pixels of the original image are plotted as points (Figure 1). This representation allows us to readily evaluate and compare the maximum magnitude of the measured field configurations in every direction, as well as to more easily detect qualitative changes. The scalar electrostatic potential images are directly compared through relative difference maps that show the increase or decrease in magnitude at every pixel of the imaged region, allowing for a more spatially detailed analysis.

Results

Analysis of the influence of convergence semi-angle shows how an increased angle leads to higher susceptibility to the aberrations studied, despite the improved resolution. In the case of defocus, a maximum relative change above 30% is determined in the electrostatic field images for an angle of 30 mrad, at the limit of image interpretability, whereas the impact grows at a slower rate with increasing defocus for angle of 21 mrad. Additionally, overfocus primarily affects quantification, while underfocus results in more qualitative changes to the electrostatic configurations, albeit with a reduced quantitative impact. Two-fold astigmatism has a more pronounced impact in the field configurations, with maximum relative magnitude changes higher than 60% and stronger qualitative effects. The influence of this asymmetric aberration is shown to have a resonance effect with the orientation of the segmented detector, varying the identified magnitude of quantitative and qualitative impacts.
The electrostatic potential images show the same trend as that identified in the field configurations; however, the average relative changes identified are much lower, demonstrating an improvement in image quality due to the integration applied.

Conclusions
Following the procedure described, the relative quantitative and qualitative changes in electrostatic field and potential images due to the influence of key experimental parameters are identified. Differences in impact between imaging at over- and underfocus are determined and the more complex impact of asymmetric aberrations is analysed by considering the influence of two-fold astigmatism, identifiying a resonance effect with the orientation of the segmented detector.

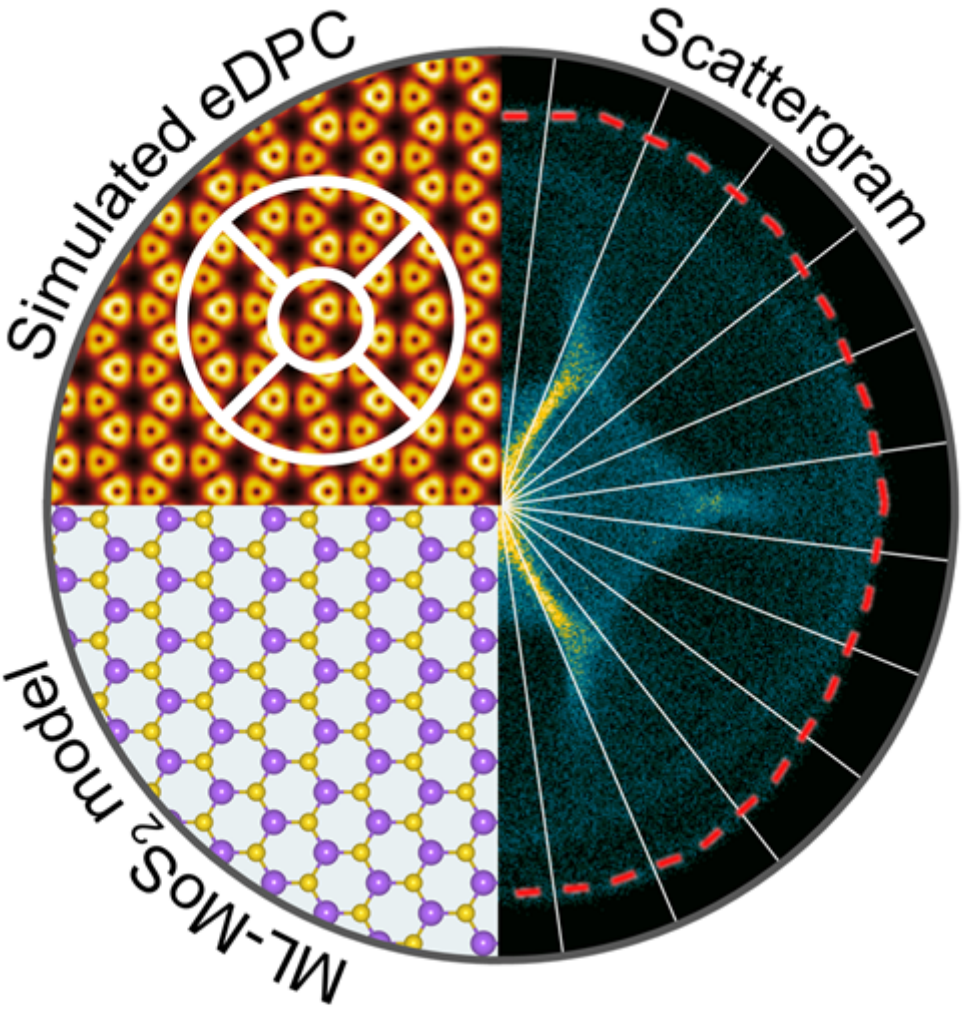

Figure 1 – Structural model of monolayer MoS_2 used in the simulations, aberration-free eDPC image with standard detector orientation overlaid, and corresponding scattergram showing delineated perimeter.

Keywords:

DPC-STEM; multislice image simulations; aberrations

Reference:

[1] Ishikawa, R., et al, Nat. Commun. 9 (2018), p. 3878.
[2] Müller-Caspary, K., et al, Phys. Rev. B 98 (2018), p. 121408.
[3] Fang, S., et al, Nat. Commun. 10 (2019), p. 1127.
[4] Calderon V., S., et al, Nano Letters 21(24) (2021), p.10157.
[5] Burger, J., et al, Ultramicroscopy 219 (2020), p. 113118.

928

Reconstruction of Angstrom resolution exit-waves by the application of drift-corrected phase-shifting off-axis electron holography

Jonas Lindner[1], Ulrich Ross[2], Tobias Meyer[1], Victor Boureau[3], Michael Seibt[2], Christian Jooss[1,4]
[1]1 Institute of Materials Physics, University Goettingen, Goettingen, Germany, [2]2, 4th Institute of Physics – Solids and Nanostructures, University of Goettingen, Germany, [3]Interdisciplinary Center for Electron Microscopy, École Polytechnique Fédérale de Lausanne, Lausanne, Switzerland, [4]4 International Center for Advanced Studies of Energy Conversion (ICASEC), University of Goettingen, Goettingen, Germany

Poster Group 2

Background

Off-axis electron holography is a phase retrieval technique which enables access to the full complex-valued exit-wave of thin samples. The potential distribution at interfaces obtained from the measured phase information is highly relevant for in-situ experiments. Combining off-axis holography with the capabilities of an environmental TEM offers the ability for exit-wave reconstruction under external bias and in catalysis relevant gases and material systems. However, the conventional holography Fourier-reconstruction suffers from a trade-off between spatial and phase resolution caused by the fringe spacing and visibility. To tackle the open fundamentally questions in catalysis research, e.g. the atomic structure of the electrolyte-solid interface, the identification of active reaction sites and the influence of surface faceting, atomic resolution is highly desired. Therefore, state-of-the-art phase retrieval techniques must be adapted to the particular requirements of in-situ studies. Phase-shifting electron holography bypasses the spatial resolution limit by real-space evaluation of hologram series. However, to reach atomic resolution in reconstructed hologram-series, special care is needed to correct sample and biprism drift.

Methods

Phase-shifting holography acquires a series of holograms formed by tilted incident waves. This results in a shift of the hologram fringes, that are modulated by the potential of the specimen. If specimen and biprism drift are carefully corrected, the cosine intensity dependency of the hologram series can be used for linear fits of the local amplitude and phase of the exit wave. This obviates the use of the low-pass aperture which is necessary for the conventional reconstruction of off-axis holograms in the Fourier domain. The upper bound of the spatial resolution is thus only limited by the performance characteristics of the instrument, while the low-frequency information is also retained.

Results

Previous implementations of phase-shifting holography have been limited by the independent drift of biprism and sample and allowing for medium spatial resolution. We improve the reconstruction process by introducing a drift correction scheme and demonstrate exit wave reconstruction on platinum. The reconstructed exit-waves show reliable phase information at the 1 Å information limit of the used Titan 80-300 kV environmental transmission electron microscope. Simultaneously, the omission of the trade-off between fringe spacing and visibility leads to phase resolutions up to $2\pi/452$ rad at moderate birpism voltages of 250 V (fringe spacing 1 Å). The obtained phase and amplitude information is validated at a thin Pt sample due to the excellent matching to frozen-lattice multi-slice image simulations.

Conclusions

In conclusion, we demonstrate the successful method improvement of the phase-shifting holography reconstruction process by introducing novel drift correction of the mixed signals of biprism and sample drifts. The reconstructed exit-waves of a thin platinum sample show spatial resolution up to the 1 Å information limit of the microscope simultaneously with a phase resolution up to 2π/452 rad. The exit-waves are in excellent agreement with multi-slice frozen lattice image simulations and preserve the high- and low-frequency information. The published method is applicable in any TEM equipped with a single electron biprism and thus allows to achieve high resolution off-axis holography in various instruments including those for in-situ applications. A software implementation for the acquisition, calibration and reconstruction is provided. The combination of environmental TEM and high-resolution phase-shifting electron holography grants access to the platinum-water interface at the atomic scale in ongoing studies.

Keywords:

atomic-scale, off-axis-holography, exit-wave reconstruction, ETEM

Reference:

Q. Ru, G. Lai, K. Aoyama, J. Endo, and A. Tonomura, “Principle and application of phase-shifting electron holography,” Ultramicroscopy 55 (2), 209–220 (1994).
Lindner, J., Ross, U., Meyer, T., Boureau, V., Seibt, M., & Jooss, C. (2024). Reconstruction of Angstrom resolution exit-waves by the application of drift-corrected phase-shifting off-axis electron holography. Ultramicroscopy, 256, 113880.
Barthel, J. (2018). Dr. Probe: A software for high-resolution STEM image simulation. Ultramicroscopy, 193, 1-11.

947

Engineering electron-electron interaction for advanced quantum metrology in electron microscopy

Phd Caterina Chiari[1,2], Prof Marco Beleggia[2], Dr Vincenzo Grillo[1]
[1]Centro S3, CNR - Istituto di Nanoscienze, Modena, Italy, [2]Department of Physics, Informatics and Mathematics, University of Modena, Modena, Italy

Poster Group 2

Background incl. aims:
Electron microscopy (EM) is a fundamental instrument for our comprehension of nanoscale materials and biological samples, providing unparalleled resolution and structural information.
Standard electron microscopy uses beams where a single electron at a time forms the image. However, the recent demonstration of interacting electrons in Ultrafast TEM experiments [1,2] has opened up the possibility of a more complex electron beam characterized by strong electron-electron, mainly Coulomb, interaction.
In fact, electron-electron repulsion may significantly impact the spatial arrangement of beam electrons, leading to collective phenomena such as space charge, beam dispersion, and beam instability. While this is considered detrimental to image resolution and contrast, harnessing this new degree of freedom may be a new tool for electron microscopy and metrology.
In particular, electron-electron interactions can be represented as a non-linear Schrödinger equation and could bring quantum advantage in metrology.
This could be important in increasing the accuracy of measurements or reducing dose demand in imaging delicate matter (e.g., proteins). In fact, quantum discrimination theory [3] has helped us to ascertain the minimum number of electrons needed to discriminate between two particles, which depends on the superposition integral of the wave function corresponding to the imaging of the two particles. Unfortunately, unitary evolution of electrons in a microscope, even in the presence of beam shaping, cannot overcome such limitations. Conversely, the non-unitary wave evolution in multiple electron beams with "self-interaction" could potentially overcome this limitation.
Here, we aim to explore the feasibility of this new TEM metrology concept through quantitative wave simulations.

Methods:
We are using here a simplified mean field Hartree scheme [5] connected to multislice propagation of the electron wave function. We employ a modified multislice code [4], implemented in Python, to simulate the effects of electron-electron interactions alongside propagation. At each slice, the electron density is used to self-consistently calculate the self-interaction Coulomb potential.
In our simulation we used a Laguerre-Gauss (LG) multi-electron beam with an orbital angular momentum (OAM) of 10. The nm sized beam traverses here a cumulative distance of 280 nm.
For comparison we also investigated the behavior of a single-electron LG beam.

Results:
Our findings (as shown in the figures below) reveal that by increasing electron density (number of electrons per bunch) the gold atom becomes more visible, and that upon self interaction and propagation the overlap integral [1], starts to decrease. This suggests that particle discrimination could be improved for interacting electron beam, if the electron density is sufficiently large.

In other words two initially identical multi-electron wave functions, where one of them is scattered by a single gold atom, progressively differentiate with propagation distance. The nontrivial evolution of the wave can be also interpreted in terms of vortex beam instability.

Conclusion:
In this preliminary study, we showcased with a relatively simple example how electron-electron interactions, generally considered detrimental to imaging and analysis, could potentially be exploited to enhance the discrimination between electron wave functions.

Figure Caption:
Fig.1 The amplitude (a,b) and phase (c,d) of the wavefront of a single electron LG beam (OAM=10) in the final () slice with and without gold, respectively. In e) the overlap integral as a function of propagation distance (slice number, with each slice comprising 14 nm) remains constant at a value of 1, denoting unitarian propagation.
The amplitude (f,g) and phase (h,i) of the wavefront of a multi-electron LG beam (OAM=10) in the final () slice with and without gold, respectively. In l) the overlap integral begins to exhibit a different trend, decreasing in value. This is attributed to the non-unitarity, arising from electron-electron interactions.

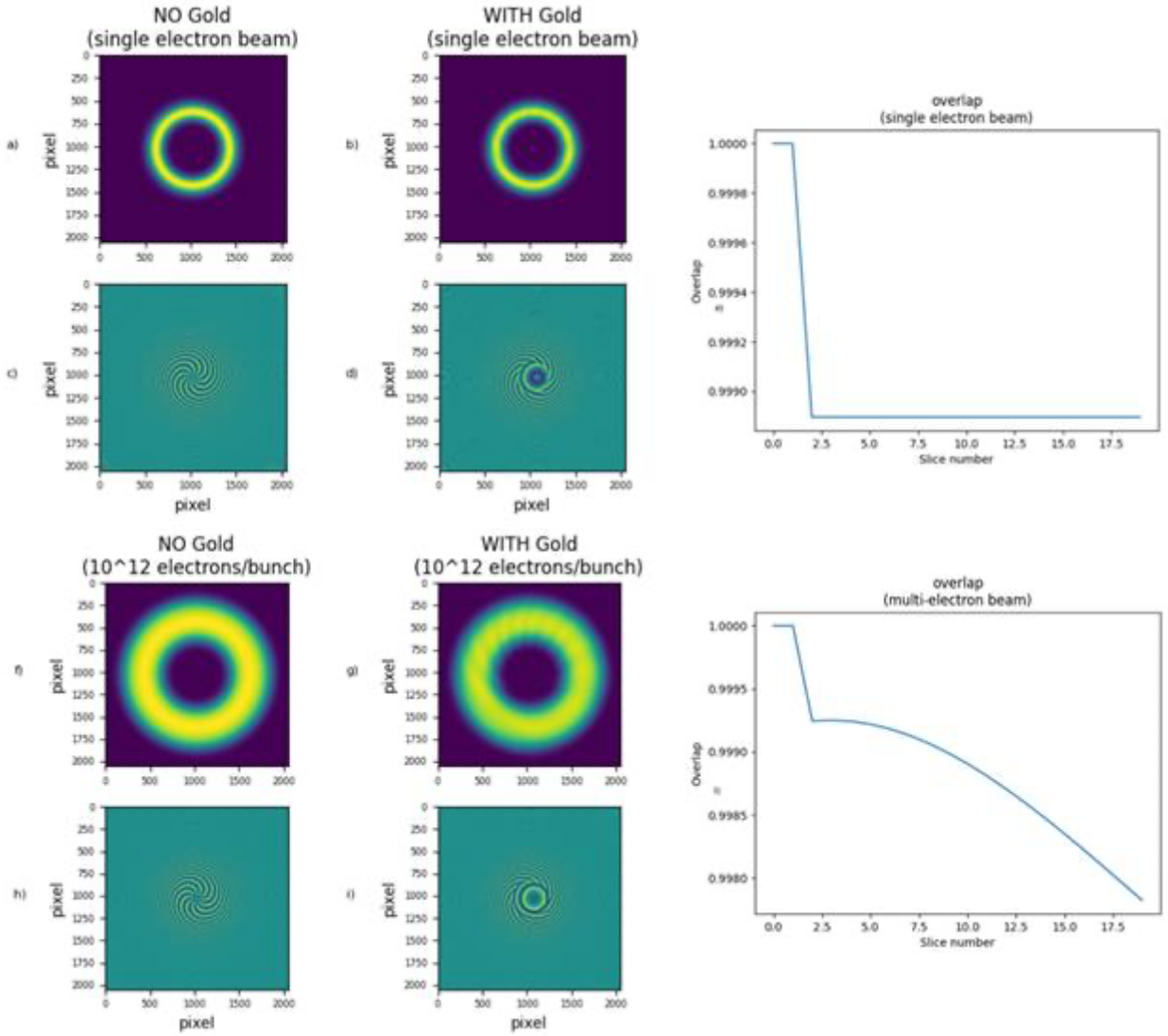

Keywords:

Electron microscopy, multislice, electron interactions,

Reference:

[1] Haindl, R. Et al., Nature Phys. 19 (2023) 10, 1410-1417, 10.1109/IVNC57695.2023.10188964.
[2] Meier, S. Et al., Nat. Phys. 19, 1402–1409 (2023). https://doi.org/10.1038/s41567-023-02059-7.
[3] Troiani, F. Et al, arXiv:2001.08918v1, Phys. Rev. A 102, 043510 (2020).
[4] Cowley, J. M. & Moodie, A. F. (1957). Acta Cryst., 10, 609-619.
[5] Mutzafi, M. Et al., Nat Commun 8, 650 (2017). https://doi.org/10.1038/s41467-017-00651-z.

949

Mean inner potential measurement by correlated EFTEM and phase-shifting holography

Dr. Ing. Ulrich Ross[1], Dr. Christoph Flathmann[1], M.Sc. Jonas Lindner[2], Dr. Tobias Meyer[2], Dr. Andreas Beyer[3], Dr. Jürgen Belz[3], Prof. Dr. Kerstin Volz[3], Prof. Dr. Christian Jooss[2,4], Prof. Dr. Michael Seibt[1]
[1]4th Institute of Physics - Solids and Naonstructures, Georg-August-University Goettingen, Goettingen, Germany, [2]Institute of Materials Physics, Georg-August-University Goettingen, Goettingen, Germany, [3]Department of Physics and Materials Science Center, Philipps-University Marburg, Marburg, Germany, [4]International Center for Advanced Studies of Energy Conversion (ICASEC), Georg-August-University Goettingen, Goettingen, Germany

Poster Group 2

Scientific Background
The mean inner potential (MIP) is an intrinsic material property describing the volume average of the atomic electrostatic potentials in a specimen. Accordingly, it depends on the atomic composition and structure and is sensitive to impurities. Typical values for the MIP lie on the order of 10-30V. However, literature values for common materials can vary by several volts, while values for less-common materials are often unavailable. Since the projected MIP across a homogeneous sample should be constant, the typically used off-axis holography approach involves reconstruction of the gradient of the projected MIP from a sample with a known wedge angle created by cleaving along lattice planes.
This approach has several limitations. Cleaving samples is only practical for single-crystalline, ideal samples. Alternatively, FIB-milling can be used to create the wedge profile, but this results in local deviations from the desired wedge angle as well as significant surface damage. Therefore, the reconstructed phase must be correlated to the local thickness of the material. It is imperative that the local thickness of the sample is known with a high spatial resolution, which then can be matched to the reconstructed phase at similar length-scale. The latter is particularly problematic, since the common Fourier sideband phase reconstruction introduces a low-pass envelope that degrades the spatial resolution of the phase map. We aim to improve the precision of the MIP measurement by correlating EFTEM thickness and off-axis holography phase with high fidelity using phase-shifting holography [1].
Methods
We have recently demonstrated the capability of phase-shifting holography with systematic beam tilt to reconstruct the complex exit-wave of a sample up to Angstrom resolution [2]. Here, we make use of the biprism drift in order to reconstruct the projected potential at lower magnifications, which allows us to reach a spatial resolution up to the pixel size of the camera device while still maintaining a large field of view. We demonstrate this method on a FIB-milled wedge from a lattice-matched heteroepitaxial AlAs-GaAs multilayer sample [3].
Wedge-shaped samples from AlAs-GaAs multiayers are prepared by Ga+ focused ion-beam milling and low-kV cleaning using stage and milling pattern rotations to optimize the wedge angle. The local thickness is mapped by EFTEM using the log-ratio technique. In order to reduce the uncertainty from the mean-free-path prediction, the crystalline part of the thickness wedge is measured by convergent beam electron diffraction (CBED). With the assumption that the FIB-damaged volume outside the sample edge is of homogeneous thickness, we thus calibrate the EFTEM thickness gradient at the sample tilt of the CBED two-beam condition. We then record series of off-axis holograms in Lorentz-TEM mode with a biprism voltage of 200V at zone-axis, two-beam and weakly diffracting tilt conditions. The random drift of the biprism position is used in place of a systematic beam tilt, in order to generate a phase-shifting series. The holography data is then aligned and a narrow band of

high visibility of the fringes in the vacuum region is selected in order to improve the cosine fit for phase-shifting reconstruction.

Results

Taking into account differences in magnification and lens rotation from the projection system, we are able to correlate local projected potential and local thickness with sub-nanometre precision (see Fig.1). Collecting all the data pairs and performing a linear regression results in an excellent fit to the linear phase prediction at kinematical conditions. However, results for different sample tilts also highlight the need for a dynamical scattering correction. The method thus is well-suited for homogeneous samples and uniform diffraction conditions.

Conclusions

Phase-shifting is a powerful tool to improve the correlation between off-axis holography and other TEM methods. Results at suitably large tilts off zone axis are in good argeement with literature, although MIP values appear to be systematically slightly larger than previously reported. Particular care must be taken in order to minimize or, barring that, account for the different influence of preparation damage and dynamical diffraction.

Caption

Fig.1: Measurements from AlAs-GaAs heteroepitaxial multilayers near the surface to the FIB-Pt layer, for MIP measurement. EFTEM t/λ thickness map (a), single-hologram phase reconstruction with an aperture of 1/3rd of the carrier frequency (b), and phase-shifting phase reconstruction from a subset of 90 individual holograms (c). Insets show magnified views of the amplitude of the reconstructed wave at the interface to the nanocrystalline FIB-Pt, with the approximate position of the surface marked by the dashed lines. All measurements were taken at weakly-diffracting sample tilt.

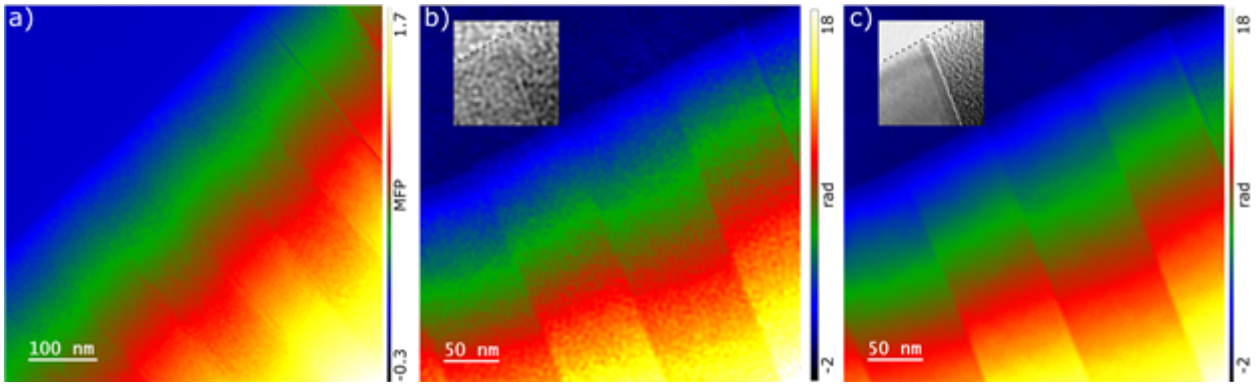

Keywords:

Off-axis Holography, Mean Inner Potential

Reference:

[1] Q. Ru, G. Lai, K. Aoyama, J. Endo, and A. Tonomura, Principle and application of phase-shifting electron holography (1994). Ultramicroscopy, 55(2), 209–220

[2] J. Lindner, U. Ross, T. Meyer, V. Boureau, M. Seibt, & C. Jooss (2024), Reconstruction of Angstrom resolution exit-waves by the application of drift-corrected phase-shifting off-axis electron holography. Ultramicroscopy, 256, 113880

[3] V. S. Chejarla, S. Ahmed, J. Belz, J. Scheunert, A. Beyer, K. Volz (2023), Measuring Spatially-Resolved Potential Drops at Semiconductor Hetero-Interfaces Using 4D-STEM. Small Methods, 7, 2300453

985

Thin Film Phase Plates for Cryo TEM: Fabrication, and Characterization Using Electron Holography

Marcus Hufe[1], Mads Larsen[1], Prof. Stephan Keller[1], Prof. Marco Beleggia[1,2], Associate Professor Paul Kempen[1]
[1]Technical University of Denmark, Copenhagen, Denmark, [2]University of Modena and Reggio Emilia, Modena, Italy

Poster Group 2

BACKGROUND

Phase plates for transmission electron microscopy (TEM) have been a research field since 2001 and are of continuing interest to enhance contrast and increase resolution when imaging biological samples [1]. Unfortunately, biological samples are weak-phase objects in the electron microscope, providing minimal inherent contrast. This is in part because our detectors are only sensitive to variations in electron intensity and not phase. There are different approaches to overcome these limitations, including heavy metal staining (mass-thickness contrast), defocus phase contrast, and phase plate induced phase contrast.

We utilize phase plates to induce phase contrast. The most promising phase plates for soft-matter imaging are thin-film-based. These phase plates suffer from several limitations that plague their widespread implementation. These challenges include contamination, ease of installation and use, lack of reproducibility, and lack of full understanding and control of the induced phase shift [2]. We aim to develop, design, fabricate, implement and use these phase plate devices to reliably improve the contrast when imaging biological samples while staying close to focus, and that are easy to install, align, and use continuously.

METHODS

In this work we are developing thin film based phase plate devices, operating in Zernike and Hilbert mode respectively, to enhance phase contrast at minimal defocus. We are utilizing cleanroom technology to fabricate these devices to be reproducible and with known parameters. We are employing established CMOS thin film processes including dry and wet chemical etching and thin film deposition to create our devices. These phase plates, when installed in the back-focal plane of our TEMs, introduce a phase shift of $\Delta\phi = \pi/2$ (pi-half), or π (pi) respectively, to the scattered beam. The phase shift produced by a thin film is governed by the mean inner potential of the film, the film thickness and the accelerating voltage of the electron microscope. Using the cleanroom to fabricate these devices gives us both knowledge and control of the induced phase shift [3].

We are also employing the electron holography technique to measure the phase shift induced by our thin films. For that a bi-prism, in our case a biased gold wire, is placed in the selected area diffraction (SAD) plane of our TEM. With this we can make the part of the beam going through our material interfere with a reference part going through vacuum. We are thus creating a hologram in the image plane that contains the phase information of the beam going through the material relative to vacuum. After mathematical procedures to reconstruct and unwrap the phase information we can map the phase shift induced by our thin film material [4, 5].

RESULTS

We are able to utilize off-axis electron holography to reliably characterize the phase shift induced by the thin film material of our devices. Employing the accelerating voltage, the known film thickness, and the measured phase shift, we can determine the mean inner potential for the material. With the mean inner potential in hand we can now produce phase plate devices with the correct thickness to induce the target phase shift. With these devices we are able to optimize the contrast from a variety of weak-phase objects yielding TEM images with both higher resolution and higher contrast.

CONCLUSIONS

With the aforementioned approaches and techniques we are able to build a reliable device that improves the contrast when we image bio samples while keeping the defocus value very close to focus. The device can be reliably aligned in diffraction mode when mounted in the back-focal plane. We can address the most common drawbacks of material-based phase plates: we can make usage simple by installing them in the back-focal plane and alignment by aligning at the material edge visible in diffraction mode. Via employing electron holography we can also track the phase shift induced by our devices, which in turn improves the interpretability of phase contrast images.

Keywords:

Phase Plates, Electron Holography, TEM

Reference:

[1] R. Danev et al., Practical factors affecting the performance of a thin-film phase plate for transmission
electron microscopy, 2009, Ultramicroscopy 109: 312
[2] M. Obermair et al., Analyzing contrast in cryo-transmission electron microscopy: Comparison of electrostatic Zach phase plates and hole-free phase plates, 2020, Ultramicroscopy 218: 113086
[3] M. Malac et al., Phase plates in the TEM: operating principles and applications, 2021, Microscopy Vol. 70, No. 1: 75
[4] C. T. Koch, A. Lubk, Off-axis and inline electron holography: A quantitative comparison, 2010, Ultramicroscopy 110: 460
[5] T. Latychevskaia et al., Off-axis and inline electron holography: Experimental comparison, 2010, Ultramicroscopy 110: 472

989

Characterization of Cu doped zeolite by MicroED and electron ptychography

Mr. Masahiko Shimizu[1], Dr. Katsuaki Nakazawa[2], Dr. Kazutaka Mitsuishi[2], Dr. Hajime Matsumoto[1], Dr. Hisashi Shima[1], Dr. Takahiko Takewaki[1], Dr. Ayako Hashimoto[2,3]
[1]Mitsubishi Chemical corporation, Yokohama, Japan, [2]National Institute for Materials Science, Tsukuba, Japan, [3]University of Tsukuba, Tsukuba, Japan

Poster Group 2

Background incl. aims
Selective catalytic reduction (SCR) of NOx by ammonia has been widely applied to the removal of pollutants from diesel gas engines, and Cu doped small pore zeolites are known to exhibit excellent NOx conversion activity and N_2 selectivity. In particular, Cu doped CHA type zeolites (Cu-CHA) have been widely used in automobiles. One of the requirements for practical SCR catalysts is hydrothermal stability to withstand the harsh environment of over 700°C water vapor, and Cu-CHA is known to suffer hydrothermal degradation[1]. The origin of this degradation is proposed to be atomic-scale structural changes such as degradation of the CHA framework and local coordination environment changes of Cu atoms[2]. However, there are few studies of direct observation of this degradation reaction at the atomic level. The reason is that zeolite is an extremely electron sensitive material, so in widely used TEM technique it is difficult to observe zeolites in atomic resolution due to the poor electron beam efficiency. In this study, direct observation of Cu-CHA was performed using microcrystal electron diffraction (MicroED), which allows to analyze crystal structure at low electron doses, and electron ptychography[3], which utilizes 4D-STEM technology to achieve high electron beam efficiency.

Methods
Zeolite sample preparation: Cu-CHA was synthesized by the method described in the paper[3] (Sample A). The synthesized sample was kept at 800°C for 5 hours under 10%-water vapor/air circulation to test its hydrothermal durability (Sample B). Two types of samples were dispersed on carbon TEM grids for MicroED and TEM observation.
Preliminary observation by Micro ED: Sample A was analyzed by a Micro ED system (XtaLAB Synergy-ED, Rigaku/JEOL). The acceleration voltage was 200 kV, and diffraction patterns were obtained from -50 to 50 degrees in 0.5 degree increments. Structural analysis from the set of the diffraction patterns was performed by CrysAlis (Rigaku/JEOL).
Electron ptychography observation: For the two types of samples (Sample A and B) were heated on a hot plate at 200°C in the air for 20 minutes just before TEM observation for removing water and contaminants. For the ptychography observation, an aberration-corrected TEM (JEM-ARM200F, JEOL) equipped with a high-speed pixelated STEM detector (4Dcanvas™, JEOL) was used. The acceleration voltage was 200 kV. The convergence angle was 13.5 mrad, the probe current was 0.059 pA (49 e- per point), real-space pixels were 512×512, and diffraction patterns were acquired with 264×66 pixels and binned to 66×66 by post-processing. The frame time was fixed at 7500 fps.

Results
Fig. (a) shows the crystal structure of Cu-CHA ([100] orientation) determined from MicroED result. The reliability factor R in this analysis is 0.16 (<0.2), this suggests that the determined structure provides the highest reproducibility of the obtained set of the diffraction patterns. The atoms are shown as displacement ellipsoids in Fig.(a), and the Cu atom positions are predicted to be spread out. Fig. (b) shows the phase images obtained by electron ptychography after the hydrothermal durability test. It suggests that the Cu site is changed after the hydrothermal durability test, while no structural changes in the CHA framework were observed.

Conclusion

To investigate the origin of hydrothermal degregation of Cu doped CHA type zeolite, which is useful as an SCR catalyst, MicroED analysis and electron ptychography observations were performed. The results suggest that the Cu site is changed without modifying the structure of the CHA framework after the hydrothermal degradation.

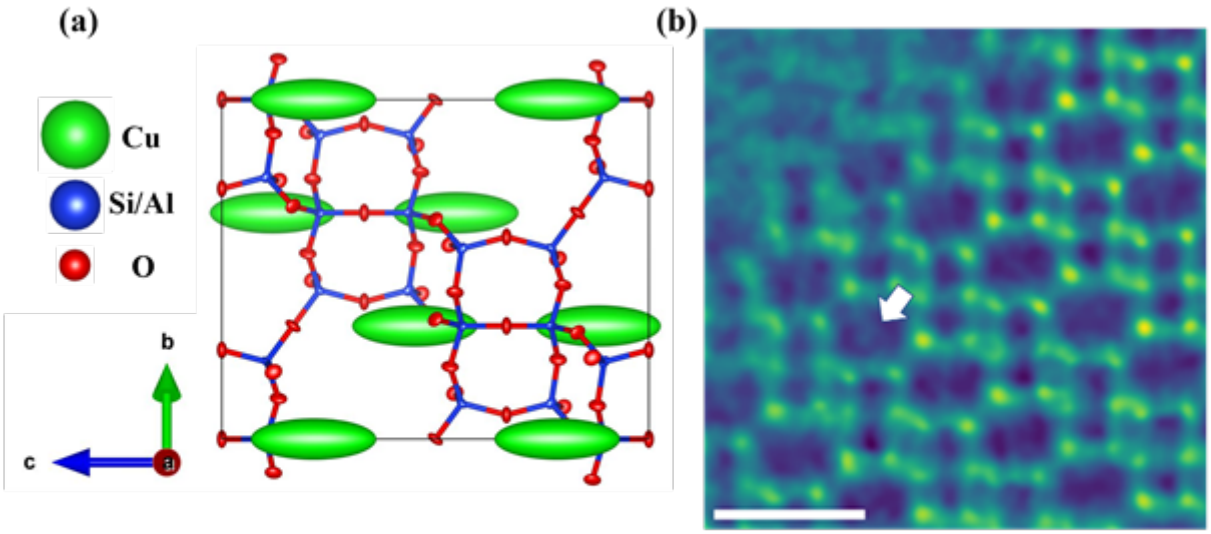

Fig .(a) Cu-CHA structure from Micro ED result. The atoms are shown as displacement ellipsoids (Probability 50%) from [100] direction. (b) Phase image of Cu-CHA after the hydrothermal deterioration test. The scale bar is 1 nm. The arrow indicates Cu site with high possibility.

Keywords:

Electron ptychography, low-dose imaging

Reference:

1. Shan, Y. et al. A comparative study of the activity and hydrothermal stability of Al-rich Cu-SSZ-39 and Cu-SSZ-13. Appl. Catal. B Environ. 264, 118511 (2020).
2. Schmieg, S. J. et al. Thermal durability of Cu-CHA NH_3-SCR catalysts for diesel NO reduction. Catal. Today 184, 252–261 (2012).
3. Mitsuishi, K. et al. Direct observation of Cu in high-silica chabazite zeolite by electron ptychography using Wigner distribution deconvolution. Sci. Rep. 13, 316 (2023).

1049

Revealing Nanostructural Dynamics: Exploring Inelastic Scattering in Electron Microscopy

Phd Caterina Chiari[1,2], Prof. Marco Beleggia[1], Dr Vincenzo Grillo[2]
[1]University of Modena and Reggio Emilia, Modena, Italy, [2]S3 CNR Nano, Modena, Italy

Poster Group 2

Background incl. aims:
Inelastic electron-matter interactions are pivotal for probing the dynamic behavior and electronic structure of materials at the nanoscale. Electron microscopy techniques like electron energy loss spectroscopy (EELS) and energy-filtered transmission electron microscopy (EFTEM) utilize inelastic scattering as a powerful tool for identifying chemical composition, mapping elemental distributions, and elucidating bonding configurations with exceptional spatial resolution [1,2].
A captivating consequence of inelastic scattering is that each electron beam, arriving at the sample after inelastic collisions, interacts with a different (e.g. excited) state. With inelastic processes like ionization, each collision contributes to the establishment of a plasma-like state within the sample. Consequently, it is pertinent to ascertain the final state of the sample after these interactions. Also, what is generally referred to as radiation damage, which may progressively change the very structure of the sample, is entirely a consequence of inelastic collisions. It becomes then extremely important to determine the state of the sample during and after electron irradiation, including, among many other effects, electron-hole recombination.
In this context, since that the relevant cross-sections are modified alongside the evolving sample, we aim to track the formation and dynamics of new molecules, molecular fragments and generated electrons resulting from inelastic scattering.
Additionally, exploring the effects of structured or shaped beams, adds another dimension to reveal the benefits and hindrances of inelastic scattering in electron microscopy. By employing beam-shaping techniques, it may become possible to modulate and control different scattering channels thereby driving the evolution of the sample.

Methods:
Our study commences with an analytical derivation of the wave function, decomposed in elastic and inelastic partial waves, originating from the electron-hydrogen atom interaction [2,3,4]. This choice has the unique advantage of providing analytical results from beginning to end. We present our findings with a set of plots describing visually the ionization of a hydrogen atom, and the subsequent formation of a secondary electron, highlighting the distinctions between elastic and inelastic scattering.

Results:
Representing the primary beam as a plane wave interacting with the hydrogen atom, we obtain scattered spherical outgoing waves modulated in amplitude and phase by the elastic and inelastic scattering factors. The latter (left side of Fig.1 a) shows a more pronounced forward-scattering angular distribution than the former, and, strictly speaking, should also exhibit a longer wavelength. This occurs because the primary beam loses momentum, transferring it to the hydrogen atom's electron. With an energy loss set at 20 eV in this example, the electron is expelled through ionization and becomes a secondary. However, being proportional to the momentum transfer, the wavelength variation of the primary remains very small. The ejected electron is also depicted as a plane wave for simplicity, although it should be more correctly represented by a Coulomb wave function [3,4].

Conclusion:
In this preliminary study, we demonstrate how even a simple specimen as a hydrogen atom, undergoes modifications due to electron beam irradiation. The monitoring of any sample is fundamental in electron microscopy to track the alterations occurring in it and to control its behavior. This is crucial, as inelastic scattering leads to heating or damage effects, emphasizing the necessity of comprehending these interactions for proficient sample analysis and manipulation.

Figure caption:
Fig. 1 (a) Elastic and inelastic scattering processes representation. k_i and k_f are the primary initial and final momentum respectively, while q is the transfer one.
ksin is the initial momentum of the electron bounded to the hydrogen atom, while ksfin is that of the ejected electron according to momentum conservation: k_s^in+q= k_s^fin.
The angular distribution of the scattered wave function is broader for elastic collisions than for inelastic ones. This is reflected in the scattering factor f(θ) which appears narrower in the inelastic case (b).

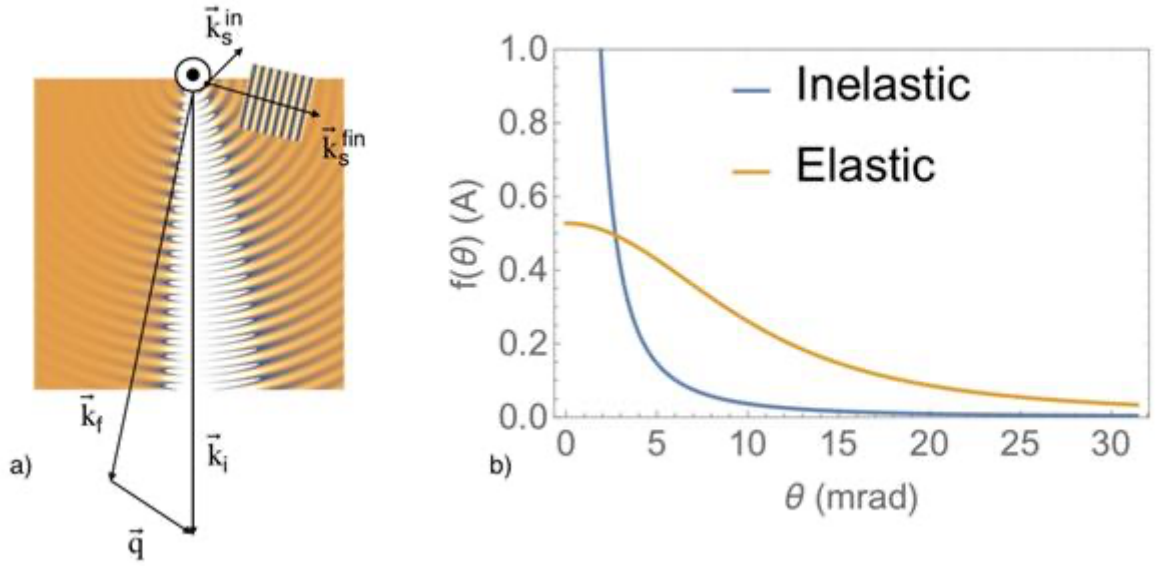

Keywords:

Electron microscopy, Inelastic scattering

Reference:

[1] Egerton, R.F., Physical Principles of Electron Microscopy, Springer, 2005.
[2] Landau, L. and Lifshits, E, Quantum mechanics: non relativistic theory, Pergamon Press, 1977.
[3] Sakurai, J.J., Modern Quantum mechanics, Addison-Wesley Publishing Company, 1994.
[4] Gottfried, K, Quantum mechanics: fundamentals, Springer, 2003.

1066

Electrons phase reconstruction using Kramers-Kronig relations

Dr. Yang Yin[1], Dr. Wenhao He[1], Prof. Changlin Zheng[1]
[1]Department of Physics,Fudan University, Shanghai, China

Poster Group 2

Background incl. aims
Phase imaging plays an important role in electron microscopy, particularly in mapping electric and magnetic fields at the nano and atomic scale. In this presentation we introduce a new electron phase imaging approach based on Kramers-Kronig (KK) relations, which is originally developed for optical imaging [1, 2].

Methods
According to the Kramers-Kronig relations, the real and imaginary parts of a complex function transform into each other when the function is analytical in the upper half-plane. This results in a clear link between the amplitude and phase of the exit wave. As a first attempt, we applied such KK method to reconstruct the phase of off-axis electron hologram. The experiments were performed on a Thermo Fisher Scientific Themis Z transmission electron microscope fitted with an electron biprism. An off-axis electron hologram of nano particles was then recorded using a CETA -S camera (see Fig.1). We applied the KK reconstruction on the electron holograms, the detailed reconstruction procedure is illustrated in Fig. 1. We also performed the conventional Fourier transform reconstruction for comparison.

Results :
The reconstructed amplitude and phase images based on KK relations are shown in Fig.1. Further comparsion with Fourier transform method reveals that the KK reconstruction results are consistent with Fourier transform method.

Conclusion
Here, we show that the Kramers-Kronig relation can be used to recover phase information from electron holograms. This method not only provides an alternative to conventional Fourier transform reconstruction but also helps surpass bandwidth limits when using a digital aperture in conventional Fourier transform reconstruction.

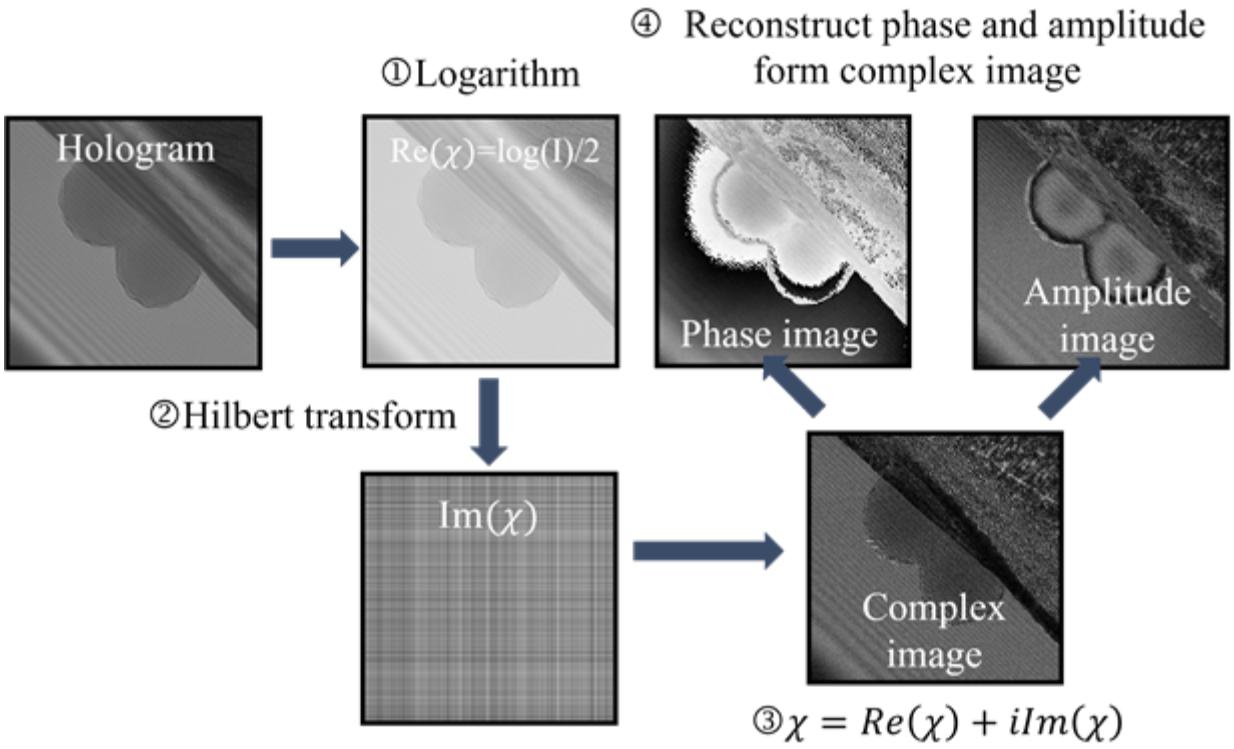

Keywords:

holography, Kramers-Kronig relations

Reference:

[1] Y. Baek and Y. Park. (2021). Nat. Photonics 15, 5.
[2] Y. Baek, K. Lee, S. Shin, and Y. Park. (2019). OPTICA 6, 45.

1088

Quarantotto: a 48-segment STEM detector for enhanced STEM performance and new applications

Dr Stefano Vespucci[1], Dr Eric G.T. Bosch[1], Dr Ivan Lazić[1], Bert de Vries[1], Dr Ricardo Egoavil[1], Dr Bert Freitag[1], Dr Tim Grieb[2], Dr Florian F. Krause[2], Dr Martin Eickhoff[2], Prof Andreas Rosenauer[2]
[1]Thermo Fisher Scientific, Eindhoven, The Netherlands, [2]Institute of Solid-State Physics, University of Bremen, Bremen, Germany

Poster Group 2

Background incl. aims

In scanning transmission electron microscopy (STEM) the image formation process requires the acquisition of convergent beam electron diffraction (CBED) patterns, at every position of the probe on the sample. Traditionally, disc or ring detectors capture only part of CBED signal within their area, enabling annular bright field (ABF) or annular dark field (ADF) STEM imaging. The center-of-mass (COM) of the CBED pattern provides an essential information on the sample, as the COM vector represents the projected electric field of the sample, the gradient (differential) of the projected electrostatic potential [1, 2]. In thin samples, the projected electrostatic potential is encoded in the phase of the electron wave passing through the specimen, and for this reason these COM-based techniques are referred to as differential-phase-contrast (DPC) techniques.

DPC-STEM techniques have emerged as a powerful tool, offering unprecedented insights into electric and magnetic properties of materials at nano and atomic scale. Integrated DPC-STEM technique (iDPC-STEM) [2] allows efficient imaging of light elements (including hydrogen) next to heavy ones, beam sensitive materials including Zeolites, Metal-Organic-Frameworks (MOFs) at sub-Å scale, as well as cryo-biological nanoparticles at near-atomic resolution [3].

DPC-STEM and iDPC-STEM are implemented in the simplest way by exploiting a four-quadrant detector [1], as this is sufficient for obtaining a good representation of the COM vector. At the other extreme, cameras with larger number of pixels can be used to record the full CBED patterns. This approach is known as 4D-STEM and enables additional reconstruction techniques such as ptychography. However, due to readout limitations, the acquisition speed of cameras (10 to 100µs dwell-time) is much lower than of single/multi-segment detectors (100ns dwell-time). While the precision of 4D-STEM methods benefits from larger number of pixels, many practical applications require dwell-times of 1µs, or smaller, making the use of cameras not an ideal choice.

In this work, we propose an intermediate solution based on a 48-segment detector, called Quarantotto. With this approach, the acquisition speed can be as fast as with a single segment, while, at the same time, the larger number of segments improve the COM measurement. This leads to contrast transfer improvement for DPC-STEM and enables implementation of new applications, such as aberration measurements [4] and segmented ptychography.

Methods

Although four segments provide very accurate results for most applications, there are cases (e.g. thicker samples and heavy atoms) where the effects of the 4-fold symmetry of the detector is reflected in the corresponding contrast-transfer-function (CTF). The CTF improves by increasing the number of detector segments as the COM vector can be precisely computed and an ideal version of iDPC-STEM, called iCOM-STEM, can be obtained. When a smaller number of larger segments is used,

the positions of their geometrical-gravity-centers are used (the DPC mask in Fig. 1a-d bottom) to map their integral signals and compute COM of the CBED.

Quantification of the atomic electric field based on COM was used to demonstrate how the number of segments in segmented-STEM detector affects the accuracy of the measurement compared to cameras [5].
Quarantotto, the newly proposed solid-state detector, Fig. 1a-d top row, consists of 48 segments arranged in 3 rings of 8, 16 and 24 segments of equal area. All 48 segments can be simultaneously read out at a speed of 100ns dwell-time. The improvement in the CTF for the DPC-STEM and iDPC-STEM techniques with the 48-segment detector, is demonstrated against the three sub-configurations of the detector. The first two sub-configurations are two orientations of a regular 4-quadrant detector (Fig 1a and b), the third one is an 8-segment detector consisting of 8 pie-pieces (Fig. c).

In addition to DPC-STEM and iDPC-STEM, the 48-segment STEM detector enables efficient implementation of new techniques, such as segmented-ptychography, where the reconstructed CBED patterns are matched with the measurement segment by segment, and fast probe aberration measurements, where the shifts between the 48 segment images based on the aberration function are matched with the measured segment image shifts. In the past, these techniques have not been fully explored because of the lack of a detector featuring both enough segments and high speed, but now possible with the 48 segments detector.

Results

Quarantotto was used to demonstrate a more rotationally symmetric CTF when compared to four quadrant detectors. Figure 1 shows a direct comparison between iDPC-STEM images of gold islands on amorphous carbon, acquired at 300keV and convergent semi angle of the beam of 30mrad, obtained with the two possible 4-quadrant configurations (Fig. 1a-b), 8-segment azimuthal segment configuration (Fig. 1c) and the full 48-segment detector (Fig. 1d), respectively. For each image, the bottom row shows the FFT where the bottom-left insets show the DPC mask (x-direction), while the bottom-right insets show the theoretical CTF [1] using given detector configuration.

The FFTs of the iDPC-STEM images reflect the corresponding symmetry of the CTFs. The possible undesired effects of the noncentral symmetrical CTFs of 4-quadrant configurations are largely mitigated with 8-quadrant configuration and eliminated using the 48-segment configuration. The CTF of the 48-segment configuration is practically indistinguishable from the ideal rotationally symmetric situation of a camera.

The detector has been successfully utilized to measure and tune the aberrations of the microscope. This was achieved by measuring the shifts between the 48 segment images and fitting them to the expected shifts based on the aberration function. The image in Figure 1 was obtained after correcting for these measured aberrations.

Quarantotto has also been benchmarked against EMPAD to validate the precision of the electric field measurement across a GaN-GaAlN nanowire structure.

Conclusion

The 48-segment detector was used to demonstrate an improvement in (i)DPC-STEM performance when compared to the 4 and 8-quadrant detectors. It has been successfully used to measure the electric fields across a GaN-GaAlN nanowire structure and to tune the optical aberrations of the

microscope. Overall, the Quarantotto detector represents a significant advancement, offering improved imaging at ultimate speed, larger field of view measurements, and the implementation of new techniques.

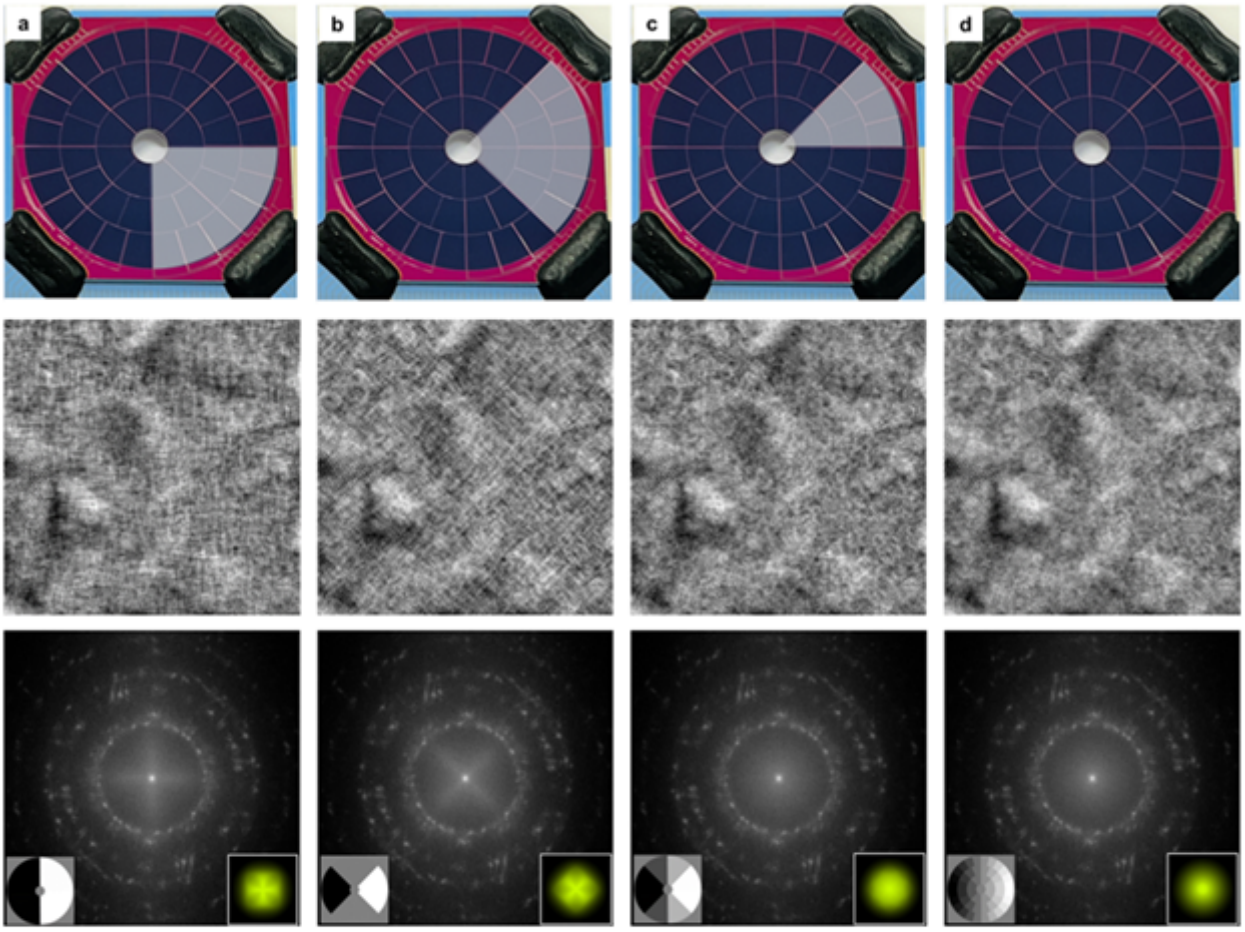

Figure 1: Top row: image of 48-segment detector with four different (sub-)configurations indicated. Middle row: iDPC-STEM images of gold on carbon sample using corresponding detector configurations, acquired at 300kV with convergence semi angle of the beam of 30mrad. Botom row: FFT of the images showing the imprint of the CTFs. Left inserts are DPC masks, right inserts are theoretical CTFs. Scanning is aligned with the orientation of the detector (from left to right and from top to bottom). (a, b) Two possible 4-quadrant configurations. Note the crosses both in the image and FFT aligned with CTF crosses. (c) Azimuthal 8-segment configuration. The central star reflecting the CTF symmetry is hardly noticeable. (d) Full 48 segment configuration. Full central symmetrical FFT and CTF.

Keywords:

Multi-segment-detector, iDPC-STEM, iCOM-STEM, Ptychography, Aberration-Correction

Reference:

[1] I. Lazić, E.G.T. Bosch, Advances in Imaging and Electron Physics 199 (2017) 75-184.
[2] I. Lazić, E.G.T. Bosch and S. Lazar, Ultramicroscopy 160 (2016) 265-280.
[3] I. Lazić, et. al., Nature Methods 19 (2022) 1126
[4] A.R. Lupini, M.Chi, S. Jesse, Journal of Microscopy 263, (2016) 43–50
[5] T. Grieb, et. al., Journal of Microscopy (2024) 1–7.

1103

Low-dose 4D-STEM cryo-tomography of biological samples

Dr. Shahar Seifer[1], Shai Kiriati[1], Dr. Peter Kirchweger[1], Prof. Michael Elbaum[1]
[1]Weizmann Institute of Science, Rehovot, Israel

Poster Group 2

Background incl. aims
4D-STEM provides a copious amount of information that must be reduced for interpretion. The challenge is compounded in the context of low dose exposure in beam-sensitive specimens. We describe several data processing approaches for tomographic reconstruction that result in improved 3D mapping of biological samples.

Methods
4D STEM collects a 2D diffraction pattern at each pixel in real space. Summation of electron counts over masked areas define virtual detectors in the form of annular rings and azimuthal sectors. A tilt series of projection images provide data for tomography, from which 3D reconstructions are generated for each virtual detector individually. Principal component analysis (PCA) of annuli yields a separation of amplitude and phase contrast. Alternatively, center of mass (COM) and differential phase contrast (DPC), generated from azimuthal segments, reveal phase gradients. By manipulation of parallax corrections, which appear as image shifts, the phase contrast extracted by integrated virtual differential phase contrast (iDPC) can be separated into parts that originate from distinct contributions of the contrast transfer function, aiding in interpretation. Finally, by collection of a large scattering range, information accessible in the virtual rings in the dark field is also interpretable as a differential cross section, which decomposes to elastic and inelastic scattering contributions depending on the scattering angle.

Results
3D reconstructions are applicable on either the virtual rings or sectors. Applying parallax manipulation over the virtual DPC is particularly useful and shares common aspects with ptychography techniques. The differential cross section data fits predictions in elastic scattering and plasmon generation in several amorphous non-metallic materials.

Conclusion
4D-STEM in tilt series can be applied routinely to generate 3D imaging that demonstrates improvement over simple dark-field or incoherent bright-field STEM. In parallel, the direct measurement of differential scattering cross section provides indications on atomic composition.

Keywords:

4D-STEM tomography; ptychography; DPC; cryo-TEM

Reference:

1. Seifer et al, “Optimizing contrast in automated 4D-STEM cryo-tomography”, https://doi.org/10.1101/2024.02.23.581684
2. Seifer et al, “Quantitative atomic cross section analysis by 4D-STEM and EELS”, Ultramicroscopy 2024, https://doi.org/10.1016/j.ultramic.2024.113936
3. Seifer et al, “Flexible STEM with Simultaneous Phase and Depth Contrast”, M&M 2021, https://doi.org/doi:10.1017/S1431927621012861

1128

Nanoparticle Self Diffraction in the TEM: A proposal

Prof. Stefan Nimmrichter[1], Prof. Dennis Rätzel[2,3], Prof. Peter Schattschneider[4,5], Prof. Philipp Haslinger[4,6]
[1]Naturwissenschaftlich-Technische Fakultät, Universität Siegen,, Siegen, Germany , [2]Institut für Physik, Humboldt-Universität zu Berlin, Berlin, Germany, [3]ZARM, University of Bremen, Bremen, Germany, [4]USTEM, TU Wien, Vienna, Austria, [5]Institute of Solid State Physics, TU Wien, Vienna, Austria, [6]Vienna Center for Quantum Science and Technology, Atominstitut, TU Wien, Vienna, Austria

Poster Group 2

Background and aims
Entanglement in the TEM has been proposed to study the superposition of mesoscopic quantum states and their decoherence via the reduced density matrix of the probe electron [1]. Here, we take this idea further and discuss the possibility to prepare a massive nanoparticle in a quantum superposition of distinct momentum states and observe its interference. Contrary to previous proposals for nanoparticle diffraction at optical standing-wave gratings [2], the spatial and temporal coherence requirements are substantially lower. TEM-assisted diffraction might be therefore a viable alternative route towards new mass records in matter-wave interferometry.
Methods
We propose to diffract a single electron on a (crystalline) nanoparticle of about 50 nm radius and lattice plane distance d. By virtue of momentum conservation, each Bragg reflection $g_n=2\pi n/d$ imparts a momentum of $nhg/2\pi$ onto the center of mass (CM) of the nanoparticle (red dot in Fig. 1A). Detecting the electron in the image plane (Fig. 1B) then prepares the nanoparticle in a quantum superposition of wave packets with different momenta – a Schrödinger kitten state with a relative phase conditioned on the detected electron position. As the particle propagates freely in time (Fig. 1C), the wave packets disperse and interference fringes form. A position measurement, e.g., in an optical dipole trap (Fig. 1D), would reveal these fringes, demonstrating the quantum wave nature of the nanoparticle's CM. This can be viewed as resulting from the diffraction of the nanoparticle on its own crystal lattice.
Results
We predict fringe patterns caused by quantum interference, different from both a classical mixture of individually spreading states that would not show fringes, and from a semiclassical model of Moiré fringes, which presumes that the Wigner function of the nanoparticle be non-negative at all times. For didactical reasons, we demonstrate the principle in Fig. 2 showing the density matrix of a hypothetical particle's CM with an initial position spread of the pure state of d/20. ξ/d is the main diagonal, η/d shows the degree of coherence. The red curve is the density profile. A realistic scenario with a crystalline nanoparticle in the mass regime of 10^6 to 10^8 atomic mass units will be benchmarked against the semiclassical model.
Conclusion
In a dedicated TEM the observation of macroscopic quantum interference should be feasible.

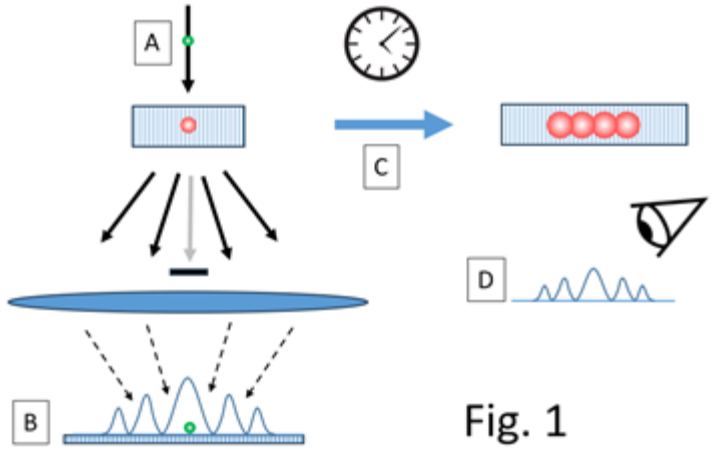

Fig. 1

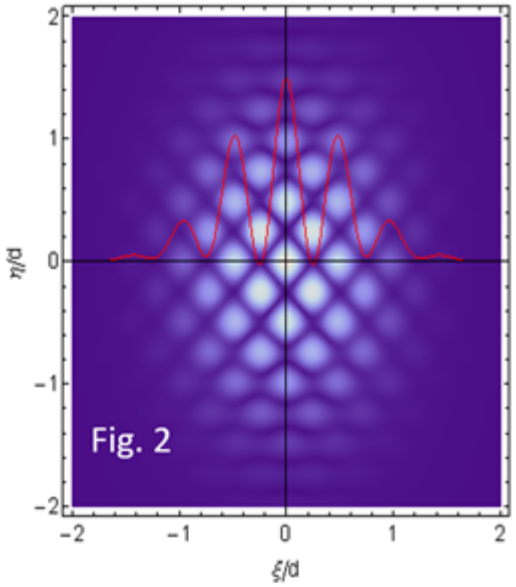

Fig. 2

Keywords:

Entanglement, matter-wave interference, cat-states, coherence

Reference:

1. Schattschneider, P. and Löffler, S.: Ultramicroscopy 190 (2018) 39
2. Bateman, J., Nimmrichter, S., Hornberger, K. et al. Nat Commun 5, 4788 (2014)

1296

Optimized Bright Field STEM Imaging for Detecting Molecules absorbed within Zeolite Pores

Yu Xia[1], Tom Willhammar[1]
[1]Department of Materials and Environmental Chemistry, Stockholm University, Stockholm, Sweden

Poster Group 1

Background incl. aims
Zeolites, characterized by their large and regular pores, are utilized to filter target molecules from mixtures, purify effluent by removing pollutants and in catalysis. Atomic resolution imaging of small molecules in pores will contribute to elucidate host-guest interactions between small molecules and porous structures and understand diverse molecular absorption/desorption behaviors in pores. Scanning transmission electron microscopy (STEM) is a powerful technique to capture interpretable atom-scale images, facilitating localized structural analyses. Recognizing the inherent sensitivity of zeolites and molecules to electron beam exposure, low electron dose imaging techniques, including the differential phase contrast (DPC) employing segmented detectors and 4D-STEM using pixelated detectors, have been developed. Pixelated detectors employed by 4D-STEM offer superior electron collection efficiency with fine resolution and high signal-to-noise ratio (SNR) at probe positions[1]. However, pixelated detectors entail higher costs and longer dwell time compared to segmented counterparts. The integrated DPC (iDPC) technique has shown its power in imaging light elements with low-dose conditions. Recently, a newly developed optimum bright-field (OBF) STEM technique demonstrates enhanced SNR relative to iDPC[23] OBF images are reconstructed by combining the images captured by segmented detectors. Each segmented image is weighted by a frequency filter for the contribution to the Fourier component of the reconstructed OBF image, where the frequency filters are built using phase contrast transfer functions (PCTFs) for the segmented detector[2]. Here, the OBF-STEM technique with a custom-made python package is utilized for the efficient detection of molecules within the pores of ZSM-5 zeolite using a four-segmented detector.
Methods
The theoretical framework of the OBF STEM image can be derived from the single side band (SSB) ptychography[4], where the specimen is weakly electron scattering. The exit wave function M(k ,Q) is given by the convolution of the entrance probe wavefunction ψ(k)·ψ^* (k-Q) on the specimen with the pupil function A(k) A^* (k +Q) , where Q is the spatial frequency of the probe at spaced position r on the specimen in Fourier space. Therefore, the PCTF can be calculated by T^* (k)T(k -Q)-T(k) T^* (k +Q) , where T(k) is the aperture transfer function defined as the multiplication of the aperture function with the probe wave function in reciprocal space. In a segmented detector, the STEM image intensity of the i-th segment I_i (r) is described mathematically as ∫I(k ,r) D_i (k)𝑑k, where D_i (k) is the i-th segmented detector response function in reciprocal space and I(k, r) is the inverse Fourier transform of the diffraction pattern (|M(k,Q)|^2). The OBF STEM image is reconstructed by combining the segmented images weighted by frequency filters in reciprocal space, or combining the convolution of each segmented image with a corresponding point spread function (PSF) in real space[2]. For maximizing the SNR of the reconstructed OBF image, the PCTFs in the segmented detector are optimized by incorporating real-valued functions, such as high/low bandpass filters [2]. In this work, a custom-made python package is developed to calculate the PCTFs and the corresponding real-valued functions for OBF STEM image reconstruction. The specimen of ZSM-5 zeolite absorbed pollutants was imaged with the convergence semi-angle of 21 mrad on an aberration-corrected FEI Titan Cubed Themis Z microscope operated at 300 kV. A four-segmented detector was employed to capture images using a beam current around 4.7 pA and a dwell time of 2 µs per pixel within a collection angle range of 8-42 mrad, with a camera length of 185 mm.
Results

The ZSM-5 with pollutants in pores was imaged along the [0 1 0] direction under a dose rate of 856 e-/Å². iDPC image (Figure a) and OBF image (Figure b) were reconstructed using the same dataset. Compared with the iDPC image, OBF image demonstrates clearer structural details due to its higher contrast and SNR, evident in line profiles and the cropped image (Figure d) from the same area in iDPC and OBF images. The superior contrast and finer resolution of OBF image enable more distinct observation of pollutants (marked by arrows in the line profiles) within pores than that of the iDPC image.

Conclusion

OBF-STEM images were reconstructed using the custom-made python package. This package implements algorithms to compute the PCTFs and the corresponding real-valued filters for image reconstruction. The reconstructed OBF image demonstrates enhanced contrast and SNR, giving clearer discernment of structural features. Importantly, features within the pores of ZSM-5 were distinctly distinguished in the OBF images compared to those reconstructed iDPC images. These findings imply that the OBF technique, employing a high-speed segmented detector, represents a promising approach for low-dose imaging of molecules encapsulated within the pores of zeolites.

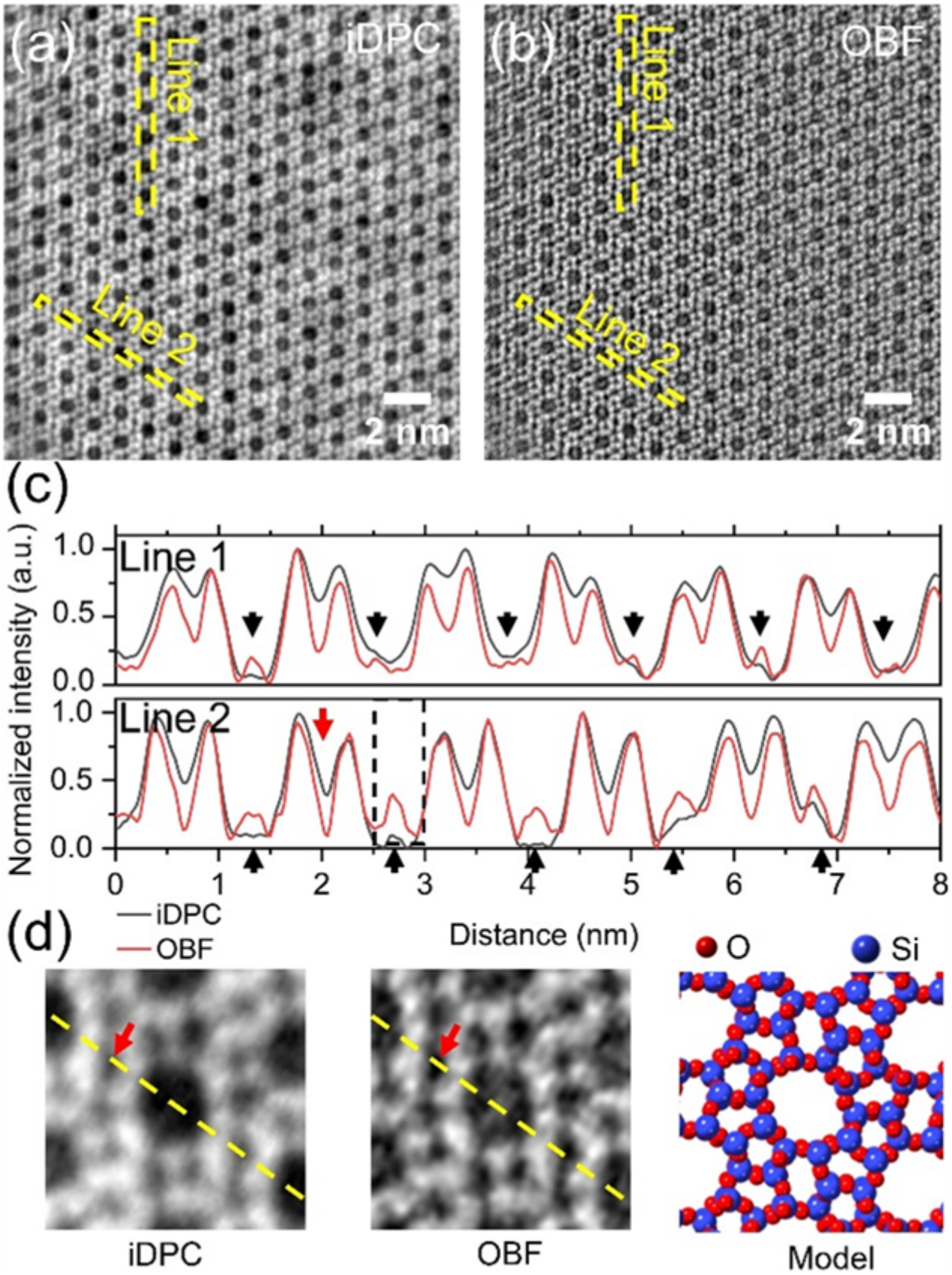

Keywords:

STEM, segmented detectors, low-dose imaging

Reference:

1. O'Leary, C. M. et al.. Ultramicroscopy 221, (2021).
2. Ooe, K., Seki, T., Ikuhara, Y. & Shibata, N. Ultramicroscopy 220, 113133 (2021).
3. Ooe, K. et al. Sci. Adv. (2023) doi:10.1126/sciadv.adf6865.

4. Rodenburg, J. M., Mccallum, B. C. & Nellist, P. D. Ultramicroscopy 48 (1993).